UNIVERSIDAD DE GRANADA
FACULTAD DE CIENCIAS
DEPARTAMENTO DE MICROBIOLOGÍA

EFECTO DE *STENOTROPHOMONAS BENTONITICA* BII-R7 SOBRE LA MOVILIDAD DE SELENIO, CURIO Y EUROPIO EN EL MARCO DEL SISTEMA DE ALMACENAMIENTO GEOLÓGICO PROFUNDO DE RESIDUOS RADIACTIVOS

EFFECT OF *STENOTROPHOMONAS BENTONITICA* BII-R7 ON THE MOBILITY OF SELENIUM, CURIUM, AND EUROPIUM WITHIN THE DEEP GEOLOGICAL REPOSITORY SYSTEM OF RADIOACTIVE WASTE

Programa Oficial de Doctorado en Biología Fundamental y de Sistemas

Miguel Ángel Ruiz Fresneda

TESIS DOCTORAL
Granada, 2019

Universidad de Granada
Facultad de Ciencias
Departamento de Microbiología

EFECTO DE *STENOTROPHOMONAS BENTONITICA* BII-R7 SOBRE LA MOVILIDAD DE SELENIO, CURIO Y EUROPIO EN EL MARCO DEL SISTEMA DE ALMACENAMIENTO GEOLÓGICO PROFUNDO DE RESIDUOS RADIACTIVOS

EFFECT OF *STENOTROPHOMONAS BENTONITICA* BII-R7 ON THE MOBILITY OF SELENIUM, CURIUM, AND EUROPIUM WITHIN THE DEEP GEOLOGICAL REPOSITORY SYSTEM OF RADIOACTIVE WASTE

Memoria presentada por el graduado en Biología D. Miguel Ángel Ruiz Fresneda para aspirar al Grado de Doctor por la Universidad de Granada con mención internacional.
Esta tesis ha sido dirigida por D. Mohamed Larbi Merroun, Profesor Titular de la Universidad de Granada.

V° B° del Director

Mohamed Larbi Merroun
Profesor Titular de Microbiología
Universidad de Granada

El doctorando

Miguel Ángel Ruiz Fresneda

Editor: Universidad de Granada. Tesis Doctorales
Autor: Miguel Ángel Ruiz Fresneda
ISBN: 978-84-1117-277-6
URI: http://hdl.handle.net/10481/74160

Esta Tesis Doctoral ha sido realizada en el Departamento de Microbiología (Facultad de Ciencias) de la Universidad de Granada durante los años 2015-2019 dentro del grupo de investigación Mixobacterias (BIO 103).

Para la realización de este trabajo el doctorando disfrutó de un contrato de investigador con cargo al Proyecto Europeo MIND *"Microbiology In Nuclear waste Disposal",* financiado por el programa "*Euroatom research and training program 2014-2018 under Grant Agreement no. 661880 (H2020 Programme)*", siendo el Dr. Mohamed Larbi Merroun el investigador principal de dicho proyecto en la Universidad de Granada. Parte de esta Tesis Doctoral también ha sido financiada por el "*European Regional Development Fund (ERDF)-co-financed Grants CGL2012-36505 and CGL2014-59616-R (Ministerio de Ciencia e Innovación, Spain; 80% funded by ERDF)".*

Además, el doctorando disfrutó de ayudas para la realización de estancias en centros de investigación extranjeros:

- Beca de "Estancias Breves en Centros de Investigación Nacionales y Extranjeros". Otorgada por el Plan Propio de investigación de la Universidad de Granada en Diciembre de 2016 para una estancia de 2 meses en el centro de investigación Helmholtz-Zentrum Dresden-Rossendorf (HZDR) localizado en Dresden (Alemania).

- Beca de "Movilidad Internacional de Jóvenes Investigadores de Programas de Doctorado de la Universidad de Granada". Otorgada por el Vicerrectorado de Internacionalización de la Universidad de Granada en Mayo de 2017 para una estancia de 3 meses en la Universidades de Sheffield y Sheffield Hallam (Sheffield, Reino Unido).

- Beca de Movilidad Internacional otorgada por la "*European Radioecology Alliance*" en Septiembre de 2018 para una estancia de 2 meses en el centro de investigación Helmholtz-Zentrum Dresden-Rossendorf (HZDR) localizado en Dresden (Alemania).

Durante el transcurso de esta Tesis Doctoral se han llevado a cabo estancias de investigación en los siguientes centros extranjeros:

- **Department of Biogeocemistry, Institute of Resource Ecology, Helmholtz-Zentrum Dresden-Rossendorf (HZDR), Dresden, Alemania.** Tema: *Study of the molecular interactions of uranium and europium with bacterial strains isolated from Spanish bentonites.* Duración: 60 días (17/05/2016-15/07/2016).

- **Department of Geography, The University of Sheffield, Sheffield, Reino Unido**. Tema: *Purification and spectroscopic characterization of selenium nanoparticles produced by the bacterial strain Stenotrophomonas bentonitica*. Duración: 93 días (27/08/2017-27/11/2017).

- **Biomolecular Sciences Research Center, Faculty of Health and Wellbeing, Sheffield Hallam University, Sheffield, Reino Unido.** Tema: *Purification and spectroscopic characterization of selenium nanoparticles produced by the bacterial strain Stenotrophomonas bentonitica.* Duración: 93 días (27/08/2017-27/11/2017).

- **MARS beamline, SOLEIL Synchrotron, Saint-Aubin, Paris, France.** Tema: *XAS characterization of reduced selenium produced by the bentonite-isolate Stenotrophomonas bentonitica*. Duración: 4 días (20/04/2018-23/04/2018).

- **Department of Biogeocemistry, Institute of Resource Ecology, Helmholtz-Zentrum Dresden-Rossendorf (HZDR), Dresden, Alemania.** Tema: *Study of the molecular interactions of uranium and europium with the bacterial strain Stenotrophomonas bentonitica isolated from Spanish bentonites.* Duración: 62 días (03/09/2018-03/11/2018).

Los resultados obtenidos durante la realización de esta Tesis Doctoral han sido publicados o se están preparando para su publicación en revistas científicas de impacto, así como en congresos tanto a nivel nacional como internacional:

1) Artículos científicos publicados con los resultados obtenidos durante esta Tesis Doctoral:

- **Ruiz-Fresneda M.A.**; Delgado-Martin J.; Gómez-Bolivar J.; Fernández-Cantos M.V.; Bosch-Estévez G.; Martínez-Moreno M.F. and Merroun M.L. Green synthesis and biotransformation of amorphous Se nanospheres to trigonal 1D Se nanostructures: impact on Se mobility within the concept of radioactive waste disposal. Environ. Sci. Nano. 2018; 5:2103-2116.

- Sánchez-Castro I.; **Ruiz-Fresneda M.A.**; Bakkali M.; Kämpfer P.; Glaeser S.P.; Busse H.J.; López-Fernández M.; Martínez-Rodríguez P. and Merroun M.L. *Stenotrophomonas bentonitica* sp. nov., isolated from bentonite formations. Int. J. Syst. Evol. Microbiol. 2017; 67(8):2779–2786.

2) Resultados obtenidos durante esta Tesis Doctoral presentados en congresos a nivel nacional e internacional:

- **Ruiz-Fresneda, M.A.***; Eswayah A.S.; Gomez-Bolivar J.; Romero-Gonzalez M.; Gardiner P.H.E. and Merroun M.L. Bioproduction of selenium nanostructures and volatile compounds within the concept of deep geological repository. Joint G16-ABWET Conference. 6-7 December, 2018, Naples, Italy. Comunicación oral.

- **Ruiz-Fresneda M.A.***; Gómez-Bolívar J.; Delgado-Martín J.; Fernández-Cantos M.V. and Merroun M.L. Reduction of selenite to amorphous and crystalline selenium nanostructures by *Stenotrophomonas bentonitica*: impact on selenium mobility within the concept of radioactive waste repositories. MIND Project Annual Meeting. 7-9 May, 2018, Lausanne, Switzerland. Comunicación oral.

- **Ruiz-Fresneda M.A.***; Gómez-Bolívar J.; Fernández-Cantos M.V.; Delgado-Martín J. and Merroun M.L. Microscopic and structural characterization of selenium nanoparticles produced by *Stenotrophomonas bentonitica*. Annual conference 2018, Microbiology Society. 10-13 April, 2018, Birmingham, UK. Póster.

- Merroun M.L.*; **Ruiz-Fresneda M.A.** and Gómez-Bolívar J. Anaerobic reduction of Se^{IV} by bacterial strain isolated from Spanish bentonites: multidisciplinary approach characterization. Selenium 2017. 13-17 August, 2017, Stockholm, Sweden. Comunicación oral.

- **Ruiz-Fresneda M.A.***; Gómez-Bolívar J.; Fernández-Cantos M.V.; Delgado-Martín J.; Cherkouk A.; Moll H. and Merroun M.L. Speciation of Se^{IV} and Eu^{III} associated with *Stenotrophomonas bentonitica* BII-R7 isolated from Spanish bentonites. Goldschmidt Conference 2017. 13-18 August, 2017, Paris, France. Póster.

- **Ruiz-Fresneda M.A.***; Gómez-Bolívar J.; Sánchez-Castro I.; Cherkouk A.; Moll H. and Merroun M.L. Interactions of Se^{IV} and Eu^{III} with the indigenous bentonite bacterial specie *Stenotrophomonas bentonitica*. 16th International Clay Conference (ICC). 17-21 July, 2017, Granada, Spain. Comunicación oral.

- Gómez-Bolívar J.*; **Ruiz-Fresneda M.A.** and Merroun M.L. Microbial/metal interactions with metals: microscopic characterization. Scandem 2017. 5-9 June, 2017, Reykjavik, Iceland. Comunicación oral.

- **Ruiz-Fresneda M.A.***; Gómez-Bolívar J.; Sánchez-Castro I.; Cherkouk A.; Moll H. and Merroun M.L. The speciation of selenium and europium associated with bacteria isolated from Spanish bentonites. 2017 MIND Project Annual Meeting. 3-5 May, 2017, Prague, Czech Republic. Comunicación oral.

- Martínez-Moreno M.F.*; **Ruiz-Fresneda M.A.** and Merroun M.L. Morphological and structural characterization of selenium nanoparticles produced biologically by the bacterial strain *Stenotrophomonas bentonitica* BII-R7. IV Workshop de Jóvenes Biotecnólogos. 3-4 April, 2017, Granada, Spain. Comunicación oral.

- Delgado-Martín J.*; Fernandez-Cantos M.V.*; **Ruiz-Fresneda M.A.** and Merroun M.L. Tolerance to Se^{IV} and Se^{VI} by the bacterial strain *Stenotrophomonas bentonitica* BII-R7. IV Workshop de Jóvenes Biotecnólogos. 3-4 April, 2017, Granada, Spain. Póster.

- **Ruiz-Fresneda, M.A.***; Gómez-Bolívar, J.; Sánchez-Castro, I. and Merroun, M.L. Enzymatic reduction of Se^{IV} by *Stenotrophomonas* sp. BII-R7 under aerobic and anaerobic conditions: multidisciplinary approach study. 10thInternational BioMetals Symposium. 10-15 July, 2016, Dresden, Germany. Comunicación oral.

- **Ruiz-Fresneda, M.A.**; Gómez-Bolívar, J.*; Sánchez-Castro, I. and Merroun, M.L. Reduction of Se^{IV} by *Stenotrophomonas* sp. BII-R7 isolated from Spanish bentonites: microscopic and spectroscopic characterization. Geomicrobiology Network, Research in Progress Meeting. 13-14 June, 2016, Bangor, UK. Póster.

- Martínez-Rodríguez, P.*; Sánchez-Castro, I.; López-Fernández, M.; **Ruiz-Fresneda, M.A.**; Gómez-Bolívar, J.; Jroundi, F. and Merroun, M.L. Aislamiento y caracterización de cepas bacterianas con potencial em estrategias de biorremediación y otras aplicaciones biotecnológicas. XVI Reunión Del Grupo Especializado em Taxonomía y Filogenia de la Sociedad Española de Microbiología. 8-10 June, 2016, Santiago de Compostela, Spain. Comunicación oral.

- **Ruiz-Fresneda, M.A.***; Gómez-Bolívar, J.; Sánchez-Castro, I. and Merroun, M.L. Study of the interactions of Se^{IV} and the bacterial strain *Stenotrophomonas* sp. BII-R7 for deep geological storage purposes. III Workshop de Jóvenes Biotecnólogos. 9-10 May, 2016, Granada, Spain. Comunicación oral.

- **Ruiz-Fresneda, M.A.***; Gómez-Bolívar, J.; Sánchez-Castro, I. and Merroun, M.L. Anaerobic reduction of Se^{IV} by bacterial strain isolated from Spanish bentonites. 2016 MIND Project Annual Meeting. 2-4 May, 2016, Granada, Spain. Comunicación oral.

- **Ruiz-Fresneda, M.A.***; Sánchez-Castro, I. and Merroun, M.L. Fabrication and molecular scale characterization of selenium nanoparticles produced by *Stenotrophomonas* sp. BII-R7. NanoSpain2016 Conference. 15-18 March, 2016, Logroño, Spain. Comunicación oral.

- Sánchez-Castro, I.*; López-Fernández, M.; **Ruiz-Fresneda, M.A.**; Bakkali, M.; Guenther, A.; Solari, P.L. and Merroun, M.L. Biomineralization of Se and U by the bacterial strain *Stenotrophomonas* sp. BII-R7: microscopic, spectroscopic and genomic characterization. GMDM 2015 Workshop On Mineral Reactivity And Biomineralization Processes. 25 November, 2015, Granada, Spain. Comunicación oral.

- **Ruiz-Fresneda, M.A.***; Sánchez-Castro, I.; Merroun, M.L. Spectroscopic and microscopic characterization of selenium nanoparticles produced by *Stenotrophomonas* sp. BII-R7. Focused Meeting 2015: Industrial Applications Of Metal-Microbe Interactions. 9-10 November, 2015, London, UK. Póster.

- López-Fernández, M.; Sánchez-Castro, I.*****; Bakkali, M.; **Ruiz-Fresneda, M.A.**; Guenther, A.; Solari, P.L. and Merroun, M.L. Linking genomic structure of *Stenotrophomonas* sp. BII-R7 and its potential for bioremediation purposes. 2015 Goldschmidt International Conference. 16-21 August, 2015, Prague, Czech Republic. Comunicación oral.

***** Conferenciante

3) Premios y otros reconocimientos obtenidos durante esta Tesis Doctoral por los resultados presentados en congresos a nivel nacional e internacional:

- Premio CARL ZEISS por la excelente comunicación oral presentada durante el Congreso Internacional "*10th International BioMetals Symposium 2016*" celebrado en Dresden (Alemania) del 10 al 15 de Julio de 2016, bajo el título "*Reduction of Se^{IV} by Stenotrophomonas sp. BII-R7 under aerobic and anaerobic conditions: multidisciplinary approach study*".

- Reconocimiento por parte del Presidente del Consejo Social de la Universidad de Granada con motivo de la concesión del Premio CARL ZEISS arriba mencionado.

El doctorando/The doctoral candidate **Miguel Ángel Ruiz Fresneda** y el director de la tesis/and the thesis supervisor **Mohamed Larbi Merroun**:

Garantizamos, al firmar esta tesis doctoral, que el trabajo ha sido realizado por el doctorando bajo la dirección de los directores de la tesis y hasta donde nuestro conocimiento alcanza, en la realización del trabajo, se han respetado los derechos de otros autores a ser citados, cuando se han utilizado sus resultados o publicaciones.

/

Guarantee, by signing this doctoral thesis, that the work has been done by the doctoral candidate under the direction of the thesis supervisors and, as far as our knowledge reaches, in the performance of the work, the rights of other authors to be cited (when their results or publications have been used) have been respected.

Lugar y fecha / Place and date:

Director de la Tesis / Thesis supervisor

Doctorando / Doctoral candidate

Firma / Signed

Firma / Signed

“Daría todo lo que sé por la mitad de lo que ignoro”

(René Descartes)

RELACIÓN DE ACRÓNIMOS

AGP: Almacenamiento Geológico Profundo

ANDRA: Agence Nationale pour la gestión des Déchets Radioactifs

ANI: Average Nucleotide Identity

ATR-FTIR: Attenuated Total Reflection-Fourier Transform Infrared

BSA: Bovine Serum Albumin

CMI: Concentración Mínima Inhibitoria

dDDH: Digital DNA-DNA hybridizations

DGR: Deep Geological Repository

$DiOC_6$: 3,3'-dihexyloxacarbocyanine iodide

EBR-I: Experimental Breeder Reactor I

ED: Electron Diffraction

EDX: Energy Dispersive X-ray

EPS: Extracellular Polymeric Substance

ESEM: Environmental scanning electron microscopy

EW: Exempt Waste

EXAFS: X-ray Absorption Fine Structure

FDA: Fluorescein Diacetate

FEG-ESEM: Field Emission Gun Environmental Scanning Electron Microscopy

FFT: Fast Fourier Transform

FT: Fourier Transform

FTIR: Fourier Transform Infrared Spectroscopy

GC-MS: Gas Chromatography - Mass Spectrometry

GGDC: Genome-to-Genome Distance Calculation

HAADF-STEM: High Angle Annular Dark Field Scanning Transmission Electron Microscopy

HLRW: High-Level Radioactive Waste

HLW: High Level Waste

HPLC: High-Performance Liquid Chromatography

HRSTEM: High-Resolution Scanning Transmission Electron Microscopy

IAEA: International Atomic Energy Agency

ICP-MS: Inductively Coupled Plasm-Mass Spectometry

ILW: Intermediate Level Waste

ISA: Isosaccharinic acid/Ácido isosacarínico

LB: Luria-Bertani

LLW: Low Level Waste

LTPs: all species Living Tree Project

MIC: Minimal Inhibitory Concentration

NB: Nutrient Broth

NEA: Nuclear Energy Agency

OMV: Outer Membrane Vesicle

PI: Propidium Iodide

SAED: Selected-Area Electron Diffraction

STEM: Scanning-Transmission Electron Microscopy

TOC: Total Organic Carbon

TRLFS: Time-Resolved Laser-induced Fluorescence Spectroscopy

VLLW: Very Low Level Waste

VP-FESEM: Variable Pressure Field Emission Scanning Electron Microscopy

VSLW: Very Short-Lived Waste

XANES: X-ray Absorption Near-Edge Structure

XAS: X-ray Absorption Spectroscopy

XPS: X-ray Photoelectron Spectroscopy

XRD: X-ray Diffraction

ÍNDICE

RESUMEN

La cada vez mayor producción de residuos radiactivos debido al extenso uso de energía nuclear se está convirtiendo, en la actualidad, en un problema ambiental a escala global para el medio ambiente debido a sus graves riesgos asociados. Es bien sabido que estos residuos altamente peligrosos contienen materiales contaminados con radionúclidos, que deben ser almacenados durante largos periodos de tiempo hasta que su radiotoxicidad disminuya hasta niveles naturales. Por esta razón, la implementación de los almacenamientos geológicos profundos (AGPs) ha sido considerada por muchos países para su depósito seguro en un futuro próximo. Este sistema está basado en la encapsulación de residuos radiactivos en contenedores de acero, hierro o cemento, que serán depositados bajo tierra a una profundidad de 500-1000 m. Además, estos contenedores estarán rodeados por barreras naturales (roca hospedante) y de ingeniería (materiales de arcilla, cemento, etc.) para su protección mecánica, hidráulica y térmica. De hecho, las formaciones arcillosas jugarán un papel crucial en muchos diseños de AGP tanto como roca hospedante y como barrera de ingeniería en países como Francia, Bélgica y Suiza. Concretamente en España, arcillas de bentonita del Parque Natural de Cabo de Gata (Almería) se han seleccionado como material de referencia para barreras de ingeniería, debido a sus excelentes propiedades físicas y geoquímicas.

Una amplia distribución de microorganismos se ha descrito previamente en numerosos materiales seleccionados para su uso como barrera en los AGPs, incluyendo formaciones bentoníticas. Muchos estudios han evidenciado el papel que los procesos microbianos pueden tener sobre la corrosión metálica de contenedores, la transformación de minerales, la producción de gases y la movilidad de los radionúclidos presentes en los residuos radiactivos, entre otras cosas. Como consecuencia de ello, los microorganismos podrían afectar la seguridad de los sistemas de AGP. Diversos mecanismos microbianos como biotransformación, biosorción, biomineralización y bioacumulación se han descrito con anterioridad por su involucración en la interacción con radionúclidos, probablemente afectando su movilización a través de estos almacenamientos. Entre los radionúclidos presentes en los residuos radiactivos, el selenio (Se) y el curio (Cm) son de gran interés. El Se es un componente común del combustible nuclear gastado, existente en los residuos radiactivos principalmente en forma del isótopo ^{79}Se (3.7 x 10^5 años de vida media). Este elemento puede existir en la naturaleza en diferentes estados de oxidación: +VI, +IV, 0, y –II. El selenito (Se^{IV}) y el selenato (Se^{VI}) son las formas más solubles y tóxicas, mientras que el Se elemental (Se^0) y el seleniuro (Se^{-II}) son básicamente insolubles. Por otro lado, el Cm es un elemento altamente radiotóxico también presente en el combustible nuclear gastado, principalmente en forma de los isótopos ^{247}Cm and ^{248}Cm. Las excelentes

propiedades luminiscentes de este elemento, como representante de actínidos trivalentes (An^{III}), son idóneas para el estudio de su especiación química a concentraciones relevantes para el medio ambiente. De la misma manera, el europio (Eu), análogo inactivo de An^{III}, también presenta excelentes propiedades luminiscentes. Debido a su inactividad, el Eu es un elemento ideal para estudios de especiación sobre An^{III}.

El principal objetivo de esta Tesis Doctoral consistió en estudiar el papel de la cepa bacteriana aislada de bentonitas, *Stenotrophomonas bentonitica,* sobre la especiación y movilización de Se, Cm y Eu simulando las condiciones de los sistemas de AGP (aerobiosis, anaerobiosis y alcalinidad) con el objetivo de evaluar su impacto sobre la seguridad de los mismos. Para este fin, se empleó una metodología multidisciplinar combinando técnicas espectroscópicas, microscópicas y microbiológicas. Se estima que unas condiciones aerobias dominarán los AGPs después de su cierre, ya que el oxígeno se introducirá durante su construcción y periodos operacionales. Posteriormente, se establecerá un ambiente anóxico. Además, condiciones alcalinas (~pH 10-12) dominarán en aquellos almacenamientos que utilicen materiales cementosos como referencia.

En primer lugar, la cepa de estudio, previamente aislada de formaciones bentoníticas españolas durante estudios de diversidad dependientes de cultivo, se analizó a nivel molecular y fenotípico. Los análisis indicaron claramente que este aislado representa una nueva especie dentro del género *Stenotrophomonas*, para el cual se propuso el nombre *Stenotrophomonas bentonitica*, con BII-$R7^T$ como cepa tipo (= LMG 29893^T = CECT 9180^T = DSM 103927^T). De acuerdo con la literatura revisada, otras especies dentro del género *Stenotrophomonas* muestran una elevada tolerancia a numerosos elementos tóxicos como cadmio, zinc, selenio, cobre, telurio, uranio, etc. En este sentido, el genoma de *S. bentonitica* contiene genes que codifican para enzimas específicas (glutatión reductasa, tiorredoxina reductasa, fosfatasa alcalina, etc.) previamente descritas por su implicación en la tolerancia e inmovilización de elementos peligrosos para el ambiente como el Se y algunos actínidos (ej. uranio). Estos estudios genómicos también revelaron la presencia de genes codificantes para la formación de biopelículas (*flhA, flhB, fliR, fliQ, fliP, fliN, fliM, slp*), que podrían incentivar la inmovilización de estos elementos en el marco de los sistemas de AGP a través de diferentes mecanismos de interacción como la biosorción o la acumulación intracelular.

En segundo lugar, se evaluó el impacto de *S. bentonitica* sobre la especiación química de Se bajo condiciones aerobias. Las células de *S. bentonitica* fueron capaces de reducir Se^{IV} a Se^0 tal y como indicaron los precipitados rojos producidos en los cultivos suplementados con este oxoanión. El contenido total de Se^{IV} fue completamente reducido cuando las células se

cultivaron bajo diferentes concentraciones iniciales. A pesar de que el crecimiento, la viabilidad, y la actividad bacteriana se vieron afectadas negativamente por el Se^{IV}, las células fueron capaces de crecer y mantenerse viables y activas. El Se^{IV} fue reducido a Se^{0} en forma de nanopartículas de Se (SeNPs) con diferentes formas (esférica, hexagonal, poligonal, nanofibras o nanohilos) y propiedades cristalinas (amorfas y trigonales cristalinas), tal y como revelaron los análisis con microscopia (HAADF/STEM-*high angle annular dark field scanning transmission electron microscopy*) y difracción de rayos X (XRD-*X-ray diffraction*). Inicialmente, se sintetizaron nanoesferas de Se amorfo (a-Se) tras 24 h de incubación, las cuáles empezaron a formar agregados tras 48 y 72 h. Finalmente, tras 144 h de incubación, se detectaron SeNPs cristalinas con una estructura trigonal en forma de hexágonos, polígonos y nanofibras. Por lo tanto, se propuso un proceso de transformación dependiente del tiempo desde nanoesferas de a-Se a diferentes nanoestructuras de Se trigonal (t-Se), en el cual la materia orgánica (probablemente correspondiente a proteínas tipo flagelo) asociada a las nanopartículas parece estar involucrada. Posteriores estudios espectroscópicos (ATR-FTIR-*attenuated total reflectance-Fourier transform infrared spectroscopy* y XPS-*X-ray photoelectron spectroscopy*) y microscópicos sobre SeNPs purificadas demostraron la presencia de materia orgánica rica en grupos amino recubriendo las mismas. Estos resultados confirmaron el posible rol de las proteínas en la síntesis y transformación de SeNPs. Sin embargo, estudios adicionales son necesarios para un mejor entendimiento sobre el papel específico de estas envolturas proteicas. La estructura local de las nanoestructuras de Se producidas biológicamente se investigó, además, mediante espectroscopia de absorción de rayos X (XAS-*X-ray absorption spectroscopy*). El análisis mediante XANES (*X-ray absorption near edge region spectroscopy*) confirmó el estado de oxidación 0 de estas nanoestructuras de Se. Por otro lado, el análisis mediante EXAFS (*extended x-ray absorption fine structure*) nos permitió confirmar su estructura tanto amorfa como cristalina. Los mayores valores obtenidos del factor Debye-Waller (σ^2) de la primera esfera de coordinación (Se-Se_1) en la muestra incubada durante 24 h, en comparación con las muestras de 72 y 144 h, indicaron un aumento en el orden estructural conforme aumenta el tiempo de incubación. Estos resultados apoyaron el proceso de transformación y cristalización previamente sugerido a partir de los resultados obtenidos mediante microscopia y espectroscopia. Finalmente, la detección de compuestos volátiles metilados de Se como DMDSe (*dimethyl diselenide*) y DMDSeS (*dimethyl selenenyl sulphide*) producidos por las células de *S. bentonitica*, evidenció la implicación del proceso de volatilización como mecanismo de interacción. Este hecho, también confirmó la habilidad de las células para reducir Se^{IV} a especies metiladas de menor toxicidad en un estado de oxidación –II.

La reducción biológica de Se^{IV} se estudió también bajo condiciones anaeróbicas y alcalinas simulando las esperadas en los AGPs. A diferencia de los experimentos en aerobiosis descritos

anteriormente, bajo estas condiciones más desfavorables se detectó la ausencia de crecimiento microbiano y una menor viabilidad y actividad metabólica. Sin embargo, las células de *S. bentonitica* mostraron su capacidad para reducir Se^{IV} anaeróbicamente desde pH neutro hasta alcalino (pH 7-10) tal y como indicaron los precipitados rojos observados. De forma similar a los resultados obtenidos en condiciones aerobias, los productos de Se procedentes de este proceso de reducción se acumularon en forma de diferentes SeNPs rodeadas por materia orgánica y proteínas tipo flagelo. La presencia de nanoestructuras de t-Se, además de otras fases termodinámicas intermedias como a-Se y Se monoclínico (m-Se), confirmaron un proceso de transformación similar al descrito anteriormente bajo condiciones aerobias. Sin embargo, la menor cantidad de nanoestructuras de t-Se encontradas bajo condiciones anaerobias y alcalinas, sugirieron un mecanismo de transformación de mayor lentitud, probablemente provocado por este ambiente de mayor estrés. Los bajos niveles de crecimiento, actividad y viabilidad parecen afectar al proceso de reducción y al de transformación hacia cristales de Se.

En definitiva, el estudio de las interacciones moleculares con Se bajo condiciones aerobias, anaerobias y alcalinas demostraron el impacto sustancial de los procesos microbianos llevados a cabo por *S. bentonitica* sobre la especiación y movilidad del Se. El Se producido en forma de cristales de Se^0 y de compuestos metilados como resultado de un proceso de reducción, podrían tener un papel beneficioso en la seguridad de los sistemas de AGP debido a su conocida menor movilidad y toxicidad, respectivamente.

Finalmente, se analizaron tanto aeróbica como anaeróbicamente las interacciones moleculares de Cm^{III} y Eu^{III} con *S. bentonitica*. Un gran número de técnicas incluyendo espectroscopia, microscopia, y titulaciones potenciométricas se emplearon para llevar a cabo un estudio más completo y exhaustivo. Las titulaciones potenciométricas proporcionaron datos cuantitativos sobre los tipos y concentraciones de los grupos funcionales de la superficie celular implicados en la unión de Eu^{III}. Según esta técnica, los grupos fosfato podrían actuar como el principal sitio de unión para la interacción. Los resultados de espectroscopia infrarroja (ATR-FTIR) concordaron con la implicación de los grupos fosfato y sugirieron, además, que los grupos carboxilo podrían formar complejos puente de unión con el Eu^{III}. Los análisis realizados con espectroscopia de fotoelectrones emitidos por rayos X (XPS) también sugirieron que los grupos carboxilos presentes en determinados ácidos orgánicos, como el acetato, podrían participar en la interacción con el Eu^{III}. Adicionalmente, la espectroscopia de fluorescencia (TRLFS-*time-resolved laser-induced fluorescence spectroscopy*) confirmó la participación de los grupos carboxilo y fosforilo en la acomplejación de Cm^{III}/Eu^{III} al comparar los parámetros de luminiscencia obtenidos con la bibliografía publicada. Por último, los análisis de microscopia mostraron que *S. bentonitica* interacciona con Eu^{III} principalmente a través de un proceso de

biosorción sobre la superficie celular. Sin embargo, la presencia de precipitados de Eu^{III} intra- y extracelulares indicó que otros mecanismos como la bioacumulación o la bioprecipitación podrían estar involucrados en dicha interacción. De hecho, los estudios cinéticos apoyaron claramente el posible rol de más de un mecanismo de interacción. En definitiva, los estudios moleculares sobre las interacciones con Eu^{III}/Cm^{III} bajo condiciones aeróbicas y anaeróbicas demostraron la influencia de los procesos microbianos llevados a cabo por *S. bentonitica* en la movilidad de Eu^{III} y Cm^{III}. Los resultados obtenidos proponen que *S. bentonitica* juega un papel importante en la inmovilización de An^{III} a través de su biosorción y su potencial habilidad para formar biopelículas dentro de los sistemas de AGP. Además, la más que probable bioprecipitación de An^{III} por las células podría también dar lugar a su inmovilización. Sin embargo, la poca cantidad de precipitados de Eu^{III} intracelulares encontrados, descartó la acumulación intracelular como un mecanismo con un impacto significativo en los repositorios. En cualquier caso, más estudios y evidencias son necesarios para elucidar el rol específico de *S. bentonitica* sobre la seguridad de los futuros almacenamientos geológicos de residuos radiactivos.

El estudio de las interacciones microbianas con radionúclidos será de gran utilidad para la predicción del impacto microbiano sobre el funcionamiento y seguridad de los almacenamientos de residuos radiactivos, así como en el desarrollo de estrategias apropiadas de biorremediación y en la fabricación ecológica de nanopartículas con un gran potencial en numerosas aplicaciones industriales y médicas.

SUMMARY

Nowadays, the increasing generation of radioactive waste due to the extensive use of the nuclear industry is becoming a global environmental concern for the environment due to their serious associated risks. It is well known that these extremely hazardous residues contain materials contaminated with radionuclides, which must be stored for a long period of time until their radiotoxicity decrease to natural levels. For this purpose, the implementation of the deep geological repositories (DGRs) has been considered by many countries for their safely disposal in the near future. This system is based on the encapsulation of radioactive wastes in steel, iron or concrete containers that will be placed underground at a depth of 500-1000 m. In addition, the containers will be surrounded by natural (host rocks) and engineered barriers (bentonite, cementitious materials, etc.) for their mechanical, hydraulic, and thermal protection. Indeed, the clay formations will play a crucial role in many DGR design as host rock and engineered-barrier in countries such as France, Belgium, and Switzerland. Specifically, in Spain, bentonite clays from Cabo de Gata (Almería) have been selected as a reference material for engineered barriers because of their well characterized physical and geochemical properties.

A widely distribution of microorganisms has been previously reported in many materials selected for their use as barrier for DGR, including bentonite formations. Many studies have evidenced the role that microbial processes may play on the metal corrosion of containers, transformation of clay minerals, gas production, and mobility of radionuclides present in radioactive wastes, among others. As a consequence, microorganisms could affect the safety of the DGR system. Several microbial mechanisms such as biotransformation, biosorption, biomineralization, and bioaccumulation have been previously described to be involved in the radionuclide interaction, probably affecting their migration behavior through the disposal. Among the radionuclides present in radioactive waste, selenium (Se) and curium (Cm) are of great interest. Se is a common component of the spent nuclear fuel present in radioactive waste mainly as ^{79}Se isotope (half life 3.7 x 10^5 years). This element can exist in nature in different oxidation states: +VI, +IV, 0, and –II. Selenite (Se^{IV}) and selenate (Se^{VI}) are the more soluble and toxic forms, while elemental Se (Se^0) and selenide (Se^{-II}) are basically insoluble. On the other hand, Cm is a highly radiotoxic element also present in nuclear spent fuel mainly as ^{247}Cm and ^{248}Cm isotopes. The excellent luminescence properties of this element, as a representative of trivalent actinides (An^{III}), are suitable for the study of their chemical speciation at environmentally relevant concentration**.** In the same way, europium (Eu), an inactive analogue of An^{III}, also provide excellent luminescence properties. This inactivity makes Eu an optimal element for speciation studies about An^{III}.

The main objective of this Doctoral Thesis is to study the role of the bentonite-isolated bacterium *Stenotrophomonas bentonitica* on the speciation and migration behaviour of Se, Cm, and Eu simulating geodisposal conditions (aerobic, anaerobic, alkaline) with the aim of evaluating its impact on the safety of the DGR system. For this purpose, a multidisciplinary approach combining spectroscopic, microscopic, and microbiological techniques was employed. Aerobic conditions are expected to dominate the DGRs after closure since oxygen will enter during the construction and operational periods. After that, anoxic conditions will be established. In addition, alkaline conditions (~ pH 10-12) will dominate in those disposal that use cementitious materials as reference.

Firstly, the bacterial strain of study, previously isolated from Spanish bentonite formations during a culture-dependent microbial diversity study, was analysed at molecular and phenotypic level. These analyses clearly indicated that the isolate represents a novel species within the genus *Stenotrophomonas*, for which the name *Stenotrophomonas bentonitica* sp. nov. was proposed with BII-R7^T as the type strain (= LMG 29893^T = CECT 9180^T = DSM 103927^T). According to the literature reviewed, other species within the genus *Stenotrophomonas* show high tolerance to numerous toxic elements such as cadmium, zinc, selenium, copper, tellurium, uranium etc. In this sense, the genome of *S. bentonitica* contains genes coding for specific enzymes (glutathione reductase, thioredoxin reductase, alkaline phosphatase, etc.), previously described for their involvement in tolerating and immobilizing environmentally hazardous elements such as Se and some actinides (e.g. uranium). These genomic studies also revealed the presence of genes coding for proteins involved in the formation of biofilms (*flhA, flhB, fliR, fliQ, fliP, fliN, fliM, slp*), which could enhance the immobilization of these elements within the DGR system through different interaction mechanisms such as biosorption or intracellular accumulation.

Secondly, the impact of *S. bentonitica* on the chemical speciation of Se under aerobic conditions was evaluated. *S. bentonitica* cells are able to reduce Se^{IV} to Se^0 as indicated by the red precipitates produced in the cultures supplemented with this oxyanion. The total Se^{IV} content was completely reduced when the cells were grown under different initial concentrations, indicating the high efficiency of the cells reducing Se^{IV}. Despite the bacterial growth, viability, and activity was negatively affected by Se^{IV}, the cells were able to grow and maintain both viability and activity. Se^{IV} was reduced to Se^0 in form of nanoparticles with different shapes (spherical, hexagonal, polygonal and nanowires) and crystallographic properties (amorphous and trigonal) as by revealed microscopy (HAADF/STEM-high-angle annular dark field scanning transmission electron microscopy) and X-ray diffraction (XRD). Amorphous Se (a-Se) nanospheres were initially synthesized after 24 h of incubation and then, they started to form

aggregates after 48 to 72 h. After 144 h, crystalline selenium nanoparticles (SeNPs) with trigonal structure in form of hexagons, polygons and nanowires were also detected. A time-dependent transformation process from a-Se nanospheres to different trigonal Se (t-Se) nanostructures was proposed, in which organic matter (probably corresponding to flagella-like proteins) attached to the nanoparticles seems to be involved. Further spectroscopic (ATR-FTIR-attenuated total reflectance-Fourier transform infrared spectroscopy and XPS-X-ray photoelectron spectroscopy) and microscopic studies of the purified SeNPs demonstrated the presence of amine rich organic matter coating them. These results confirmed the possible role of proteins in the synthesis and transformation of SeNPs. However, additional studies are needed to better understand the specific role of protein coating. The local structure of the bioproduced Se nanostructures was further investigated by X-ray absorption spectroscopy (XAS). X-ray absorption near edge region spectroscopy (XANES) confirmed the zero-valent oxidation state of these Se nanostructures. In addition, extended x-ray absorption fine structure (EXAFS) confirmed their amorphous and crystalline structure. The higher Debye-Waller factor (σ^2) values of Se-Se_1 shell in the sample incubated for 24 h comparing with 72 and 144 h samples, indicated an increase in the structural order with the incubation time. These results would support the transformation and crystallization process previously suggested by microscopic and spectroscopic techniques. Finally, the detection of volatile methylated Se species such as dimethyl diselenide (DMDSe) and dimethyl selenenyl sulphide (DMDSeS) produced by *S. bentonitica* cells pointed out the involvement of volatilization as interaction mechanism. This fact also confirmed the ability of the cells to reduce Se^{IV} to the less toxic methylated species in the -II oxidation state.

The biological reduction of Se^{IV} was also studied under anaerobic and alkaline conditions simulating those expected in DGRs. In contrast to aerobic experiments mentioned above, no cell growth and a lower viability and activity were detected under these more stressful conditions. However, the cells of *S. bentonitica* showed their capacity to reduce Se^{IV} anaerobically from neutral to alkaline pH (pH 7-10) as indicated by the observed red precipitates. Similarly to the results obtained aerobically, the Se products derived from the reduction process were accumulated in form of different SeNPs surrounded by organic matter and flagella-like proteins. The presence of t-Se nanostructures in addition to other intermediate thermodynamic phases such as a-Se and monoclinic Se (m-Se) confirmed a similar transformation process as previously described under aerobic conditions. However, the lower amount of t-Se nanostructures observed under anaerobic and alkaline conditions suggested a slower transformation mechanism probably influenced by this stressful environment. The low levels of cell proliferation, activity, and viability seem to affect the reduction and transformation to Se crystals.

Definitely, the study of the molecular interactions with Se under aerobic, anaerobic, and alkaline conditions demonstrated the substantial impact of microbial processes derived from *S. bentonitica* on Se speciation and mobility. The Se produced in form of Se^0 crystals and methylated compounds as a result of the reduction process may play an important beneficial role on the safety of the geodisposal system due to their well-documented lower mobility and toxicity, respectively.

Finally, the molecular interactions of Cm^{III} and Eu^{III} with *S. bentonitica* were analysed both aerobically and anaerobically. A large number of techniques including spectroscopy, microscopy, and potentiometric titrations were employed to provide a more comprehensive and complete study. Potentiometric titrations provided quantitative data about the type and concentration of functional groups from the cell surfaces involved in the Eu^{III} coordination. According to this technique, phosphate groups could serve as the main binding site involved on the interaction. ATR-FTIR results agreed with the implication of phosphate groups and also suggested that carboxyl groups could form bidentate bridging complexes with Eu^{III}. XPS analysis also suggested carboxyl groups from organic acids such as acetate to participate in the Eu^{III} complexation. Additionally, TRLFS (time-resolved laser-induced fluorescence spectroscopy) confirmed the phosphoryl and carboxyl groups to be involved in the Cm^{III}/Eu^{III} complexation by comparing the luminescence parameters obtained with the published literature. Finally, microscopic analyses showed that *S. bentonitica* mainly interact with Eu^{III} by a biosorption process on the cell surface. However, the presence of intracellular and extracellular Eu^{III} precipitates pointed out that other mechanisms such as bioaccumulation or bioprecipitation could be implicated in the interaction. Indeed, kinetic studies clearly supported the possible role of more than one mechanism. Definitely, the study of the molecular interactions with Eu^{III}/Cm^{III} under aerobic and anaerobic conditions demonstrated the influence of microbial processes derived from *S. bentonitica* on Eu^{III}/Cm^{III} mobility. The obtained results proposed *S. bentonitica* to play an important role in the immobilization of An^{III} through their biosorption and the potential ability of the cells to form biofilms within the DGR system. Additionally, the probable bioprecipitation of An^{III} by the cells could also lead to their immobilization. However, the low amount of intracellular Eu^{III} precipitates, discarded bioaccumulation as a mechanism with a significant impact in the repositories. In any case, more studies and evidences are necessary to elucidate the specific role of *S. bentonitica* on the safety of the future repositories of radioactive waste.

Fundamental understanding of the microbial interactions with radionuclides will be useful in predicting the microbial impacts on the performance of the radioactive waste repositories as

well as in developing appropriate bioremediation strategies, and environmentally-friendly fabrication of nanoparticles with potential industrial and medical applications.

INTRODUCCIÓN

1. Radiactividad y sus efectos perjudiciales

La radiactividad es un proceso por el cual determinados elementos químicos emiten radiaciones como consecuencia de la desintegración espontánea de su núcleo atómico. Este fenómeno es característico de isótopos inestables que tienden a descomponerse de forma directa o progresiva en isótopos de mayor estabilidad, a la vez que emiten radiaciones (Porcelli, 2018). Estos isótopos radiactivos, también conocidos por el nombre de radionúclidos, pueden emitir tres tipos de radiaciones ionizantes:

- Radiación alfa (α): consiste en la emisión de partículas compuestas por dos protones y dos neutrones (núcleos de helio) como consecuencia de la desintegración del núcleo atómico. Estas partículas son poco penetrantes y pueden ser detenidas por la ropa, hojas de papel, o la propia piel. Sin embargo, pueden causar daños celulares severos si son ingeridas a través de alimentos o del aire.

- Radiación beta (β): consiste en la emisión de un electrón o un positrón (partícula de igual tamaño y masa que un electrón pero con carga positiva) tras la desintegración del núcleo atómico. Presentan un mayor poder penetrante que las partículas alfa debido a su menor masa, pudiendo incluso penetrar la piel unos pocos centímetros. Sin embargo, su principal peligro reside en la emisión interna a partir de su ingesta.

- Radiación gamma (γ): se trata de ondas electromagnéticas procedentes de un núcleo inestable. Es la radiación de mayor capacidad penetrante al no tener ni masa ni carga eléctrica. Es, por tanto, la más dañina para los seres vivos al poder atravesar completamente el cuerpo humano. Son necesarias capas muy gruesas o densas de materiales de alto número atómico para detenerlas.

Los llamados isótopos radiactivos naturales de vida larga fueron incorporados a rocas y suelos durante la formación de la Tierra, procedentes de la nucleosíntesis estelar (Porcelli, 2018). Estos isótopos no pueden ser formados bajo las condiciones terrestres, por lo que su cantidad y radiactividad están en continuo decrecimiento desde el origen de la Tierra. Sin embargo, la elevada vida media de estos isótopos hace que su radiactividad se mantenga hasta el día de hoy. De hecho, al estar todavía en proceso de desintegración, son muy utilizados en geocronología para la determinación de la edad de los diferentes acontecimientos geológicos ocurridos a lo

largo de la historia. Otro tipo de isótopos naturales son los formados en la atmósfera por reacciones nucleares de rayos cósmicos con los átomos presentes en la misma (Kónya y Nagy, 2018). Sin embargo, en la actualidad, son más numerosos en la naturaleza los isótopos radiactivos creados artificialmente. Estos radioisótopos artificiales proceden principalmente de las actividades de la industria nuclear, así como de residuos de laboratorios de investigación, nucleares, médicos, e industriales. Algunos existentes en residuos nucleares como el ^{79}Se, el ^{95}Zr, o el ^{109}Pd presentan una reactividad no muy elevada, pero debido a su elevada vida media deben ser almacenados de forma segura (Kónya y Nagy, 2018).

La contaminación radiactiva de los ambientes naturales puede tener efectos perjudiciales para los seres vivos dependiendo de numerosos factores, tales como el tejido afectado, el tipo de radiación, la dosis recibida, etc. Básicamente, el principal efecto de la radiactividad en los seres vivos consiste en la radiólisis del agua, principal componente de los sistemas biológicos, que conduce a la generación de radicales libres. La formación de radicales libres es debida al carácter ionizante de las radiaciones emitidas, que por su elevada energía son capaces de extraer electrones ligados a los átomos con los que interaccionan. Como bien es sabido, los radicales libres pueden provocar cambios estructurales en biomoléculas, impidiendo así que lleven a cabo su función biológica. El ejemplo más claro lo encontramos en las moléculas de ADN, en las que daños irreversibles en su estructura química pueden dar lugar a diferentes tipos de cáncer. El uso de materiales de construcción (granitos, esquistos, etc.) enriquecidos con isótopos radiactivos puede aumentar la dosis de radiación en las inmediaciones de construcciones y edificios, teniendo efectos nocivos para el ser humano. Por ejemplo, el isótopo radiactivo ^{222}Rn, procedente de la serie de desintegración del ^{238}U, es un gas móvil e inerte que puede escapar de rocas y suelos y acumularse dentro de los edificios (Porcelli, 2018). Uno de los principales problemas derivados de esta exposición radiactiva es la acumulación de radionúclidos en el organismo al inhalar aires o ingerir alimentos contaminados con los mismos y su inclusión en la cadena trófica.

Del mismo modo, la presencia de radioisótopos en la naturaleza puede causar problemas ambientales de gran preocupación para la sociedad. Uno de los principales riesgos ambientales y humanos asociados al uso de radioisótopos provienen de los accidentes en reactores nucleares, así como de la gestión de residuos radiactivos (Zhang et al., 2019). La posible liberación al entorno de radionúclidos procedentes de actividades nucleares pueden ocasionar problemas ambientales y sociales de gran calibre (Prăvălie y Bandoc, 2018). Desde el año 1950, aproximadamente unos 20 accidentes nucleares han tenido lugar en todo el mundo hasta el día de hoy (Burns, 2012; Lelieveld et al., 2012). De todos ellos, el conocido como mayor desastre nuclear de la historia, fue el ocurrido en Chernóbil (Ucrania) el 26 de Abril del año 1986 (Figura

1). Este accidente produjo la mayor liberación de material radiactivo al medio ambiente hasta la fecha (Burns, 2012; UNSCEAR, 2013). Entre los radionúclidos liberados, caben destacar por su peligrosidad los radionúclidos ^{137}Cs y ^{131}I.

Figura 1. Accidente nuclear ocurrido en el reactor 4 de la planta nuclear de Chernóbil (Ucrania) el 26 de Abril del año 1986 (http://time.com/4306694/chernobly-30-american-physicist/).

En definitiva, tanto los radioisótopos naturales como artificiales se encuentran distribuidos por toda la naturaleza (atmósfera, hidrosfera, litosfera), siendo un riesgo para la salud de todos los organismos vivos y para la sostenibilidad del medio ambiente. Sin embargo, son aquellos producidos artificialmente como consecuencia de actividades nucleares, los que en la actualidad suponen un mayor riesgo. Por ello, el estudio y evaluación para la mejora de la seguridad nuclear y de la gestión y almacenamiento de residuos radiactivos, deben ser primordiales para garantizar el bienestar de los seres vivos y del ambiente que les rodea.

2. Energía nuclear y producción de residuos radiactivos

La demanda de energía a escala global está aumentando considerablemente en la actualidad debido al elevado crecimiento demográfico y al incremento de las actividades industriales. La naturaleza no renovable de los combustibles fósiles, principal fuente de energía mundial hoy en día, junto con las conocidas limitaciones de las energías renovables, hacen primordial la búsqueda de nuevas alternativas como la energía nuclear.

El uso de la energía nuclear empezó en la década de 1950, cuando el primer reactor, el Experimental Breeder Reactor I (EBR-I) (Figura 2), fue construido en Estados Unidos. Entre los

años 1970 y 1985 se produjo un importante desarrollo global de la tecnología nuclear, pasando de 70 reactores nucleares a principios de 1970, a unos 360 en 1985. Posteriormente, tuvo lugar un pequeño retroceso en el desarrollo nuclear debido a algunos acontecimientos que tuvieron una gran repercusión mediática, como son, el accidente nuclear de Chernóbil y el aumento de interés en el petróleo por las grandes economías mundiales debido a su reducción de precios a partir de 1980 (Albino et al., 2014). Estos sucesos tuvieron un gran impacto en la sociedad acerca del uso de esta tecnología. De hecho, algunos países declararon el no uso de la energía nuclear. A pesar de ello, otros países como Japón, India o China continuaron con sus proyectos, los cuales se mantienen hasta el día de hoy. En la actualidad, la energía nuclear se encuentra en expansión en todo el mundo debido, en gran medida, a las fuertes inversiones en la construcción de reactores, al aumento del precio de los combustibles fósiles y a la creciente preocupación por el cambio climático (Prăvălie y Bandoc, 2018).

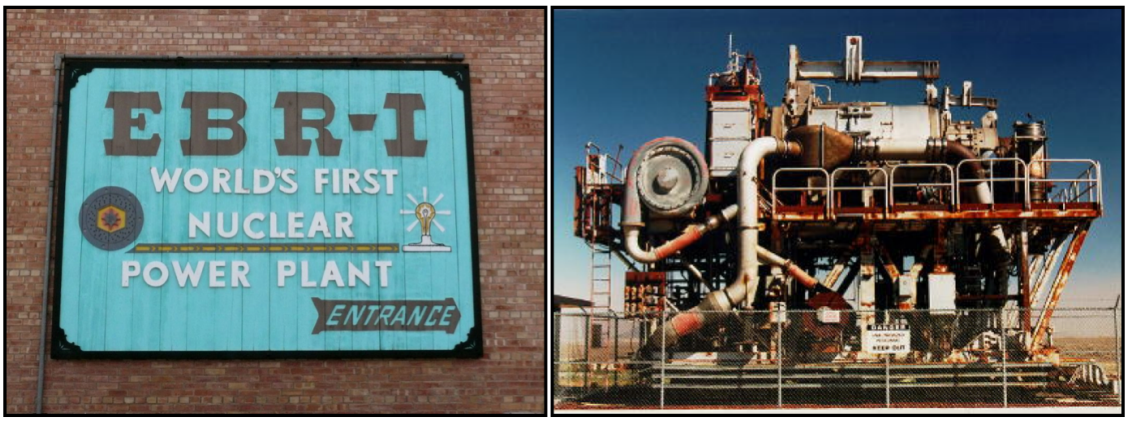

Figura 2. Instalaciones del Reactor Experimental Breeder (EBR-I), la primera planta de energía nuclear experimental del mundo (https://www.smithsonianmag.com/travel/tour-worlds-first-nuclear-power-plant-idaho-180956006/) (http://expdvl.com/internet/TRAVEL/WWWOZ~1.NET/~CHRISP/EBR.HTM).

Desde el punto de vista económico, la energía nuclear es una importante fuente de ingresos en numerosos países, al ser una de las principales fuentes de energía. Se estima que cubre el 11 % de la producción total de electricidad en todo el mundo (IAEA, 2015). Sin embargo, el uso de combustibles fósiles como fuente de energía es todavía dominante e incluso se estima que cubrirá hasta un 50% de la energía global hasta el año 2050 (Don MacElroy, 2016). El dominio de los combustibles fósiles en este sector en los últimos 50 años ha provocado la emisión de cantidades descomunales de carbono a la atmósfera, causando la aceleración del cambio climático (Ballantyne et al., 2012). Se calcula que unas 350 billones de toneladas de carbono se han emitido entre 1959 y 2010 (Ballantyne et al., 2012). El uso de la energía nuclear podría ser una oportunidad para combatir el calentamiento global, uno de los problemas medioambientales más serios al que nos enfrentamos hoy día en el mundo (Rockström et al., 2009). Los bajos niveles de emisión de carbono liberados por la industria nuclear (NEA, 2015), hacen de ella una

buena opción para la descarbonización del modelo energético global. En concreto, se estima que este tipo de energía ha evitado la liberación de 60 billones de toneladas de dióxido de carbono desde 1970 (IAEA, 2016). Por supuesto, para este fin, se hace necesario el uso simultáneo de otras estrategias que reduzcan la emisión de dióxido de carbono, como la instauración de energías renovables.

A pesar de lo citado anteriormente, el uso de la energía nuclear se encuentra en continua controversia debido a los importantes riesgos asociados que conlleva, como por ejemplo, la contaminación ambiental y la generación de residuos radiactivos contaminados con radionúclidos. El difícil almacenamiento seguro y permanente de los residuos radiactivos generados, supone una amenaza para la sociedad y el medio ambiente. La IAEA (*International Atomic Energy Agency*), junto con otras organizaciones, se encarga de la gestión y regulación de los residuos radiactivos. Según la guía de seguridad de la IAEA (IAEA, 2009a), el sistema de clasificación actual de residuos radiactivos, basado en aspectos de seguridad a largo plazo, contempla 6 tipos de residuos:

- **Desechos exentos** (EW-*Exempt Waste*): contienen concentraciones de radionúclidos tan pequeñas que no están sometidos a las reglas de disposición de protección radiológica.

- **Desechos de periodo muy corto** (VSLW-*Very Short-Lived Waste*): son aquellos que contienen radionúclidos con periodos de semidesintegración muy cortos y cuyas concentraciones de actividad están por encima de las establecidas para los exentos. Estos residuos son almacenados hasta que su actividad se reduce por debajo de estos niveles. Se trata principalmente de radionúclidos procedentes de aplicaciones industriales y médicas. Aunque el límite de los periodos de semidesintegración no se puede establecer, ya que depende de la duración del almacenamiento y de la actividad inicial, este tipo de residuos se suele aplicar a aquellos con radionúclidos con periodos de 100 días aproximadamente.

- **Desechos de actividad muy baja** (VLLW-*Very Low Level Waste*): son desechos con niveles de concentración de actividad cercanos a los niveles especificados para la exención o ligeramente por encima. Se trata de desechos que suelen contener radionúclidos naturales procedentes de la minería. El nivel de seguridad óptimo para estos residuos se puede conseguir mediante su disposición final en instalaciones superficiales, al presentar un riesgo más limitado en comparación con clases de residuos superiores.

- **Desechos de baja actividad** (LLW-*Low Level Waste*): aquellos que contienen una cantidad de material radiactivo que sea necesario su aislamiento y contención durante periodos limitados de hasta algunos cientos de años. Se trata de residuos cuyo contenido de actividad se encuentra justo por encima del nivel establecido para los VLLW.

- **Desechos de actividad intermedia** (ILW-*Intermediate Level Waste*): contienen cantidades de radionúclidos con periodos de semidesintegración largos que requieren un mayor grado de aislamiento de los ecosistemas del que ofrece la disposición en instalaciones superficiales. Para ello, su disposición final se lleva a cabo a una profundidad de entre decenas y varios cientos de metros. Los menores efectos de erosión y la menor probabilidad de intrusión humana otorgan una mayor seguridad a este tipo de disposiciones.

- **Desechos de alta actividad** (HLW-*High Level Waste*): son aquellos residuos que contienen concentraciones tan grandes de radionúclidos que requieren un mayor grado de contención y aislamiento que los ILW para garantizar la seguridad a largo plazo. Para ello, su disposición final geológica se realiza a elevadas profundidades mediante el uso de barreras artificiales. Los HLW generan grandes cantidades de calor como consecuencia de la desintegración radiactiva, que puede durar siglos. Por ello, hay que tener en cuenta la disipación de calor a la hora de diseñar las instalaciones que los contengan. Se trata principalmente de residuos procedentes de la industria nuclear, cuyos niveles de concentración de actividad oscila entre los 10^4-10^6 TBq/m^3. Los HLW son los residuos más peligrosos, ya que son capaces de persistir en el ambiente hasta unos cien mil años (Horvath y Rachlew, 2016). Su producción es alarmante, con más de 12000 toneladas al año (Gerstner, 2009). Actualmente, se estima que aproximadamente unos 250.000 toneladas de HLW necesitan almacenamiento en todo el mundo (World Nuclear Association, www.world-nuclear.org/info/ inf104.html.).

Es importante aclarar que los límites de concentración de actividad radiactiva entre las diferentes clases de residuos no se pueden especificar de forma general, ya que dependen del tipo de instalación, evaluación de seguridad del emplazamiento, tipo de radionúclidos contenidos, parámetros geológicos y técnicos, etc. Es el organismo regulador o las autoridades nacionales los que pueden determinar donde se clasifican los desechos basándose en justificaciones de seguridad genéricas. Por tanto, este sistema de clasificación consiste en una guía de seguridad orientativa internacional sobre como cumplir los requisitos de seguridad.

La elevada generación de estos residuos supone un problema ambiental de primer orden al que hay que encontrar solución. En este sentido, el reprocesamiento del combustible nuclear gastado puede resolver de forma parcial este problema. Según la IAEA en unos de sus informes de 2009 (IAEA, 2009b), unas 5600 toneladas son reprocesadas al año. Sin embargo, es evidente que la cantidad de residuos generados es mucho mayor y, en consecuencia, el problema no puede ser solventado exclusivamente con este método. Es por ello que en los últimos años el consenso político y científico internacional ha declarado que la gestión y disposición más viable de residuos radiactivos consiste en su almacenamiento geológico profundo (AGP) (NEA, 2010).

3. Sistemas de Almacenamiento Geológico Profundo de residuos radiactivos

El concepto de AGP fue acuñado en el año 1995 por el comité de gestión de residuos de la NEA (*Nuclear Energy Agency)* (Vuori, 1995). Los AGPs se basan en el almacenamiento de residuos radiactivos en contenedores situados entre unos 500-1000 metros bajo la superficie mediante un sistema multi-barrera, con el objetivo de aislarlos del medio por cientos de miles de años (Figura 3). Estos sistemas comprenden barreras naturales, como la propia roca hospedante del emplazamiento geológico, y barreras artificiales o de ingeniería, como los contenedores y los materiales de sellamiento (Ma et al., 2018). Arcillas, rocas cristalinas (granitos, rocas metamórficas de alto grado, etc.) y depósitos salinos son las principales formaciones geológicas seleccionadas por sus características físico-químicas como posible barrera natural (Ahonen et al., 2016). Las formaciones arcillosas son una de las principales opciones como roca hospedante en países como Francia, Bélgica y Suiza debido a sus excelentes propiedades, mientras que las formaciones geológicas de granito han sido seleccionadas en países como Finlandia, Suecia, Canadá y República Checa. Por último, Estados Unidos está contemplando el uso de formaciones de sales, que fueron las primeras consideradas para su uso en los almacenamientos de residuos radiactivos (Ahonen et al., 2016). Por otro lado, el material y diseño de las barreras artificiales dependen, entre otras cosas, del tipo de residuos y de la naturaleza de la roca hospedante. Los contenedores pueden ser de metal (hierro o cobre) o de hormigón, mientras que como material de sellamiento se puede usar cemento o arcillas como las bentonitas.

Según recientes estudios los materiales cementosos proporcionarían un ambiente alcalino que prevendría la posible disolución, y por tanto la movilización, de los radionúclidos en aguas subterráneas (Abrahamsen et al., 2015). Además, estos materiales también actuarían como blindaje contra la radiación (Abrahamsen et al., 2015). Se estima que en este tipo de sistemas cementosos el pH varíe a lo largo del tiempo, con un elevado pH inicial superior a 12,5 y su posterior reducción y equilibrio a pH 8-10 con la entrada de aguas subterráneas (Berner, 1992). Por supuesto, otros factores como la radiación, los microorganismos o el tipo de residuos

podrían afectar la fluctuación del pH. Por otra parte, en la mayoría de almacenamientos se prevé que después de un periodo inicial corto en condiciones aerobias, debido a la presencia de oxígeno atrapado durante la construcción, predomine un ambiente reductor y anaerobio. Estas condiciones serán debidas principalmente a la escasez de oxígeno bajo tierra, la disolución de minerales reducidos presentes y la presencia de determinados aceptores y donadores de electrones, entre otras cosas (Duro et al., 2014). Los ambientes reductores son esenciales para evitar la movilidad de numerosos radionúclidos al afectar su especiación química mediante procesos de reducción.

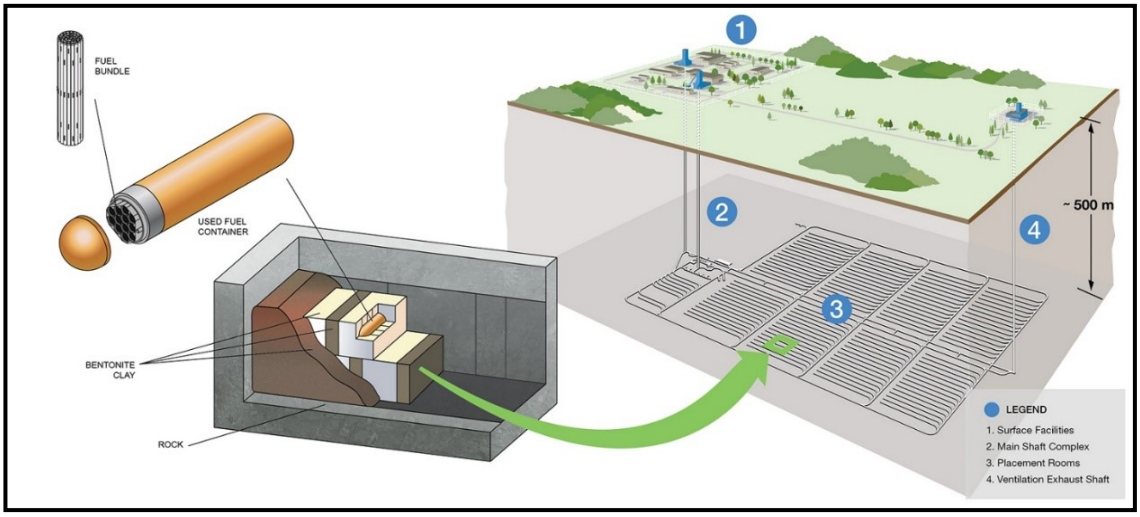

Figura 3. Concepto de almacenamiento geológico profundo según la *Nuclear Waste Management Organization* (NWMO) (http://www.edram.info/index.php?id=218).

En la actualidad, los AGPs son la opción más ampliamente aceptada por la comunidad científica para el almacenamiento final de los residuos radiactivos de alta actividad, así como para los de intermedia actividad de larga vida media. Por otra parte, se tiene previsto que los residuos de actividad baja e intermedia de vida media corta sean depositados en repositorios de superficie o a unos cuantas decenas de metros de profundidad. Muchos países ya han comenzado a planear e incluso construir su propio almacenamiento de residuos radiactivos. China ha anunciado la preselección de un plan nacional de almacenamiento de residuos de alta actividad en zonas geológicas de granito en la provincia de Gansu. Por su parte, Francia, uno de los mayores productores de energía nuclear, está diseñando a través de la agencia ANDRA (*Agence Nationale pour la gestión des Déchets Radioactifs*) un AGP denominado Cigéo, sobre un emplazamiento de rocas arcillosas situado al este del país. El objetivo es almacenar HLW e ILW de larga vida media usando un sistema basado en materiales de cemento, tanto para su encapsulación como para su aislamiento y sellamiento. En países como Suiza, República Checa,

Finlandia, Suecia, Alemania o el Reino Unido también se están planeando AGPs basados en materiales de cemento (IAEA, 2018).

4. Radionúclidos de interés presentes en los residuos radiactivos.

Tal y como ya hemos mencionado, los residuos radiactivos contienen radionúclidos que pueden afectar la seguridad ambiental y humana. Aunque no todos los radionúclidos presentan un impacto significativo en este sentido, si son de relevancia aquellos que por diversos factores como el tipo de radiación emitida, la concentración, o el periodo de semidesintegración, presentan un mayor riesgo en términos de seguridad. El estudio de algunos isótopos radiactivos de selenio (^{79}Se), de actínidos trivalentes (An^{III}) como el curio (^{247}Cm, ^{248}Cm) y el americio (^{242}Am), y de otros actínidos como el neptunio (^{237}Np) o el uranio (^{235}U) es de elevada importancia debido a su radiotoxicidad (Hamed et al., 2017; Kooyman et al., 2018).

El selenio (Se) es un elemento que se encuentra ampliamente distribuido por la naturaleza (ambientes acuáticos, atmosféricos, terrestres, etc.) en diferentes estados de oxidación: selenato (Se^{VI}), selenito (Se^{IV}), selenio elemental (Se^0) y seleniuro (Se^{-II}). Es bien sabido que la solubilidad, y por tanto la movilidad, de un elemento viene determinada en gran medida por su especiación o estado de oxidación, además de otros factores como el pH y el potencial redox (Eh) (Breynaert et al., 2010; Di Gregorio et al., 2005). El Se^{VI} y el Se^{IV}, las formas más solubles y tóxicas, predominan en ambientes oxidantes (Breynaert et al., 2010; Lehto y Hou, 2011). Por el contrario, el Se^0 y los seleniuros metilados son básicamente insolubles (Ranjard et al., 2003) y predominan en ambientes reductores. Los radionúclidos de Se no aparecen en cantidades significativas en la naturaleza. La mayoría de ellos presentan una vida media corta que oscila entre los 20 segundos (para el ^{77m}Se) y 120 días (para el ^{75}Se). El único de potencial interés por su peligrosidad para el medio ambiente y para la seguridad a largo plazo de los almacenamientos de residuos radiactivos es el ^{79}Se, debido a su elevada vida media ($3{,}7 \times 10^5$ años) y movilidad en los ambientes geológicos (Atwood, 2010). El radioisótopo ^{79}Se es un emisor beta producido principalmente por la fisión del ^{235}U y otros radionúclidos como el ^{239}Pu, aunque, en menor medida, también se origina como consecuencia de la activación neutrónica del ^{78}Se presente en los materiales de construcción de los reactores de fisión (Atwood, 2010). Se trata de un componente característico de los HLW y es, sin duda, el principal radionúclido de Se presente en los mismos (Ikonen et al., 2016). Al ser un radionúclido artificial, la única posible fuente de ^{79}Se en la naturaleza sería su liberación a partir de los residuos generados en las centrales nucleares, así como de accidentes nucleares. En tal caso, se prevé que sea liberado en forma de Se^{VI} y Se^{IV} y que su comportamiento sea idéntico al del Se no radiactivo existente en la naturaleza (Atwood, 2010). No obstante, algunos cálculos termodinámicos indican que

también podría estar en los estados 0 y –II debido a su interacción con el hierro presente en los contenedores metálicos que contienen los residuos (Altmann, 2008).

Uno de los An^{III} de mayor interés presente en los residuos radiactivos es el curio (Cm). El Cm es un radionúclido muy tóxico debido a la actividad alfa de algunos de sus isótopos, como el ^{247}Cm y el ^{248}Cm, existentes en el combustible nuclear gastado (Gorietti et al., 2017; Kooyman et al., 2018). Este elemento es también el principal artífice del calor por desintegración nuclear producido en los residuos nucleares, un factor limitante en cuanto a la gestión y almacenamiento de los mismos. La producción de calor requiere un mayor espacio en los almacenamientos para que haya una mejor adecuación y disipación de la temperatura (Chabert et al., 2012). Por tanto, la eliminación del calor producido supondría una ventaja a la hora de depositar los residuos. El enfoque actual consiste en almacenar los residuos que contengan estos radionúclidos durante 120 años y esperar la disipación natural del calor producido antes de su almacenamiento bajo tierra (Kooyman et al., 2018). Muchos de los trabajos enfocados en el estudio del Cm, utilizan el elemento europio (Eu) como representante inactivo de An^{III}. Esta inactividad, junto con sus excepcionales propiedades luminiscentes (Ansoborlo et al., 2007), hacen que el Eu sea ideal para estos estudios, ya que los experimentos realizados con este elemento pueden ser extrapolados tanto al Cm como al resto de An^{III}. Otros actínidos como el Am y el Np también son responsables de la elevada radiotoxicidad a largo plazo del combustible nuclear, así como de la gran cantidad de calor producido por desintegración nuclear (Kooyman et al., 2018).

Como ya se ha comentado con anterioridad, la movilidad de los radionúclidos se puede ver afectada por numerosos factores, entre los que se encuentran, el pH, el potencial redox y la especiación química. Sin embargo, aún no se ha mencionado el impacto que pueden tener los microorganismos tanto en la movilidad de los radionúclidos como en la seguridad de los AGPs.

5. Diversidad e influencia de los microorganismos en los sistemas de AGP.

Hoy día es bien conocida la presencia de microorganismos en las formaciones geológicas consideradas para el almacenamiento de residuos radiactivos, tales como granitos, arcillas, depósitos de sales, etc. en las que se ha detectado una amplia diversidad microbiana (Bachran et al., 2018; López-Fernández et al., 2018a, 2015; Pedersen, 2013). En este sentido, no solo hay que tener en cuenta la microbiología autóctona de los materiales y formaciones geológicas de los AGPs, ya que una amplia gama de microorganismos pueden ser introducidos durante la construcción de los mismos.

En aquellos países que han optado por el uso de arcillas en sus respectivos AGPs, se están llevando y se han llevado a cabo estudios de diversidad, actividad y viabilidad microbiana con el objetivo de investigar la influencia de los procesos microbianos en la seguridad de estos sistemas. Es el caso de la arcilla Opalinus de Suiza, la Callavo-Oxfordian de Francia, las bentonitas de Cabo Gata de España, o las arcillas Boom de Bélgica (Bengtsson y Pedersen, 2016; López-Fernández et al., 2014; Schlegel et al., 2016; Smart et al., 2017). Las formaciones arcillosas de bentonita obtenidas de Cabo de Gata (Almería, España) han sido caracterizadas y descritas como adecuadas para su uso como barrera artificial en los AGPs debido a sus propiedades mineralógicas, físico-químicas, hidráulicas, mecánicas y geoquímicas (Villar et al., 2006). Concretamente, las bentonitas procedentes del depósito de Cortijo de Archidona (Almería, España) se han seleccionado como material español de referencia debido principalmente a sus óptimas propiedades de compactación (Villar et al., 2006). Los estudios de López-Fernández et al. (2018a; 2015; 2014) demostraron la elevada biodiversidad microbiana presente en estas bentonitas (Figura 4). La mayoría de especies identificadas correspondieron a microorganismos aeróbicos facultativos y estrictos. Algunos de ellos han sido descritos previamente por su habilidad para interaccionar con radionúclidos y metales pesados presentes en residuos radiactivos mediante diversos mecanismos. Es el caso de géneros bacterianos como *Acidovorax, Variovorax, Pseudomonas, Stenotrophomonas y Ralstonia* (Choudhary y Sar, 2009; Gerber et al., 2016; Hedrich et al., 2011; Hupert-Kocurek et al., 2013; Ruiz-Fresneda et al., 2018). Recientemente se ha demostrado la capacidad de la bacteria *Acidovorax facilis* para interaccionar con U^{VI}, principalmente a través de un proceso de biosorción a la superficie celular (Gerber et al., 2016). Otras especies bacterianas como *Stenotrophomonas bentonitica* presentan una gran versatilidad al poder interaccionar con Se^{IV}, Cm^{III}, o U^{VI} a través de diferentes procesos como reducción, biosorción y acumulación intracelular (López-Fernández et al., 2014; Ruiz-Fresneda et al., 2018; Capítulo II y V).

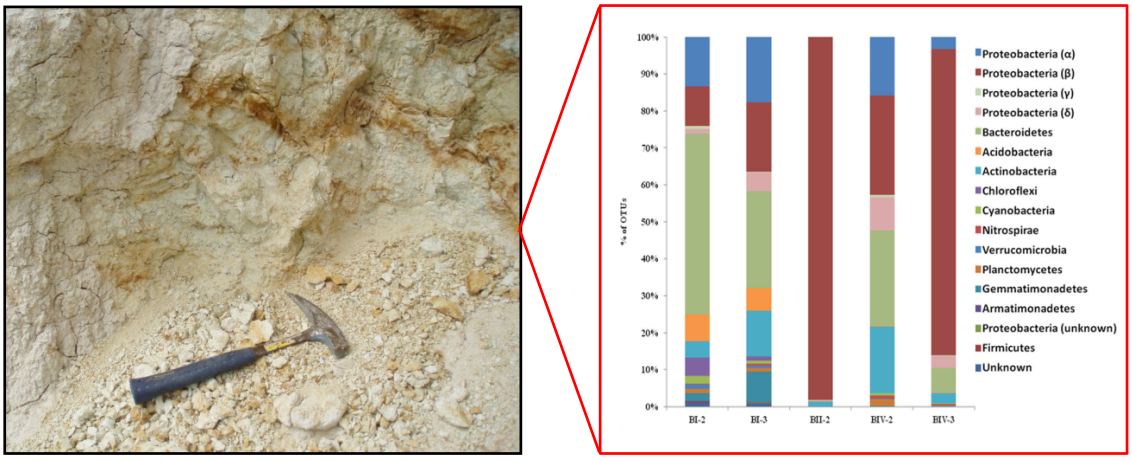

Figura 4. Análisis de la biodiversidad microbiana presente en muestras de bentonitas obtenidas de Cabo de Gata (Almería, España) mediante secuenciación Illumina (modificado de López-Fernández et al. 2015).

En definitiva, los almacenamientos geológicos no van a ser ambientes estériles. Aunque las condiciones no sean óptimas, van a estar presentes los nutrientes necesarios (donadores y aceptores de electrones, fuentes de carbono, nitrógeno, fósforo, etc.) para la existencia de actividad metabólica microbiana. Como los microorganismos pueden sobrevivir y estar activos, tienen que ser considerados cuando los residuos sean almacenados. Por todo ello, el estudio de los procesos microbianos y su posible efecto en la seguridad de los almacenamientos de residuos radiactivos es de gran interés. Entre ellos cabe destacar principalmente: la corrosión de los contenedores metálicos utilizados para depositar los residuos radiactivos, la producción microbiana de gases y la interacción microbiana con radionúclidos y materiales orgánicos presentes en los residuos.

5.1. Biocorrosión de los contenedores metálicos.

El fenómeno de biocorrosión consiste en el deterioro de materiales como el hiero, acero, hormigón o rocas a través de reacciones electroquímicas llevadas a cabo por microorganismos (Videla y Herrera, 2009). La formación de sustancias químicas corrosivas (sulfuros, acetatos, nitritos, ácidos, etc.) como consecuencia del metabolismo microbiano, contribuyen a este proceso de corrosión de los contenedores, que actúan como primera barrera de los residuos radiactivos (Leupin et al., 2017). Las bacterias sulfato-reductoras, las oxido-reductoras del hierro, y aquellas productoras de ácidos orgánicos, son los principales microorganismos implicados en la biocorrosión (Féron y Crusset, 2014; Leupin et al., 2017). De entre las anteriormente mencionadas cabe destacar a las bacterias sulfato-reductoras, debido a su capacidad de producir ácido sulfhídrico (H_2S) como principal agente corrosivo (Bagnoud et al., 2016a). Además, experimentos llevados a cabo en los últimos años en el Laboratorio Subterráneo Mont Terri, indican que las bacterias del género *Pseudomonas* presentes en aguas de poro de las arcillas Opalinus, están involucradas en la producción de ácidos orgánicos (Bagnoud et al., 2016a), los cuáles podrían intervenir en procesos de corrosión. En definitiva, el estudio de este fenómeno simulando las condiciones presentes en los almacenamientos es de gran interés, ya que podría dar lugar a la liberación de los radionúclidos en los alrededores del almacenamiento. Sin embargo, la corrosión no sólo puede afectar a la liberación de radionúclidos, sino que también puede dar lugar a la formación de gases como H_2 tal y como veremos a continuación.

5.2. Producción microbiana de gases.

La producción de gases como consecuencia de la actividad microbiana (principalmente H_2, CO_2 y CH_4) puede dar lugar al aumento de la presión dentro de los repositorios, comprometiendo la integridad de las arcillas como barreras (Bagnoud et al., 2016b). El CH_4 puede ser producido a través de la metanogénesis llevada a cabo por algunos microorganismos y mediante reacciones producidas entre el H_2 y los carbonos inorgánicos (CO_2 y CO) presentes (Kietäväinen y Purkamo, 2015). Por otra parte, la generación de H_2 puede ser debida a la corrosión anóxica de contenedores metálicos (Senior et al., 2017) y a la radiólisis del agua (Le Caër, 2011), además de como consecuencia de la actividad microbiana (Bagnoud et al., 2016a). El H_2 producido puede ser utilizado por los microorganismos como fuente de energía para el crecimiento microbiano mediante la producción de CH_4 y la reducción de sulfatos (Libert et al., 2011). Recientemente se están llevando a cabo estudios metagenómicos y metaproteómicos sobre la comunidad microbiana presente en las arcillas Opalinus, simulando las condiciones presentes en los repositorios, para determinar el papel de rutas metabólicas microbianas sobre la seguridad de los AGPs. Estos análisis indicaron la elevada contribución del género bacteriano *Pseudomonas* en la oxidación de H_2 a través de la reducción de sulfato (Bagnoud et al., 2016a; Smart et al., 2017). En este caso, al contrario que lo mencionado anteriormente, el uso de H_2 por los microorganismos supondría un impacto positivo sobre los AGPs al disminuir el exceso de presión ejercido por este gas (Bagnoud et al., 2016b). Las bacterias sulfato-reductoras de la familia Peptococcaceae también parecen intervenir en la formación de H_2S como consecuencia de la respiración de sulfatos y de CO_2 a partir de la oxidación de acetatos y otros compuestos orgánicos (Bagnoud et al., 2016a). El CO_2 generado puede disolverse en el agua de poro, precipitar mediante su interacción con materiales cementosos o difundirse en forma gaseosa, dependiendo de la zona donde se produzca dentro de los almacenamientos (Bagnoud et al., 2016a).

En definitiva, los microorganismos podrían tener un papel tanto beneficioso como perjudicial en la seguridad de estos repositorios en cuanto a la formación y utilización de gases. Sin embargo debido a la gran cantidad de procesos y ciclos biogeoquímicos que tendrán lugar, es difícil determinar el rol específico de los mismos. De todas formas, el estudio del metabolismo microbiano debe ser considerado a la hora de evaluar la seguridad de los almacenamientos de residuos radiactivos. Por ello, numerosos estudios se están llevando a cabo en la actualidad con la finalidad de aclarar este tema.

5.3. Interacción microbiana con materia orgánica.

La seguridad de los AGPs puede verse comprometida por la posible interacción entre la materia orgánica que requiere almacenamiento geológico, la radiación, y los microorganismos presentes en estos repositorios (Meleshyn, 2011). Los polímeros halogenados (PVC), el betún, los materiales de celulosa (papel, ropa, madera) y las resinas de intercambio iónico son materiales orgánicos de origen antropogénico que al estar contaminados con radionúclidos forman parte de residuos de intermedia actividad (Abrahamsen et al., 2015; Von Schenck y Källström, 2014). Estos materiales están sometidos a duras condiciones durante su almacenamiento, ya que están expuestos a radiaciones, a la acción de microorganismos y a difíciles condiciones químicas (pH alcalinos) en un ambiente anaerobio. Como consecuencia de ello, pueden ser degradados radiolítica, química y biológicamente, dando lugar a productos de degradación (acetato, lactato, etc.) que pueden afectar a la especiación de los radionúclidos y por tanto, a la movilización de los mismos (Abrahamsen et al., 2015). Diesen et al. (2017) comprobaron que productos de degradación procedentes de materiales celulósicos, como el ácido isosacarínico (ISA-*isosaccharinic acid*), intervienen en la solubilización y movilización de Eu^{III}. Sin embargo, algunos microorganismos también son capaces de degradar el ISA y otros agentes acomplejantes bajo condiciones alcalinas semejantes a las esperadas en los futuros AGPs, pudiendo evitar así la movilización de los radionúclidos presentes (Bassil et al., 2015). Además, estos productos de degradación orgánicos pueden ser utilizados por el metabolismo microbiano como fuente de energía, de carbono y de electrones, favoreciendo su viabilidad y supervivencia en los alrededores de los almacenamientos (Bassil et al., 2015).

5.4. Movilización de radionúclidos por microorganismos.

Es bien sabido que los radionúclidos no pueden ser degradados, pero si pueden ser transformados a formas de menor toxicidad. Uno de los principales responsables que pueden intervenir en esta transformación son los microorganismos. Esto se debe gracias a la tolerancia que presentan determinados microbios a la toxicidad de algunos elementos y a otro tipo de condiciones estresantes como la radiación, desecación o la presencia de agentes oxidantes (Brim et al., 2000). En este sentido, se ha descrito una amplia variedad de bacterias con elevada resistencia a elementos como uranio, níquel, cobre, cadmio, selenio, cesio y estroncio, pertenecientes a géneros como *Bacillus, Pseudomonas, Stenotrophomonas o Serratia,* (Paterson-Beedle et al., 2006; Ruiz-Fresneda et al., 2018; Shukla et al., 2017).

La actividad microbiana puede afectar la solubilidad y migración de los radionúclidos de forma indirecta mediante la alteración de las condiciones geoquímicas de los almacenamientos (pH,

Eh, etc.). Estas alteraciones pueden dar lugar a cambios en el estado de oxidación de determinados radionúclidos, afectando a su solubilidad y movilidad a través de los repositorios. Por otro lado, los microorganismos también pueden interaccionar de forma directa con elementos presentes en residuos radiactivos como el Se, el Cm o el U mediante diferentes procesos como bioacumulación intracelular, biotransformación, biosorción y biomineralización, afectando la movilización de los mismos (Merroun et al., 2011; Moll et al., 2014; Ruiz-Fresneda et al., 2018; Shukla et al., 2017) (Figura 5).

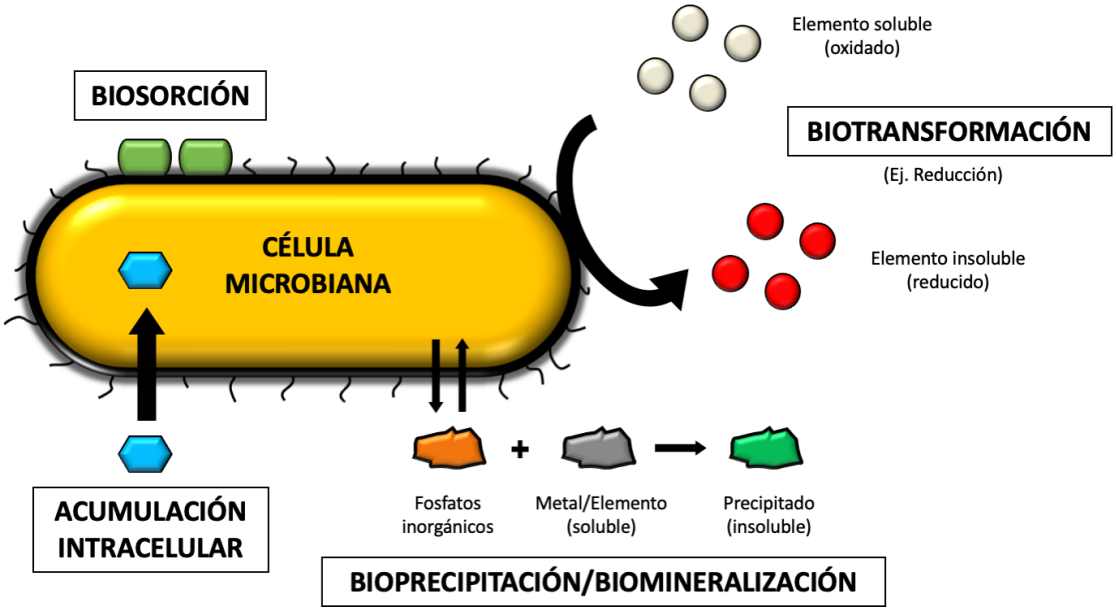

Figura 5. Esquema representativo de los principales procesos microbianos involucrados en la movilización de metales y radionúclidos.

- Biotransformación.

Es un proceso que tiene lugar cuando un elemento determinado cambia su estructura química como consecuencia de la actividad microbiana. Las reacciones oxidación-reducción (redox) llevadas a cabo por microorganismos pueden provocar cambios en el estado de oxidación de numerosos metales y radionúclidos (Francis y Nancharaiah, 2015). La biorreducción de sus formas oxidadas, solubles y móviles, a formas reducidas, puede dar lugar a su inmovilización (Rui et al., 2013). Muchos de ellos llevan a cabo este proceso mediante el uso de enzimas. La reducción enzimática de radionúclidos y metales pesados por bacterias se ha descrito ampliamente con anterioridad. Diversas bacterias pueden mediar en la reducción de la forma oxidada y soluble de uranio (U^{VI}) a su forma insoluble (U^{IV}), sobre todo aquellas anaerobias que utilizan U^{VI} como aceptor final de electrones (Kolhe et al., 2018). De entre los principales géneros descritos capaces de llevar a cabo esta reducción caben destacar a *Geobacter,*

Desulfovibrio, y Shewanella (Cologgi et al., 2014; Grouzdev et al., 2018; Stylo et al., 2015). Por su parte, las formas oxidadas de otros elementos como el Se (Se^{VI} y Se^{IV}) también pueden ser reducidas a Se^{0} de menor solubilidad por géneros bacterianos como *Bacillus* o *Stenotrophomonas*, entre otros (Kora, 2018; Lampis et al., 2017; Tan et al., 2016).

- Biosorción.

La biosorción puede ser definida como el secuestro de iones metálicos positivamente cargados por componentes de la superficie celular cargados negativamente a través de interacciones físico-químicas (Gadd, 2004; Prakash et al., 2013). Esta unión puede ser debida a interacciones electrostáticas entre ligandos cargados, intercambio iónico y a procesos de complejación y de quelación (Diep et al., 2018; Yang et al., 2015). Por todo ello, se trata de un proceso pasivo que incluso puede llevarse a cabo a través de fragmentos celulares y biomasa microbiana muerta (Ayangbenro y Babalola, 2017; Fomina y Gadd, 2014). La biosorción puede ser directa, mediante la interacción de cationes metálicos con los grupos funcionales aniónicos de la paredes celulares, o indirecta, con polímeros extracelulares (EPS), proteínas de la capa S y cápsulas de algunas bacterias (Dobrowolski et al., 2017; Merroun et al., 2005).

- Bioacumulación intracelular.

Según Tabak et al. (2005) la bioacumulación consiste en la retención y concentración de una determinada sustancia dentro de un organismo. Al contrario que la biosorción, la bioacumulación es un proceso metabólicamente activo, en el que los microorganismos introducen un determinado radionúclido o metal pesado en el espacio intracelular, utilizando para ello un sistema de transporte (Diep et al., 2018). Se trata por tanto de un proceso más lento y que requiere de un mayor consumo energético. Una vez dentro, los radionúclidos pueden ser secuestrados por proteínas, así como ser envueltos en membranas lipídicas, vacuolas y otros sistemas de almacenamiento (Mishra y Malik, 2013).
Algunos autores indican que la bioacumulación puede estar estrechamente relacionada con la biosorción, ya que requiere de rápidas interacciones con aniones presentes en componentes de la superficie celular para su posterior introducción en el espacio intracelular (Tišáková et al., 2013). Como consecuencia de ello, las propiedades moleculares del radionúclido en cuestión, así como las características de la superficie celular (contenidos en lípidos, área superficial para la acumulación, etc.) podrían afectar al proceso (Jorgensen, 2010).

- Bioprecipitación/Biomineralización.

Consiste en la precipitación de determinados metales con ligandos liberados por microorganismos (fosfatos, sulfuros, carbonatos o hidróxidos), dando lugar a la formación de complejos insolubles (Newsome et al., 2014; Shukla et al., 2017). Este proceso puede ser debido a la acción de determinadas enzimas. Algunos microorganismos son capaces de hidrolizar fosfatos orgánicos mediante la actividad fosfatasa, produciendo fosfatos inorgánicos (Pi) que precipitan con U^{VI} como fosfatos de uranio insolubles. En concreto, bacterias del género *Sphingomonas, Bacillus y Serratia* han sido descritas por su capacidad para precipitar uranio formando fosfato de uranilo como consecuencia del proceso anteriormente mencionado (Chandwadkar et al., 2018; Newsome et al., 2015; Zhang et al., 2018). Cuando el precipitado insoluble formado es un mineral, a este proceso se le suele denominar biomineralización en lugar de bioprecipitación (Kolhe et al., 2018). Es importante destacar que los metales precipitados producidos por los procesos de biomineralización/bioprecipitación no presentan cambios en su estado de oxidación, al contrario que en otros procesos anteriormente descritos como la biotransformación.

6. Mecanismos de interacción microbiana con selenio, curio y europio.

Por todo lo citado en anteriores apartados, existe un elevado interés en comprender cómo diferentes procesos microbianos afectan la movilidad de elementos de interés presentes en los residuos radiactivos, como el Se, y algunos representantes de actínidos trivalentes, como el Cm y el Eu.

6.1. Interacciones microbianas con selenio.

Los microorganismos pueden interactuar con el Se principalmente a través de procesos de biotransformación bioquímica. Son numerosos los capaces de transformar diferentes especies de Se a través de procesos de reducción-oxidación (redox), metilación y desmetilación (Eswayah et al., 2016).

La reducción microbiana de las formas oxidadas y solubles de Se (Se^{VI} y Se^{IV}) a Se^0 insoluble se ha sido descrito con anterioridad por bacterias del género *Bacillus, Comamonas, Stenotrophomonas*, *Azospirillum, y Pseudomonas,* entre otras (Figura 6) (Kora, 2018; Lampis et al., 2017; Staicu et al., 2015; Vogel et al., 2018; Wang et al., 2010). Actualmente, el número de cepas reductoras de Se^{VI} conocidas es menor que el de reductoras de Se^{IV}. El mecanismo de reducción del Se^{VI} varía entre los microorganismos estudiados hasta la fecha. Algunas especies

bacterianas como *Thauera selenatis y Seleniivibrio woodruffii* son capaces de respirar Se^{VI} al usarlo como aceptor de electrones (Butler et al., 2012; Rauschenbach et al., 2013). Por otra parte, algunas enzimas como la selenato reductasa han demostrado su habilidad para reducir Se^{VI} en cepas como *Comamonas testosteroni* S44 (Tan et al., 2018). La reducción de Se^{IV} también puede ser llevada a cabo a través de otros mecanismos enzimáticos. La nitrito reductasa, sulfito reductasa, fumarato reductasa y selenito reductasa parecen intervenir en este proceso (Basaglia et al., 2007; Song et al., 2017; Wang et al., 2018; Zheng et al., 2014). Además, reacciones mediadas por compuestos con grupos tiol (-SH) también han sido estudiadas. Con especial interés se ha investigado la participación del glutatión (GSH) en la reducción de Se^{IV}. Kessi y Hanselmann (2004) comprobaron que el GSH y la enzima glutatión reductasa (GR) intervienen en la reducción de Se^{IV} a Se^{0} en *Rhodospirillum rubrum* mediante una serie de reacciones. Los estudios de Antonioli et al. (2007) llevados a cabo con la cepa *S. maltophilia* SeITe02 apoyan este mecanismo al sugerir que, efectivamente, el GSH y la GR intervienen en el proceso de reducción de Se^{IV} llevado a cabo por esta bacteria.

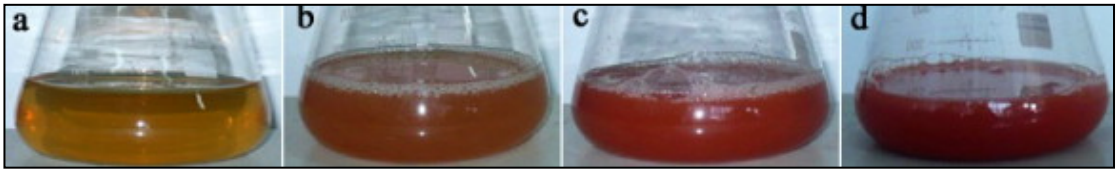

Figura 6. Cambio de color indicativo de la reducción de Se^{IV} a Se^{0} en cultivos bacterianos de *Bacillus subtilis* tras su incubación a 35º C durante 12, 24, 36 y 48 horas (a-d) (Wang et al., 2010).

En la mayoría de los casos, los productos de Se^{0} reducidos se presentan formando nanopartículas de selenio (SeNPs), conocidas por su uso en numerosas aplicaciones, tanto médicas como industriales (Wadhwani et al., 2016). Estas nanopartículas pueden presentar diferentes propiedades físico-químicas (morfología, tamaño, forma) que afectan a su solubilidad y movilidad por el ambiente (Buchs et al., 2013; Jain et al., 2017; Keller et al., 2010). *Rhodopseudomonas palustris N* y *Zooglea ramigera* son capaces de producir esferas de Se de naturaleza amorfa a escala nanométrica (Li et al., 2014a; Srivastava y Mukhopadhyay, 2013). Los estudios de Benko et al. (2012) demostraron la menor toxicidad de las nanoesferas de Se en comparación con las formas oxidadas (Se^{VI} y Se^{IV}). Sin embargo, existe una cierta controversia en este aspecto ya que diferentes estudios indican lo contrario (Li et al., 2008). La formación de "nanofibras o nanohilos" (del inglés *nanowire*) de Se por parte de microorganismos presentes en lodos granulares anaeróbicos también ha sido comprobada por Jain et al. (2017). Estos autores indicaron la menor estabilidad coloidal y movilidad de estas nanoestructuras en comparación con nanoesferas producidas biológicamente. Por otro lado, la cristalinidad de algunas nanoestructuras de Se también parece afectar a la inmovilización de las mismas al aumentar su coeficiente de sedimentación (Lenz et al., 2009).

Algunos estudios han revelado la presencia de capas de materia orgánica, compuestas principalmente por proteínas y polisacáridos, envolviendo las nanoestructuras de Se producidas biológicamente (Dobias et al., 2011; Kamnev et al., 2017). Las propiedades físico-químicas, y por tanto la movilidad, de las nanoestructuras de Se pueden verse ampliamente afectadas por la presencia de estas capas orgánicas asociadas (Jain et al., 2017). Además, algunos autores también han sugerido el papel de las proteínas durante la síntesis y la transformación de SeNPs, así como controlando el tamaño de las mismas (Dobias et al., 2011; Wang et al., 2010). Según Wang et al. (2010), las proteínas producidas por la bacteria *Bacillus subtilis* intervienen en la transformación de nanoesferas a nanofibras de Se trigonal cristalino (Figura 7). Aunque el mecanismo exacto de transformación se desconoce, lo que parece indiscutible es el papel directo de las células y sus proteínas durante el proceso.

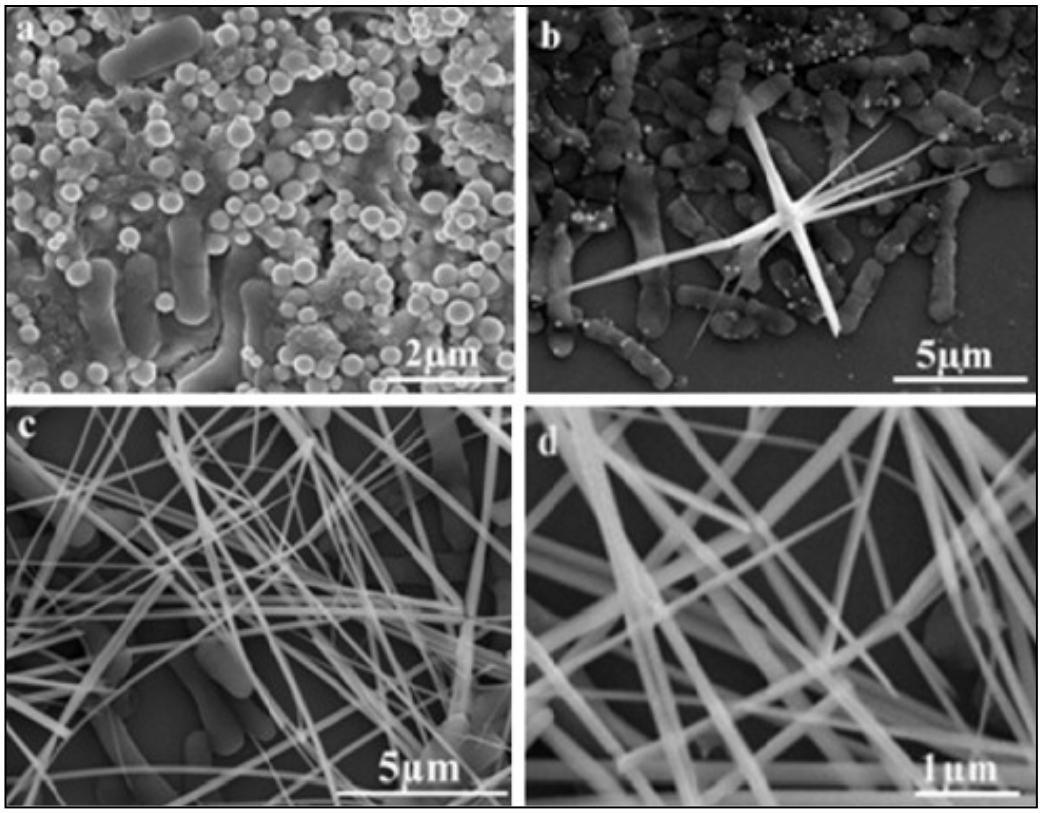

Figura 7. Imágenes de microscopia del proceso de transformación de nanoesferas a nanofibras de Se producidas por la especie bacteriana *Bacillus subtillis* (Wang et al., 2010)**.**

Los compuestos metilados de seleniuro son, al igual que el Se^0, formas básicamente insolubles y poco biodisponibles para los seres vivos (Ranjard et al., 2003). Por esta razón, la metilación de Se es considerada como uno de los más importantes procesos de transformación relacionados con la biorremediación. Se trata de un mecanismo de detoxificación para microorganismos, ya que los compuestos volátiles metilados de Se son notablemente de menor toxicidad que las formas oxidadas (Frankenberger y Arshad, 2001; Ranjard et al., 2003). La producción de

seleniuros metilados como consecuencia de la metilación de Se ha sido comprobada en diferentes especies bacterianas como *Methylococcus capsulatus*, *Methylosinus trichosporium* OB3b, *S. maltophilia y P. stutzeri* NT-I (Dungan et al., 2003; Eswayah et al., 2017; Kagami et al., 2013). Estas especies son capaces de producir compuestos volátiles como el dimetil seleniuro (*dimethyl selenide*-DMSe, CH_3SeCH_3), el dimetil diselenio (*dimethyl diselenide*-DMDSe, $CH_3SeSeCH_3$) y el dimetil selenio sulfuro (*dimethyl selenenyl sulphide*-DMSeS, CH_3SeSCH_3). Hasta la fecha, se han propuesto diversos mecanismos para la biometilación de Se. Chasteen y Bentley (2003) sugirieron que el Se^0 es reducido a la forma seleniuro (H-Se-X), que posteriormente es metilada a CH_3SeCH_3 y CH_3SeH. Otros mecanismos proponen de forma similar la formación de CH_3SeCH_3 a partir de Se^{IV} mediante una serie de reacciones de reducción y metilación (Challenger, 1945).

Finalmente, diversos estudios han indicado la oxidación de Se^0 y Se^{IV} por microorganismos presentes en suelos (Dowdle y Oremland, 1998; Sarathchandra y Watkinson, 1981). Sin embargo, a diferencia de los procesos de reducción, el bajo índice de oxidación de las formas reducidas de Se hacen que este proceso no sea considerado de relevancia para el medio ambiente (Eswayah et al., 2016; Losi y Frankenberger, 1998). Del mismo modo, los procesos de desmetilación de compuestos de Se no suelen tenerse en consideración debido a las bajas tasas a las que se producen estas reacciones (Eswayah et al., 2016).

6.2. Interacciones microbianas con curio/europio.

El estudio de las interacciones entre representantes de actínidos trivalentes (Cm y Eu) y microorganismos que estarán presentes en los AGPs es indispensable para predecir y evaluar la seguridad de los mismos. Diferentes mecanismos de interacción como biosorción, biomineralización/bioprecipitación o acumulación intracelular pueden afectar la movilidad en el ambiente de estos elementos.

La biosorción es uno de los principales mecanismos de interacción que intervienen en el caso del Cm y del Eu. La superficie celular de numerosas bacterias presentan una alta densidad de grupos funcionales que pueden servir como punto de unión de determinados elementos y cationes metálicos (Moll et al., 2014; Reitz et al., 2011). Concretamente, los grupos carboxilos presentes en la capa de peptidoglucano de la pared celular de bacterias gram-positivas parecen actuar como los principales sitios de unión de actínidos (Barkleit et al., 2009). Por otra parte, los grupos carboxilo, fosforilo, hidroxilo y amino presentes en la membrana externa de lipopolisacáridos (LPS), característica de bacterias gram-negativas, también tienen la capacidad de actuar como ligando de actínidos como el U, el Cm y el Np (Moll et al., 2009). Diferentes

especies bacterianas como *P. fluorescence* y *Sporomusa* sp. MT-2.99 se han caracterizado por su habilidad para la biosorción de Cm^{III} y Eu^{III} (Moll et al., 2014, 2013). En el caso de *Sporomusa* sp. MT-2.99, mediante espectroscopía de fluorescencia (TRLFS-*Time-Resolved Laser-induced Fluorescence Spectroscopy*), se pudo determinar la especiación y estructura de los complejos de superficie formados con Cm^{III} y Eu^{III}. Los resultados reflejaron que los grupos carboxilo y fosforilo son los responsables de la unión de Cm^{III} y Eu^{III} a la superficie celular de esta bacteria (Moll et al., 2014). No solo células bacterianas se han analizado mediante esta técnica. Recientemente, estudios llevados a cabo sobre la levadura *Rhodotorula mucilaginosa* BII-R8, aislada de bentonitas españolas, revelaron su habilidad para retener en la superficie celular tanto Cm^{III} como Eu^{III} (López-Fernández et al., 2018b) (Figura 8). Del mismo modo que los trabajos citados anteriormente, los grupos carboxilos y fosforilos presentes en las envueltas celulares de *R. mucilaginosa* BII-R8 parecen intervenir en la interacción de estos dos elementos según los resultados obtenidos mediante TRLFS. Según sus investigaciones, se trata de la primera levadura descrita hasta la fecha por su capacidad de interaccionar con Cm y Eu. La arqueas también pueden interaccionar con Cm^{III} y Eu^{III} tal y como indicaron los estudios realizados sobre *Halobacterium noricense* $DSM15987^{T}$ (Bader et al., 2019), donde los grupos fosfato y carboxílicos superficiales y liberados por las células parecen actuar como sitios de unión. Otras técnicas como la espectroscopía infrarroja (ATR/FTIR-*attenuated total reflectance-Fourier transform infrared spectroscopy*) o la espectroscopía fotoelectrónica de rayos X (XPS-*X-ray photoelectron spectroscopy*) pueden ser de gran utilidad para la caracterización de los complejos Cm^{III}/Eu^{III} formados durante su biosorción. Maleke et al., (2019) demostraron la posible implicación de grupos carboxilo, carbonilo y fosfato en la biosorción de Eu^{III} por la bacteria *Thermus scotoductus* SA-01 según datos obtenidos mediante ATR-FTIR. Además, sugirieron la formación de carbonatos de Eu^{III} a nivel superficial tal y como indicaron los análisis con XPS.

Otros mecanismos como la bioacumulación y la biomineralización/bioprecipitación también presentan un papel destacado en la interacción microbiana con Cm^{III}/Eu^{III}. La especie bacteriana *Thermus scotoductus* SA-01 es capaz de acumular intracelular y extracelularmente precipitados de Eu^{III} sobreviviendo bajo concentraciones superiores a las normalmente encontradas en la naturaleza (hasta 1 mM Eu) (Maleke et al., 2019) (Figura 9). El análisis de estas muestras mediante varias técnicas espectroscópicas sugirieron que la presencia de acúmulos extracelulares puede ser debida a un proceso de biomineralización, a partir de la formación de carbonatos producidos mediante la reacción del CO_2, procedente de la respiración, con radicales OH^-. Estos resultados evidencian que varios mecanismos de interacción pueden tener lugar simultáneamente en una célula cuando se encuentra expuesta a un agente estresante como es, en este caso, el Eu^{III}.

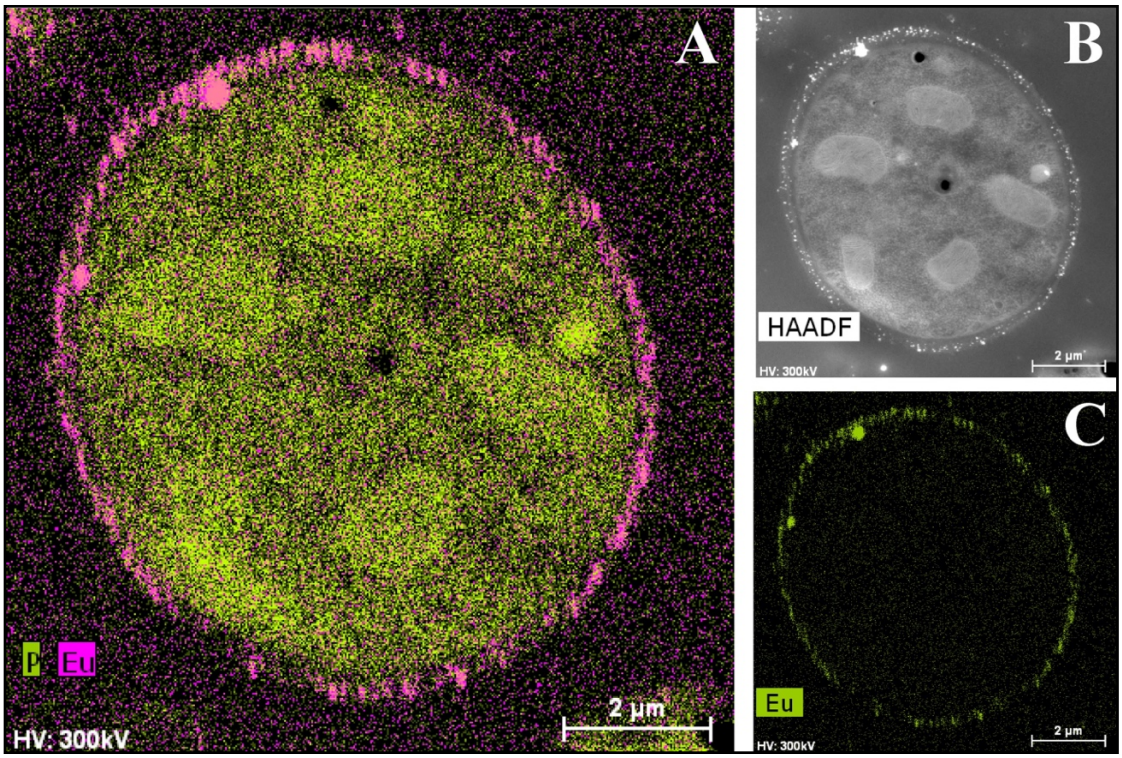

Figura 8. Imágenes de microscopia mostrando la biosorción de Eu en la superficie celular de *Rhodotorula mucilaginosa* BII-R8 (López-Fernández et al., 2018b).

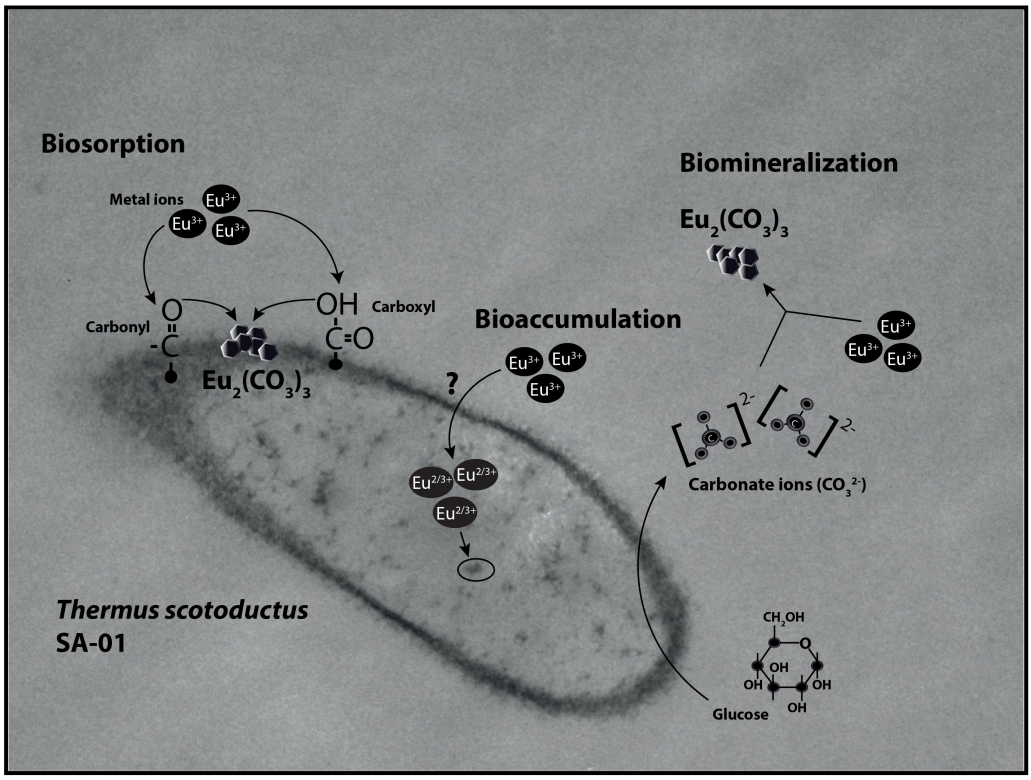

Figura 9. Ilustración esquemática sobre los mecanismos de interacción de *Thermus scotoductus* SA-01 con europio (Maleke et al., 2019).

Los procesos de biosorción y bioacumulación microbianos podrían tener un papel importante en la inmovilización de Cm^{III}, Eu^{III} y otros elementos tóxicos mediante la fijación de biomasa microbiana en soportes inertes a través de la formación de biopelículas (Gadd, 2009). Por otra parte, la biomineralización también daría lugar a la inmovilización de estos elementos debido a la formación de precipitados insolubles (Shukla et al., 2017). Por todo ello, el estudio de las interacciones microbianas con actínidos (Cm^{III}) y elementos análogos (Eu^{III}) está adquiriendo un especial interés en los últimos años, tanto para la evaluación de la seguridad de los repositorios de residuos radiactivos, como para fines de biorremediación de ambientes contaminados.

OBJETIVOS

Hasta la fecha, multitud de trabajos han tratado de investigar el impacto que tienen los procesos microbianos sobre la movilidad de elementos presentes en los desechos radiactivos. Sin embargo, todavía se desconocen numerosos aspectos sobre el efecto que los microorganismos pueden ejercer sobre los radionúclidos bajo las diferentes condiciones que existirán en los futuros almacenamientos geológicos profundos (AGPs) de residuos radiactivos, tales como aerobiosis, anaerobiosis, alcalinidad, presencia de compuestos donadores y aceptores de electrones, etc.

La presente tesis doctoral trata de estudiar la influencia de la bacteria *Stenotrophomonas bentonitica* BII-R7, aislada de bentonitas de Cabo de Gata (Almería, España) que se han seleccionado como material de referencia para su uso en los AGPs, sobre la movilidad de selenio (Se), curio (Cm) y europio (Eu) con el fin de evaluar su efecto sobre la seguridad de los almacenamientos de residuos radiactivos.

En base a lo anterior, los objetivos específicos para el desarrollo de esta tesis doctoral son:

1- Caracterización molecular, fisiológica y bioquímica de la cepa bacteriana *S. bentonitica* BII-R7, seleccionada para su uso en los experimentos de interacciones con Se, Cm y Eu.

2- Estudio de los mecanismos de reducción y volatilización de Se por *S. bentonitica* BII-R7 mediante técnicas espectroscópicas, microscópicas y microbiológicas bajo condiciones aerobias, anaerobias y alcalinas relevantes para los sistemas de AGP.

3- Elucidación de los mecanismos de interacción de *S. bentonitica* BII-R7 con Cm (actínido trivalente) y Eu (análogo inactivo de actínidos trivalentes) mediante el uso de una metodología multidisciplinar bajo condiciones aerobias y anaerobias de relevancia para los sistemas de AGP.

MATERIALS AND METHODS

1. Molecular and phenotypic characterization of the strain *Stenotrophomonas* sp. BII-R7 isolated from bentonite formations

A large number of microbial strains were isolated in a study targeting the culture-dependent microbial diversity occurring in bentonite formations from southern Spain. This investigation aimed at understanding the impact of microbial processes on the performance of this type of material for deep geological disposal of nuclear wastes (López-Fernández et al., 2014). By using standard dilution plating technique on different culture media, including oligotrophic R2A medium (Reasoner and Geldreich, 1985), Luria–Bertani (LB) medium (Miller, 1972) and Nutrient Broth (NB), 32 microbial isolates (31 bacterial strains and 1 fungal strain) were isolated and characterized. The strain BII-R7^T, affiliated to the genus *Stenotrophomonas* (family *Xanthomonadaceae*, order *Xanthomonadales*, class *Gammaproteobacteria*) based on 16S rRNA gene sequence divergence (López-Fernández et al., 2014), was further investigated.

1.1. Molecular analysis

For detailed phylogenetic placement of the strain BII-R7^T, its 16S rRNA gene sequence was aligned with the SILVA Incremental Aligner (SINA; v1.2.11; Pruesse, Peplies, and Glöckner 2012) and implemented into the "All species living tree project" (LTPs; Yarza et al. 2008) using the ARB software package release 5.2 (Ludwig et al., 2004) for analysis. Additionally, sequences not included in the LTP database were obtained from GenBank (http://www.ncbi.nlm.nih.gov/) and added to the database. Finally, the sequence alignment was checked manually. Pairwise sequence similarities were calculated using the ARB Neighbor-joining tool, without the application of an evolutionary model. Phylogenetic trees were calculated with the maximum-likelihood method using RAxML version 7.04 (Stamatakis, 2006) with General Time Reversible-GAMMA (GTR-GAMMA) and rapid bootstrap analysis, the maximum-parsimony method using DNAPARS v 3.6 (Felsenstein, 2005), and the neighbor-joining method using ARB Neighbor-joining and the Jukes-Cantor correction (Jukes and Cantor, 1969).

Sequencing of the draft genome of BII-R7^T (GenBank accession number MKCZ00000000) allowed genomic analyses which clearly separated this strain from established species within the genus *Stenotrophomonas*. Reference genome sequences corresponding to type strains from all other species belonging to this genus were obtained from public databases (Patil et al., 2016).

Calculation of average nucleotide identity (ANI) with only the orthologous genes (Ortho-ANI; Lee et al. 2016) was performed for the comparative analysis of available *Stenotrophomonas* spp. genome sequences with BII-R7^T genome sequence. Similar indices were calculated by using different algorithms like original ANI value by Ortho-ANI software (Lee et al., 2016), ANI value by *EzBioCloud* ANI Calculator (Yoon et al., 2017), and ANI value obtained through Kostas lab ANI Calculator (Goris et al., 2007), which supported Ortho-ANI values obtained initially. Digital DNA-DNA hybridizations (dDDH) were determined online at http://ggdc.dsmz.de/distcalc2.php using the Genome-to-Genome Distance Calculation (GGDC) version 2.0 as described in Meier-Kolthoff et al. (2013). Additionally, DNA G+C contents were calculated in-silico in all cases.

1.2. Phenotypic analysis

The morphology of cells grown on LB broth at 28 ºC for 24 h with shaking at 160 rpm was observed by scanning electron microscopy (Quanta 400; FEI). Gram staining, cell motility and the presence of flagella were determined according to Komagata (1985). At physiological level, catalase activity was determined by assessing bubble production in 3 % (v/v) H_2O_2, and oxidase activity by using a 1 % (w/v) solution of tetramethyl-p-phenylenediamine (Kovacs, 1956). The growth capacity at various temperatures (4–42 ºC), NaCl concentrations (0.5-5 % at 28 ºC) and pH values (pH 4.0–13.0 at 28 ºC) was determined in TSB culture medium. About oxygen requirements, anaerobic growth was analyzed by cultivating strain BII-R7^T in serum bottles containing R2A broth, supplemented with thioglycolate (1 g/L) and the upper gas phase replaced with nitrogen.

Carbon sources utilization, acid production from carbon sources and some physiological characteristics were determined by using the API 20NE (48 h, 28 ºC), API 50CH (inoculated with AUX medium, 48 h, 28 ºC) and API ZYM (4 h, 28 ºC) galleries, respectively, according to the instructions of the manufacturer (bioMérieux) and the methods of Kämpfer et al.(1991).

Biomasses subjected to extraction of polyamines, quinones and polar lipids were grown in PYE broth [0.3 % peptone from casein (w/v), 0.3 % yeast extract (w/v), pH 7.2] at 28 °C. Polyamines were extracted from biomasses harvested at the late exponential growth phase according to the protocol of J. Busse and Auling (1988). HPLC (high-performance liquid chromatography) equipment was described by Stolz et al. (2007) and conditions for HPLC analysis were described by Busse et al. (1997). Quinones and polar lipids were extracted from biomass harvested at the stationary growth phase applying the integrated protocol of Tindall (1990a;

1990b) and Altenburger et al. (1996). The HPLC equipment used for quinone analysis was described recently (Stolz et al., 2007).

Biomass for fatty acid analysis was harvested after growth on TSA at 28 °C for 48 h. The analysis was performed as described by Kämpfer and Kroppenstedt (1996). Fatty acids were separated with a 5898A gas chromatograph (Hewlett Packard), respective peaks were automatically integrated and fatty acid names and percentages were determined with the Sherlock MIDI software v. 2.1 (TSBA v. 4.1).

2. Interactions of the bacterium *Stenotrophomonas bentonitica* with selenium

2.1. Bacterial strain and growth conditions

The bacterial strain used in the present Doctoral Thesis, recently described as a novel species named *S. bentonitica* BII-R7^T (Sánchez-Castro et al. 2017a; Capítulo I), was isolated from Spanish bentonites collected from Cabo de Gata (Almeria, Spain) (López-Fernández et al., 2014). Genome analysis revealed the presence of enzymes described for their ability to reduce selenite (Se^{IV}) to elemental Se (Se^0) like glutathione-related enzymes and NADH-dependent enzymes (Sánchez-Castro et al. 2017b). The cells were grown aerobically in LB broth medium (tryptone 10 g/l, yeast extract 5 g/l and NaCl 10 g/l, pH 7.0 ± 0.2) at 28 ºC and 180 rpm on a rotary shaker.

2.2. Preparation of Se^{IV} stock solution

Sodium selenite (Na_2SeO_3) (Sigma-Aldrich) was prepared as a 1M stock solution by dissolving appropriate quantities in distilled water. Finally, the solution was sterilized by filtration using 0.22-µm syringe filters (Sartorius®).

2.3. Bacterial synthesis, extraction, and purification of selenium nanoparticles

Selenium nanoparticles (SeNPs) were synthesized aerobically after contact of *S. bentonitica* with 2 mM Se^{IV}. After period of 48 and 144 h of incubation, the SeNPs were extracted and purified following the method described by Sonkusre (2014). Finally, purified SeNPs were spread onto LB agar plates to check the efficiency of the extraction process.

2.4. Se^{IV} tolerance studies of *S. bentonitica*

2.4.1. Reduction of SeIV under aerobic, anaerobic and alkaline conditions

The potential of *S. bentonitica* to tolerate Se^{IV} was assayed by growing the cells aerobically in LB liquid medium supplemented with increasing concentrations of sodium selenite. Untreated (control) and Se^{IV}-treated cells were incubated at 28 ºC by shaking at 180 rpm. In addition, dead cells obtained by heating the biomass at 90 ºC and LB broth containing Se^{IV} (abiotic) were used as controls.

For anaerobic assays, degassed and washed cell solution was inoculated in R2A medium, previously degassed using N_2, and supplemented with different electron donors (sodium acetate, citric acid, pyruvic acid, etc.) and acceptors (sodium nitrate, iron(III) hydroxide, ferric citrate, etc.). Prior to the inoculation, Se^{IV} at different concentrations was added to the medium. Finally, the suspensions were incubated at 28 ºC. Se^{IV}-untreated cells and R2A medium containing Se^{IV} were used as controls.

The Se^{IV} reduction ability of *S. bentonitica* was also assayed anaerobically under alkaline conditions (from pH 8 to 11) relevant for the deep geological repository (DGR) system. The samples were prepared as described above using sodium acetate and sodium nitrate as electron donor and acceptor, respectively. The pH of the solutions was adjusted by addition of acid ($HClO_4$) or base (NaOH) using a pH-meter CRISON© micro pH 2002 and sterilized by filtration through 0.22 μm nitrocellulose filters prior to degassing.

2.4.2. Determination of the minimum inhibitory concentration (MIC) of Se^{IV} for the bacterial growth

The minimum inhibitory concentrations (MICs) of Se^{IV} were determined in triplicates. Cells of the isolate were grown to late exponential phase to a final optical density (O.D) of 0.9 (at 600 nm) in LB broth and washed twice with 0.9% NaCl. Finally, 10 μl of the cell suspension was inoculated to LB agar supplemented with increasing concentrations of Se^{IV} from 1 to 400 mM. Afterwards, the plates were incubated at 28 ºC for 48 h. The MIC was defined as the lowest concentration of the element at which complete inhibition of colony formation is observed (Rossbach et al., 2000).

2.4.3. *Effect of selenite on the bacterial growth*

Cell growth of *S. bentonitica* both in the presence and absence of Se^{IV} was evaluated by quantifying the total protein content in bacterial cell extracts using a modification of the method of Dhanjal and Cameotra (2010). The total protein content was correlated with the increase in the cell growth. A 1 ml aliquot of bacterial culture was taken at different time intervals to measure growth based on the protein content of the cells by using Bradford reagent (Bio-Rad®). Bovine serum albumin (BSA) was used as a standard. All measurements were performed in triplicate.

2.4.4. *Quantification of biological Se^{IV} reduction rate*

The Se^{IV} reduction rate of *S. bentonitica* was assayed aerobically in LB liquid medium supplemented with different initial Se^{IV} concentration (0.1, 0.25 and 2 mM). After different times of incubation (0, 6, 24, 48, 120 and 144 h) 1 ml of the samples were taken and centrifuged (10000 x g; 15 min; room temperature) to remove the cells and other debris. The Se^{IV} concentration in the resultant supernatant was determined by using a Perkin Elmer Flexar HPLC pump attached to a Hamilton PRP-X100 column (4.6 x 250 mm) and coupled to a Perkin Elmer ICP-MS NexION350X. Ammonium citrate (5 mM; pH 5.2) containing methanol (2% *v/v*) was employed as mobile phase to achieve the separation at a flow rate of 1 ml min^{-1}. Se^{IV} amended-media without bacterial cells were used as controls. All samples were prepared in triplicate. In addition, a standard calibration curve with different solutions of known Se^{IV} concentrations was elaborated.

2.4.5. *Flow cytometry*

The cell viability and the metabolic activity of *S. bentonitica* in the presence of Se^{IV} under oxic and anoxic conditions were determined by using flow cytometry technique. Flow cytometry is a useful tool for the analysis of multiple individual parameters from cell populations (Givan, 2011). This analytical technique consists of a capillary tube in which the cells (or other particles) are flowing individually in front of one or more light sources (laser beams) (Picot et al., 2012) (Figure 1). The signals coming from the cells as a result of their illumination (scattered lights and fluorescent emissions) could then be detected and analyzed by a specific software. Flow cytometry is used in a broad range of research applications for biology including: cell counting, immuno-phenotyping, cell proliferation, multi-parametric DNA analysis, fluorescent protein, etc. (Picot et al., 2012). Emission fluorescence from the cells is quantitatively proportional to excitation intensity of the fluorochrome employed.

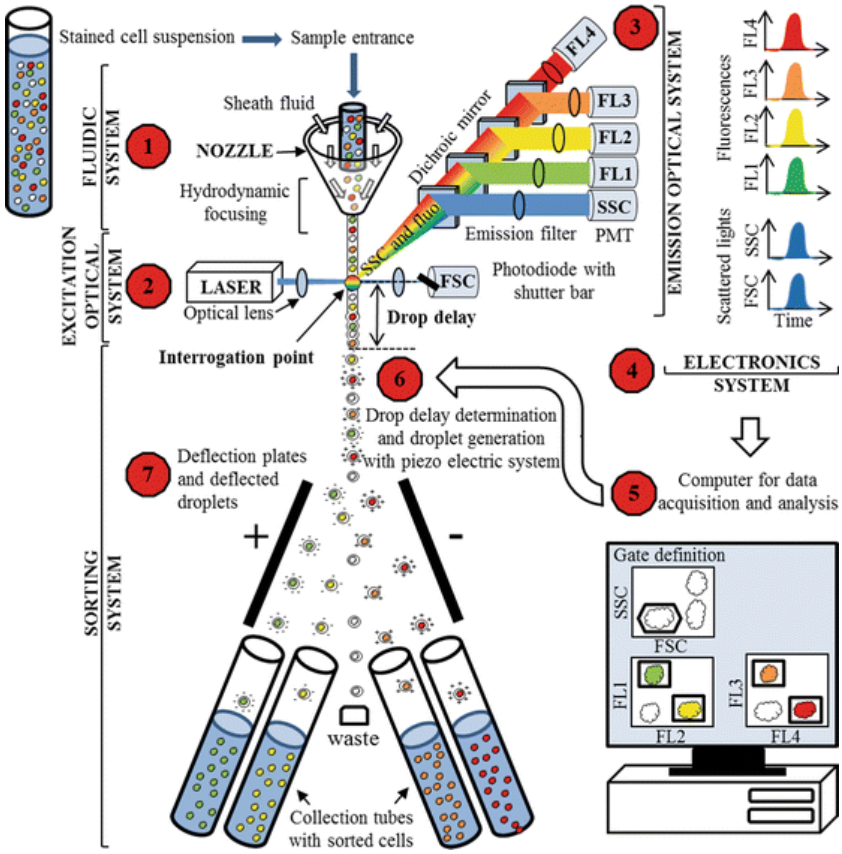

Figure 1. Schematic diagram of the flow cytometry principle (Picot et al., 2012).

In this study, the cells of *S. bentonitica* were stained with fluorescein diacetate (FDA) and propidium iodide (PI) for the cell viability test. The fluorescent dye FDA can diffuse across intact cell membranes (living cells) being enzimatically hidrolyzed to green fluorescent products (Stubberfield and Shaw, 1990). In contrast, PI is an intercalating DNA-binding dye exclusive of dead cells with injured cell membranes, which stains them in red (Givan, 2011). For the metabolic activity test, the fluorescent dye 3,3'-dihexyloxacarbocyanine iodide ($DiOC_6$) was employed. $DiOC_6$ is a positively charged lipophilic dye which binds to the membrane of actively growing cells (David et al., 2011). The samples were analysed by Forward Scatter using a FACSCantoII™ cytometer (Becton Dickinson) available from Centro de Instrumentación Científica at Universidad de Granada (Granada, Spain).

2.4.6. Detection and identification of volatile Se compounds

A combined thermal desorption GC-MS (Gas Chromatography – Mass Spectrometry) system (Figure 2) was employed for the detection and identification of selenium (Se) volatile species produced by *S. bentonitica*. GC-MS consists in a combination of two different analytical techniques. The GC separates different compounds in a sample into pulses of pure chemicals

based on their volatility by flowing an inert gas (mobile phase), which carries the sample, through a stationary phase fixed in the column (Skoog et al., 2007; Hussain and Maqbool, 2014). The mobile phase is usually an inert gas such as helium or an un-reactive gas such as nitrogen, and the stationary phase is a microscopic layer of liquid or polymer on an inert solid support, inside glass or metal tubing, called a column. The compounds in a sample are separated from each other because some take longer to pass through the column than others. Finally, the different compounds are collected and identified by MS according to their mass-to-charge ratio (m/z) (Hussain and Maqbool, 2014). The thermal desorption technique is used as a preconcentration technique for GC–MS. This system utilizes heat to increase the volatility of the compounds, enabling their separation.

Analysis of the samples was performed on a combined termal desorption GC-MS system (7890A-GC with 5975C-MS, Agilent Technologies), available from Biomolecular Sciences Research Centre at Sheffield Hallam University (Sheffield, United Kingdom).

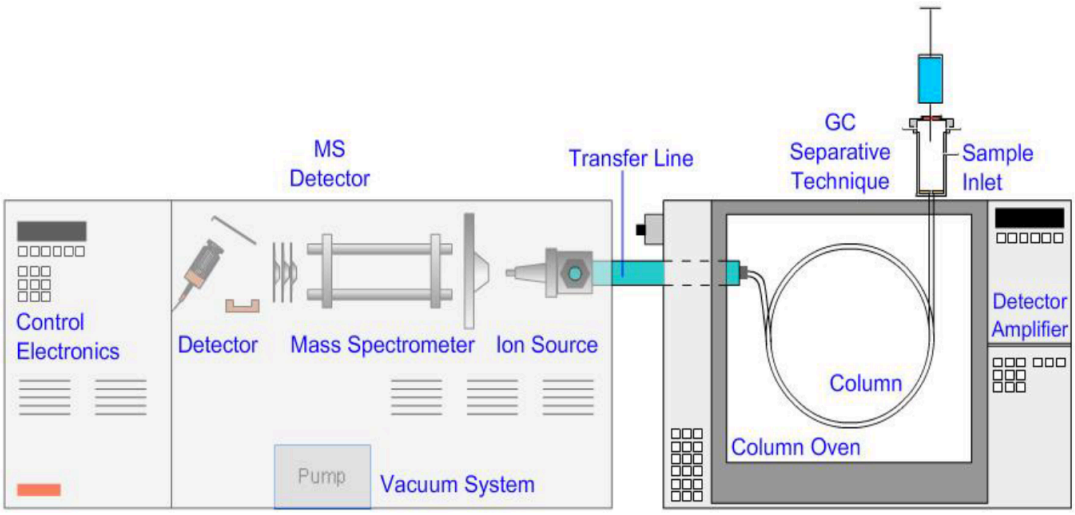

Figure 2. Schematic diagram of a GC-MS system (www.chromacademy.com) (Żymankowska-Kumon, 2016).

3. Interactions of the bacterium *Stenotrophomonas bentonitica* with curium and europium

3.1. Bacterial strain and culturing conditions

The bacterial strain *S. bentonitica* BII-R7 was cultured following the same methodology as described above (see section 2.1.).

3.2. Preparation of Eu^{III} and Cm^{III} stock solutions

An stock solution of Eu^{III} was prepared by dissolving europium chloride ($EuCl_3 \cdot 6H_2O$) (Sigma-Aldrich) in 0.1 M HCl to a final concentration of 10 mM. For the experiments, an Eu^{III} working solution was prepared diluting the stock in 0.1 M $NaClO_4$ to a final concentration of 0.03 mM. On the other hand, a stock solution of the long-lived curium isotope ^{248}Cm (half-life: 3.4×105 years) was used as described in López-Fernández et al. (2018b).

3.3. Potentiometric Titration

Potentiometric titrations is a chemical method of analysis in which the endpoint of the titration is monitored with an indicator electrode that records the change of the potential as a function of the volume of an added titrant of known concentration (Hulanicki et al., 2013). This technique is frequently used in the study of numerous reactions, such as protonation and complexation. A large number of potentiometric studies have been conducted in the last years to characterize the protonation behaviour of bacterial cell walls (Merroun et al., 2011; Moll et al., 2014; Yu et al., 2014). Potentiometric titration data clearly indicate the pH range in which bacterial surfaces can adsorb and desorb protons from solution, and consequently, the pH range in which the proton-active functional groups from the bacterial surface can interact with aqueous ions through adsorption reactions. A wide variety of functional groups present in bacterial cell walls (hydroxyl, phosphoryl, amino, and carboxylate) provide binding sites for metals and other toxic elements (Fein et al., 2005; Merroun et al., 2011; Ojeda et al., 2008). This technique is very useful to determine the type and abundance of functional groups of cell walls. Therefore, knowledge of the concentration and characteristics of functional groups on the cells surfaces is crucial to understand the interaction mechanisms of bacterial cells with surrounding metals and other elements. However, the experimental data from potentiometric titrations measurements cannot be used alone to identify and quantify the surface ligands. A combination of potentiometric titrations and different spectroscopic techniques allow a more comprehensive characterization of the bacterial cell surface.

In the present work, the cell surface properties of *S. bentonitica* cells were examined aerobically to better understand the interaction mechanism involved in the molecular binding of Eu^{III} to the functional groups from cell surfaces. All titrations were performed using a Metrohm Titrando 906 automatic titrator (Metrohm, UK) at 25 ºC available from the Systems and Process Engineering Centre at Swansea University (Swansea, United Kingdom). The titrator was set to add successive acid or base only after a drift equal or less than 5 mV min^{-1} was achieved.

3.4. Biosorption experiments

Kinetics studies of Eu^{III} binding were performed in order to estimate the adsorption efficiency of Eu^{III} by *S. bentonitica* cells under both aerobic and anaerobic conditions. For this purpose, the resultant supernatant collected after Eu^{III}-bacteria interaction was mixed with HNO_3 and measured by inductively coupled plasm-mass spectometry (ICP-MS) to estimate the Eu^{III} concentration. The amount of Eu^{III} adsorbed to the cells was calculated by subtracting the amount obtained in the supernatant from the initial Eu^{III} concentration.

4. Spectroscopic characterization of selenium, curium, and europium products

4.1. Attenuated total reflection-Fourier transform infrared (ATR-FTIR) Spectroscopy

Infrared (IR) spectroscopy uses the absorption of IR radiation by the molecular bonds to identify the bond types that can absorb energy by oscillating, vibrating, and rotating (Mattox, 2010). An IR spectrum of a sample is generated by scanning the intensity of IR radiation before and after passage of the IR beam through the sample (Figure 3). The IR spectrum is displayed by plotting the quantity $T = I_S / I_R$ as a function of wavenumbers, where T is the transmittance, I_S the intensity of the IR beam after and I_R before passing through the sample (Naumann, 2000). In most cases the absorbance A is used (A = - log T), since the absorbance at a given wavelength is directly proportional to the concentration of a sample according to Beer's law. The IR spectra of most materials consist of a large number of absorption bands, which originate from the interaction between discrete light quanta and mechanical motions (vibrational and rotational modes) of the molecules which are excited by the absorption of IR radiation (Naumann, 2000). Since the components of biological samples are usually present as solids, liquids or solutions, only vibrational modes are observed. Consequently, IR spectra of biological specimens are only vibrational spectra (Colthup et al., 1990). In contrast to classic dispersive IR spectroscopy, FTIR spectroscopy applies an interferometric modulation of radiation, providing a higher frequency resolution and a faster analysis time (Mattox, 2010). In FTIR spectrometers, the interference patterns of the modulated signals from interferograms are amplified, digitized, computer stored and transformed into a spectrum by the Fast Fourier transform (FFT) algorithm (Beekes et al., 2007; Naumann, 2000). This technique is oftently used for the study of microbiological samples. IR absorption bands observed in the region between approximately 800 and 4000 cm^{-1} can often be assigned to particular functional groups (Naumann, 2000). These absorption bands are also sensitive to structural changes, molecular interactions, membrane constitution, lipid–protein interaction, etc.

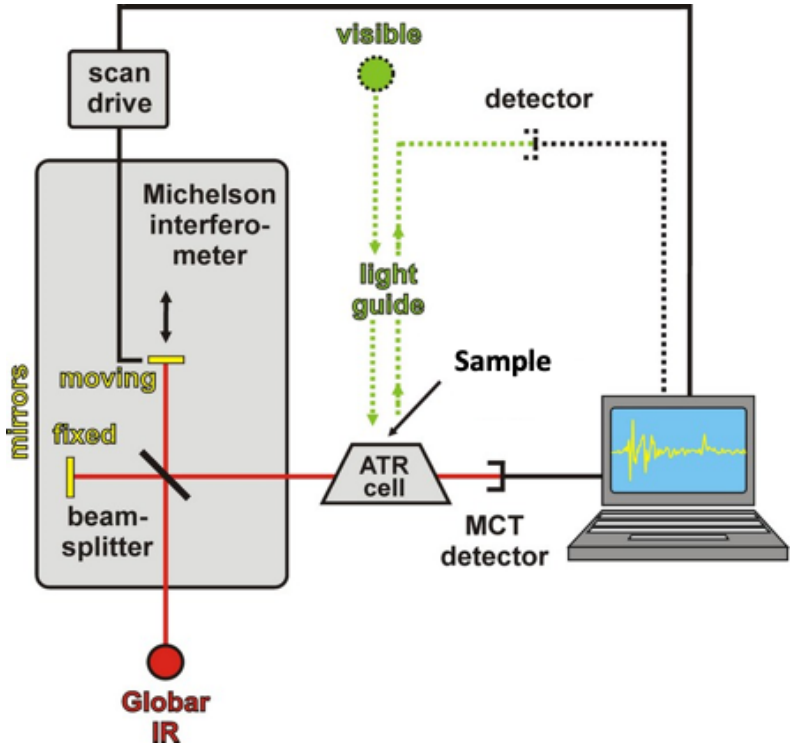

Figure 3. Schematic illustration of FTIR spectrometer equipped with ATR-cell (modified from http://www.biocenter.helsinki.fi/bi/biophys/methods_ftir.html).

In the present work, this technique was employed to study the nature of functional groups from the *S. bentonitica* cells involved in the interaction with Se and Eu. In addition we investigated the presence of organic molecules attached to the SeNPs produced by this bacterium. For the Se samples, ATR-FTIR measurements were performed on a Perkin Elmer Spectrum One FT-IR spectrometer available from the Department of Geography at The University of Sheffield (Sheffield, United Kingdom). This instrument was equipped with a Silver Gate Evolution ATR accessory consisting of a germanium crystal. For the Eu samples, ATR-FTIR measurements were performed on a Perkin Elmer Spectrum Two spectrometer, available from the Systems and Process Engineering Centre at Swansea University (Swansea, United Kingdom). This instrument was equipped with a ATR accessory, consisting of a diamond crystal at a fixed angle of 45º.

4.2. X-ray photoelectron spectroscopy (XPS).

XPS is a surface-sensitive technique that analyzes the energy of the photoelectrons (50–2000 eV) that are emitted when a surface is bombarded with X-rays in a vacuum environment (Mattox, 2010). Vacuum is required to maximise the free path of electrons and increase the probability of their detection. The energy of these electrons is characteristic of the bombarded atom and allowing the elemental composition, chemical state and electronic state of the

elements within a material (Mattox, 2010). XPS has developed into a useful analytical technique with many applications in different branches of physics, chemistry, and biology. It provides information about the electronic states and structure in solids, liquids, and gases (Sharma and Beard, 1990).

In the present work, this technique was employed to determine the functional groups from the *S. bentonitica* cells involved in the interaction with Se and Eu. The oxidation state of the Se and Eu products was also analyzed. The measurements were carried out using a KRATOS SUPRA instrument with a monochromated aluminium source.

4.3. X-ray diffraction (XRD)

XRD is a powerful non-destructive and analytical technique used for the characterization of crystalline materials. It provides information on structures, phases, texture, and other structural parameters such as average grain size, crystallinity, strain, and crystal defects (Kohli, 2012). XRD is based on constructive interference of monochromatic beam of X-rays scattered at specific angles from each set of lattice planes in a crystalline sample (Figure 4). The interaction of the incident X-rays with the sample produces constructive interference when conditions satisfy Bragg´s Law ($n\lambda=2d \sin \theta$) (Bish and Post, 1989). This law relates the wavelength of electromagnetic radiation to the diffraction angle and the lattice spacing in a crystalline sample. By scanning the sample through a range of 2θ angles, all possible diffraction directions of the lattice should be attained due to the random orientation of the powdered material. Finally, the diffracted X-rays are detected and processed. The peak intensities are determined by the atomic positions within the lattice planes. Therefore, the XRD pattern is the fingerprint of periodic atomic arrangements in a given material (Kohli, 2012). Standard database for X-ray powder diffraction patterns enables quick phase identification for a large variety of crystalline samples based on the comparison of d-spacings obtained with standard reference patterns (Fultz and Howe, 2008).

In this work we determined the size and crystalline phase of biogenic SeNPs produced by *S. bentonitica* cells. X-ray patterns were obtained with a Bruker D8 Advanced diffractometer associated to a LINXEYE detector available at the University of Granada. The obtained diffractograms were analysed using the software DIFFRAC PLUS.

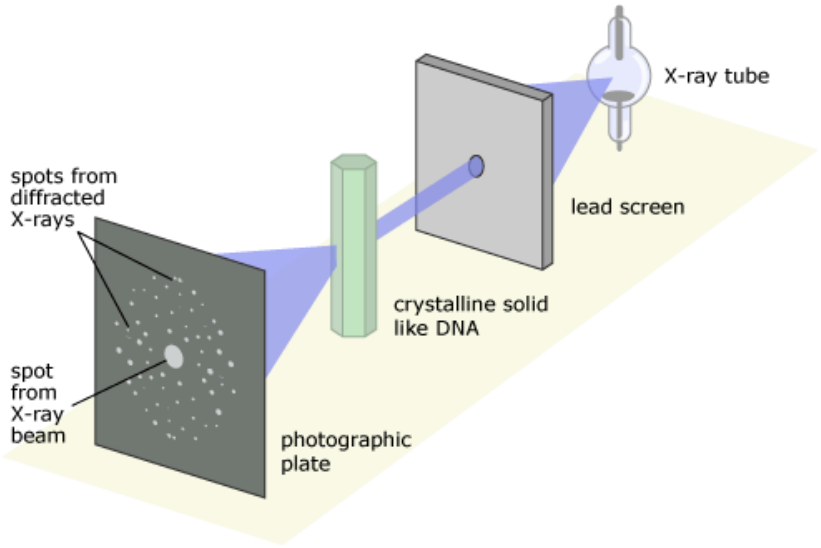

Figure 4. Schematic diagram of a X-ray diffraction system (https://undsci.berkeley.edu/article/0_0_0/dna_04).

4.4. X-ray absorption spectroscopy (XAS)

XAS was applied for complementary chemical characterization of the biologically produced Se nanostructures. Se K–edge X-ray absorption spectra were collected at the MARS beamline at the SOLEIL synchrotron facility (ring operated at 2.75 GeV with 400 mA) (Figure 5), which is the French bending magnet beamline dedicated to the study of radioactive materials (Sitaud et al., 2012), using a Si(220) double-crystal monochromator with horizontal dynamical focusing, and Pt-coated mirrors for vertical focusing and rejection of higher harmonics (Solari et al., 2009).

Figure 5. SOLEIL synchroton facilities located in Plateau de Saclay in Saint Aubin París (France) https://www.destination-paris-saclay.com/fr/actualites/a-la-une.php.

XAS is a well-established analytical technique used extensively for the characterization of the local chemical structure of different materials including semiconductors in solid or liquid, crystalline or amorphous, bulk or nanoscale form (Schnohr and Ridgway, 2015). Through this technique, a sample of interest is bombarded with x-rays of determined energy. Some of these x-rays are absorbed by the atoms in the sample, inducing the excitation of a core electron (Calvin, 2013). Once the absorption is determined and quantified for one energy of incident x-rays, the energy is changed slightly and the process repeated. By stepping through a range of energies in this way, a spectrum is created. The sharp rise typical of XAS spectrum is generally called the edge. At energies below the edge, incident x-rays do not have energy enough to excite electrons, while above the edge they do (Calvin, 2013). The XAS spectrum is commonly divided into the extended x-ray absorption fine structure (EXAFS) and the x-ray absorption near-edge structure (XANES) region (Figure 6). The EXAFS region comprises the oscilllations above the edge and provides reliable structural information concerning the local, short-range coordination environment and the chemical and electronic structure of specific sites within materials, including the number, chemical nature, and distance of neighboring atoms from the atomic site of interest (Ormerod, 2001). XANES region includes peaks and other features near or on the edge and basically provides information about the oxidation state of the atoms.

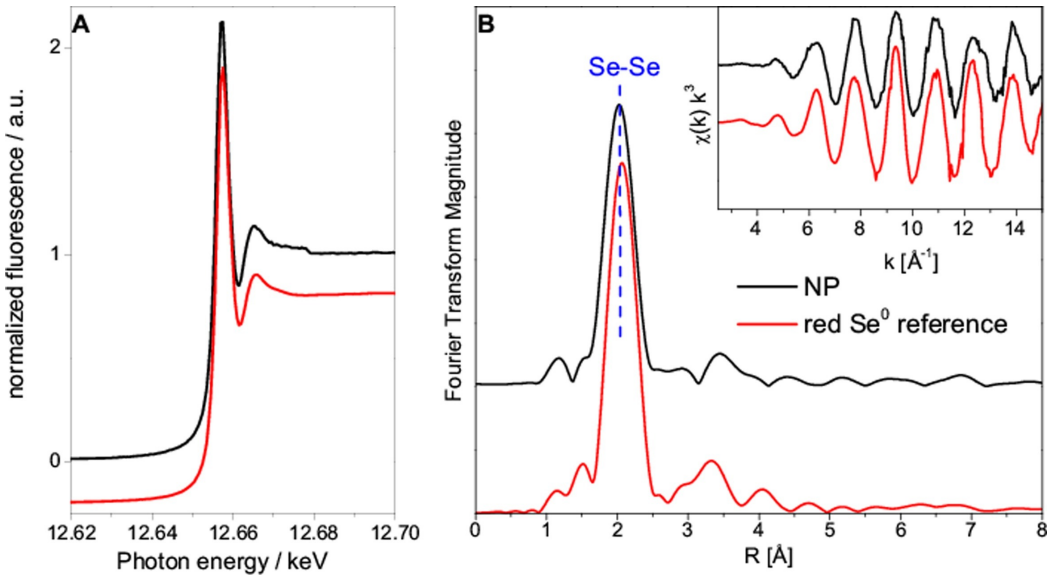

Figure 6. An example of Se-K XAS spectra of microbially formed SeNPs. XANES (A), and EXAFS Fourier Transform magnitude and k3-weighted EXAFS spectra as insert (B) (Vogel et al., 2018).

4.5. Time-resolved laser-induced fluorescence spectroscopy (TRLFS) analysis

TRLFS is a useful technique for the identification of certain actinide or lanthanide species resulting from various biogeochemical processes (Collins et al., 2011). Fluorescent metal ions

emmit fluorescence emission spectra and decay lifetimes when irradiated with laser pulses. This phenomenon occurs as a consequence of their transition from electronically excited states to the ground-state. Analysis of the emision spectra and lifetimes allows the identification of different chemical species produced of a fluorescent metal ion (Collins et al., 2011; Saito et al., 2015). Changes in metal speciation could lead to changes in fluorescence intensity, spectral shape, and decay lifetimes since metal ion fluorescence is sensitive to the inner-sphere coordination environment. For this reason, analysis of the obtained fluorescence decay can often reveal the presence of two or more species with similar fluorescence spectra but considerably different decay lifetimes (Günther et al., 2007; Saito et al., 2010).

TRLFS has been mainly applied to studies of actinide speciation in aqueous and solid phases as well as coordination of metal ions sorbed to mineral and bacterial surfaces (Collins et al., 2011). The TRLFS capability to analyse metal ion speciation under environmentally relevant micromolar to picomolar concentrations is of great significance for the application of this technology in systems of biogeochemical interest. In the present work, TRLFS measurements were done in order to determine the microbial functional groups from *S. bentonitica* involved in the Eu^{III}/Cm^{III}-bacteria interaction. For this purpose, the time-resolved luminescence spectra were recorded using a unique pulsed flash lamp pumped Nd:YAG-OPO laser system (Powerlite Precision II 9020 laser equipped with a Green PANTHER EX OPO from Continuum, Santa Clara, CA, USA). The luminescence spectra were detected using an optical multi-channel analyzer-system, consisting of an Oriel MS 257 monochromator and spectrograph with a 300 or 1200 line mm^{-1} grating and an AndoriStar ICCD camera (Lot-Oriel Group, Darmstadt, Germany). A more detailed description of the experimental setup and data evaluation of the luminescence spectra is described in Capítulo V.

5. Microscopic characterization of selenium and europium products

5.1. STEM-HAADF analysis

The morphology, elemental composition analysis and cellular location of Se and Eu products were analysed by using Scanning-Transmission Electron Microscopy (STEM) equipped with energy dispersive X-ray (EDX). EDX analysis was performed at 300 kV using a spot size of 4 Å and a live counting time of 50 s. In addition, the structural characterization of Se nanostructures was performed by using selected-area electron diffraction (SAED) and high-resolution TEM combined with FFT. All the samples were examined under High-Angle Annular Dark Field Scanning Transmission Electron Microscope (HAADF-STEM) FEI TITAN G2 80-300 (Figure 7) available from Centro de Instrumentación Científica at Universidad de

Granada (Granada, Spain). STEM specimen holders were cleaned by plasma prior to STEM analysis to minimize contamination.

5.2. VP-FESEM analysis

Variable Pressure Field Emission Scanning Electron Microscopy (VP-FESEM) equipped with an X-ray detector Raman spectroscopy system enabled an in situ 3-D structural and elemental characterization of the reduced Se produced by the cells of *S. bentonitica*. The samples were prepared as described in Ruiz-Fresneda et al. (2018) and analysed under Variable Pressure Field Emission Scanning Electron Microscope Zeiss SUPRA 40VP, available from Centro de Instrumentación Científica at Universidad de Granada (Granada, Spain).

5.3. FEG-ESEM analysis

Field Emission Gun Environmental Scanning Electron Microscopy (FEG-ESEM) equipped with secondary and circular backscatter electron detectors (ETD and CBS) enabled to determine the presence of organic matter surrounding the biogenic Se nanostructures. For this purpose, the samples were prepared as described in Ruiz-Fresneda et al. (2018) and analysed under FEG-SEM Microscope FEI QEMSCAN 650F.

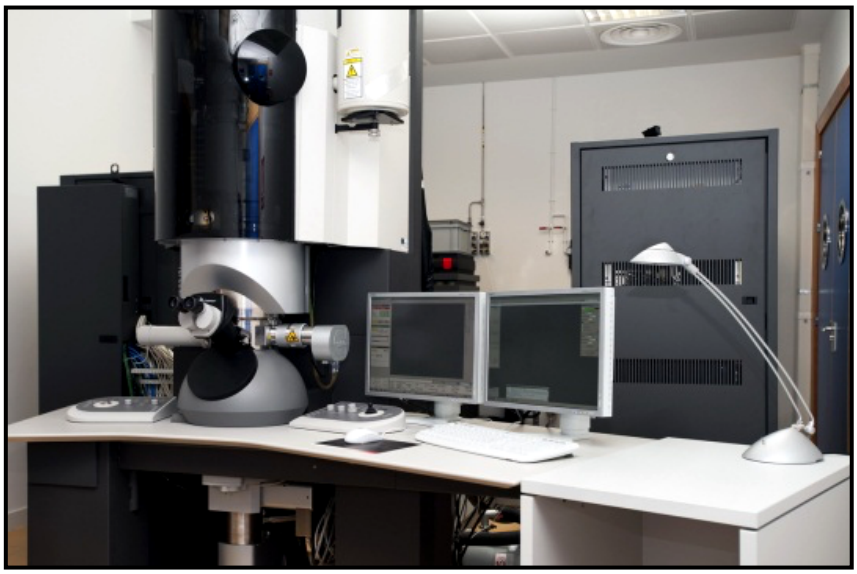

Figure 7. High-Angle Annular Dark Field Scanning Transmission Electron Microscope FEI TITAN G2 80-300 available at Centro de Instrumentación Científica (Universidad de Granada) (https://cic.ugr.es/servicios-y-unidades/ficha.php?codServicio=6&unidad=28).

CAPÍTULO I:

Stenotrophomonas bentonitica sp. nov., isolated from bentonite formations

Iván Sánchez-Castro[1], **Miguel A. Ruiz-Fresneda[1]**, Mohammed Bakkali[2], Peter Kämpfer[3], Stefanie P. Glaeser[3], Hans-Jürgen Busse[4], Margarita López-Fernández[1]†, Pablo Martínez-Rodríguez[1], Mohamed L. Merroun[1]

[1] Departamento de Microbiología, Campus de Fuentenueva, Universidad de Granada, 18071 Granada, Spain

[2] Departamento de Genética, Campus de Fuentenueva, Universidad de Granada, 18071 Granada, Spain

[3] Institut für Angewandte Mikrobiologie, Justus-Liebig-Universität Giessen, D-35392 Giessen, Germany

[4] Institut für Mikrobiologie, Veterinärmedizinische Universität Wien, A-1210 Wien, Austria

†Present address: Centre for Ecology and Evolution in Microbial Model Systems (EEMiS), Linnaeus University, Kalmar, Sweden

INTERNATIONAL JOURNAL OF SYSTEMATIC AND EVOLUTIONARY MICROBIOLOGY

TAXONOMIC DESCRIPTION
Sánchez-Castro *et al.*, *Int J Syst Evol Microbiol*
DOI 10.1099/ijsem.0.002016

MICROBIOLOGY SOCIETY

OPEN MICROBIOLOGY

Stenotrophomonas bentonitica sp. nov., isolated from bentonite formations

Iván Sánchez-Castro,[1,*] Miguel Angel Ruiz-Fresneda,[1] Mohammed Bakkali,[2] Peter Kämpfer,[3] Stefanie P. Glaeser,[3] Hans Jürgen Busse,[4] Margarita López-Fernández,[1]† Pablo Martínez-Rodríguez[1] and Mohamed Larbi Merroun[1]

Este capítulo ha sido publicado en la revista International Journal of Systematic and Evolutionary Microbiology (10.1099/ijsem.0.002016): *Sánchez-Castro, I., **Ruiz-Fresneda, M.A.**, Bakkali, M., Kämpfer, P., Glaeser, S.P., Busse, H.J., López-Fernández, M., Martínez-Rodríguez, P., Merroun, M.L., 2017a. Stenotrophomonas bentonitica sp. nov., isolated from bentonite formations. Int. J. Syst. Evol. Microbiol. 67 (8), 2779–2786. https://doi.org/10.1099/ijsem.0.002016*

1. Abstract

A Gram-stain negative, rod-shaped, aerobic bacterial strain, BII-R7^T, was isolated during a study targeting the culture-dependent microbial diversity occurring in bentonite formations from southern Spain. Comparative 16S rRNA gene sequence analysis showed that BII-R7^T represented a member of the genus *Stenotrophomonas* (class *Gammaproteobacteria*), and was related most closely to *Stenotrophomonas rhizophila* e-p10^T (99.2 % sequence similarity), followed by *Stenotrophomonas pavanii* ICB 89^T (98.5 %), *Stenotrophomonas maltophilia* IAM 12423^T, *Stenotrophomonas chelatiphaga* LPM-5^T, and *Stenotrophomonas tumulicola* T5916-2-1b^T (all 98.3 %). Pairwise sequence similarities to all other type strains of species of the genus *Stenotrophomonas* were below 98 %. Genome-based calculations (orthologous average nucleotide identity, original average nucleotide identity, genome-to-genome distance and DNA G+C percentage) indicated clearly that the isolate represents a novel species within this genus. Different phenotypic analyses, such as the detection of a quinone system composed of the major compound ubiquinone Q-8 and a fatty acid profile with iso-$C_{15:0}$ and anteiso-$C_{15:0}$ as major components, supported this finding at the same time as contributing to a comprehensive characterization of BII-R7^T. Based on this polyphasic approach comprising phenotypic and genotypic/molecular characterization, BII-R7^T can be differentiated clearly from its phylogenetic neighbours, establishing a novel species for which the name *Stenotrophomonas bentonitica* sp. nov. is proposed with BII-R7^T as the type strain (= LMG 29893^T = CECT 9180^T = DSM 103927^T).

Keywords: *Stenotrophomonas*; BII-R7^T; bentonite; ANI value

A large number of microbial strains were isolated in a study targeting the culture-dependent microbial diversity occurring in bentonite formations from southern Spain. This investigation aimed at understanding the impact of microbial processes on the performance of this type of material for deep geological disposal of nuclear wastes (López-Fernández et al., 2014). By using standard dilution plating technique on different culture media, including oligotrophic R2A medium (Reasoner and Geldreich, 1985), Luria–Bertani (LB) medium (Miller, 1972) and Nutrient Broth (NB), 32 microbial isolates (31 bacterial strains and 1 fungal strain) were isolated and characterized. The strain BII-R7^T, affiliated to the genus *Stenotrophomonas* (family *Xanthomonadaceae*, order *Xanthomonadales*, class *Gammaproteobacteria*) on the basis of 16S rRNA gene sequence divergence (López-Fernández et al., 2014), was further investigated.

Species of the genus *Stenotrophomonas* possess an important ecological role in the element cycle in nature (Ikemoto et al., 1980) and various potential biotechnological applications, for example as bioremediation agents (Binks et al., 1995; Ge and Ge, 2016; Ghosh and Saha, 2013; Merroun and Selenska-Pobell, 2008; Ryan et al., 2009) and are considered as potential plant growth-promoting and biocontrol organisms (Berg and Ballin, 1994; Nakayama et al., 1999), becoming a widely studied group. In this sense, the bacterial strain BII-R7^T showed high uranium and selenium tolerance, being able to grow up to 6 mM U (López-Fernández et al., 2014) and 100 mM Se (Ruiz-Fresneda MA, Gómez-Bolívar J, Sánchez-Castro I, Merroun ML, unpublished data). The taxonomy of the genus *Stenotrophomonas* has been subject to considerable revision over recent years. Originally, this genus was proposed when the species *Xanthomonas maltophilia* was reclassified as *Stenotrophomonas maltophilia* (Palleroni and Bradbury, 1993), and subsequently accommodated in the class *Gammaproteobacteria* (Moore et al., 1997). At the time of writing, the genus *Stenotrophomonas* comprises 13 species with validly published names isolated from a large range of natural and artificial environments and geographical regions including *S. maltophilia* (Palleroni and Bradbury, 1993), *Stenotrophomonas nitritireducens* (Finkmann et al., 2000), *Stenotrophomonas acidaminiphila* (Assih et al., 2002), *Stenotrophomonas rhizophila* (Wolf et al., 2002), *Stenotrophomonas koreensis* (Yang et al., 2006), *Stenotrophomonas humi* (Heylen et al., 2007), *Stenotrophomonas terrae* (Heylen et al., 2007), *Stenotrophomonas chelatiphaga* (Kaparullina et al., 2009), *Stenotrophomonas ginsengisoli* (Kim et al., 2010), *Stenotrophomonas panacihumi* (Yi et al., 2010), *Stenotrophomonas daejeonensis* (Lee et al., 2011), *Stenotrophomonas pavanii* (Ramos et al., 2011) and *Stenotrophomonas tumulicola* (Handa et al., 2016).

So far, species within the genus *Stenotrophomonas* have been described as being Gram-stain negative, non-endospore forming, rod-shaped, resistant to certain antibiotics and metals, and catalase-positive. Moreover, the predominant cellular fatty acid component is $C_{15:0}$ iso and the

DNA G+C content is between 64.0 and 69.1 % (Assih et al., 2002; Finkmann et al., 2000; Handa et al., 2016; Heylen et al., 2007; Kaparullina et al., 2009; Kim et al., 2010; Lee et al., 2011; Palleroni and Bradbury, 1993; Ramos et al., 2011; Wolf et al., 2002; Yang et al., 2006; Yi et al., 2010). BII-R7^T displays all these common characteristics. This fact, together with 16S rRNA gene sequencing (López-Fernández et al., 2014), confirms that BII-R7^T represents a member of the genus *Stenotrophomonas*. However, considering that 16S rRNA gene is not discriminative enough to classify certain strains at species level within this genus (Svensson-Stadler et al., 2012), a polyphasic approach comprising phenotypic and genotypic/molecular assays was employed to study the relationship of BII-R7^T with species of the genus *Stenotrophomonas*.

As a preliminary molecular characterization, almost the complete 16S rRNA gene was re-sequenced according to previously described methods (López-Fernández et al., 2014). The resulting sequence (1385 bp; GenBank accession number LT622838) was almost identical to original sequence (1454 bp; GenBank accession number HG800055) (López-Fernández et al., 2014) when aligning with the SILVA Incremental Aligner (SINA; v1.2.11) (Pruesse et al., 2012). For detailed phylogenetic placement of BII-R7^T, its 16S rRNA gene sequence was aligned with the SILVA Incremental Aligner and implemented into the "All species living tree project" (LTP) (Yarza et al., 2008) using the ARB software package release 5.2 (Ludwig et al., 2004) for analysis. Additionally, sequences not included in the LTP database were obtained from GenBank (http://www.ncbi.nlm.nih.gov/) and added to the database. Finally, the sequence alignment was checked manually. Pairwise sequence similarities were determined in ARB using the ARB Neighbour-joining tool without the application of an evolutionary model. Phylogenetic trees were reconstructed with the maximum-likelihood method using RAxML version 7.04 (Stamatakis, 2006) with General Time Reversible-GAMMA (GTR-GAMMA) and rapid bootstrap analysis, the maximum-parsimony method using DNAPARS v 3.6 (Felsenstein, 2005) and the neighbour-joining methods using ARB Neighbour-joining and the Jukes-Cantor correction (Jukes and Cantor, 1969). Independent of the applied treeing method, BII-R7^T was placed within the genus *Stenotrophomonas* and formed a distinct cluster with the type strain of *S. rhizophila* but not with any other type strains of species of the genus *Stenotrophomonas* (Figure 1). The clustering of the two strains was always supported by high bootstrap values. The two strains shared 98.8 % 16S rRNA gene sequence similarity among each other, based on the BLAST analysis in EzTaxon (Yoon et al., 2017), and 99.2 % sequence similarities based on the analysis in ARB. Pairwise 16S rRNA gene sequence similarities (calculated in ARB) between BII-R7^T and other type strains of the genus *Stenotrophomonas* were between 96.6 to 98.5 % 16S rRNA gene sequence similarity (Table S1). Sequence similarities of BII-R7^T to type strains of *S. pavanii* (98.5 %), *S. maltophilia*, *S. chelatiphaga*, and *S. tumulicola* (all 98.3 %) were above 98

%. All other sequence similarities were below 98 %. Phylogenetic analysis also included 16S rRNA gene sequences of strains misclassified as *Pseudomonas* species (Figure 1); pairwise 16S rRNA gene sequence similarities of BII-R7^T to those strains were always below 98.0 % (Table S1).

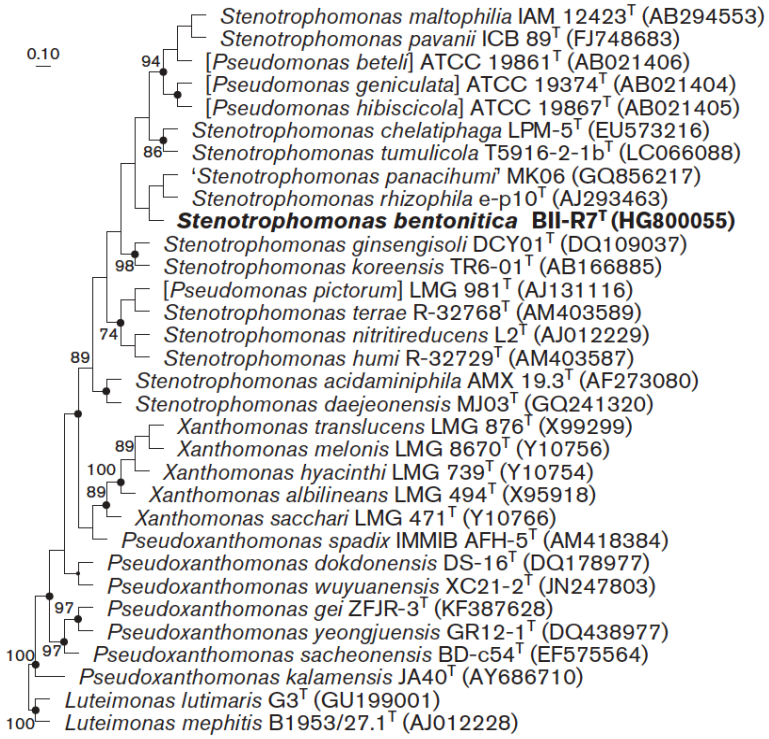

Figure 1. Maximum-likelihood phylogenetic tree based on nearly full-length 16S rRNA gene sequence of BII-R7^T and type strains of species of the genus *Stenotrophomonas* as well as species wrongly classified as members of the genus *Pseudomonas* and other related taxa. The 16S rRNA gene sequences of the type strains of *Luteimonas mephitis* and *Luteimonas lutimaris* were used as outgroups. Analysis based on 16S rRNA gene sequences between gene termini 67 and 1448 (according to the *Escherichia coli* numbering (Brosius et al., 1981)). Sequence accession numbers are given in parentheses, including the BII-R7^T sequence obtained originally in this work. Circles at branch point represent those branch points which were also present in the phylogenetic trees obtained with other treeing methods. Bootstrap values greater than 70 % are shown at branch points (percentages of 100 re-samplings). Bar, 0.1 substitutions per sequence position.

For more detailed phylogenetic analysis, nucleotide sequences of the *gyrB* region 1 and *gyrB* region 2 were analyzed according to the methods of Svensson-Stadler et al. (2012) including the *gyrB* gene sequences of all type strains of species of the genus *Stenotrophomonas*. The partial gene sequences of BII-R7^T were obtained from the genome sequence generated for the strain (see below). Reference sequences were taken either from Svensson-Stadler et al. (2012), Handa et al. (2016) or from published type strain genomes. The analysis was performed in MEGA 7 version 7.0 (Kumar et al., 2016). The nucleotide sequences alignment was obtained by the alignment of respective amino acid sequences using ClustalW implemented in MEGA7 and the

phylogenetic trees were reconstructed using the maximum-likelihood method and the GTR method (Nei and Kumar, 2000). The final tree based on 100 replications (bootstrap analysis). Pairwise sequence similarities were calculated based on the determination of *p*-distances using MEGA7. In the obtained phylogenetic trees, BII-R7^T clustered either with the type strain of *S. chelatiphaga* and subsequently with *S. rhizophila* (*gyrB*, region 1, Figure 2A) or directly with the type strain of *S. rhizophila* (*gyrB*, region 2, Figure 2B). Pairwise sequence similarities for both partial gene sequences for BII-R7^T to other species of the genus *Stenotrophomonas* were all below 90% (Tables S2 and S3) which supported the placement of BII-R7^T to a novel species according to Svensson-Stadler et al. (2012).

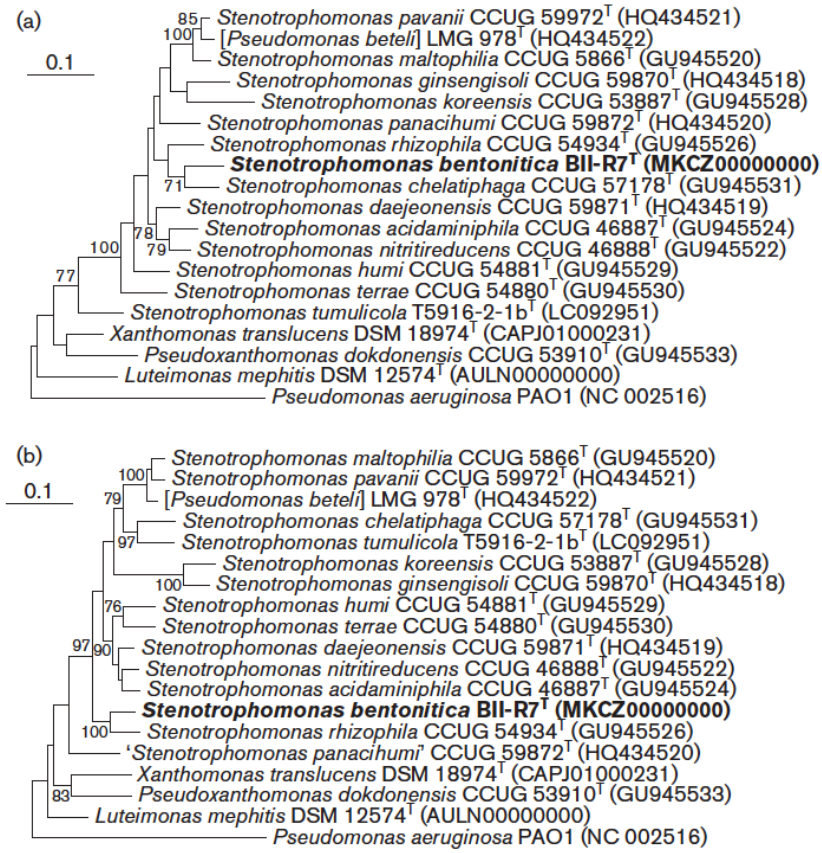

Figure 2. Maximum-likelihood phylogenetic tree based on partial *gyrB* gene sequence (a: region 1, b: region 2, according to Svensson-Stadler et al. (2012) of BII-R7^T and type strains of species of the genus *Stenotrophomonas* as well as species wrongly classified as members of the genus *Pseudomonas* and other related taxa. The *gyrB* gene sequences of *Luteimonas mephitis* and *Pseudomonas aeruginosa* were used as outgroup. Sequence accession numbers are given in parentheses. The trees were reconstructed in MEGA7 with the maximum-likelihood method using the GTR model and 100 replications. Bootstrap values greater than 70 % are shown at branch points (percentages of 100 re-samplings). Bar, 0.1 substitutions per sequence position.

Sequencing of the draft genome of BII-R7^T (GenBank accession number MKCZ00000000) allowed genomic analyses which clearly separated this strain from established species within the genus *Stenotrophomonas* and four other strains misclassified as *Pseudomonas* species. Reference genome sequences corresponding to type strains from all other species belonging to

these genera were obtained from public databases (Patil et al., 2016). Analysis of average nucleotide identity (ANI) with only the orthologous genes (Ortho-ANI) (Lee et al., 2016) produced values below the proposed 95-96 % threshold for the species boundary (Richter and Rossello-Mora, 2009) between BII-R7^T and reference genomes (Table 1). Based on this algorithm, the most closely related species with a validly published name was *S. rhizophila* DSM 14405^T with an Ortho-ANI value of 85.5 %. Moreover, as previously observed when using 16S rRNA gene sequence analysis, *S. pavanii* and *S. maltophilia* (together with *Pseudomonas geniculata*, *P. beteli* and *P. hibiscicola*, considered as synonyms of *S. maltophilia* (Anzai et al., 2000) followed *S. rhizophila* as most closely related species to BII-R7^T with Ortho-ANI values higher than 81.6 %. In this case, *S. tumulicola* was not considered since its genome was not available at the time. Similar indices calculated by different methods (original ANI value by Ortho-ANI software, ANI value by *EzBioCloud* website (http://www.ezbiocloud.net/tools/ani) based on algorithm published by Goris et al. (2007) and ANI value obtained through *Kostas lab* website (http://enve-omics.ce.gatech.edu/ani/) supported these results consistently (Table 1). The digital DNA-DNA hybridizations (dDDH) were determined online at http://ggdc.dsmz.de/distcalc2.php using the Genome-to-Genome Distance Calculation (GGDC) version 2.0 as described in Meier-Kolthoff et al. (2013) (Table 1). These calculations produced in silico DNA–DNA hybridization values well below the 70 %, threshold to delimit a bacterial species (Stackebrandt et al., 2002; Wayne et al., 1987). BII-R7^T and *S. rhizophila* were found to have a dDDH value of 29.9 % [identities/high-scoring segment pair (HSP) length formula], with a probability of equal to or above 70 % DDH of 0.1 %. All other comparisons resulted in lower dDDH values (Table 1). DNA G+C contents were calculated in-silico in all cases (Table 1). In the case of BII-R7^T it was 66.4 %, whereas those for the type strains of the closest relatives *S. rhizophila* and *S. pavanii* were 67.3 % and 66.9 %.

Based on DNA-based comparisons presented above, the four species of the genus *Stenotrophomonas* phylogenetically most closely related to BII-R7^T (*S. pavanii*, *S. maltophilia*, *S. rhizophila* and *S. chelatiphaga*) were compared with BII-R7^T. The other distantly related remaining species of the genus *Stenotrophomonas* were not included in this comparative survey. Certain cultural, physiological, chemotaxonomic and biochemical key features of these strains of members of the genus *Stenotrophomonas* were analyzed, even if these analyses had been performed in previous studies, in order to guarantee a comprehensive comparative study.

Table 1. Genome-based comparisons of BII-R7^T and other type strains of members of the genus *Stenotrophomonas* and *Pseudomonas* (misclassified) type strain genomes retrieved from Patil et al. (2016).

Reference strain	Ortho-ANI % (OAT)	Original ANI % (OrAT)	ANI % (EzBioCloud)	ANI calculation (Kostas Lab)	GGDC distance (DSMZ)*	mol% G+C (BII-R7^T =66.49 %)
Stenotrophomonas maltophilia ATCC 13637^T	81.6	80.8	80.9	83.3 (82.9–83.0)†	25.0	66.1
Stenotrophomonas rhizophila DSM 14405^T	85.5	85.0	85.1	86.0 (85.7–85.7)	29.9	67.3
Stenotrophomonas chelatiphaga DSM 21508^T	81.2	80.5	80.5	82.7 (82.4–82.4)	24.3	66.5
Stenotrophomonas acidaminiphila JCM 13310^T	81.0	80.3	80.3	82.5 (82.1–82.2)	24.3	68.0
Stenotrophomonas daejeonensis JCM 16244^T	81.0	80.1	80.1	82.2 (81.9–81.9)	24.1	67.8
Stenotrophomonas ginsengisoli DSM 24757^T	76.7	75.9	76.0	79.6 (79.4–79.5)	20.8	64.4
Stenotrophomonas humi DSM 18929^T	79.0	78.2	78.3	81.2 (80.8–80.8)	22.7	63.4
Stenotrophomonas koreensis DSM 17805^T	76.7	75.8	75.9	79.8 (79.6–79.5)	20.8	65.5
Stenotrophomonas nitritireducens DSM 12575^T	81.1	80.4	80.5	83.1 (82.5–82.5)	24.5	66.0
'*Stenotrophomonas panacihumi*' JCM 16536	79.1	78.3	78.3	81.2 (80.9–80.9)	22.5	68.0
Stenotrophomonas pavanii DSM 25135^T	81.7	80.9	81.0	83.3 (83.0–82.9)	25.2	66.9
Stenotrophomonas terrae DSM 18941^T	79.0	78.2	78.3	81.3 (80.9–80.9)	22.6	63.9
Pseudomonas pictorum JCM 9942^T	80.0	79.1	79.8	81.8 (81.6–81.5)	23.0	66.0
Pseudomonas geniculata JCM 13324^T	81.8	80.9	81.6	83.3 (82.9–82.8)	25.0	66.2
Pseudomonas beteli LMG 978^T	81.8	81.0	81.6	83.3 (83.0–83.0)	25.0	66.8
Pseudomonas hibiscicola ATCC 19867^T	81.6	80.9	81.5	83.2 (82.8–82.8)	24.8	66.4

*DDH estimate (identities/HSP length formula).

†Two-way ANI (One-way ANI 1–One-way ANI 2).

The morphology of cells grown on LB broth at 28 ºC for 24 h with shaking at 160 rpm was observed by scanning electron microscopy (Quanta 400, FEI; Figure S1). Gram staining, cell motility and the presence of flagella were determined according to the method of Komagata (1985). At physiological level, catalase activity was determined by assessing bubble production in 3 % (v/v) H_2O_2, and oxidase activity by using a 1 % (w/v) solution of tetramethyl-p-phenylenediamine (Kovacs, 1956). The growth capacity at various temperatures (4, 15, 20, 28, 37 and 40 ºC), NaCl concentrations (0, 0.5, 1, 1.5, 2.5 and 5 % at 28 ºC) and pH values (pH 4.0–13.0 using increments of 1.0 pH units at 28 ºC) was determined in TSB culture medium, except in the case of 0 % NaCl test which was performed in R2A culture medium. Anaerobic growth was not detected when cultivating BII-R7^T in serum bottles containing R2A broth, supplemented with thioglycolate (1 g/L) and the upper gas phase replaced with nitrogen. However, the ability to reduce nitrate indicates that anaerobic growth might occur under certain circumstances. Carbon sources utilization, acid production from carbon sources and some physiological characteristics were determined by using the API 20NE (48 h, 28 ºC), API 50CH (inoculated with AUX medium, 48 h, 28 ºC) and API ZYM (4 h, 28 ºC) galleries, respectively, according to the instructions of the manufacturer (bioMérieux) and the methods of Kämpfer et al. (1991). Some of these cultural and physiological characteristics of BII-R7^T, including carbon sources utilization and acid formation from these carbon sources, were compared with those of the reference strains (Table 2), and some differences were detected.

Table 2. Differential phenotypic characteristics between *Stenotrophomonas bentonitica* sp. nov. and phylogenetically closest species of the genus *Stenotrophomonas* with validly published names.

Strains: 1, BII-R7^T; 2, *S. rhizophila* DSM 14405^T; 3, *S. pavanii* DSM 25135^T; 4, *S. maltophilia* DSM 50170^T; 5, *S. chelatiphaga* DSM 21508^T. All data from this study. All strains were positive for catalase and protease (gelatin hydrolysis) activity and for acid formation from D-glucose, D-mannose and D-maltose. All strains were negative for acid formation from lactose, D-mannitol, dulcitol, adonitol, inositol, sorbitol, L-arabinose, raffinose, L-rhamnose, D-xylose, cellobiose, methyl-D-glucoside, melibiose and D-arabitol. All strains hydrolysed: aesculin, oNP-ß-D-galactopyranoside, pNP-α-D-glucopyranoside, pNP-ß-D-glucopyranoside, Bis-pNP-phosphate, pNP-phenyl-phosphonate, pNP-phosphoryl-choline, L-alanine-pNA, L-glutamate-gamma-3-carboxy-pNA and L-proline-pNA but did not hydrolyse pNP-ß-D-glucuronide. All strains utilised as sole source of carbon: N-Acetyl-D-galactosamine, N-Acetyl-D-glucosamine, D-glucose, D-maltose, D-mannose, acetate, propionate, fumarate, DL-lactate, malate, pyruvate, D-ribose, salicin and D-trehalose. None of the tested strains utilised: L-arabinose, D-galactose, D-gluconate, L-rhamnose, D-adonitol, D-inositol, D-mannitol, sorbitol, putrescine, adipate, 4-aminobutyrate, azelate, DL-3-hydroxybutyrate, itaconate, mesaconate, oxoglutarate, suberate, ß-alanine, L-aspartate, L-leucine, L-phenylalanine, L-serine, L-tryptophane, 3-hydroxybenzoate, 4-hydroxybenzoate and phenylacetate. Symbols: +, positive; -, negative; w, weakly positive.

Characteristic	1	2	3	4	5
Growth at/with:					
4 °C	–	+	–	–	–
40 °C	–	–	–	–	+
pH 12	–	–	+	–	–
5 % NaCl	–	–	–	+	–
Motility	–	–	–	+	+
Indole production	–	–	–	–	+
Nitrate reduction to nitrite	+	+	–	+	–
Hydrolysis of:					
pNP-β-D-xylopyranoside	+	+	+	–	–
Enzyme activity:					
Oxidase	–	+	–	–	+
Urease	–	–	–	+	–
β-Galactosidase	w	w	+	w	+
Utilization of:					
D-Fructose	–	–	+	+	–
Sucrose	–	+	+	+	–
D-Xylose	+	+	+	–	+
Maltitol	–	+	–	+	–
L-Histidine	–	–	+	+	+
Cellobiose	+	–	+	+	+
Glutarate	+	–	–	–	–
Melibiose	+	+	+	–	–
cis-Aconitate	–	–	+	+	–
trans-Aconitate	–	–	+	+	–
L-Alanine	–	–	+	+	+
L-Ornithine	–	–	–	+	–
L-Proline	–	–	+	+	+
p-Arbutin	+	–	+	+	–
Acid formation from:					
D-Galactose	–	–	–	–	+
Salicin	–	+	+	–	–

Biomasses subjected to extraction of polyamines, quinones and polar lipids were grown in PYE broth [0.3 % peptone from casein (w/v), 0.3 % yeast extract (w/v), pH 7.2] at 28 °C. Polyamines were extracted from biomasses harvested at the late exponential growth phase according to the protocol of Busse and Auling, (1988). HPLC equipment was described by Stolz et al. (2007) and conditions for HPLC analysis were described by Busse et al. (1997). The polyamine pattern of BII-R7^T consisted of the major polyamine spermidine [90.0 µmol (g dry weight)$^{-1}$], moderate amounts of spermine [8.5 µmol (g dry weight)$^{-1}$] and traces [< 0.2 µmol (g dry weight)$^{-1}$] of cadaverine, putrescine and 1,3-diaminopropane. This polyamine pattern was very similar to that of *S. chelatiphaga* DSM 21508^T which was found to contain also spermidine as the major polyamine [78.8 µmol (g dry weight)$^{-1}$], moderate amounts of spermine [6.2 µmol (g dry weight)$^{-1}$] and traces [< 0.2 µmol (g dry weight)$^{-1}$] of cadaverine, putrescine and 1,3-diaminopropane. On the other hand, the absence of significant amounts of cadaverine distinguish BII-R7^T and *S. chelatiphaga* DSM 21508^T from other species of the genus

Stenotrophomonas. *S. rhizophila* DSM 14405^T was found to contain a polyamine pattern consisting of the major polyamines spermidine [87.1 µmol (g dry weight)$^{-1}$] and cadaverine [17.5 µmol (g dry weight)$^{-1}$] and moderate amounts of spermine [4.5 µmol (g dry weight)$^{-1}$] and the polyamine pattern of *S. pavanii* DSM 25135^T contained the major polyamines spermidine [58.3 µmol (g dry weight)$^{-1}$] and cadaverine [16.3 µmol (g dry weight)$^{-1}$], small amounts of spermine [2.3 µmol (g dry weight)$^{-1}$] and traces [< 0.2 µmol (g dry weight)$^{-1}$] of putrescine. The polyamine pattern with high amounts of cadaverine resembles that of *S. maltophilia* which has been reported to show a pattern with almost equal amounts of cadaverine and spermidine (Auling et al., 1991).

Quinones and polar lipids were extracted from biomass harvested at the stationary growth phase applying the integrated protocol of Tindall (1990a; 1990b) and Altenburger et al. (1996). The HPLC equipment used for quinone analysis has benn described recently (Stolz et al., 2007). The quinone system consisted of ubiquinone Q-8 (98.8 %) and Q-7 (1.2 %). The polar lipid profiles (Figure S2) of BII-R7^T and the reference species showed the presence of the major lipid diphosphatidylglycerol, moderate amounts of phosphatidylglycerol and phosphatidylethanolamine and minor amounts of the unidentified aminophospholipid APL1. In the case of BII-R7^T and *S. chelatiphaga* DSM 21508^T their polar lipid profiles were almost identical showing only some small quantitative differences in the lipids detected. Also, *S. rhizophila* DSM 14405^T was highly similar but some minor lipids were not detected in this species (phospholipid PL1, and the two lipids L2 and L3, only visible after detecting total lipids). *S. pavanii* DSM 25135^T was distinguishable from BII-R7^T based on the presence of unidentified lipids including glycolipid GL1, aminolipid AL1, lipid L4 and phospholipid PL2. *S. maltophilia* DSM 50170^T could be distinguished from BII-R7^T by the presence of the unidentified lipids aminolipid AL2 and the two lipids L5 and L6 and absence of lipids L1, L2 and L3.

Biomass for fatty acid analysis was harvested after growth on TSA at 28 °C for 48 h. The analysis was performed as described by Kämpfer and Kroppenstedt (1996). Fatty acids were separated with a 5898A gas chromatograph (Hewlett Packard), respective peaks were automatically integrated and fatty acid names and percentages were determined with the Sherlock MIDI software v. 2.1 (TSBA v. 4.1). The fatty acid profiles of BII-R7^T was consistent with the profiles described for species of genus *Stenotrophomonas* as shown in Table 3, with the predominant unsaturated fatty acid iso-$C_{15:0}$ and anteiso-$C_{15:0}$ and a variety of iso-branched hydroxylated fatty acids, typical for representatives of the genus *Stenotrophomonas* (Table 3).

Table 3. Fatty acid compositions of BII-R7^T and other members of the genus *Stenotrophomonas*. Strains: 1, BII-R7^T; 2, *S. rhizophila* DSM 14405^T; 3, *S. pavanii* DSM 25135^T; 4, *S. maltophilia* DSM 50170^T; 5, *S. chelatiphaga* DSM 21508^T. All data from this study. Strains were grown on TSA at 28°C for 48 prior to analysis. Symbols: -, not detected.

Fatty acid	1	2	3	4	5
$C_{10:0}$	–	0.6	0.6	0.9	2.0
iso-$C_{11:0}$	3.7	3.0	3.3	3.0	4.2
Unknown ECL* 11.799	1.0	0.7	1.3	1.5	1.6
iso-$C_{11:0}$ 3-OH	2.0	1.6	1.4	1.8	2.9
iso-$C_{13:0}$	–	–	–	–	2.2
anteiso-$C_{13:0}$	–	–	–	–	2.0
iso-$C_{12:0}$ 3-OH	–	0.4	–	–	1.1
$C_{12:0}$ 3-OH	3.6	2.0	1.6	4.1	4.3
iso-$C_{14:0}$	1.4	1.0	0.8	–	4.0
$C_{14:0}$	2.3	1.0	1.9	2.5	15.8
iso-$C_{13:0}$ 3-OH	3.2	1.8	3.4	3.3	1.9
$C_{13:0}$ 2-OH	1.7	0.9	0.9	–	1.6
iso-$C_{15:1}$	1.1	1.6	–	–	6.3
iso-$C_{15:0}$	23.8	17.9	30.1	29.4	10.6
anteiso-$C_{15:0}$	19.4	22.2	23.3	13.3	10.8
$C_{15:0}$	0.9	0.7	–	–	1.4
iso-$C_{16:0}$	4.0	3.7	1.9	–	1.1
$C_{16:1}\omega 9c$	2.3	3.2	2.2	4.2	3.9
Summed feature 3†	9.2	8.4	6.1	8.3	13.7
$C_{16:0}$	9.4	8.6	7.0	13.7	7.4
iso-$C_{17:1}\omega 9c$	7.5	10.0	4.0	3.9	1.5
iso-$C_{17:0}$	2.8	4.8	4.2	4.7	–
anteiso-$C_{17:0}$	–	0.9	1.0	–	–
$C_{17:1}\omega 8c$	–	0.7	–	–	–
cyclo-$C_{17:0}$	1.7	1.6	2.4	–	–
$C_{18:1}\omega 9c$	–	1.0	1.7	2.2	–
$C_{18:1}\omega 7c$	–	1.4	0.9	1.7	–

*ECL, equivalent chain length.

†Summed feature 3: $C_{16:1}\omega 7c$/ikso-$C_{15:0}$ 2-OH.

BII-R7^T shows molecular and phenotypic characteristics typical of the genus *Stenotrophomonas* while it can be clearly differentiated from other members of this genus by a number of significant characteristics. At molecular level, the 16S rRNA and *gyrB* phylogenetic analyses and the different genome-based indices calculated confirmed unequivocally the status of the BII-R7^T as a novel species and that *S. rhizophila*, *S. maltophilia*, *S. pavanii* and *S. chelatiphaga* are the most closely species within the genus. Besides these differences at DNA-level, these four most closely related species of the genus *Stenotrophomonas* can be distinguished with

regard to several phenotypic features (Table 2). Although results on polar lipid and polyamine analyses showed high similarity between BII-R7^T and *S. chelatiphaga* DSM 21508^T, these strains presented contrasting results regarding other aspects such as fatty acid composition (Table 3), motility, indole production capacity and certain enzymatic activities like oxidase (Table 2). In the case of the recently described novel species of the genus *Stenotrophomonas*, *S. tumulicola*, a comprehensive comparison was performed at different levels based on the data obtained for BII-R7^T in this study and the data extracted from the publication of Handa et al. (2016). 16S rRNA and *gyrB* genes sequence differences (Table S1-S3) were supported by a number of phenotypic differences such as growth inhibition in presence of 5 % NaCl, lack of cell motility and ability to reduce nitrates to nitrites.

On this basis, BII-R7^T represents a novel species of the genus *Stenotrophomonas*, for which the name *Stenotrophomonas bentonitica* sp. nov. is proposed.

2. Description of *Stenotrophomonas bentonitica* sp. nov.

Stenotrophomonas bentonitica (ben.to.ni'ti.ca. N.L. fem. adj. *bentonitica* referring to bentonite, the type of clay from which this bacterium was isolated).

Cells are Gram-stain negative, aerobic, non-motile, with no flagella and do not form endospores. When grown on LB agar at 28 ºC for 3 days, colonies are light yellow, smooth, convex and circular. Under these growing conditions, cells are straight rods 0.45-0.65 μm in width and 0.92-1.55 μm in length and occurred singly or in pairs. Growth takes place at 15-37 °C but not at 4 or 40 ºC (optimum is 28 ºC) at pH 5–10 but not at pH 4 or 11 (optimum at pH 7) and with 0–2.5 % NaCl but not with 5 % NaCl. The organism is able to reduce nitrate to nitrite but not to N_2. Catalase, leucine arylamidase, protease, esterase, esterase lipase, acid and alkaline phosphatase, naphtol-AS-BI- phosphohydrolase and β-glucosidase activities are positive but oxidase activity is negative. No indole production occurs. The strain is able to utilize the following carbon sources: D-xylose, cellobiose, glutarate, α-D-melibiose, p-arbutin, N-acetyl-D-galactosamine, N-acetyl-D-glucosamine, D-glucose, D-maltose, D-mannose, acetate, propionate, fumarate, DL-lactate, malate, pyruvate, D-ribose, salicin and D-trehalose. The predominant fatty acids are iso-$C_{15:0}$ and anteiso-$C_{15:0}$. In addition a variety of iso-branched hydroxylated fatty acids are produced. The polyamine pattern contains the major polyamine spermidine, moderate amounts of spermine and traces of cadaverine, putrescine and 1,3-diaminopropane. The quinone system is composed of the major compound ubiquinone Q-8 and small amounts of Q-7. The polar lipid profile contains the major lipid diphosphatidylglycerol,

moderate amounts of phosphatidylglycerol, and phosphatidylethanolamine and minor amounts of an unidentified aminophospholipid, a phospholipid, and three lipids.

The type strain is *Stenotrophomonas bentonitica* BII-R7^{T} (= LMG 29893^{T} = CECT 9180^{T} = DSM 103927^{T}), and was isolated from bentonite formations. The DNA G+C content of the type strain is 66.5 %.

3. Acknowledgements

The authors acknowledge the Euratom research and training programme 2014–2018 under grant agreement number 661880. We thank Ramón Roselló-Móra for his invaluable assistance and comments during the different stages of this work and Professor Bernhard Schink for help with etymology. First author wants to thank also Fritz Oehl and Javier Palenzuela for sharing their interest and knowledge on taxonomy.

4. Funding information

This study was supported by the European Regional Development Fund (ERDF)-co-financed Grants CGL2012-36505 and CGL2014-59616-R (Ministerio de Ciencia e Innovación, Spain; 80% funded by ERDF) and the Introduction to Research Fellowship for Master students of the University of Granada.

5. Conflicts of interest

The authors declare that there are no conflicts of interest.

6. Ethical statement

No experiments with humans or animals were carried out.

7. Supplementary material

Table S1. Pairwise 16S rRNA gene sequences similarities of strain BII-R7^{T} to type strains of all *Stenotrophomonas* species as well as wrongly classified *Pseudomonas* species. Pairwise 16S rRNA gene sequence similarities were determined in ARB using the ARB Neighbour-joining tool without using an evolutionary model for sequence similarity calculations. Red highest (100%) to green lowers 16S rRNA gene sequence similarities.

	***S. bentonitica* BII-R7^{T} (HG800055)**	*S. rhizophila* e-p10^{T} (AJ293463)	*S. panacihumi* MK06^{T} (GQ856217)	*S. maltophilia* IAM 12423^{T} (AB294553)	*S. pavanii* ICB 89^{T} (FJ748683)	[*P. beteli*] ATCC 19861^{T} (AB021406)	[*P. geniculata*] ATCC 19374^{T} (AB021404)	[*P. hibiscicola*] ATCC 19867^{T} (AB021405)	*S. chelatiphaga* LPM-5^{T} (EU573216)	*S. tumulicola* T5916-2-1b^{T} (LC066089)	*S. ginsengisoli* DCY01^{T} (DQ109037)	*S. koreensis* TR6-01^{T} (AB166885)	[*P. pictorum*] LMG 981^{T} (AJ131116)	*S. terrae* R-32768^{T} (AM403589)	*S. nitritireducens* L2^{T} (AJ012229)	*S. humi* R-32729^{T} (AM403587)	*S. acidaminiphila* AMX19^{T} (AF273080)	*S. onas daejeonensis* MJ03^{T} (GQ241320)
***Stenotrophomonas bentonitica* BII-R7^{T} (HG800055)**	100	99.2	97.9	98.3	98.5	97.8	97.9	97.7	98.3	98.3	97	97.2	97.3	97.3	97.4	97.8	96.8	96.6
Stenotrophomonas rhizophila e-p10^{T} (AJ293463)	99.2	100	98.7	97.9	98.1	97.5	97.9	97.7	98.3	98.4	96.5	97.1	97.3	97.4	97.3	97.6	96.9	96.3
Stenotrophmonas panacihumi MK06^{T} (GQ856217)	97.9	98.7	100	97.4	97.6	97	97.3	97.1	97.7	97.8	96	96.4	96.4	96.6	96.6	97	96.3	96.1
Stenotrophomonas maltophilia IAM 12423^{T} (AB294553)	98.3	97.9	97.4	100	99.7	99.4	99.4	99.5	98.6	98.6	96.6	97.2	97.1	97.4	97.5	97.5	97.2	97
Stenotrophomonas pavanii ICB 89^{T} (FJ748683)	98.5	98.1	97.6	99.7	100	99.1	99.3	99.2	98.6	98.7	96.7	97.3	97.1	97.4	97.5	97.6	97.2	97
[*Pseudomonas beteli*] ATCC 19861^{T} (AB021406)	97.8	97.5	97	99.4	99.1	100	99.2	99.3	98.2	98.3	96.7	97	96.6	97	97.2	97	97.1	96.9
[*Pseudomonas geniculata*] ATCC 19374^{T} (AB021404)	97.9	97.9	97.3	99.4	99.3	99.2	100	99.5	98.6	98.7	96.8	97.7	97	97.4	97.2	97.2	97.2	96.5
[*Pseudomonas hibiscicola*] ATCC 19867^{T} (AB021405)	97.7	97.7	97.1	99.5	99.2	99.3	99.5	100	98.4	98.5	96.9	97.3	96.8	97.1	97	97	97	96.6
Stenotrophomonas chelatiphaga LPM-5^{T} (EU573216)	98.3	98.3	97.7	98.6	98.6	98.2	98.6	98.4	100	99.4	97.4	97.6	97.1	97.4	97.2	97.4	97	97
Stenotrophimonas tumulicola T5916-2-1b^{T} (LC066089)	98.3	98.4	97.8	98.6	98.7	98.3	98.7	98.5	99.4	100	97.1	97.7	97.4	97.6	97.4	97.7	97.4	97
Stenotrophomonas ginsengisoli DCY01^{T} (DQ109037)	97	96.5	96	96.6	96.7	96.7	96.8	96.9	97.4	97.1	100	98.2	96.7	96.8	96.5	97.1	96.3	96.6
Stenotrophomonas koreensis TR6-01^{T} (AB166885)	97.2	97.1	96.4	97.2	97.3	97	97.7	97.3	97.6	97.7	98.2	100	96.9	97.5	97.3	97.1	97.5	96.5
[*Pseudomonas pictorum*] LMG 981^{T} (AJ131116)	97.3	97.3	96.4	97.1	97.1	96.6	97	96.8	97.1	97.4	96.7	96.9	100	98.8	98.7	98.7	98.1	96.9
Stenotrophomonas terrae R-32768^{T} (AM403589)	97.3	97.4	96.6	97.4	97.4	97	97.4	97.1	97.4	97.6	96.8	97.5	98.8	100	99.3	99	98.6	97.1
Stenotrophomonas nitritireducens L2^{T} (AJ012229)	97.4	97.3	96.6	97.5	97.5	97.2	97.2	97	97.2	97.4	96.5	97.3	98.7	99.3	100	99.1	98.5	97.4
Stenotrophomonas humi R-32729^{T} (AM403587)	97.8	97.6	97	97.5	97.6	97	97.2	97	97.4	97.7	97.1	97.1	98.7	99	99.1	100	98	97.4
Stenotrophomonas acidaminiphila AMX19^{T} (AF273080)	96.8	96.9	96.3	97.2	97.2	97.1	97.2	97	97	97.4	96.3	97.5	98.1	98.6	98.5	98	100	98.3
Stenotrophomonas daejeonensis MJ03^{T} (GQ241320)	96.6	96.3	96.1	97	97	96.9	96.5	96.6	97	97	96.6	96.5	96.9	97.1	97.4	97.4	98.3	100

Table S2. Pairwise *gyrB* gene (region 1) sequences similarities of strain BII-R7^{T} and type strains of species of the genus *Stenotrophomonas* as well as the wrongly-classified strain *Pseudomonas beteli*. Pairwise *gyrB* gene sequence similarities were calculated based on *p*-distances in MEGA 7. Red highest (100%) to green lowers *gyrB* gene sequence similarities.

	S. bentonitica BII-R7^{T} (MKCZ00000000)	*S. chelatiphaga* CCUG 57178^{T} (GU945517)	*S. daejeonensis* CCUG 59871^{T} (HQ434503)	*S. rhizophila* CCUG 54934^{T} (GU945512)	*S. pavanii* CCUG 59972^{T} (HQ434505)	[*P. beteli*] LMG 978^{T} (HQ434506)	*S. ginsengisoli* CCUG 59870^{T} (HQ434502)	*S. nitritireducens* CCUG 46888^{T} (GU945508)	*S. acidaminiphila* CCUG 46887^{T} (GU945510)	*S. maltophilia* CCUG 5866^{T} (GU945506)	*S. terrae* CCUG 54880^{T} (GU945516)	*S. panacihumi* CCUG 59872^{T} (HQ434504)	*S. humi* CCUG 54881^{T} (GU945515)	*S. tumulicola* T5916-2-1b^{T} (LC092950)	*S. koreensis* CCUG 53887^{T} (GU945514)
S. bentonitica BII-R7^{T} (MKCZ00000000)	100.0	89.9	89.3	89.1	88.2	88.1	87.7	87.6	87.3	87.1	86.7	86.4	86.2	83.3	83.0
S. chelatiphaga CCUG 57178^{T} (GU945517)	89.9	100.0	88.3	89.0	87.7	88.1	87.3	87.5	86.9	87.6	85.9	86.4	88.6	83.1	83.0
S. daejeonensis CCUG 59871^{T} (HQ434503)	89.3	88.3	100.0	90.4	90.5	90.0	87.8	92.2	92.1	89.5	88.4	90.0	90.4	84.2	85.5
S. rhizophila CCUG 54934^{T} (GU945512)	89.1	89.0	90.4	100.0	89.3	89.2	87.4	89.0	87.6	88.3	87.0	87.5	89.0	83.7	85.5
S. pavanii CCUG 59972^{T} (HQ434505)	88.2	87.7	90.5	89.3	100.0	96.6	88.2	89.8	89.5	95.4	85.2	88.4	88.9	82.2	85.1
[*P. beteli*] LMG 978^{T} (HQ434506)	88.1	88.1	90.0	89.2	96.6	100.0	88.4	89.9	89.5	94.8	85.4	88.2	88.9	83.1	85.3
S. ginsengisoli CCUG 59870^{T} (HQ434502)	87.7	87.3	87.8	87.4	88.2	88.4	100.0	88.1	88.2	88.5	85.1	86.7	86.7	82.2	85.4
S. nitritireducens CCUG 46888^{T} (GU945508)	87.6	87.5	92.2	89.0	89.8	89.9	88.1	100.0	92.9	89.5	87.7	89.7	88.5	83.0	86.2
S. acidaminiphila CCUG 46887^{T} (GU945510)	87.3	86.9	92.1	87.6	89.5	89.5	88.2	92.9	100.0	89.7	86.2	89.5	88.6	83.2	85.9
S. maltophilia CCUG 5866^{T} (GU945506)	87.1	87.6	89.5	88.3	95.4	94.8	88.5	89.5	89.7	100.0	84.6	88.1	88.6	82.7	86.4
S. terrae CCUG 54880^{T} (GU945516)	86.7	85.9	88.4	87.0	85.2	85.4	85.1	87.7	86.2	84.6	100.0	86.0	87.4	84.4	81.5
S. panacihumi CCUG 59872^{T} (HQ434504)	86.4	86.4	90.0	87.5	88.4	88.2	86.7	89.7	89.5	88.1	86.0	100.0	87.5	81.6	85.5
S. humi CCUG 54881^{T} (GU945515)	86.2	88.6	90.4	89.0	88.9	88.9	86.7	88.5	88.6	88.6	87.4	87.5	100.0	84.9	86.3
S. tumulicola T5916-2-1b^{T} (LC092950)	83.3	83.1	84.2	83.7	82.2	83.1	82.2	83.0	83.2	82.7	84.4	81.6	84.9	100.0	80.5
S. koreensis CCUG 53887^{T} (GU945514)	83.0	83.0	85.5	85.5	85.1	85.3	85.4	86.2	85.9	86.4	81.5	85.5	86.3	80.5	100.0

Table S3. Pairwise *gyrB* gene (region 2) sequences similarities of strain BII-R7^{T} and type strains of species of the genus *Stenotrophomonas* as well as the wrongly-classified strain *Pseudomonas beteli*. Pairwise *gyrB* gene sequence similarities were calculated based on *p*-distances in MEGA 7. Red highest (100%) to green lowers *gyrB* gene sequence similarities.

	S. bentonitica BII-R7^{T} (MKCZ00000000)	*S. rhizophila* CCUG 54934^{T} (GU945526)	*S. acidaminiphila* CCUG 46887^{T} (GU945524)	*S. pavanii* CCUG 59972^{T} (HQ434521)	*S. daejeonensis* CCUG 59871^{T} (HQ434519)	*S. nitritireducens* CCUG 46888^{T} (GU945522)	[*P. beteli*] LMG 978^{T} (HQ434522)	*S. maltophilia* CCUG 5866^{T} (GU945520)	S. humi CCUG 54881T (GU945529)	*S. tumulicola* T5916-2-1b^{T} (LC092951)	*S. terrae* CCUG 54880^{T} (GU945530)	*S. chelatiphaga* CCUG 57178^{T} (GU945531)	*S. panacihumi* CCUG 59872^{T} (HQ434520)	*S. ginsengisoli* CCUG 59870^{T} (HQ434518)	*S. koreensis* CCUG 53887^{T} (GU945528)
S. bentonitica BII-R7^{T} (MKCZ00000000)	100.0	87.2	84.4	84.3	83.9	83.7	82.6	82.5	81.9	81.5	81.5	78.3	77.7	73.5	72.5
S. rhizophila CCUG 54934^{T} (GU945526)	87.2	100.0	83.6	82.9	82.9	82.5	82.6	82.7	80.9	80.5	80.4	78.5	76.0	73.6	72.8
S. acidaminiphila CCUG 46887^{T} (GU945524)	84.4	83.6	100.0	83.3	91.4	92.1	82.2	82.6	86.8	82.3	87.1	82.2	78.8	74.6	74.6
S. pavanii CCUG 59972^{T} (HQ434521)	84.3	82.9	83.3	100.0	84.4	82.9	93.4	93.8	82.2	82.0	80.2	82.2	76.9	75.5	74.5
S. daejeonensis CCUG 59871^{T} (HQ434519)	83.9	82.9	91.4	84.4	100.0	92.3	83.3	83.6	86.8	82.2	87.5	82.3	80.8	75.0	74.5
S. nitritireducens CCUG 46888^{T} (GU945522)	83.7	82.5	92.1	82.9	92.3	100.0	83.9	82.7	86.5	81.9	87.4	82.6	78.8	75.5	74.9
[*P. beteli*] LMG 978^{T} (HQ434522)	82.6	82.6	82.2	93.4	83.3	83.9	100.0	93.8	83.2	83.2	80.4	83.3	76.2	73.9	72.9
S. maltophilia CCUG 5866^{T} (GU945520)	82.5	82.7	82.6	93.8	83.6	82.7	93.8	100.0	82.9	83.2	79.8	83.0	75.9	74.3	74.1
S. humi CCUG 54881^{T} (GU945529)	81.9	80.9	86.8	82.2	86.8	86.5	83.2	82.9	100.0	80.2	85.8	81.8	75.3	74.5	73.1
S. tumulicola T5916-2-1b^{T} (LC092951)	81.5	80.5	82.3	82.0	82.2	81.9	83.2	83.2	80.2	100.0	78.5	83.9	74.8	75.0	72.9
S. terrae CCUG 54880^{T} (GU945530)	81.5	80.4	87.1	80.2	87.5	87.4	80.4	79.8	85.8	78.5	100.0	79.4	76.7	73.2	72.4
S. chelatiphaga CCUG 57178^{T} (GU945531)	78.3	78.5	82.2	82.2	82.3	82.6	83.3	83.0	81.8	83.9	79.4	100.0	73.5	72.4	71.2
S. panacihumi CCUG 59872^{T} (HQ434520)	77.7	76.0	78.8	76.9	80.8	78.8	76.2	75.9	75.3	74.8	76.7	73.5	100.0	69.1	70.8
S. ginsengisoli CCUG 59870^{T} (HQ434518)	73.5	73.6	74.6	75.5	75.0	75.5	73.9	74.3	74.5	75.0	73.2	72.4	69.1	100.0	87.1
S. koreensis CCUG 53887^{T} (GU945528)	72.5	72.8	74.6	74.5	74.5	74.9	72.9	74.1	73.1	72.9	72.4	71.2	70.8	87.1	100.0

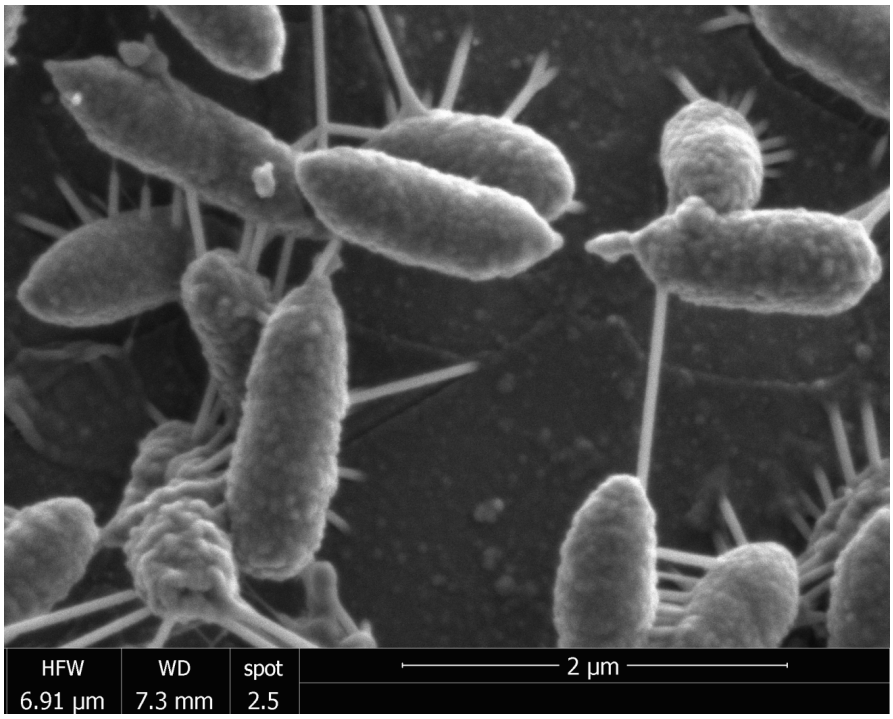

Figure S1. Scanning Electron Microscope (Quanta 400; FEI) image of BII-R7^T cells grown on LB broth at 28 ºC for 24 h with shaking at 160 rpm.

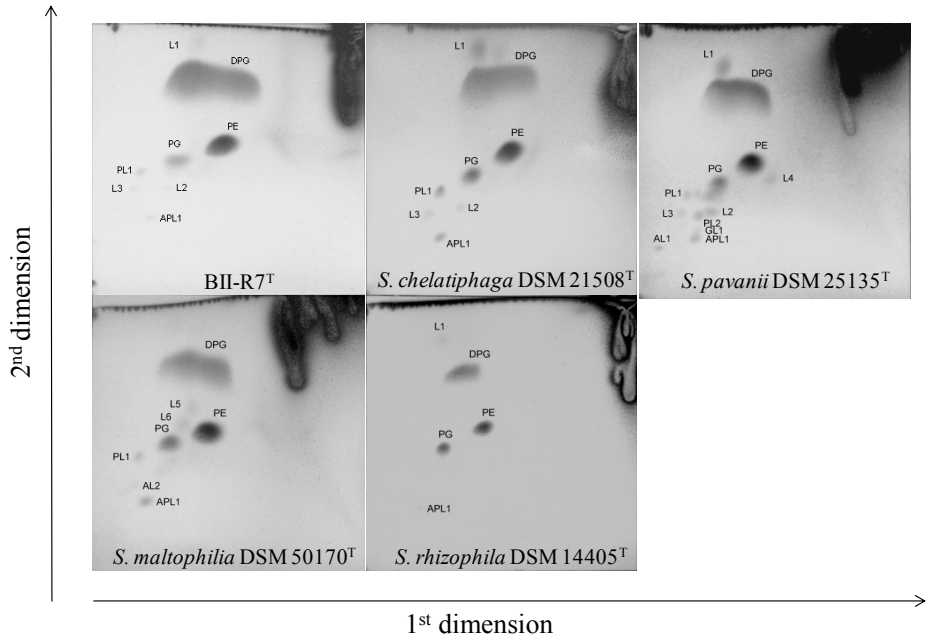

Figure S2. Polar lipid profiles of strain BII-R7^T and the species *S. pavanii* DSM 25135^T, *S. maltophilia* DSM 50170^T, *S. rhizophila* DSM 14405^T, *S. chelatiphaga* DSM 21508^T after two-dimensional thin-layer chromatography and visualized using ethanolic molybdatophosphoric acid. DPG, diphosphatidylglycerol; PG, phosphatidylglycerol; PE, phosphatidylethanolamine; GL1, unidentified glycolipid; APL1, unidentified aminophospholipid; PL1, PL2, unidentified phospholids; AL1, AL2, unidentified aminolipids; L1 – L6, unidentified polar lipid not reacting with the spray reagents specific for free amino groups, phosphate or sugar moieties.

CAPÍTULO II:

Green synthesis and biotransformation of amorphous se nanospheres to trigonal 1d se nanostructures: impact on se mobility within the concept of radioactive wastes disposal

Miguel A. Ruiz Fresneda[1], Josemaría Delgado Martín[1], Jaime Gómez Bolívar[1], María V. Fernández Cantos[1], Germán Bosch-Estévez[1], Marcos F. Martínez Moreno[1], Mohamed L. Merroun[1]

[1]Department of Microbiology, University of Granada, Granada, Spain

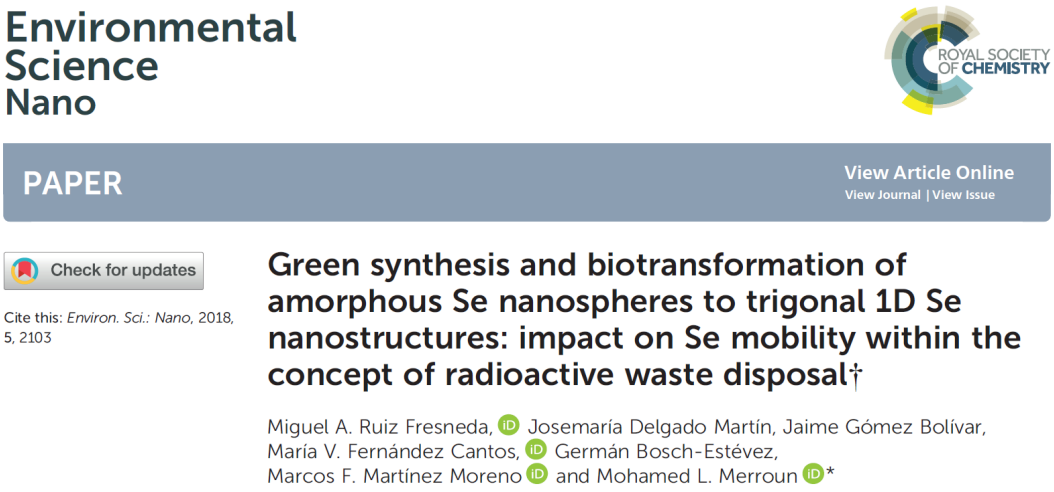

Este capítulo ha sido publicado en la revista Environmental Science: Nano (10.1039/c8en00221e): ***Ruiz-Fresneda, M.A.***, *Delgado Martín, J., Gómez Bolívar, J., Fernández Cantos, M. V., Bosch-Estévez, G., Martínez Moreno, M.F., Merroun, M.L., 2018. Green synthesis and biotransformation of amorphous Se nanospheres to trigonal 1D Se nanostructures: Impact on Se mobility within the concept of radioactive waste disposal. Environ. Sci. Nano. 5, 2103–2116. https://doi.org/10.1039/c8en00221e*

1. Abstract

Nuclear wastes containing radionuclides including selenium isotopes, Se^{79}, will be disposed in future deep geological repositories (DGR). Due to the long lifetime of these radioisotopes, studies on the impact of microbial processes on their chemical speciation would contribute significantly to understanding the risks associated with these repositories. Here we report a green method for biogenic reduction of Se^{IV}, production of amorphous Se^0 (a-Se) nanospheres and their subsequent transformation to one-dimensional (1D) trigonal selenium (t-Se) nanostructures using a combination of methods (XRD, STEM-HAADF, HRTEM/EDX, ESEM, etc.). The bacterial strain used, *Stenotrophomonas bentonitica*, was isolated from Spanish bentonites considered as artificial barriers for future Spanish repositories. After 24 h of incubation, 30-200 nm sized biogenic individual a-Se nanospheres were synthesized and then started to coalesce forming aggregates after 48 and 72 h of incubation. The 144 h sample presented a mixture of single crystal and polycrystalline 1D t-Se nanostructures with different shapes (*e.g*. nanowires, hexagonal, polygonal, etc.) and diameters of 30-400 nm, in addition to a-Se nanospheres. The HRTEM analysis showed that the 1D nanostructures presented different lattice spacing corresponding to (100), (101) and (111) planes of t-Se. Thus, a-Se nanospheres were initially synthesized and then would transform into t-Se nanostructures. STEM-HAADF and ESEM revealed that the cells and their extracellular proteins play an important role in this transformation process. Due to the low solubility of t-Se nanostructures compared to that of a-Se nanospheres and Se^{IV}, the mobility of selenium in future repositories may be significantly reduced.

Keywords: *Stenotrophomonas*, selenium nanostructures, reduction, transformation, repository

2. Introduction

Radioactive wastes produced mainly by nuclear energy industry contain materials contaminated with radionuclides (e.g. uranium, curium, selenium, etc.). Due to their toxicity, nuclear wastes will be disposed of for a long period of time until their toxicity decreases to non-hazardous levels. For this purpose, the deep geological repositories (DGRs) consisting on the encapsulation of radioactive waste in metal containers surrounded by artificial and natural barriers, have been proposed as the safest option for its disposal in the near future (IAEA, 2003). In different countries, bentonite clay formations have been selected as reference material for safety barriers in a DGR. In Spain, bentonite formations located in Cabo de Gata Natural Park (Almeria) were selected for their geochemical and mineralogical properties as artificial barrier reference materials (Villar et al., 2006). High microbial diversity of these Spanish clays was shown by means of culture dependent and independent techniques (López-Fernández et al., 2015; 2014). In addition, more than 100 microbial strains were isolated from these bentonites including a novel species of the genus *Stenotrophomonas* (*Stenotrophomonas bentonitica* BII-R7) (Sánchez-Castro et al., 2017a; Capítulo I).

The microbial communities of the selected artificial barriers can affect the safety and performance of future DGRs at 3 different levels by: i) transformation of clay minerals; ii) corrosion of metal canisters; and iii) mobilization of radionuclides through different interaction processes (Meleshyn, 2011). Microorganisms are able to interact with typical elements of radioactive wastes like selenium (Se), uranium (U) or curium (Cm) through different processes like biomineralization, biosorption or reduction leading to their mobilization or immobilization (Merroun et al., 2011; Moll et al., 2014; Prakash et al., 2009).

Selenium is considered a common component of high-level radioactive wastes (HLRW), particularly the Se^{79} isotope produced by nuclear fission reactions. Different studies have indicated Se^{79} isotope to be one of the critical radionuclides for the geological disposal of HLRW due to its ability to emit β particles (Jörg et al., 2010). Selenium can exist in the environment in different oxidation states [selenate (Se^{VI}), selenite (Se^{IV}), elemental selenium (Se^{0}) and selenide (Se^{-II})], whose toxicity is mainly related to their solubility (Di Gregorio et al., 2005). Se^{VI} and Se^{IV} are the most soluble and hence the most toxic forms of Se, being dominant species in mildly and strongly oxidizing conditions, respectively (Breynaert et al., 2010). On the other hand, Se^{0} has relatively less toxicity because of its low solubility, and it is considered the dominant species under reducing conditions (Breynaert et al., 2010). Therefore, it is important to investigate the speciation of Se associated with microbial populations occurring in different barriers in future DGRs to evaluate the safety of this kind of disposal. Different physico-

chemical and biological methods were applied to reduce Se^{VI} and Se^{IV} to produce elemental Se nanoparticles (SeNPs) (Chen et al., 2010; Li et al., 2014b). Several bacterial strains have been described for their ability to reduce toxic selenium (Se^{VI} and Se^{IV}) to less toxic forms (Se^{0}) producing NPs under different physiological conditions (Dungan et al., 2003; Lampis et al., 2014; Wadhwani et al., 2016). In general, the solubility and mobility of SeNPs seem to be affected by their physicochemical properties (size, shape, morphology, crystallinity, etc.), and also by the action of microbial processes through the synthesis of coating agents (proteins, polysaccharides, etc.) (Buchs et al., 2013; Jain et al., 2017; Keller et al., 2010).

Selenium could exist in three different allotropic forms: amorphous, monoclinic and trigonal phase (Chen et al., 2010). The trigonal selenium (t-Se) phase is one the most thermodynamically stable form of Se. This phase is characterized by its anisotropic crystal structure where the Se atoms are coordinated each other through covalent bonds forming infinite chains (Chen et al., 2010). Several studies have previously reported that bacteria can produce intracellular and extracellular amorphous Se (a-Se) nanospheres with a size ranging from 100 to 200 nm (Eswayah et al., 2017; Li et al., 2014b). To a lesser extent, few studies have also described the formation of biogenic trigonal and monoclinic selenium (t-Se and m-Se) (Prakash et al., 2009; Zhang et al., 2011). Ho et al., (2010) reported the control of organic solvents like DMSO in the transformation of biogenic a-Se nanospheres to 1D t-Se nanostructures (*e.g.* nanowires, nanoribbons, nanorods, etc.). In addition, the anaerobic biotransformation of a-Se nanospheres to t-Se nanorods has been shown for microbial granular activated sludge only under thermophilic (55 ºC) conditions (Jain et al., 2017). Biogenic Se nanorods were characterized by their low colloidal stability and high settling efficiency in comparison with the a-Se nanospheres making them highly attractive for bioremediation of Se contaminated waters (Jain et al., 2017). However, no Se nanorods were produced under mesophilic conditions (30 ºC). Here we report, the first study on the synthesis of Se nanostructures with different shapes (spherical, hexagonal, polygonal, and nanowires) and crystallographic properties under mesophilic conditions (30 ºC) by the cells of *S. bentonitica*, isolated from Spanish bentonite formations (Sánchez-Castro et al., 2017a). A scanning transmission electron microscope associated with a high angle annular field detector (STEM-HAADF) showed time-dependent transformation process of a-Se nanospheres to t-Se nanostructures with different morphologies (hexagonal, polygonal, and nanowires). Environmental scanning electron microscopy (ESEM) analysis revealed the impact of extracellular flagella-like proteins in this transformation process since the a-Se nanospheres aggregate along the axis of the flagella-like proteins whose monomers seem to embed these nanomaterials. This work provides new molecular insights into the impact of biogenic Se nanostructures on the mobility of this element and the effect of microbial processes on the

safety of the deep geological repository system. In addition, this diversity of Se nanostructure shapes will play a basic role in the development of nanoscience and technology.

3. Experimental

3.1. Bacterial strain and growth conditions

The bacterial strain used in the present work was recently described by our Research Group as a novel species named *S. bentonitica* BII-R7^T (Sánchez-Castro et al., 2017a; Capítulo I). This strain was isolated from Spanish bentonites collected from the Cabo de Gata Nature Park (Almeria, Spain) (López-Fernández et al., 2014). The cells were grown aerobically in Luria-Bertani (LB) broth medium (tryptone 10 g/l, yeast extract 5 g/l and NaCl 10 g/l, pH 7.0 ± 0.2) at 28 ºC and 180 rpm on a rotary shaker.

3.2. Metal solution preparation

Sodium selenite (Na_2SeO_3) (Sigma-Aldrich) was prepared as a 1M stock solution by dissolving appropriate quantities in distilled water. Finally, the solution was sterilized by filtration using 0.22-µm syringe filters (Sartorius®).

3.3. Determination of the minimal inhibitory concentration (MIC) of selenite for the bacterial growth

The minimal inhibitory concentrations (MICs) of Se^{IV} were determined in triplicate. Cells of the isolate were grown to the late exponential phase to a final optical density (O.D) of 0.9 (at 600 nm) in LB broth and washed twice with 0.9% NaCl. Finally, 10 µl of the cell suspension was inoculated to LB agar supplemented with increasing concentrations of Se^{IV} from 1 to 400 mM. Afterwards, the plates were incubated at 28 ºC for 48 h. The MIC was defined as the lowest concentration of the element at which complete inhibition of colony formation is observed (Rossbach et al., 2000).

3.4. X-ray diffraction (XRD)

XRD analysis was carried out to determine the size and crystalline phase of biogenic Se nanoparticles. *S. bentonitica* cells treated with 2 mM of Se^{IV} for 144 h were centrifuged at 10000 x g for 10 min and the resultant pellet was washed with double distilled water. The washed samples were dried at 28 ºC for 24 h. X-ray patterns of the biogenic SeNPs were

obtained with a Bruker D8 Advanced diffractometer associated to a LINXEYE detector available at the University of Granada. The obtained diffractograms were analysed using the software DIFFRAC PLUS. In order to calculate the average size of the nanoparticles, the Scherrer´equation ($D = k\lambda/\beta\cos\theta$) was used, where k is a constant whose value is approximately 0.9, λ is the wavelength of X-ray, β is the width in radians of the peak due to size effect and θ is the Bragg´s diffraction angle. Specifically, the particle size of the sample was estimated from the line width of the (101) XRD peak.

3.5. VP-FESEM and Raman spectroscopy analysis

A variable pressure field emission scanning electron microscopy (VP-FESEM) equipped with an X-ray detector Raman spectroscopy system enabled an in situ 3-D structural and elemental characterization of the SeNPs produced by the cells. Cell suspensions supplemented with 2 mM of Se^{IV} for 144 h were fixed in 3% glutaraldehyde in 0.05 M sodium cacodylate buffer (pH 7.2) for 24 h at 4 ºC . Afterwards, the samples were washed three times with the same buffer. The resultant pellets were fixed in 1% osmium tetroxide solution (OsO_4) in cacodylate buffer before dehydration in a graded ethanol solutions in water. The critical point drying method was also used to dehydrate the samples. Finally, they were coated with carbon and stored in a desiccator. The samples were analysed under a variable pressure field emission scanning electron microscope (Zeiss SUPRA 40VP).

3.6. STEM-HAADF analysis

The morphology, elemental composition analysis and cellular location of reduced Se were analysed by using a scanning-transmission electron microscopy (STEM) equipped with an energy dispersive X-ray (EDX) spectrometer. EDX analysis was performed at 300 kV using a spot size of 4 Å and a live counting time of 50 s. The structural characterization of Se nanostructures was performed by using selected-area electron diffraction (SAED) and high-resolution TEM combined with fast Fourier transform (FFT).

STEM samples consisting of Se^{IV}-treated cells (2 mM) were prepared as described in Merroun et al., (2005) after 24, 48, 72 and 144 h of incubation. Finally, the samples were examined under a high-angle annular dark field scanning transmission electron microscope (HAADF-STEM, FEI TITAN G2 80-300). STEM specimen holders were cleaned by plasma prior to STEM analysis to minimize contamination.

3.7. FEG-ESEM

A field emission gun environmental scanning electron microscopy (FEG-ESEM) equipped with secondary and circular backscatter electron detectors (ETD and CBS) enabled the determination of the presence of organic matter surrounding the biogenic SeNPs. For this purpose, the samples described above for VP-FESEM were also analysed by using this technique. In addition, this technique was also applied to explain the biotransformation of a-Se nanospheres to t-Se nanostructures. Thus, the cells where brought into contact for 24 h with solutions containing two different types of a-Se nanospheres: 1) chemically produced (CheSeNPs); and 2) organically produced SeNPs (OrgSeNPs). Chemical SeNPs were produced by reduction of sodium selenite (5 mM) by reduced glutathione (GSH) (20 mM) at 28 ºC. OrgSeNPs were synthesized using proteins (Bovine Serum Albumin; BSA) (0.01 g/l) in addition to GSH (20 mM) and Se^{IV} (2 mM). Finally, the samples were analysed under a FEG-SEM microscope (FEI QEMSCAN 650F).

3.8. Effect of selenite on the bacterial growth

The potential of *S. bentonitica* to tolerate selenite was assayed by growing the cells in LB liquid medium (30 ml) supplemented with 2 mM of Na_2SeO_3. Untreated (control) and Se^{IV}-treated cells were incubated at 28 ºC by shaking at 180 rpm. In addition, dead cells obtained by heating the biomass at 90 ºC and LB broth containing Se^{IV} (abiotic) were used as controls. Growth was evaluated by quantifying the total protein content in bacterial cell extracts using a modification of the method of Dhanjal and Cameotra (2010). The total protein content was correlated with the increase in the cell growth. A 1 ml aliquot of bacterial culture was taken at different time intervals to measure growth based on the protein content of the cells by using Bradford reagent (Bio-Rad®). BSA was used as a standard. All the measurements were performed in triplicate.

4. Results and discussion

4.1. Bacterial reduction of Se^{IV}

The ability of *S. bentonitica* to reduce aerobically Se^{IV} to Se^0 was tested in LB liquid medium at 2 mM selenite. The colour of Se^{IV}-treated cultures of *S. bentonitica* turned intense orange-red after 24 h incubation, in contrast to untreated cultures (blanks) (Figure 1). This colour change reveals the capacity of the strain to reduce Se^{IV} to Se^0 (Sabaty et al., 2001). The Se^{IV} reduction is mediated by a biological rather than a chemical process since no colour change were observed in abiotic and dead cells control samples supplemented with Se^{IV} (Figure 1). The MIC of Se^{IV}

for the growth of the studied strain in solid media was 400 mM as red precipitates and cell growth were observed in all assayed Se^{IV} concentrations ranging from 1 to 200 mM (Figure 2). The absence of both cell growth and red precipitates were appreciated at 400 mM Se^{IV} (data not shown). This indicated the high Se tolerance of *S. bentonitica* compared to other species of the same genus like *S. maltophilia* SeITE02 and *S. maltophilia* Sm777, both of which exhibited tolerance to Se^{IV} of up to 50 mM (Di Gregorio et al., 2005; Pages et al., 2008). The high tolerance of *S. bentonitica* to selenite can also be appreciated comparing its MIC with those of strains belonging to different bacterial genera. For example, the MIC of Se^{IV} for the growth of *Rizhobium selenitireducens* strain B1 and *Comamonas testosteroni* S44 is between 8-16 mM and 100 mM, respectively (Hunter and Kuykendall, 2007; Zheng et al., 2014).

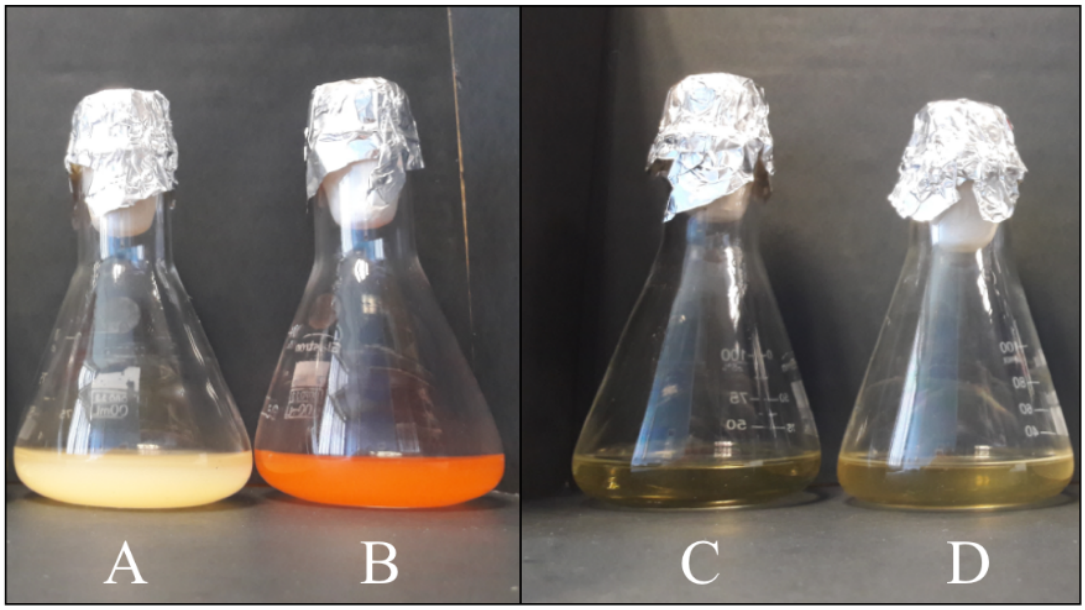

Figure 1. Cultures of *Stenotrophomonas bentonitica* in LB broth liquid medium without (A) or with 2 mM Se^{IV} (B) after 24 h showing the reduction of Se^{IV} to Se^{0} as indicated by the produced red precipitate. Abiotic (LB broth) (C) and dead cells (D) supplemented with 2 mM Se^{IV} were used as controls.

Recent studies indicated the presence of Se in tetravalent oxidation state in high-level nuclear wastes (Dardenne et al., 2015). The bioreduction of this soluble Se species to insoluble elemental Se would reduce the mobility of Se within the future DGR system. This fact makes *S. bentonitica* an excellent candidate to improve the safety of these future repositories of radioactive wastes.

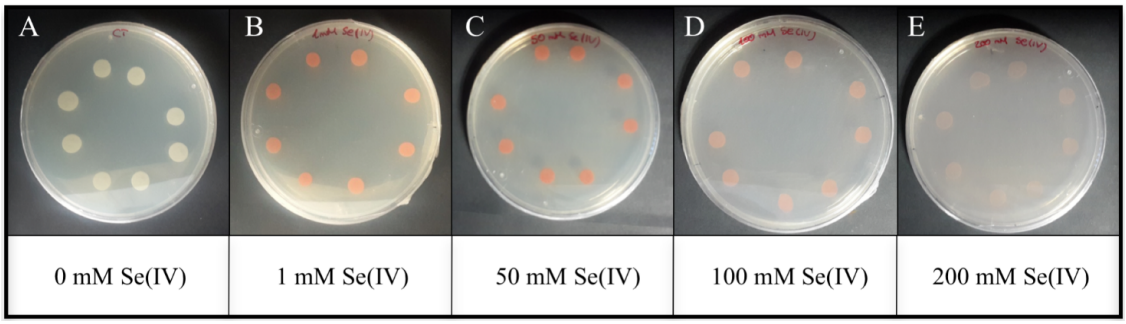

Figure 2. Growth of *Stenotrophomonas bentonitica* on LB solid medium without (A) or with 1 (B), 50 (C), 100 (D) and 200 mM (E) Se^{IV} after 48 h of incubation.

4.2. Effect of Se on the bacterial growth

In order to evaluate the biological effect of Se^{IV} towards *S. bentonitica*, the growth profile of the cells was studied and expressed as total protein content as function of time to avoid optical interferences of Se^{0} red accumulations in spectrophotometric measurements. In comparison with control (0 mM Se^{IV}), the microbial growth was negatively affected at an initial concentration of 2 mM Se^{IV} (Figure 3). It is important to note that growth of *S. bentonitica* cells presented longer lag phase of about 48 hours in the presence of Se. Vogel et al. (2018) detected that the growth of *Azospirillum brasilense* also exhibited a lag phase whose duration depends on the Se^{IV} initial concentration; 2 days at 1 mM Se^{IV} and up to 6 days when the cells were brought into contact with Se^{IV} concentration ranging from 1 to 5 mM. Furthermore, *Ralstonia metallidurans* also presented prolonged lag phase (around 30 h) at 2 mM of Se^{IV}, suggesting an adaptation of the cells to Se^{IV} stress (Roux et al., 2001). In Se^{IV}-treated cells of *S. bentonitica*, this stress could be associated with the presence of Se^{IV} which was determined to be about 50% of the initial Se^{IV} concentration at 48 h (data not shown). The optimum growth reached by the cells treated with Se^{IV} was at 144 h of incubation where the Se^{IV} concentration was about 0% (100% reduction of Se^{IV} to Se^{0}) (data not shown). It was shown that 15, 50, 60 and 100 % of Se^{IV} was reduced to Se^{0} after a period of 24, 48, 72 and 144 h time incubation, respectively (data not shown).

The lag phase observed in the present and other studies could be probably associated with differential expressions of enzymes involved in the Se^{IV} tolerance. The whole genome analysis of *S. bentonitica* revealed the presence of genes codifying enzymes described for their ability to reduce Se^{IV} to Se^{0} (Sánchez-Castro et al., 2017b). Glutathione reductase and thioredoxin reductase as well as NADH-dependent enzymes such as NADH: flavin oxidoreductase (OYE family) previously reported to be implicated in the reduction of this oxy-anion (Hunter, 2014), have been identified in the genome of *S. bentonitica*. Several mechanisms have been proposed for the reduction of selenite in microorganisms including Painter-type reaction (Kessi and

Hanselmann, 2004), thioredoxin reductase system (Yamada et al., 1997), sulphide mediated reduction (Zawadzka et al., 2006), dissimilatory reduction (Basaglia et al., 2007), etc.

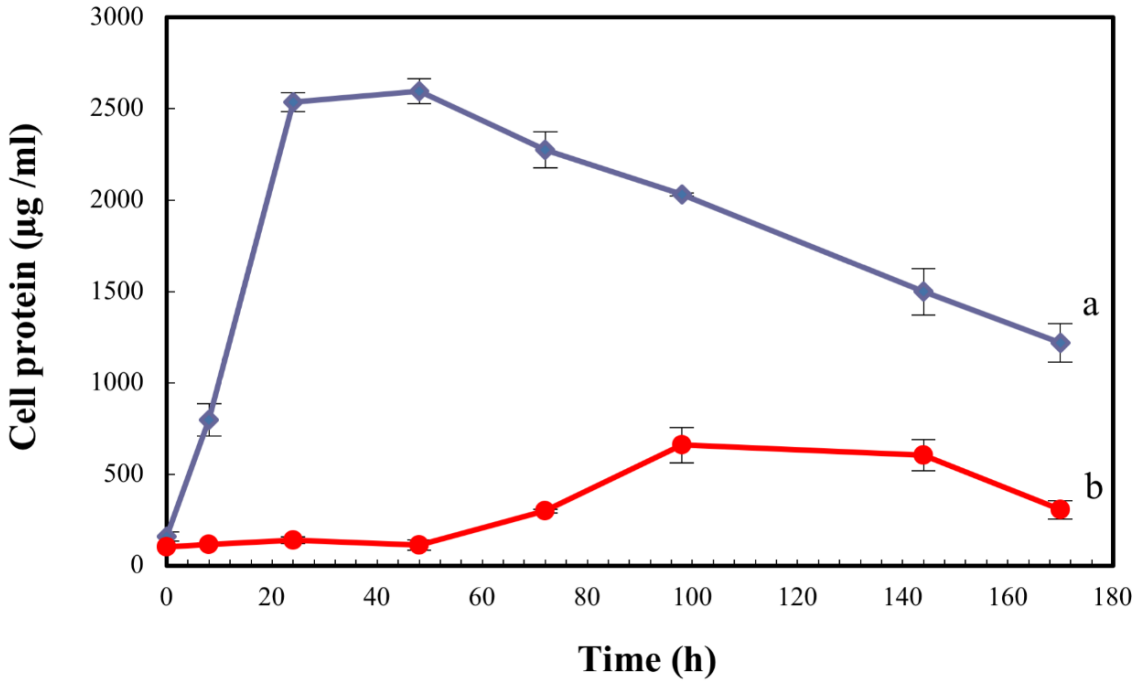

Figure 3. Growth profile of *Stenotrophomonas bentonitica* in the absence (a) and the presence of 2 mM Se^{IV} (b). Selenite was added at time zero. Standard errors are given correspondingly.

4.3. X-ray diffraction (XRD) analysis

The nature of the crystalline phase and size of reduced SeNPs produced by cells treated with 2 mM Se^{IV} for 144 h were determined by using X-ray diffraction. The XRD patterns obtained show the main peaks characteristic of crystalline t-Se (COD-9008579) at 2Θ values of 23.5°, 29.7°, 41.4°, 43.7° and 45.4° (Figure 4) corresponding to the crystal planes (100), (101), (110), (102) and (111), respectively. The average crystalline size of biogenic Se nanostructures measured by Scherrer`s equation was of about 34 nm.

These results agree well with literature data from Borghese et al. (2014) and Srivastava and Mukhopadhyay (2013) who reported the production of crystalline nanostructures by *Rhodobacter capsulatus* and *Zooglea ramigera,* respectively. The diffraction patterns corresponding to these nanoparticles show the main peaks belonging to trigonal Se^0 crystals. The production of crystalline Se nanostructures by the cells of *S. bentonitica* could be of great significance within the DGR system since the mobility of the Se through the surrounding environment may be reduced due to the low solubility of these Se nanostructures (Jain et al., 2017). Zhang et al. (2011) could not detect in the XRD pattern the presence of t-Se nanorods

previously detected by microscopic techniques after 48 h of incubation with *Pseudomonas alcaliphila*. They attributed it to the the shortage of Se nanorods and the attachment of Se nanospheres onto the surface of nanorods. Se nanospheres produced by *Bacillus* sp. SN3 have been previously reported for their amorphous nature since sharp Bragg reflections were not observed in their diffraction pattern (Prakash et al., 2009). As a consequence, amorphous nanospheres could interfere with XRD results. In our case, the XRD peak clearly showed the presence of crystalline t-Se.

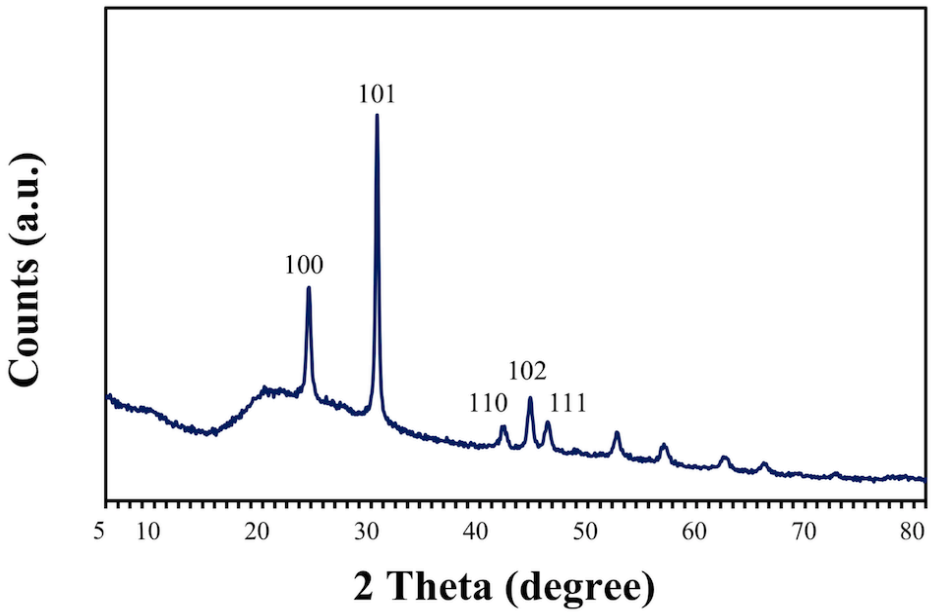

Figure 4. X-ray diffraction pattern of selenium nanoparticles synthesized by *Stenotrophomonas bentonitica* after 144 h incubation.

4.4. Microscopic characterization of Se^{IV} reduction by the *S. bentonitica* cells

VP-FESEM and Raman analysis. VP-FESEM images revealed extensive aggregations of nanospheres associated with bacterial cells after their incubation with Se^{IV} for 144 h (Figure 5A). The Raman spectrum derived from these aggregations also supports the formation of t-Se nanostructures by the appearance of peaks at 232 and 235 cm^{-1} (Figure 5B). The distinctive Raman peak corresponding to the symmetric stretching mode of t-Se is located at 235 cm^{-1}, which can be attributed to the vibration of Se helical chains (Gates et al., 2002). These results are in good agreement with XRD data. Biogenic SeNPs produced by different bacterial strains have also been characterized by using Raman spectroscopy. The Raman scattering spectrum obtained after 48 h of incubation of Se nanospheres produced by *Pseudomonas alcaliphila* showed the characteristic t-Se peak at 234 cm^{-1} (Zhang et al., 2011). *Bacillus subtillis* has also been reported for the production of t-Se nanoparticles as indicated by the distinctive signature of

t-Se at 235 cm^{-1} (Wang et al., 2010). The transformation from monoclinic Se (m-Se) to t-Se after 12 h of incubation was suggested by using this technique. In addition, EDX analysis derived from these accumulations produced by *S. bentonitica* showed that they mainly consisted of Se and sulphur (S) (Figure 5C).

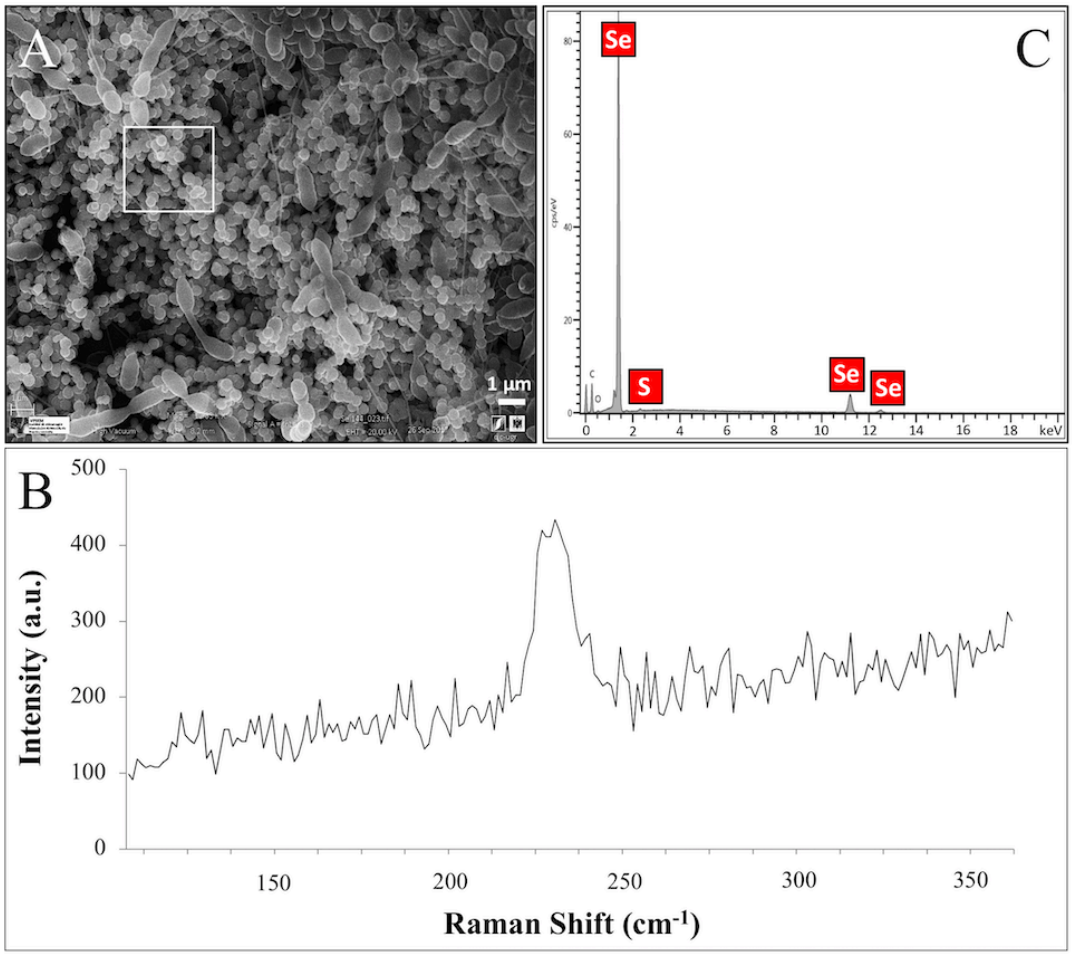

Figure 5. VP-FESEM micrographs (scale bar: 1µm) of *S. bentonitica* surrounded by extensive accumulations of Se nanospheres (A) and their respective Raman spectrum (B). EDX analysis (selected area shown) indicated the presence of Se and S in the nanospheres (C).

HAADF-STEM analysis. STEM micrographs of thin sections revealed the presence of extracellular electron-dense nanostructures when cells were grown on Se^{IV} at 2 mM for 144 h (Figure 6). Moreover, very few intracellular SeNPs were observed. The presence of both extracellular and intracellular SeNPs suggested their intracellular formation before their release into the extracellular space in response to selenite stress. Lampis et al. (2017) proposed that Se^{IV} is reduced in the cytoplasm of *S. maltophilia* SeITE02 by reaction with thiol-containing molecules to produce some intermediates that are transformed into Se^0. Once inside the cell, Se^0 is secreted out to the extracellular space through an export mechanism. Formation of vesicles from the outer membrane of Gram-negative bacteria containing periplasmic materials

(McBroom and Kuehn, 2007), is one of the possible mechanisms involved in the secretion. McBroom and Kuehn (2007) proposed that in response to stress vesicles are produced by fission of outer membrane protrusions enclosing periplasmic and stress causing materials. Then the material causing stress is released out the cells. According to other authors, a cell lysis process could be involved in the release of Se granules to the extracellular space (Di Gregorio et al., 2005; Fernández-Llamosas et al., 2016). However, further studies are needed to elucidate the way by which *S. bentonitica* releases SeNPs to the extracellular space.

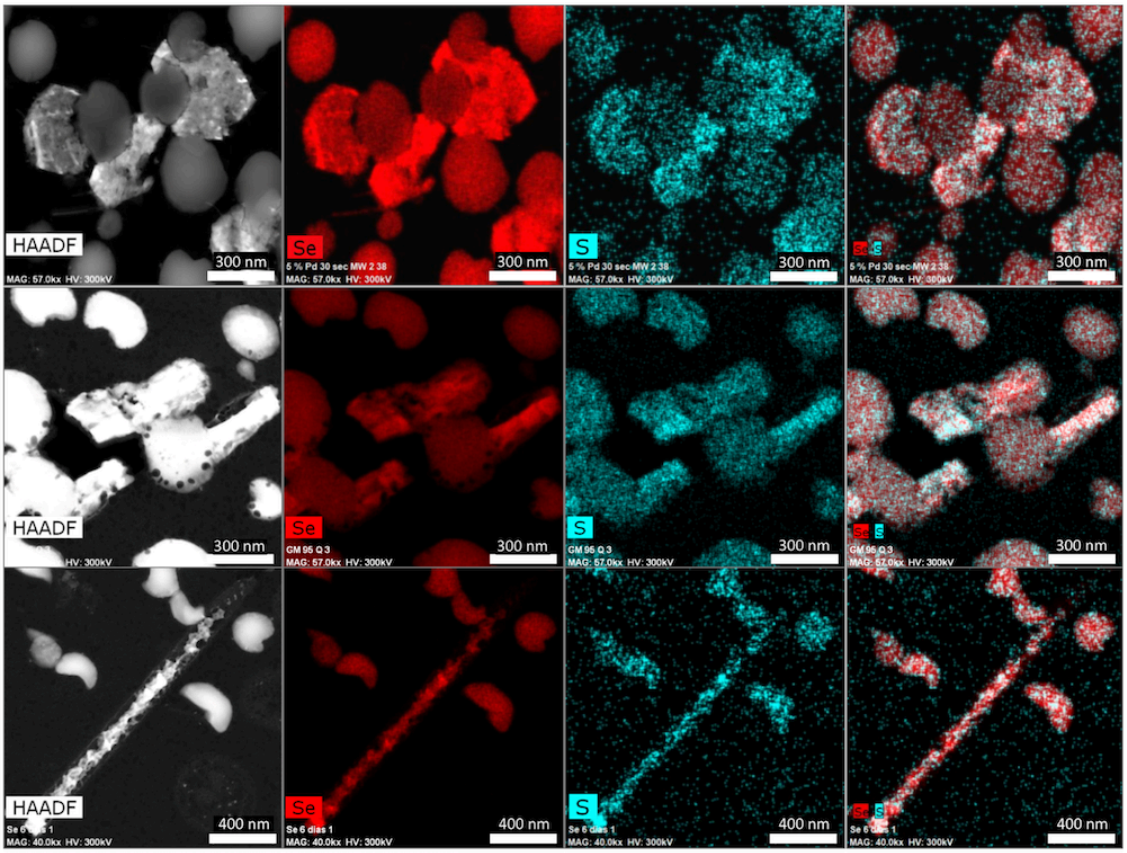

Figure 6. HAADF-STEM micrographs of a thin section showing the different morphologies (spherical, hexagonal, polygonal, and nanowires) of SeNPs produced by *S. bentonitica* after 144 h of incubation. EDX element-distribution maps confirmed that they are mainly composed of Se and S.

The Se nanostructures identified by STEM exhibited different shapes: spheres, nanowires, hexagons, polygons, etc. Energy dispersive X-ray (EDX) elemental mapping derived from these accumulations showed that they are mainly composed of Se, in addition to S (Figure 6). Many investigations reported previously the formation of biogenic SeNPs (Lampis et al., 2017; Li et al., 2014b). However, very few authors described the presence of S in these nanostructures. For instance, Vogel et al. (2018) detected S in Se nanospheres synthesized by *Azospirillum brasilense* by using EDX analysis. Combining Raman and EXAFS spectroscopy they could determine the local coordination of selenium within the biogenic SeNPs where Se is coordinated

to S atoms forming $Se_{8-n}S_n$ structured SeNPs forming 8-rings typical for amorphous Se^0 with a partial S-for-Se substitution in the 8-ring. The presence of S suggests the involvement of this element in the formation of the nanospheres. In this sense, extensive studies on the mechanisms of Se^{IV} reduction have indicated the involvement of molecules containing thiol groups (-SH) such as reduced glutathione (GSH) into the reduction of Se^{IV} to Se^0 (Kessi and Hanselmann, 2004; Tan et al., 2016). GSH is proposed to act as electron donor and reacts with selenite to form selenodiglutathione (GS-Se-SG). Selenodiglutathione reduction by glutathione reductase (GR) leads to the formation of glutathione selenopersulfide ($GS\text{-}Se^-$), which dismutates into Se^0 and GSH.

In the case of Se nanospheres, extensive accumulations of this morphology with two considerable different sizes were detected. Specifically, smaller nanospheres with diameters of 20 to 30 nm and bigger NPs around 200 nm were found (Figure 7A, 7B and 7C). EDX microanalysis indicated that they are mainly composed of Se and S (Figure 7D and 7E). In addition, the selected area electron diffraction (SAED) pattern of nanospheres indicated their amorphous nature (Figure 8A and 8B). Production of biogenic spherical SeNPs through the reduction of Se^{IV} to Se^0 by several bacterial strains has been previously reported. The strain *Rhodopseudomonas palustris* N produces nanospheres between 80 to 200 nm as indicated TEM analysis when cells grew on Se^{IV} after 8 days (Li et al., 2014a). On the other hand, Srivastava and Mukhopadhyay (2013), reported the formation of spherical SeNPs ranging from 30 to 150 nm by *Zooglea ramigera* after 48 h. Benko et al. (2012) demonstrated that biologically produced spherical SeNPs are less toxic than Se oxyanions such as Se^{IV} and Se^{VI}. However, other studies revealed that the toxicity of SeNPs can vary widely among different species (Li et al., 2008). In their experiments, Li et al. (2008) found a higher toxicity of SeNPs compared to Se^{IV} in the fish species *Oryzias latipes*.

To a lesser extent, hexagonal-shaped nanostructures from 100 to 400 nm in size were produced (Figure 8C). Their crystal structure was investigated using SAED and high-resolution scanning transmission electron microscopy (HRSTEM) combined with Fast Fourier Transform (FFT). The HRTEM image from an individual hexagonal-shaped nanoparticle showed 2 distinct lattice spacings of 0.37 and 0.29 nm corresponding to the (100) and (101) planes of t-Se, respectively (Figure 8D and 8E). The SAED pattern indicated that hexagonal-shaped nanostructures are single crystals, which can be well indexed to t-Se (Figure 8F). In addition, the lattice spacing values obtained for all the diffraction rings from the FFT of the image (Figure 8G) are in agreement with the trigonal phase of Se. The production of SeNPs with a hexagonal shape has rarely been reported. Ho et al. (2010) demonstrated the formation of Se nanoribbons with a hexagonal cross section from biogenic Se nanospheres in the presence of 80% dimethyl

sulfoxide (DMSO). As far as we know, the present work describes for the first time the biological production of crystalline hexagonal-shaped SeNPs without the addition of organic solvents under mesophilic conditions. Consequently, here we report a simpler method for the preparation of crystalline SeNPs than those previously described (Ho et al., 2010; Shin et al., 2007). We provide an economic, environmentally-friendly and promising method for the synthesis of SeNPs, well known to be useful in many industrial and medical applications. The SAED patterns and HRTEM from polygonal forms also evidenced the trigonal phase of Se (data not shown).

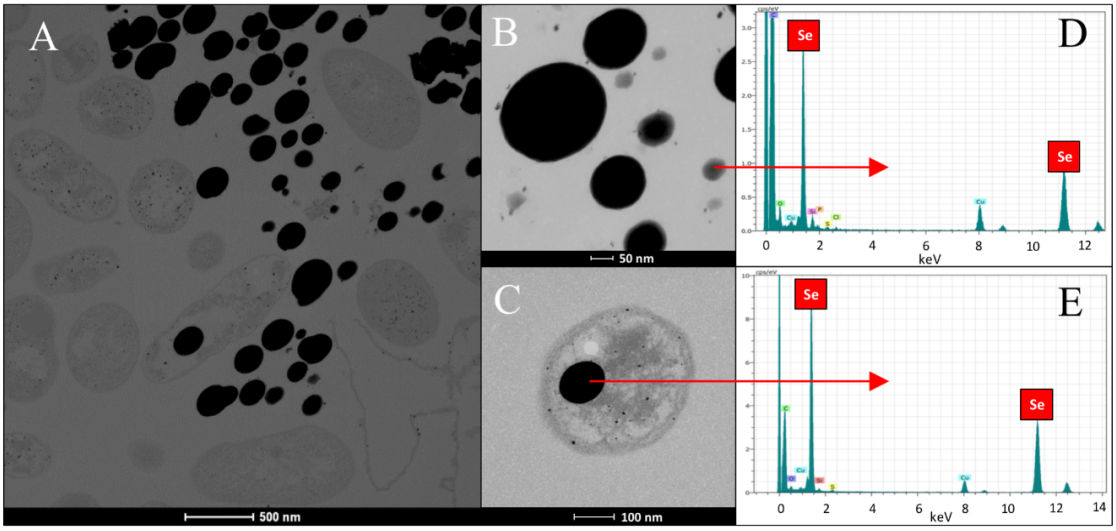

Figure 7. HAADF-STEM micrographs of a thin section showing extracellular and intracellular SeNPs with two different sizes produced by the cells of *Stenotrophomonas bentonitica* (A-C). Scale bars: 500 nm (A), 50 nm (B) and 100 nm (C). EDX analysis image of a single SeNP (D and E).

The last type of SeNP shape detected consisted of nanowires. In the same way as hexagonal and polygonal-shaped nanostructures, Se nanowires around 30 nm in diameter were found (Figure 8H) to a lesser extent comparing with nanospheres. The HRTEM image from an individual nanowire showed 2 distinct lattice spacings of 0.37 and 0.19 nm corresponding to the (100) and (111) planes of t-Se (Figure 8I and 8J). The SAED spots revealed that Se nanowires are polycrystalline (Figure 8K). In addition, the FFT of the image shown in Figure 8L further confirms the trigonal phase of selenium. These results match very well with XRD diffraction pattern described in the section above indicating the presence of t-Se ranging from 30 to 45 nm in size.

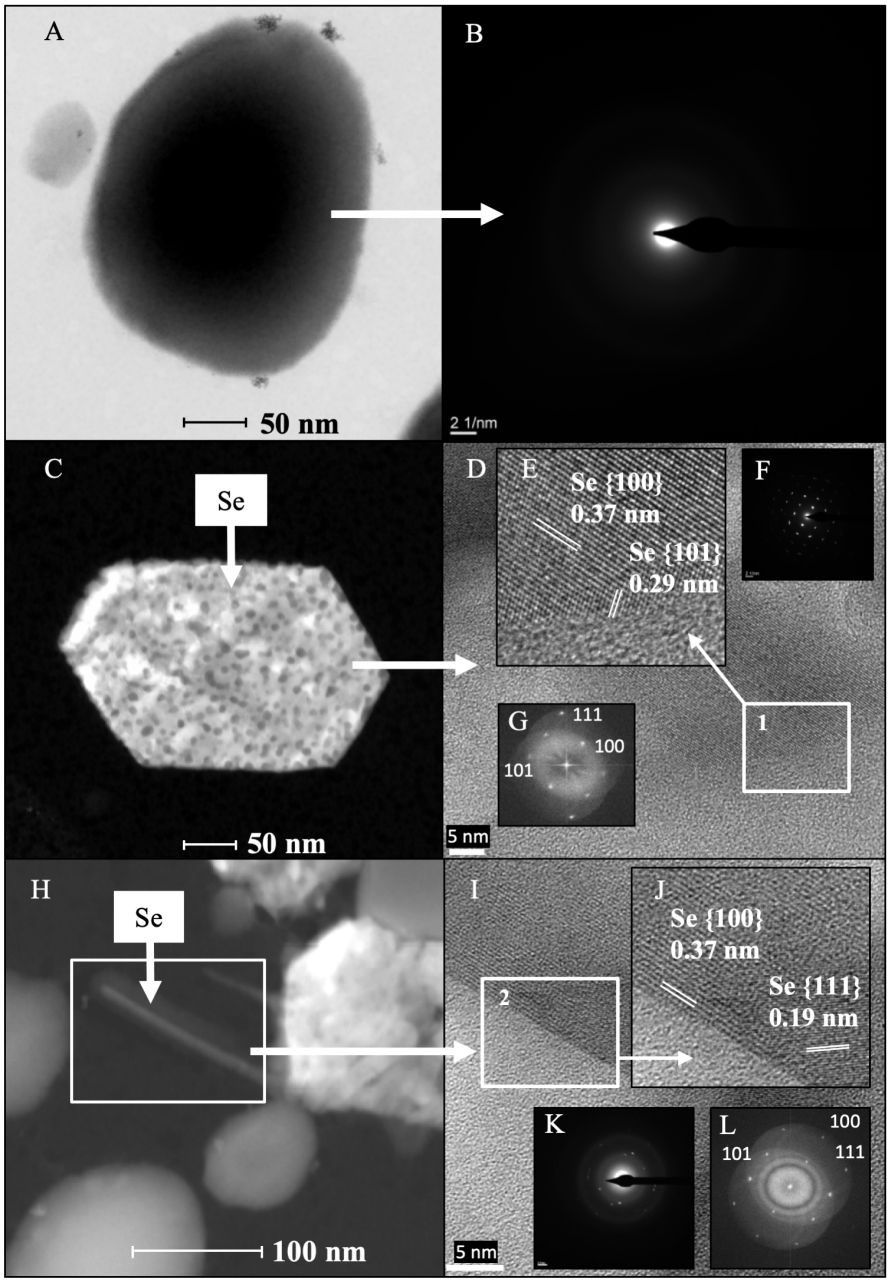

Figure 8. HAADF-STEM micrograph (A) and SAED pattern (B) of a single spherical SeNP. HAADF-STEM micrograph (C) and HRTEM image (D) of a single hexagonal-shaped SeNP. Panel E is the magnified HRTEM image corresponding to area 1. SAED pattern (F) and FFT (G) corresponding to the HRTEM of the single hexagonal-shaped SeNPs. HAADF-STEM micrograph (H) and HRTEM image (I) of a single selenium nanowire. Panel J is the magnified HRTEM image corresponding to area 2. Panel K and L show the SAED pattern and the FFT corresponding to the HRTEM of the single Se nanowire. Scale bars: 50 nm (A), 2 1/nm (B), 50 nm (C), 5 nm(D), 100 nm (H) and 5 nm (I).

The shape of Se nanostructures greatly affects their colloidal stability and surface charge, which in turn influences their mobility and the effectiveness of bioremediation (Jain et al., 2017). Jain et al. (2017) demonstrated the lower colloidal stability and mobility of biogenic Se nanorods comparing with biogenic Se nanospheres produced by anaerobic granular sludge. For this

reason, the formation Se nanowires would be beneficial for Se immobilization in future disposal of radioactive wastes. In addition to environmental purposes, SeNPs have acquired major relevance in the field of medicine owing to their antioxidative and anticancer properties. They are also extensively used in industrial applications (solar cells, photocopiers, electronics, optics, etc.) due to their semiconductor, photoelectrical and catalytic properties (Wadhwani et al., 2016).

Careful observation of TEM micrographs revealed that some nanowires are protruding out of the hexagonal and polygonal-shaped Se nanostructures (Figure 8H). This could indicate that the nanowires aggregate forming Se hexagons and polygon-shaped nanostructures. This hypothesis is supported by the discontinuous distribution of Se within these nanostructures as indicated by elemental mapping analysis, and also by the fact that hexagonal, polygonal and nanowires have the same crystalline structure (trigonal). It has been previously reported that crystallization of SeNPs increases their settleability and hence immobility through the environment (Lenz et al., 2009). For this reason, the formation of crystalline Se nanostructures may have a positive influence into the safety of DGRs due to their lower solubility and mobility.

4.5. Biotransformations of amorphous Se nanospheres to trigonal Se nanostructures

The production of different Se nanostructure shapes by the cells is a time dependent process. After an incubation period of 24 h, 30-200 nm sized biogenic individual a-Se nanospheres were synthesized (Figure 9A). The latter start to coalesce, forming aggregates after 48 and 72 h (Figure 9B and 9C). However, the cells were able to produce a mixture of single crystal and polycrystalline one-dimensional (1D) t-Se nanostructures with different shapes (*e.g.* nanowires, hexagons, polygons, etc.) and diameters of 30-400 nm, in addition to a-Se nanospheres after 144 h of incubation (Figure 9D). These results suggested the probable transformation of a-Se nanospheres to t-Se nanostructures with different shapes. This hypothesis is supported by VP-FESEM and Raman analysis results showing the aggregation and crystallization of SeNPs (see Figure 4). Li et al. (2005) and Chen et al. (2010) evidenced the synthesis of Se nanospheres and t-Se nanotubes and nanowires with HRSTEM analysis by using different chemical processes. They both suggested that spherical SeNPs are initially generated and then they transform into the more stable t-Se nanowires and nanotubes.

In order to determine the impact that bacterial cells and their components (*e.g.* proteins) can have on transformation of a-Se NPs to t-Se NPs we performed a series of control experiments where *S. bentonitica* cells were brought into contact for 24 h with chemically (CheSeNPs) and organically produced SeNPs (OrgSeNPs). The organic SeNPs were synthesized using proteins

(*i.e.* BSA) as the template and represent the early stage of biogenic formation of amorphous SeNPs. The CheSeNPs are the SeNPs produced chemically and were used as negative control (the absence of proteins and bacteria).

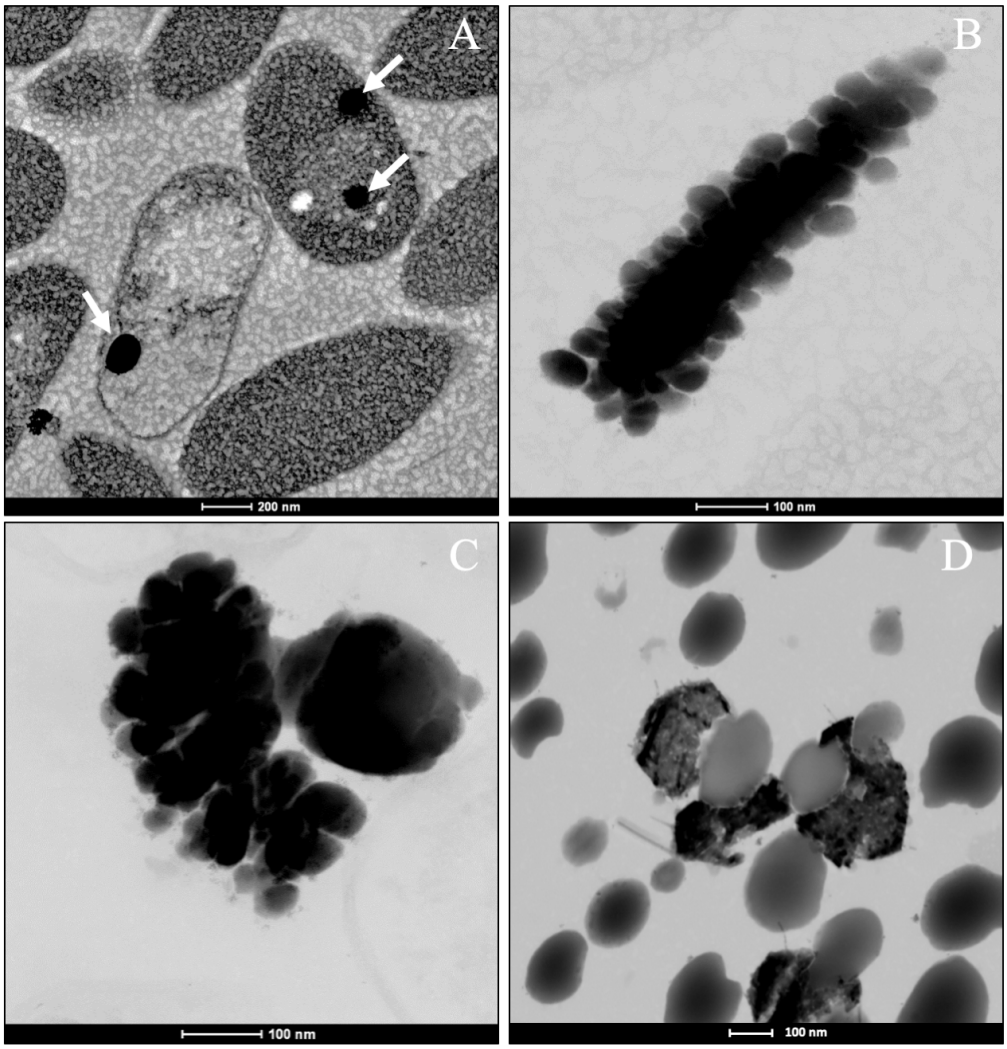

Figure 9. HAADF-STEM pictures showing individual a-Se nanospheres (white arrows) after 24 h (A) and formed aggregates after 48 h (B) and 72 h (C). A mixture of different t-Se nanostructures and a-Se nanospheres produced after 144 h (D). Scale bars: 200 nm (A), 100 nm (B-D).

When the experiment was conducted without the presence of bacteria, TEM images revealed the presence of only amorphous spherical SeNPs with homogenous size distribution in both CheSeNPs and OrgSeNPs samples (Figure S1). However, in the presence of bacteria, whilst FEG-ESEM showed a high number of individual CheSeNPs distributed in the extracellular space without any contact with the cells (Figure 10A and 10B), both Se nanowires and nanospheres associated with cells were detected (Figure 10C, 10D, 10E) when proteins (BSA) were present. EDX analysis confirmed that both nanostructures are composed of Se (Figure 10F). In the later sample, spherical SeNPs aggregates are formed by high number of individual

Se nanospheres which seem to be embedded in an organic matrix. This aggregation has been previously reported to be a crucial step during the transformation process to Se nanowires (Wang et al., 2010). The aggregation takes place along an axis which could correspond to the flagella-like proteins structures characteristic of this bacterium. Flagella-like proteins of *S. maltophilia* are composed of several thousand copies of flagellin subunits (Jucker et al., 1996), and are involved in the formation of biofilms on abiotic surfaces such as glass, Teflon, polystyrene, and stainless steel (Friedman et al., 2002; Jucker et al., 1996), as well as on biotic surfaces (Chhibber and Zgair, 2009). Bacterial flagella are also used as template for formation of different nanomaterials including pearl-necklace-like 1D silica nanotubes in aqueous solution (Wang et al., 2008). Flagellin monomers from *Pseudomonas fluorescens* were reported for its ability to form a monolayer tick protein film on the Au(111) surface through hydrophobic interactions (González Orive et al., 2014). These results suggested that organic matter (mainly proteins capping the NPs and flagella-like proteins) produced by *S. bentonitica* (Figure S2) plays an important role in the aggregation and hence in the transformation from nanospheres to nanowires.

We proposed that the transformation to t-Se nanostructures occurs once the nanospheres have been released from the cells, probably through a process of cell lysis. This is supported by the appearance of some SeNPs in the proximity of lysed cells (Figure S3). The transport of Se nanospheres across the membrane seems unlikely due to their large size and no detection of vesicles in HAADF-STEM analysis. A transformation process has been proposed where the released Se nanospheres from the intracellular space start to coalesce and probably growth on the axis of flagella-like proteins (Figure 11). Finally, they cristallyze forming the different t-Se nanostructures. However, more experimental data are needed to prove this proposed transformation mechanism model. The different Se^0 allotropes should eventually be converted to one of the most thermodynamically stable form such as t-Se. Minaev et al. (2005) reported that from a thermodynamic point of view, the transformation of amorphous Se to crystalline Se allotropes (monoclinic and trigonal Se) requires high temperatures. Specifically, the amorphous form is transformed into monoclinic Se at temperatures around 70 ºC and into hexagonal form at higher temperatures. However, in this work, the reduction of Se^{IV} to Se^0 and transformation to t-Se nanostructures by *S. bentonitica* is considered as detoxification mechanisms used by this bacterium to cope with the toxicity of Se^{IV} and it is not governed by thermodynamic law. This process is taken place at temperature of about 28 ºC for 6 days.

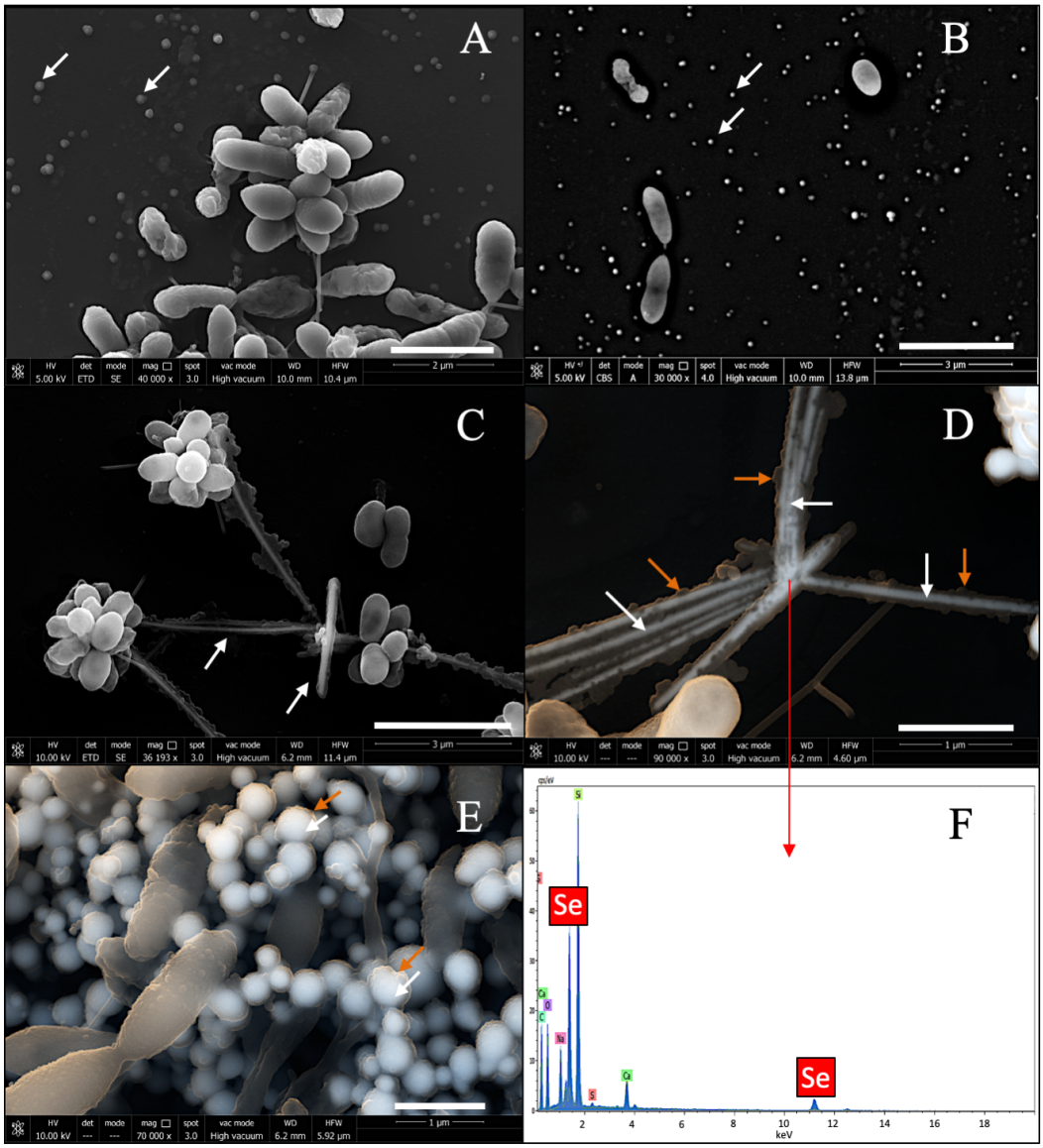

Figure 10. FEG-ESEM of CheSeNPs (white arrows) distributed within the extracellular space in the presence of *S. bentonitica* cells (A and B). Scale bars: 2 µm (A) and 3 µm (B). Selenium nanowires (white arrows) (C and D) and nanospheres (white arrows) (E) surrounded by organic matter (orange arrows) in *S. bentonitica* cultures treated with OrgSeNPs (with BSA). Scale bars: 3 µm (C) and 1 µm (D and E). EDX analysis of a single nanowire confirmed the presence of Se (F).

Many authors have reported the synthesis of SeNPs coated by organic layers mainly composed of proteins, lipids and polysaccharides (Jain et al., 2017; Kamnev et al., 2017). Ni et al. (2015) reported the first 3D electron tomographic analysis of Se^{IV} reduction by the cells of *Pseudomonas moraviensis* stanleyae providing new insights on the interactions at the nanoparticle/proteins interface. They identified the first polypeptide playing a major role on the reduction of Se^{IV} and formation of intracellular of SeNPs. This polypeptide is also involved in retaining the produced Se^{0} NPs forming complexes with the latter in the reduction site, and controlling their size. In addition, the authors demonstrated that this biopolymer layer is

acquired after intracellular NP formation, either during extracellular transport or when the NPs are outside the cell. However, the impact of bioorganic layers during the formation of SeNPs remains to be fully elucidated. In particular, the role of proteins in the transformation of SeNPs as well as in controlling the size distribution has been previously suggested (Dobias et al., 2011; Kaur et al., 2009; Wang et al., 2010). Dobias et al. (2011) demonstrated the role of AdhP, a single purified protein, on decreasing the average size of chemically produced SeNPs. On the other hand, Wang et al., (2010) reported the polyvalency of proteins during the transformation from Se nanospheres to stable Se nanowires. According to them, proteins are involved in trapping on the surface and reducing the Se^{IV} ions. In addition, they suggested that proteins excreted by *Bacillus subtilis* serve as template hindering the futher growth of m-Se and accelerating its transformation to trigonal nanowires. Although the exact mechanism of the transformation of spherical SeNPs to t-Se 1D structures in *S. bentonitica* is still unclear; the directing role of cells and their proteins is undoubtedly significant.

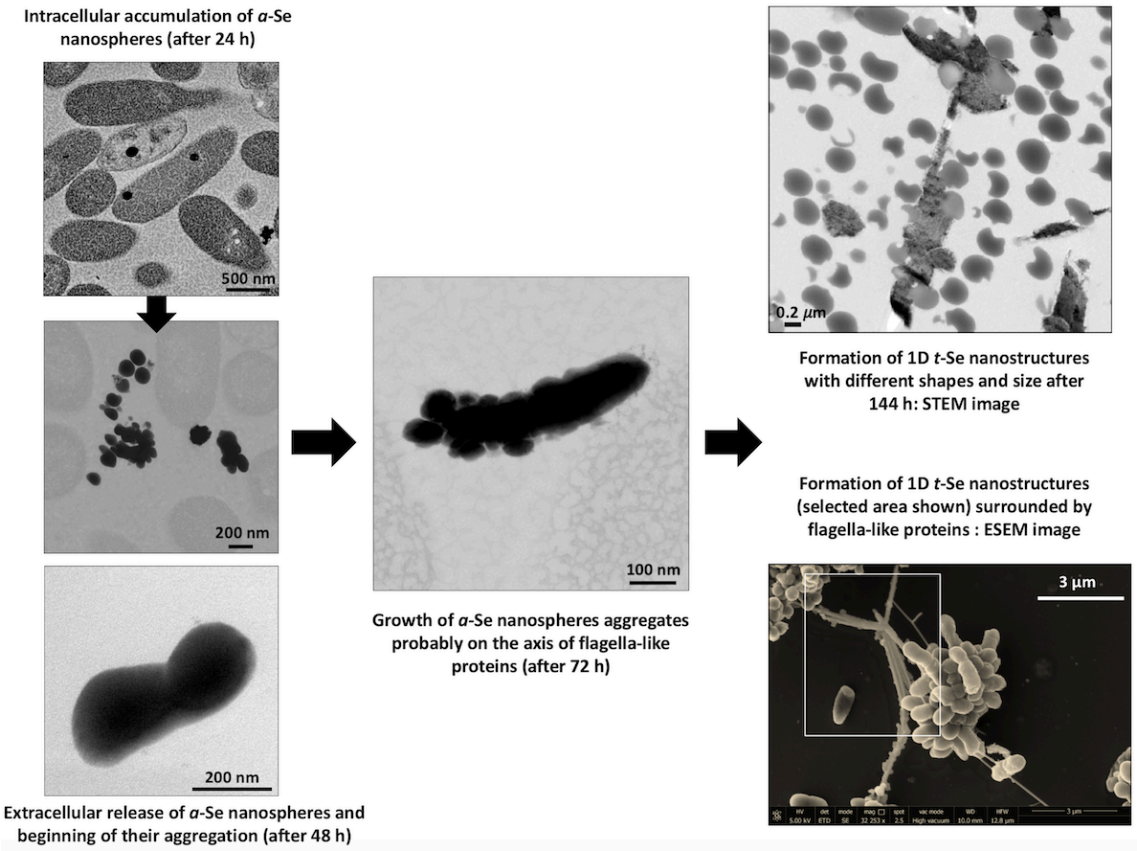

Figure 11. Proposed mechanism of time-dependent transformation of a-Se nanospheres to different 1D t-Se nanostructures.

Future studies are in progress to elucidate the molecular mechanisms of interaction between the SeNPs on the surface of purified flagella and the impact of these proteins in the transformation of spherical SeNPs to trigonal ones.

5. Conclusions

In summary, this study described the synthesis of biogenic Se nanostructures with different shapes (spherical, hexagonal, polygonal and nanowires) and distinct crystallographic properties (amorphous and trigonal structure) by the selenite-tolerant *Stenotrophomonas bentonitica*, isolated from Spanish bentonites. Time dependent SeNPs experiments showed that the cells of the strain *S. bentonitica* and their proteins are able to transform amorphous Se^0 nanospheres (a-Se) to one-dimensional (1D) trigonal selenium (t-Se) nanostructures (hexagons, polygons and nanowires) under mesophilic conditions. However, more studies are needed to determine the exact mechanism of the transformation process. The Se^{IV} reduction and production of crystalline t-Se would be of great significance within the DGR system since the mobility of Se through the surrounding environment may be reduced. The potential environmental significance of this study includes understanding of the impact of microbial processes on the transport of selenium in future radioactive repositories which in turn will help to support the implementation of planned repositories.

6. Conflicts of interest

The authors declare no competing financial interest.

7. Acknowledgements

This work was supported by Euratom research and training programme 2014-2018 under grant agreement no. 661880. The authors acknowledge the assistance of Maria del Mar Abad Ortega, Isabel Sánchez Almazo, Isabel Guerra Tschuschke and Concepción Hernández Castillo (Centro de Instrumentación Científica, University of Granada, Spain) for their help with microscopy measurements. The authors also thank of José Romero Garzón (Centro de Instrumentación Científica, University of Granada, Spain) for his assistance with the XRD measurements.

8. Supplementary material

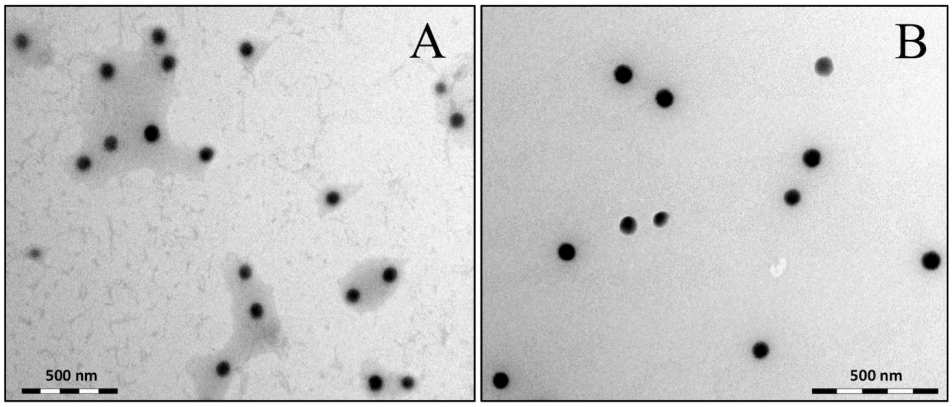

Figure S1. TEM images showing the homogenous size distribution of CheSeNPs (A) and OrgSeNPs (B) in the absence of bacteria.

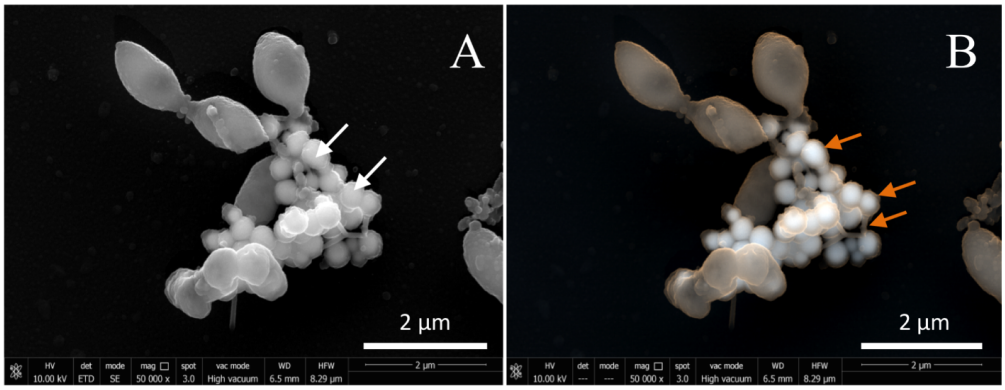

Figure 12. FEG-ESEM images showing the presence of SeNPs (white arrows) (A) and the organic material (mainly proteins coating the NPs and flagella-like proteins) (orange arrows) produced by *S. bentonitica* (B).

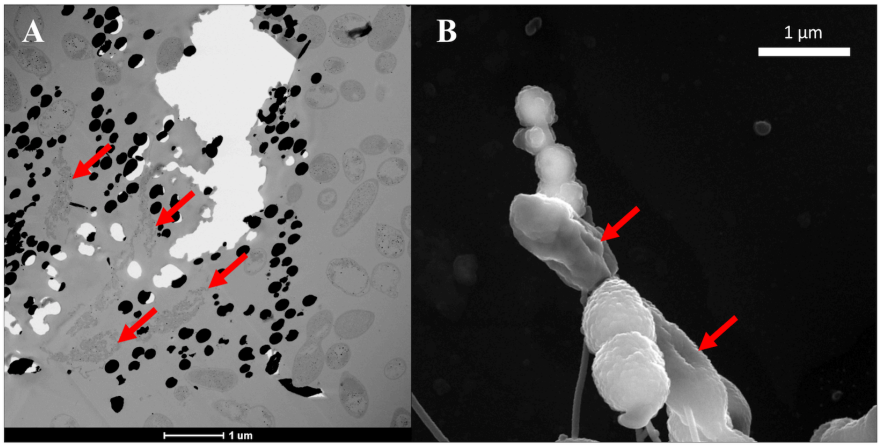

Figure S3. HAADF-STEM image showing SeNPs in the proximity of lysed cells of *S. bentonitica* (arrows) (A) and FEG-ESEM image clearly showing trans-membrane lysis tunnels in the cells (arrows) (B). Scale bars: 1 µm (A and B).

CAPÍTULO III:

Structural and chemical characterization of the Se^{IV} reduction products derived from *Stenotrophomonas bentonitica* in form of nanoparticles and volatile compounds

Miguel A. Ruiz-Fresneda[1], Abdurrahman S. Eswayah [2,3], María Romero-González [4], Philip H. E. Gardiner [2], Pier L. Solari [5], Mohamed L. Merroun[1]

[1]Department of Microbiology, University of Granada, Granada, Spain

[2]Biomolecular Sciences Research Centre, Sheffield Hallam University, Sheffield, UK

[3]Biotechnology Research Centre, Tripoli, Libya

[4]Department of Geography, University of Sheffield, Sheffield, UK

[5]MARS Beamline, Synchrotron SOLEIL, L'Orme des Merisiers, Saint-Aubin, Gif-sur-Yvette Cedex, France

To be submitted to the journal Environmental Science: Nano

1. Abstract

The deep geological repository (DGR) system is the most worldwide accepted solution for the storage of radioactive wastes in the near future. Deep disposal concept is based on a system of several passive safety natural and engineered barriers such as bentonite clays, which will be located surrounding the metal containers that include the radioactive waste. One of the most relevant long-lived radionuclides present in these residues is selenium-79 (^{79}Se), whose mobility and toxicity depends on different factors including the oxidation state, pH, and microbial processes. Therefore, study of the impact of the microbial communities from the selected barriers on the mobility of radionuclides characteristic of radioactive wastes is greatly needed. This work describes the ability of the bentonite-isolated bacterium *Stenotrophomonas bentonitica* to reduce the highly toxic selenite (Se^{IV}) to less toxic elemental Se (Se^0) forming Se nanoparticles (SeNPs) and volatile methylated Se species. The total Se^{IV} content was reduced under a wide range of concentrations (0.1-2 mM) indicating their high Se^{IV} reduction efficiency. High-angle annular dark field scanning transmission electron microscopy (HAADF-STEM) analysis of purified biogenic SeNPs extremely support the transformation process from amorphous to crystalline Se nanostructures proposed in previous studies. X-ray absorption spectroscopy (XAS) confirmed the formation of different Se^0 nanostructures (amorphous and crystalline Se). Attenuated total reflection-Fourier transform infrared spectroscopy (ATR-FTIR) and X-ray photoelectron spectroscopy (XPS) revealed the presence of amine rich organic matter coating the SeNPs, suggesting the role of proteins in their synthesis and transformation and hence affecting their environmental fate. Finally, the reduction of Se^{IV} to less toxic volatile methylated species was detected using a gas chromatography-mass spectrometry (GC-MS) system. This study demonstrates the substantial impact of microbial processes derived from *S. bentonitica* on the mobility of Se through the surroundings of the future repository system.

2. Introduction

The impact of microbial processes onto the security of the future planned deep geological repositories (DGRs) for radioactive wastes it is a current environmental concern. It is well documented that microorganisms present in these geological disposal environments would have an important role on the corrosion of metal canisters containing radioactive wastes (Smart et al., 2014). Microorganisms can also affect the speciation and hence the solubility of elements characteristic of these kind of wastes such as uranium (U), selenium (Se), curium (Cm), etc. (Krawczyk-Bärsch et al., 2018; López-Fernández et al., 2018b; Song et al., 2017). Consequently, they may have a positive or negative effect on the safety of DGRs in case of escape of radionuclides to the surrounding environment.

Se is considered an important radionuclide of interest present in radioactive wastes and spent nuclear fuel (Ikonen et al., 2016). Specifically, Se^{79} isotope formed by nuclear fission reactions is the main radioisotope of Se found in nuclear wastes (Ikonen et al., 2016). The solubility and mobility of this element depends to a great extent on its different oxidation states [selenate (Se^{VI}), selenite (Se^{IV}), elemental selenium (Se^{0}) and selenide (Se^{-II})]. In contrast to toxic and highly reactive Se oxyanions (Se^{VI} and Se^{IV}), Se^{0} and methyl selenide forms are basically insoluble and less biologically available (Ranjard et al., 2003). Microbial reduction of toxic Se oxyanions to the insoluble Se^{0} in form of nanoparticles has been previously described by many authors (Song et al., 2017; Staicu et al., 2015; Vogel et al., 2018). Some studies revealed the presence of organic coating agents (proteins) microbiologically produced surrounding the Se nanospheres (Dobias et al., 2011; Kamnev et al., 2017). The physico-chemical properties (size, morphology, crystallinity) and hence the mobility of Se nanospheres could be affected largely by the presence of these bioorganic layers (proteins, polysaccharides, etc.) associated with them (Buchs et al., 2013; Jain et al., 2017). Thus, microorganisms could have an important role in the immobilization of Se within the DGR concept as well as the bioremediation of Se contaminated environments and the production of nanostructures for biotechnological applications.

The reduction of Se oxyanions (Se^{VI} and Se^{IV}) to Se^{-II} has not been extensively investigated. However, Se^{0} can be reduced to Se^{-II} by the action of few microorganisms such as *Veillonella atypica and Bacillus selenitireducens* (Herbel et al., 2003; Pearce et al., 2008). The production of biogenic volatile methylated selenide compounds is a widespread process within bacteria to be considered. *Methylococcus capsulatus*, *Methylosinus trichosporium* OB3b, *Stenotrophomonas maltophilia*, and *Pseudomonas stutzeri* NT-I can produce Se volatile species such as dimethyl selenide (DMSe) or dimethyl diselenide (DMDSe) as a consequence of a Se methylation process (Eswayah et al., 2017; Dungan et al., 2003; Kagami et al., 2013). Several

possible mechanisms for Se biomethylation have been proposed. Chasteen (1993) suggested that methylation is preceded by the formation of Se^0 from Se^{IV}. Afterwards, Se^0 is reduced to a selenide form (H-Se-X) and subsequently methylated and converted to methane selenol and dimethyl selenide. Other proposed mechanism by Challenger (1945), not preceded by the formation of Se^0 suggested a methylation process from selenate involving several reductive and methylation steps leading to the production of DMSe. The most frequently microbiologically produced Se methylated forms detected as bacterial products are DMSe, DMDSe and dimethyl selenyl sulphide (DMSeS). However, less commonly methylated forms including dimethyl selenone, dimethyl triselenide, dimethyl selenyl disulphide, etc. have been also detected (Burra et al., 2010; Reamer and Zoller, 1980). It is noteworthy to mention that methylation of Se inorganic forms is considered a detoxification process since methyl selenide are less toxic than Se oxyanions (Frankenberger and Arshad, 2001).

Within the concept of DGR, we recently published a work describing the ability of *S. bentonitica*, isolated from Cabo de Gata´s bentonite (Almeria, Spain), to reduce Se^{IV} by producing amorphous and crystalline Se nanostructures (Ruiz-Fresneda et al., 2018). These bentonites are considered as natural analogues of artificial barriers for future Spanish repositories (Villar et al., 2006). Individual amorphous Se (a-Se) nanospheres were initially synthesized intracellularly and after a period of 48-72 h they start to coalesce forming aggregates within the extracellular space. From 144 h of incubation, different trigonal Se (t-Se) nanostructures (*e.g.* hexagons, polygons, and nanowires) were detected in addition to a-Se nanospheres. A time-dependent transformation process from a-Se nanospheres to t-Se nanostructures was proposed. Extracellular flagella-like proteins produced by the cells could play an important role into the transformation process since nanospheres seem to coalesce on the axis of these proteins forming elongated shapes. Characterization of the organic matter surrounding the Se nanoparticles (SeNPs) produced by *S. bentonitica* could be of high interest since they may be involved in their synthesis and transformation. However, no structural studies were conducted to determine the local coordination of Se within the Se nanostructures. Therefore, the main objectives of the present work are: 1) to confirm the involvement of organic matter (*e.g.* proteins) in the transformation of Se nanostructures using a combination of X-ray photoelectron spectroscopy (XPS), attenuated total reflectance-Fourier transform infrared spectroscopy (ATR-FTIR), and scanning transmission electron microscopy associated with a high-angle annular field detector (STEM-HAADF), 2) to characterize the local coordination of Se in the Se nanostructures with different morphology produced at different incubation times by means of X-ray absorption spectroscopy (XAS), and 3) to characterize the methylated Se volatile compounds (DMDSe and DMDSeS) produced by this strain using a combined thermal desorption GC-MS (gas chromatography-mass spectrometry) system. This work will provide

new molecular evidence on the impact of the bacterial strain *S. bentonitica* in the safety of the future disposal of radioactive wastes through the reduction of Se^{IV} to different Se species.

3. Experimental

3.1. Quantification of biological Se^{IV} reduction rate

The Se^{IV} reduction rate of *S. bentonitica* was determined by growing the cells aerobically in LB (Luria-Bertani) liquid medium (30 ml) supplemented with different initial Se^{IV} concentration (0.1, 0.25 and 2 mM). Se^{IV}-treated cells were incubated at 28 ºC by shaking at 180 rpm. After different times of incubation (0, 6, 24, 48, 120 and 144 h) 1 ml of the samples were taken and centrifuged (10000 x g; 15 min; room temperature) to remove the cells and other debris. The Se^{IV} concentration in the resultant supernatant was determined by using a Perkin Elmer Flexar HPLC (high performance liquid chromatography) pump attached to a Hamilton PRP-X100 column (4.6 x 250 mm) and coupled to a Perkin Elmer ICP-MS (inductively coupled plasma mass spectrometry) NexION350X. Ammonium citrate (5 mM; pH 5.2) containing methanol (2% *v/v*) was employed as mobile phase to achieve the separation at a flow rate of 1 ml min^{-1}. Se^{IV} amended-media without bacterial cells were used as controls. All samples were prepared in triplicate. In addition, a standard calibration curve with different solutions of known Se^{IV} concentrations was prepared (0.02-1 mM).

3.2. Effect of Se^{IV} on the bacterial growth

The potential of *S. bentonitica* to tolerate Se^{IV} was established by growing the cells under the same conditions described above (section 3.1.). Cell growth was evaluated by quantifying the total protein content in bacterial cell extracts using a modification of the method of Dhanjal and Cameotra (2010). The total protein content was correlated with the increase in the cell growth. A 1 ml aliquot of bacterial culture was taken at different time intervals to measure growth based on the protein content of the cells determined by using Bradford reagent (Bio-Rad®). Bovine serum albumin (BSA) was used as a standard. All measurements were performed in triplicate.

3.3. Flow cytometry

The cell viability and the metabolic activity of *S. bentonitica* in the presence of Se^{IV} under oxic conditions were determined by using flow cytometry technique. For this purpose, the bacterial species *S. bentonitica* was amended with 2 mM of Se^{IV} and incubated at 28 ºC and 180 rpm on a rotary shaker. All experiments were done in triplicates. After 24 and 144 h of incubation, the

cells were collected by centrifugation at 11000 x g and 4°C for 10 min. The resultant pellet was washed four times in phosphate buffered saline (PBS) pH 7. Then, the cells were dissolved in PBS adjusting the cellular density to approximately 10^6 cells/ml. For cell viability test, fluorescein diacetate (FDA) and propidium iodide (PI) were added into each sample to a final concentration of 20 µl/ml and 2 µl/ml respectively. For metabolic activity test, 3,30-dihexyloxacarbocyanine iodide (DiOC6) was employed to a final concentration of 20 µl/ml. Finally, the samples were analysed by Forward Scatter using a FACSCantoII™ cytometer (Becton Dickinson). Se^{IV}-free cultures and dead cells obtained by heating the biomass at 90 ºC served as controls.

3.4. Bacterial synthesis, extraction, and purification of selenium nanoparticles

SeNPs were synthesized aerobically by *S. bentonitica* under 2 mM Se^{IV} stress as previously described (section 3.1.). After period of 48 and 144 h of incubation, the SeNPs were extracted and purified following the method described by Sonkusre (2014). Finally, purified SeNPs were spread onto LB agar plates to check the efficiency of the extraction process.

3.5. Attenuated total reflectance-Fourier transform infrared spectroscopy (ATR-FTIR)

The samples of bacterial cells supplemented with 2 mM Se^{IV} were harvested after 48 and 144 h of incubation by centrifugation (11000 x g, 10 min). The precipitates were washed 3 times with distilled water and dried at 28°C. Then the samples were powdered in an agate mortar and kept in a desiccator. Finally, 1 mg of the powder was mixed with 100 mg of dried potassium bromide (KBr) and pressed forming disks. Bacterial cells solutions without Se^{IV} were used as a control. In addition, purified SeNPs extracted after 48 and 144 h incubation were analysed by this technique.

ATR-FTIR measurements were performed on a Perkin Elmer Spectrum One FT-IR spectrometer, equipped with a Silver Gate Evolution ATR accessory, consisting of a germanium crystal. A total of 200 scans for purified SeNPs and 32 for the other samples within wavenumber range from 4000 to 600 cm^{-1} were collected for each sample. Spectra obtained were baseline corrected and normalised to 1.5 absorbance (arbitrary units) using the 1650 cm^{-1} Amide I absorption band within the control sample (*S. bentonitica* biomass without Se). All data acquisition and processing were performed using the Perkin Elmer Spectrum version 3.3 to obtain peak positions and relative peak intensities.

3.6. X-ray photoelectron spectroscopy (XPS)

Both purified and cell associated SeNPs obtained as indicated for ATR-FTIR experiments under the same conditions (2 mM Se^{IV}, 48 and 144 h of incubation) were analysed by XPS. In addition, a cell biomass powder was used as control. The powder samples were all mounted by pressing them into indium foil, which was adhered using double sided carbon tape to a paper label stuck to the XPS sample mount.

The analyses were carried out using a Kratos Supra instrument with a monochromated aluminium source, and two analysis points per sample. Survey scans were collected between 1200 to 0 eV binding energy, at 160 eV pass energy, 1 eV intervals, and 300 seconds/sweep. High-resolution O 1s, N 1s, C 1s, S 2p, P 2p and Se 3d XPS spectra were also collected at 20 eV pass energy and 0.1 eV intervals for each analysis point over an appropriate energy range, with one 300 second sweep for all elements except N 1s and S 2p for which two sweeps were used. The data collected was calibrated in intensity using a transmission function characteristic of the instrument (determined using software from NPL) to make the values instrument independent. The data can then be quantified using theoretical Schofield relative sensitivity factors. All peaks positions were calibrated with respect to the C-C/C-H peak position at 285.0 eV.

3.7. HAADF-STEM analysis

The morphology and elemental composition analysis of purified SeNPs were analysed by using Transmission electron microscopy (TEM) equipped with energy dispersive X-ray (EDX). EDX analysis was performed at 300 kV using a spot size of 4 Å and a live counting time of 50 s. The structural characterization of SeNPs were analysed by using selected-area electron diffraction (SAED).

TEM samples consisting of purified SeNPs produced by *S. bentonitica* after 48 and 144 hours of incubation were prepared using the conventional negative staining. Finally, the samples were examined under HAADF-STEM microscope FEI TITAN G2 80-300. STEM specimen holders were cleaned by plasma prior to STEM analysis to minimize contamination.

3.8. X-ray absorption spectroscopy (XAS)

S. bentonitica cells were grown in LB media amended with 2 mM Se^{IV}. After 24, 72 and 144 h of incubation the cells in contact with Se^{IV} were harvested by centrifugation (10000 x g; 10 min). Then, the samples were prepared as previously described in Merroun et al. (2005) with

some modifications. The resultant pellets were washed twice with sterile double distilled water to remove the cell debris and the interfering ingredients of the growth medium and dried at 28 ºC. Then the samples were powdered in an agate mortar and kept in a desiccator. Finally, the powdered samples were prepared by spreading and pressing them onto 10 mm x 3 mm area of Kapton tape, which was sealed between additional layers. Selenium references (sodium selenate, sodium selenite, Se(0) foil and selenium sulfide) XAS data were collected in transmission mode. Each standard were prepared by mixing the powder with dried cellulose and pressed forming disks (13 mm of diameter).

Selenium K–edge X-ray absorption spectra were collected at the MARS beamline at the SOLEIL synchrotron facility (ring operated at 2.75 GeV with 400 mA), which is the French bending magnet beamline dedicated to the study of radioactive materials (Sitaud et al., 2012) using a Si(220) double-crystal monochromator with horizontal dynamical focusing, and Pt-coated mirrors for vertical focusing and rejection of higher harmonics (Solari et al., 2009). Spectra were collected in transmission mode using a 13-element Ge detector (EG & G ORTEC, USA). Data were processed following standard procedures by using the Athena/Artemis codes (Ravel and Newville, 2005). Background removal was performed by means of a pre-edge linear function. Atomic absorption was simulated with a square-spline function. The theoretical phase and amplitude functions used in data analysis were calculated with FEFF8 (Ankudinov and Ravel, 1998) using Se foil as model. The amplitude reduction factor (S_0^2) was held constant at 1.0 for the FEFF8 calculation and extended x-ray absorption fine structure (EXAFS) fits. The shift in threshold energy, ΔE_0, was varied as a global parameter in the fits.

3.9. Detection and identification of volatile Se compounds

A combined thermal desorption GC-MS system were employed for the detection and identification of Se volatile species produced by the bacterial strain *S. bentonitica*. Cultures of *S. bentonitica* were grown in the presence of Se^{IV} (0.1 and 2 mM) into 250 ml conical Quickfit® flask capped with Suba-Seals (Sigma®) to avoid the loss of gases during gas extraction with hypodermic syringes. Se^{IV}-free cultures (biotic) and Se^{IV}-amended media (abiotic) were used as controls. The gaseous samples were taken and analysed as described previously by Eswayah et al. (2017) after 24 and 144 h of incubation. The National Institute of Standards and Technology (NIST) MS search program (version 2011) was employed to identify compounds based on their mass spectrum.

4. Results

4.1. Time course experiments for Se^{IV} reduction

The time course of Se^{IV} reduction by the strain *S. bentonitica* was studied in the presence of different initial Se^{IV} concentration. Se^{IV} was completely reduced after 24, 48 and 120 h when the cells were grown on 0.1, 0.25 and 2 mM, respectively (Figure 1). Therefore, Se^{IV} removal depends on the initial concentration, where Se^{IV} is removed faster at low initial concentration (0.1 mM) than at high concentrations (2 mM). These results clearly show the high efficiency of the strain *S. bentonitica* BII-R7 in reducing Se^{IV}. No variation in Se^{IV} concentration of abiotic controls (Se^{IV} amended-media without bacterial cells) confirmed that the bacterial strain is involved in the reduction of Se^{IV} concentration (data not shown). Figure 1 also indicated the decrease of the amount of Se^{IV} per g of cell protein with time in all concentration assayed, which match with the increase in the percentage of reduced Se^{IV}.

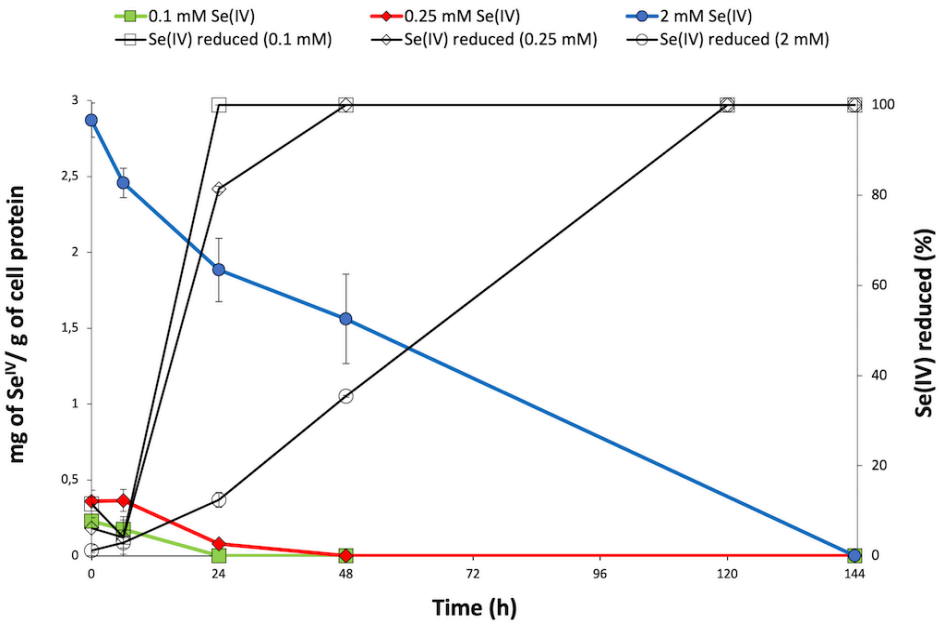

Figure 1. Time course of selenite reduction by *S. bentonitica* in the presence of 0.1 mM, 0.25 mM, and 2 mM as initial Se^{IV} concentration expressed as percentage of Se^{IV} reduced (symbols: □, ◊, ○) and amount of Se^{IV} (mg) per g of cell protein (symbols: ■, ♦, ●). Selenite was added at zero time. Each curve shows means based on the results of triplicates.

The decrease in the amount of Se^{IV} at a given initial concentration matches with the growth profile of the cells as measured by the total protein content. The presence of Se^{IV} has an inhibitory effect at the early stage of the bacterial growth as shown by the initial long lag phases in the first 48 h (Figure 2). As we have previously reported, this stress is most probably due to

the presence of Se (Ruiz-Fresneda et al. 2018). The optimal growth of Se^{IV}-treated cells was reached at 96 h (for 0.1 mM Se^{IV}) and around 144 h (for 0.25 and 2 mM Se^{IV}) once the Se^{IV} has been completely reduced.

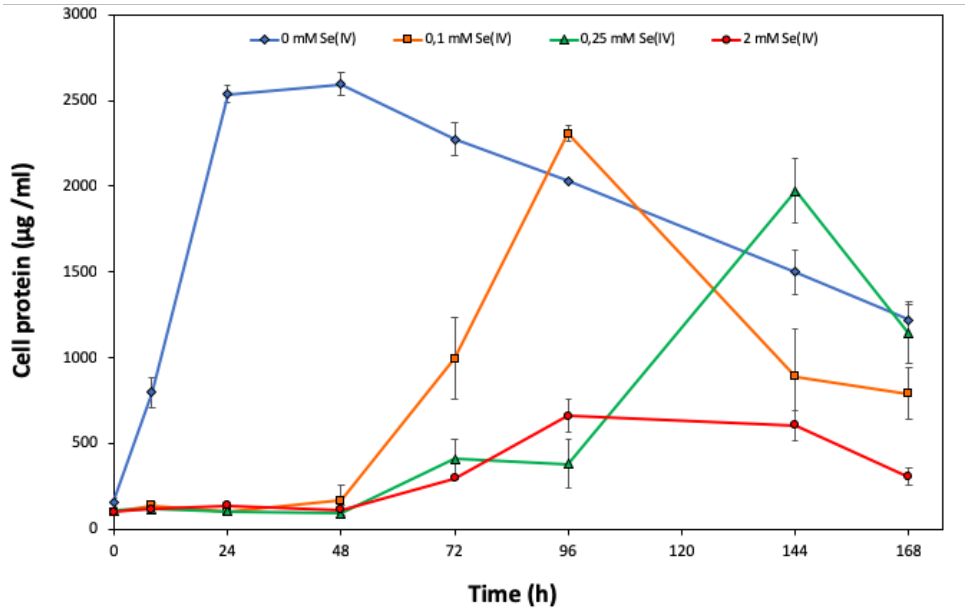

Figure 2. Growth profile of *S. bentonitica* in the absence and the presence of 0.1, 0.25, and 2 mM Se^{IV}. Selenite was added at time zero. Each curve shows means based on the results of triplicates.

The effect of Se^{IV} on cell viability of *S. bentonitica* was studied by the live-dead staining approach conducted with propidium iodide (PI) and fluorescein diacetate (FDA). PI enters to cells with damaged membranes staining nucleic acids of dead cells (Givan, 2011), while FDA stains viable cells (Stubberfield and Shaw, 1990). With regard to the metabolic activity test, the fluorescent dye $DiOC_6$ was used in order to bind polarized membranes of active cells (David et al. 2011). The percentages of viable and active cells of *S. bentonitica* population untreated and treated with an initial Se^{IV} concentration of 2 mM during 24 and 144 h are displayed in Figure 3A-B. Cell viability was affected negatively by Se^{IV}. Specifically, 46.3 and 36.4 % of cell populations were found to be viable after 24 and 144 h time incubation, respectively. In contrast, higher amount of viable cell population (100 %) was observed in untreated samples. On the other hand, the metabolic activity test showed a lower oxidative response under Se^{IV} stress. Specifically, 59 and 72.2 % were found to be active after 24 and 144 h respectively, comparing with untreated cells (97 and 97.8 % of active cells). This increase on cell activity from 59 to 72.2 % could be explained by the fact that at 24 h cells are still in the lag phase (see Figure 2), probably adapting their metabolism to respond to Se stress. Once they are able to tolerate Se they grow as observed at 144 h. The results of the flow cytometry concur with the growth curve suggesting a toxic effect of Se^{IV} on *S. bentonitica* cells.

The reduction of Se^{IV} could be also appreciated by the appearance of a red colour in Se^{IV}-amended cultures. However, under 0.1 mM Se^{IV} stress, cultures turned back from red to a mid-brown colour after 48 h incubation. This fact suggested that other further mechanism in addition to reduction seem to be involved. The absence of Se^{IV} at 48 h (Figure 1) rejects an oxidation of Se compounds as possible mechanism. However a volatilization process to methylated Se products it is possible. In fact, a characteristic garlic-like odor generated in the Se^{IV}-treated cultures suggested the formation of Se volatile species.

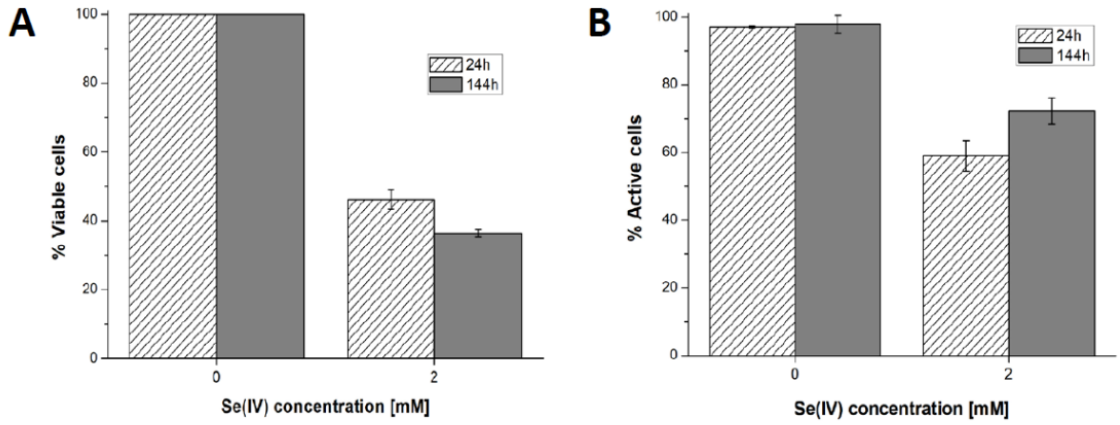

Figure 3. Percentage of viable (A) and active cells (B) of *S. bentonitica* under different Se^{IV} concentrations (0 and 2 mM) and contact times (24, and 144 h) under aerobic conditions.

4.2. Synthesis and purification of the selenium nanoparticles

The SeNPs were biogenically produced by *S. bentonitica* by reducing the oxyanion Se^{IV} to non-toxic Se^0 as described in Ruiz-Fresneda et al. (2018). The latter study revealed the formation of amorphous Se nanospheres and different crystalline Se nanostructures can be located intracellularly and extracellularly. An improved method reported by Sonkusre et al. (2014) for the recovery of the SeNPs was performed. This procedure includes cell lysis using lysozyme (Sigma®) and French press. Afterwards, the separation of the nanoparticles from cell debris was conducted by two-phase water-octanol extraction (Figure 4A). Finally, the water phase containing the SeNPs was subsequently washed with chloroform, absolute ethanol, ethanol (70%) and resuspended in water, obtaining the solution of purified SeNPs (Figure 4B). No cell growth were detected when the harvested and purified SeNPs were incubated on LB agar plates, thus indicating the high efficiency of the purification steps in removing bacterial cells.

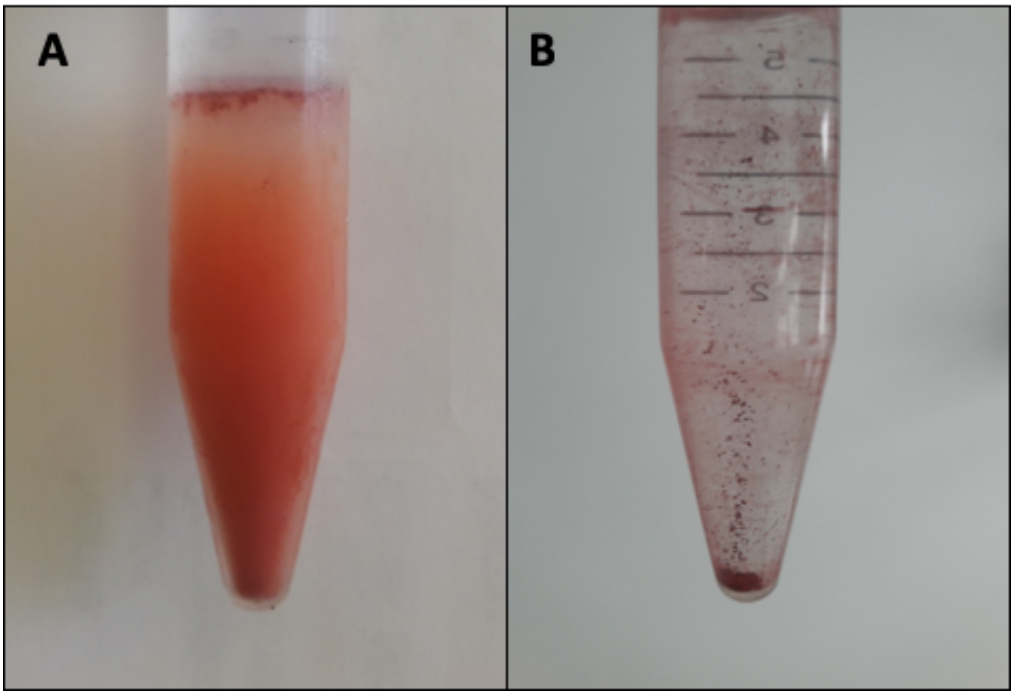

Figure 4. Separation of SeNPs from cell debris by a two-phase water-octanol extraction system (A) and final solution of purified SeNPs in water (B).

4.3. Microscopic characterization of the purified selenium nanoparticles

STEM-HAADF micrographs of purified SeNPs produced by *S. bentonitica* after 48 and 144 h of incubation showed the presence of spherical electron-dense structures with sizes ranging from 100 to 400 nm (Figure 5A and 5B). These structures frequently appeared forming aggregates (Figure 5B-C). EDX analysis and EDX elemental-distribution maps confirmed that they consisted of Se (Figure 5D-E). Additionally, the ED pattern indicated their amorphous nature (Figure 5F). Changes in the spherical morphology have been shown to occur in some Se nanospheres (Figure 5B), probably as an intermediate step in the transformation from amorphous nanospheres to trigonal Se crystals as reported in Ruiz-Fresneda et al. (2018) (Capítulo II). The presence of Se crystals in the 144 h sample also supports the proposed transformation process (Figure 6A). The HRTEM image of an individual Se nanostructure confirmed its crystallinity as indicated a d-spacing of 0.38 nm (Figure 6B). An additional d-spacing of 0.28 nm was calculated from the SAED pattern (Figure 6B inset). These d-spacings (0.38 and 0.28 nm) could correspond to (100) and (101) planes of t-Se, respectively suggesting the trigonal crystalline phase of these nanostructures.

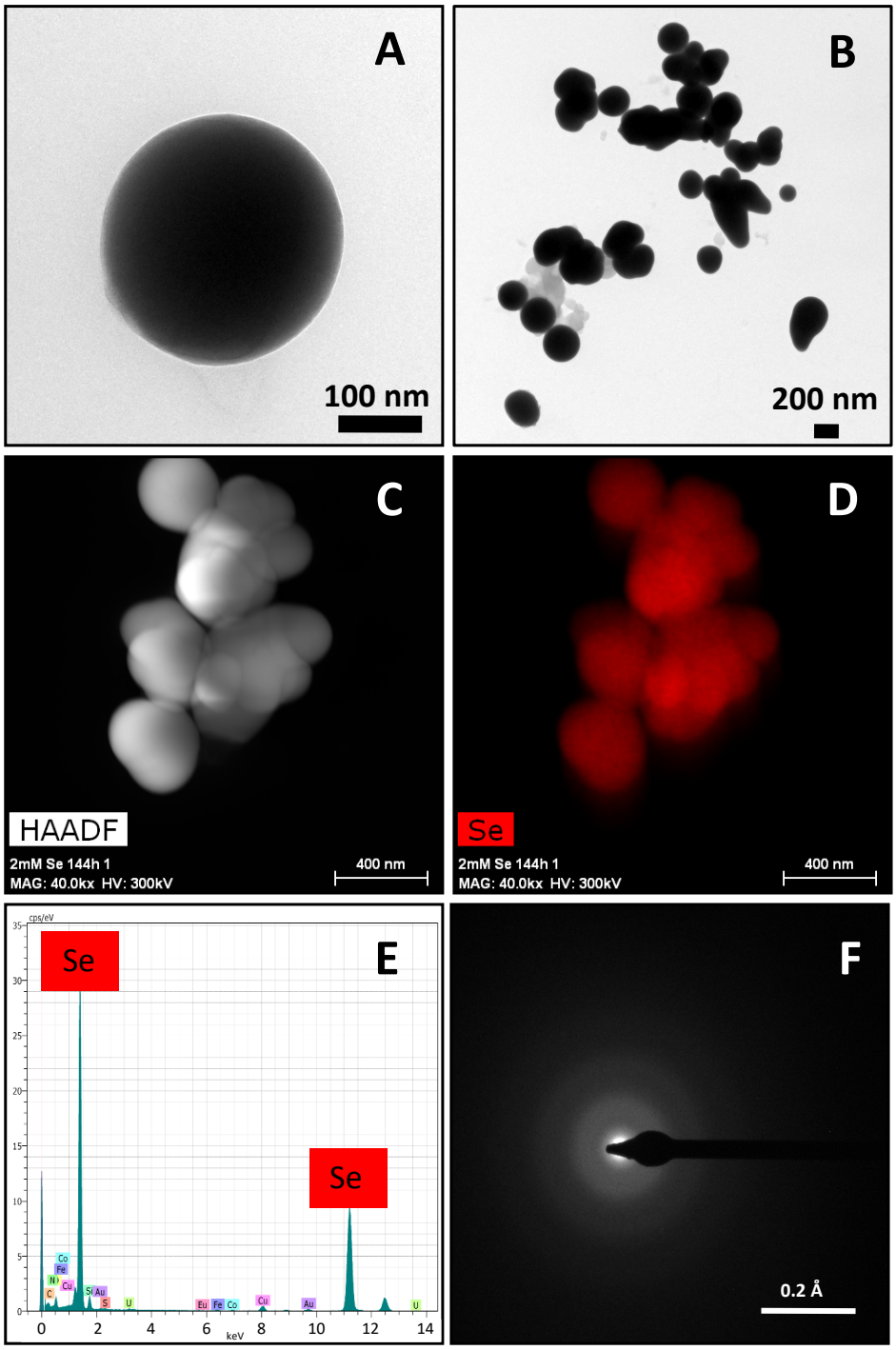

Figure 5. STEM-HAADF images showing Se nanospheres distributed individually (A) and forming aggregates (B). EDX elements distribution maps and EDX analysis indicating the Se composition of the nanospheres (C,D, and E). ED pattern derived from the Se nanospheres (F).

Negative staining of the samples allowed the detection of an organic layer coating the Se nanostructures (Figure 7); suggesting the presence of amine rich organic material. The results show the efficiency of the purification method since no cell debris was detected, and only the SeNPs are evident.

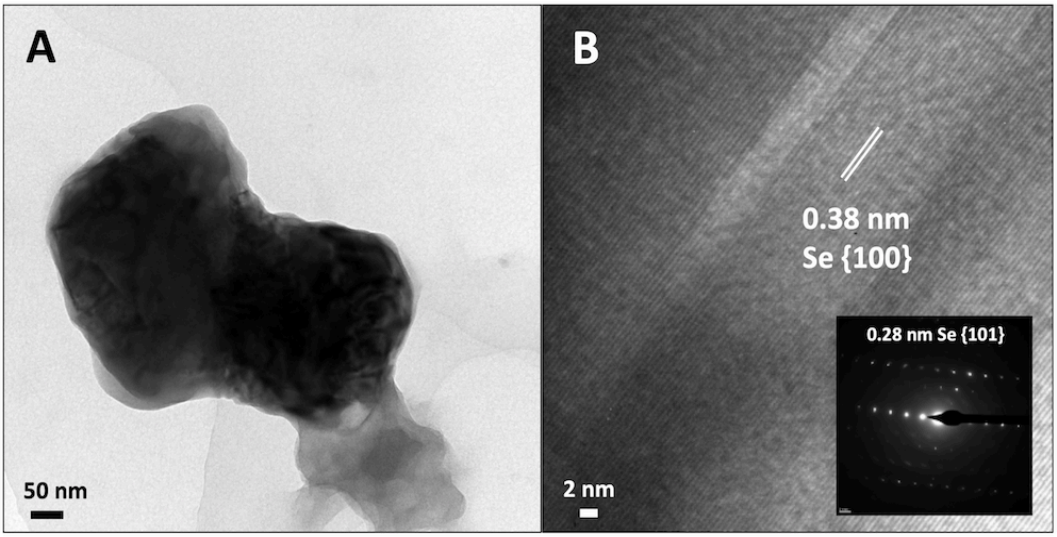

Figure 6. STEM-HAADF micrograph of a single crystalline Se nanostructure (A) and its derived HRTEM image showing a d-spacing of 0.38 nm (B). Panel inset in B shows the SAED pattern of the Se crystal.

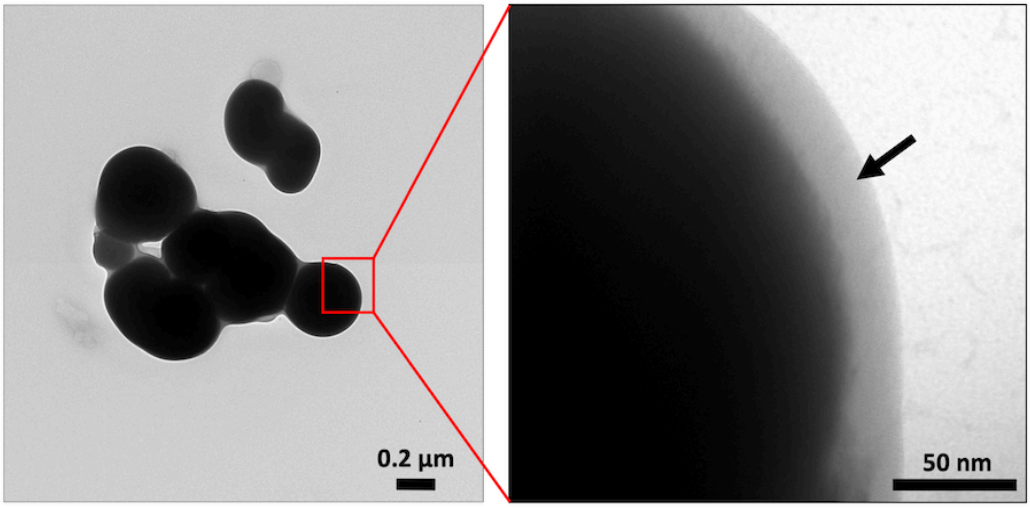

Figure 7. STEM-HAADF image showing an organic layer (arrow) coating the Se nanospheres.

4.4. Molecular and atomic interactions of microbial Se reduction products

4.4.1. ATR-FTIR analysis

ATR-FTIR spectroscopy was used to determine the possible functional groups of *S. bentonitica* cells associated with the surface of the synthesised SeNPs. ATR-FTIR spectra of the control sample (*S. bentonitica* biomass), cell associated SeNPs (*S. bentonitica* biomass in contact with 2 mM Se^{IV}) as well as purified SeNPs produced after 48 and 144 h of incubation are shown in Figure 8A and 8B, respectively. No differences in the spectra were found with increased incubation times.

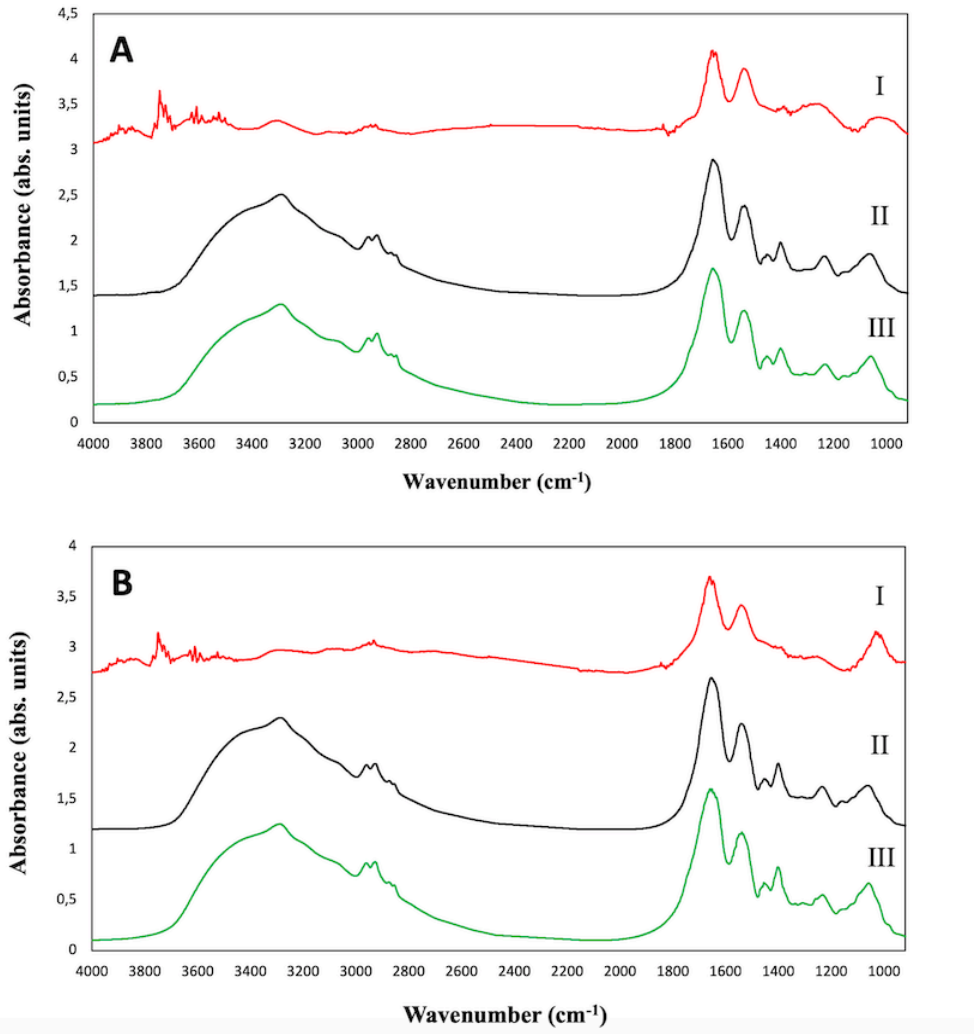

Figure 8. ATR-FTIR spectra of S. *bentonitica* biomass in the absence (I) and presence (II) of 2 mM Se^{IV}, and purified SeNPs (III) after 48 (A) and 144 h (B) of incubation.

Control spectra showed the typical ATR-FTIR spectral regions of bacterial biomass with absorption peaks within the regions dominated by stretching vibrations of functional groups in proteins, lipids and polysaccharides (Table S1). The spectra of the bacterial cells grown in the presence of Se show no remarkable shifts in the absorption bands in comparison with controls. This suggests that the amount of SeNPs in the bacterial culture was too low to give any detectable spectroscopic contribution specifically from SeNPs (Kamnev et al., 2017). In addition, the small size and mobility of the nanoparticles could make it difficult to detect noticeable changes in the spectra. In the purified SeNPs samples, the absorption bands at around 1659 and 1538 cm^{-1} mainly due to C-O vibrations corresponding to Amide I as well as N-H and C-N vibrations of peptide band attributed to Amide II of proteins were detected. The non-presence of complementary absorption bands characteristic of stretching in functional groups of proteins suggests that Amide I and II bands correspond to amino acid residues coating the SeNPs. These results confirmed the presence of organic layers composed by amine rich matter

surrounding the SeNPs as suggested by STEM-HAADF analysis. The detection of typical protein bands of isolated SeNPs biogically produced by the bacteria *Azospirillum brasilense* Sp7 and *Stenotrophomonas maltophilia* SeITE02 were also reported in other studies (Kamnev, 2008; Lampis et al., 2017).

4.4.2. XPS analysis

The composition of the surface coating the Se reduction products was also analysed by XPS. It is noteworthy that no differences between 48 and 144 h samples were detected. The most immediate difference between the purified SeNPs and the cell associated SeNPs was the shape of the survey scans (Figure 9A-B). The spectrum for the purified nanoparticles suggests a high number of photoelectrons that have been inelastically scattered such that the inelastic background is more pronounced than the photoelectron peaks. The background maxima is around the photoelectron peaks for the Se, suggesting that it consists of Se photoelectrons that have lost only a small but variable amount of kinetic energy. This suggests the SeNPs are probably entirely wrapped in a very thin layer of material. The overall surface composition determined by quantifying the survey scans showed the presence of C, N and O indicating that this material is most likely to be organic (Table S2). The purified SeNPs showed much higher Se content than the cell associated samples, but also a very high carbon concentration consistent with the Se being wrapped in a thin layer of organic material.

It was found that 4 peaks gave the best fit for the C 1s spectra, most probably due to C-C and C-H bonds, C-O and C-N which have not been resolved, C=O and O-C=O type carbon environments (Figure S1). The relative concentrations of the different components are most similar for the biomass control and the cell associated nanoparticles. However the deconvoluted carbon peak for the purified nanoparticles showed components at different positions from the other samples, suggesting a slightly different composition of the organic material (Figure S1). The oxygen high resolution spectra show a similar result with peak areas and binding energies slightly different for the purified nanoparticles than the rest of the samples (Figure S1). The high nitrogen concentrations recorded at a binding energy of approximately 400 eV are consistent with high concentrations of amine groups (Table 1; Figure S1). All samples appeared to show a second much smaller component at a slightly higher binding energy that most likely corresponds to protonated amines (Table 1; Figure S1).

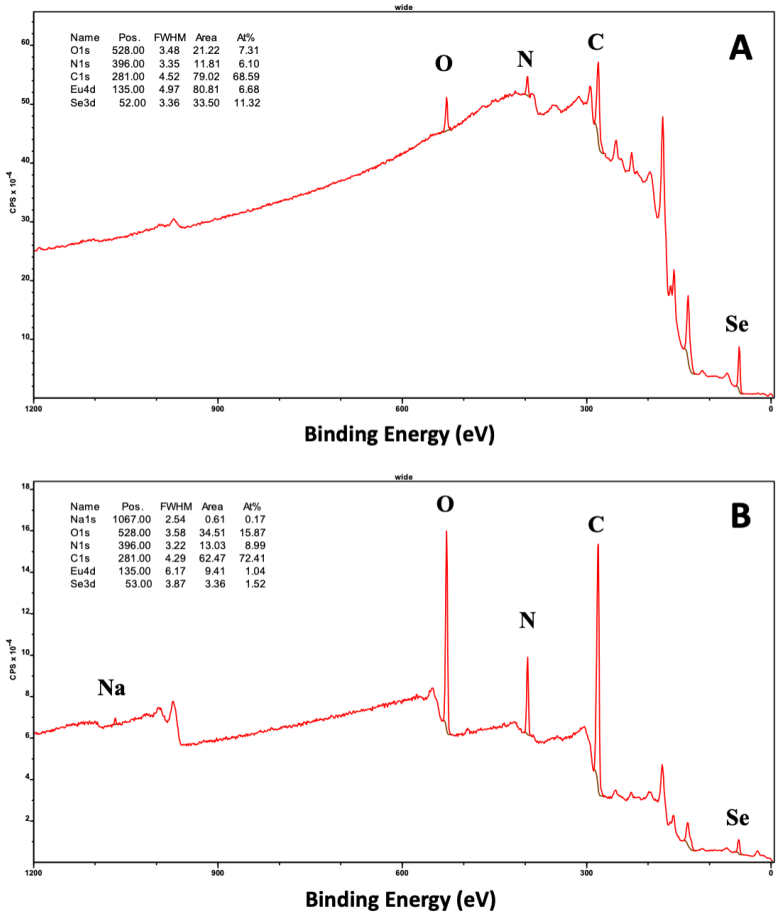

Figure 9. XPS survey scan of purified SeNPs (144 h) (A) and cell associated SeNPs (144 h) (B).

The Se 3d peak is made up of two components: the Se $3d^{3/2}$ and the Se $3d^{5/2}$. Values from the literature (https://xpssimplified.com/elements/selenium.php) suggest these are separated by 0.86 eV with a fixed area ratio of 0.735:1. The curve fits used to fit the data have these two parameters fixed. It was found that two pairs of peaks were necessary to fit each Se peak, and the widths of these pairs were allowed to vary independently. From the literature (Briggs and Seah, 1983) metallic selenium Se^0 is expected $3d^{5/2}$ at 55.1 eV, whereas Se^{IV} is expected at approximately 59.4 eV, Se^{VI} at approximately 61 eV, Se^{II} at approximately 57.7 eV and Se^{-II} at binding energies <55 eV. It has also been seen that Se^0 can be polarised leading to slightly higher binding energies (Rupp and Weser, 1975). The binding energy at 55.2 eV for the purified nanoparticles (Figure 10A) (Table 1) suggested that all the selenium is Se^0, but that approximately 50% of the signal is due to Se influenced by the outer thin layer of adsorbed organic wrapping the nanoparticles which has polarised the Se atoms, and the remainder is from a true metallic Se^0 core. The narrow peak width of the metallic Se^0 peak is typical of a metal sample. For the cell associated nanoparticles (Figure 10B) it must be remembered that the intensity of the Se signal is much smaller to start with, so the data is noisier.

Table 1. Binding energies (eV), % areas and assignment of XPS spectral bands of purified SeNPs, cell associated SeNPs, and cell biomass of after 144 h of incubation with *S. bent*onitica.

Binding Energy (eV)			% area			Assignment
Purified SeNPs	Cell associated SeNPs	Cell biomass	Purified SeNPs	Cell associated SeNPs	Cell biomass	
C 1s						
284.9	285	285	51.2	52	46.1	C-C, C-H
286.6	286.4	286.3	30.5	27.7	32	C-O, C-N
288.4	288	287.8	14.4	15.4	14.3	C=O
290.1	288	289.1	3.9	4.9	7.6	O-C=O
O 1s						
531.8	531.6	531.7	77.3	63.1	62.6	C-O
533.5	533.1	533.1	22.8	36.9	37.4	C=O
N 1s						
400.2	400.1	400.1	79.9	91.1	83.6	Amine
402.1	401.8	401.4	20.1	9	16.4	Protonated amine
Se 3d						
55.2	55.7	N/A	28.9	40.5	N/A	3d5/2
56.3	57.3	N/A	28.8	17.2	N/A	3d5/2
56.1	56.6	N/A	21.2	29.7	N/A	3d3/2
57.1	58.2	N/A	21.1	12.6	N/A	3d3/2

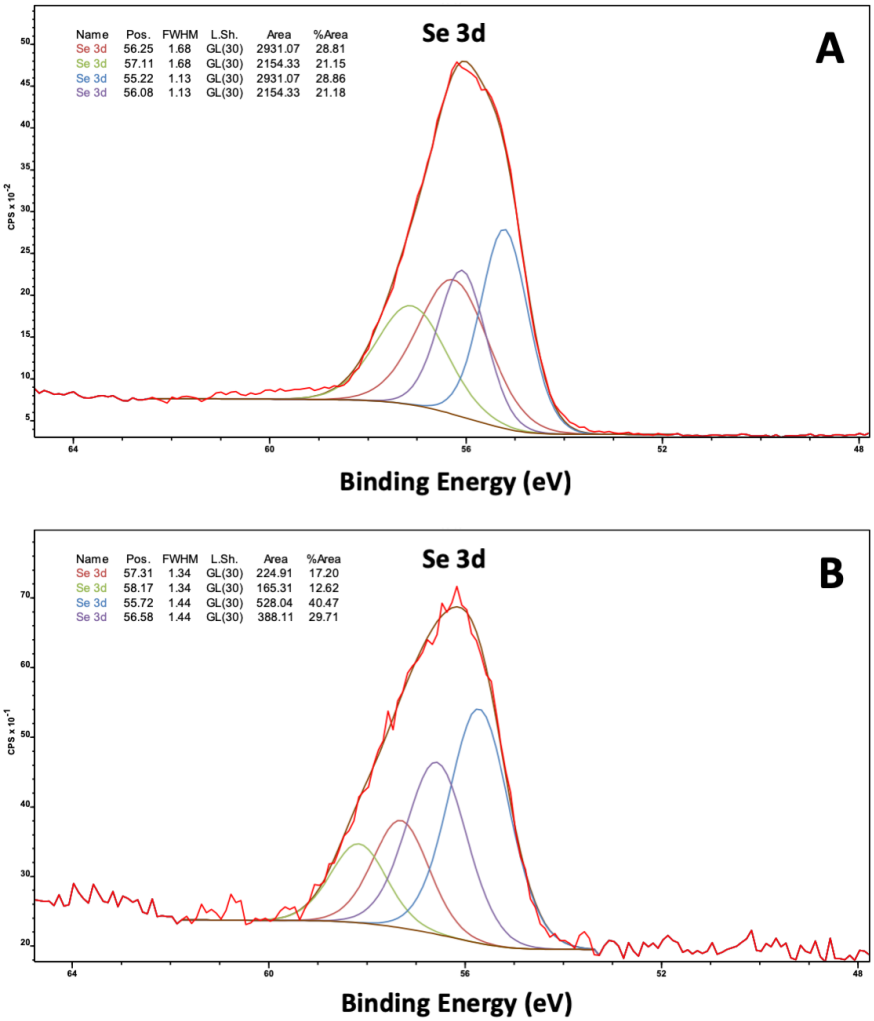

Figure 10. XPS high resolution spectra of selenium (Se 3d) from the purified SeNPs (A) and the cell associated SeNPs (B) after 144 h of incubation.

The XPS results confirmed the presence of outer layer of amine rich organic material capping the SeNPs as previously indicated HAADF-STEM and ATR-FTIR analysis. In addition, the Se reduction products seem to be present at zero-valent state (Se^0). The non-detection of binding energies corresponding to Se^{IV} agrees with the time course experiments of Se^{IV} reduction where the total content of Se^{IV} was completely reduced.

4.4.3. XAS analysis

X-ray absorption near-edge structure (XANES) analysis of biogenic SeNPs samples produced by *S. bentonitica* BII-R7 at 24, 72 y 144 h samples indicated that the local coordination of Se is dominated by Se^0 as previously suggested the colour change observed in the samples (data not shown). The Se K-edge EXAFS (extended X-ray absorption fine structure) spectra of a Se foil and of biogenic SeNPs samples produced by *S. bentonitica* BII-R7 at 24, 72 y 144h along with their corresponding Fourier transforms (FT) are presented in Figure 11. The fit parameters of the calculated spectra are summarized in Table 2.

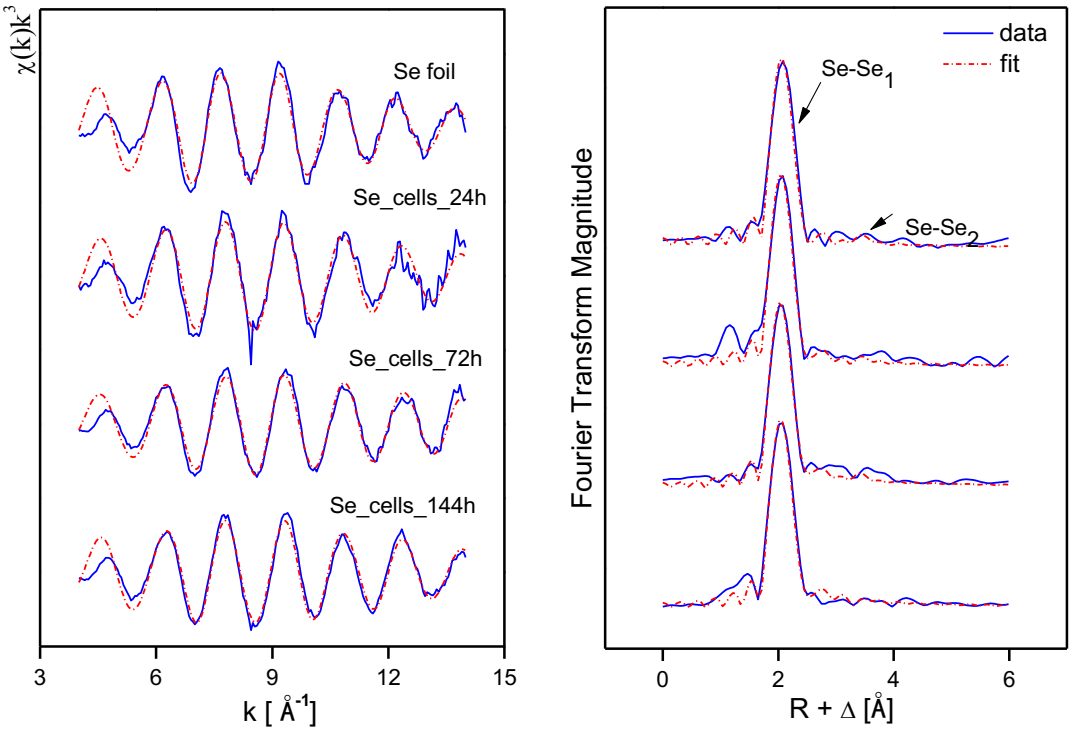

Figure 11. EXAFS spectra of Se foil and biogenic SeNPs samples produced by *S. bentonitica* at different incubation times (24, 72, and 144h) as well as their corresponding FT.

FT peak distances are reported in units of Å and are uncorrected for scattering phase shift, i.e., R + ΔR. The fit of the EXAFS spectra of the 3 experimental samples showed the presence of

two Se-Se coordination shells. The first Se-Se_1 shell was found at a bond distance of about 2.34-2.35 ± 0.02 Å. No differences were observed for the bond distance of this shell within the 3 samples. Similar bond distances values were reported for SeNPs produced by *M. capsulatus* and *M. trichosporium* (Eswayah et al., 2017) and *A. brasilense* (Vogel et al., 2018), who indicated their amorphous nature according to the bond distances obtained at 2.35 and 2.34 Å, respectively. The coordination number of this coordination sphere is ranging from 2 to 3. The Debye-Waller factor (σ^2) of this shell is ranging from 0.0022 to 0.0039 $Å^2$ in all samples, being similar to that found of the Se-Se_1 shell for biogenic SeNPs (Eswayah et al., 2017). The second Se-Se_2 coordination shell is of about 3.63- 3.70± 0.02 Å and the coordination number of this shell increases with increasing the time contact ranging from 0.2 to 0.5. These bond distances could correspond to crystalline Se as indicated by Eswayah et al. (2017) and Scheinost and Charlet (2008) who reported Se-Se coordination shells at 3.69 and 3.67-3.69 Å, respectively.

Table 2. EXAFS structural parameters of the Se foil and the biogenic SeNPs.

Sample	Shell	N[a]	R[Å][b]	σ^2 [$Å^2$][c]	ΔE[eV]
Se foil	Se-Se_1	3.4 ± 0.2	2.37	0.0044	-10.2
	Se-Se_2	0.7 ± 0.2	3.69	0.0044[d]	
Se^{IV}- Cells-24h	Se-Se_1	3.0 ± 0.2	2.35	0.0039	-9.1
	Se-Se_2	0.23 ± 0.2	3.69	0.0039[d]	
Se^{IV}- Cells-72h	Se-Se_1	2.3 ± 0.1	2.34	0.0027	-8.92
	Se-Se_2	0.25 ± 0.1	3.72	0.0027[d]	
Se^{IV}- Cells-144h	Se-Se_1	2.6 ± 0.1	2.34	0.0032	-9.4
	Se-Se_2	0.5 ± 0.1	3.63	0.0032[d]	

[a] Errors in coordination numbers are ±25% and standard deviations as estimated by EXAFSPAK
[b] errors in distance are ±0.02 Å
[c] Debye-Waller factor
[d] Debye-Waller factor (σ^2) linked to the σ^2 of Se-Se_1 path

4.5. Volatilization of selenium species by *S. bentonitica*

The headspace gas above the cultures was sampled (200 ml) and analyzed by GC-MS system in order to identify the volatile Se species. GC-MS extracted ion chromatograms for 80 m/z (specific for Se) of the samples amended with 0.1 and 2 mM Se^{IV} concentration showed the production of dimethyl diselenide (DMDSe) and dimethyl selenenyl sulphide (DMSeS) after 24 and 144 h (Figure 12A-B). No differences in the production of volatile Se species were

observed with different initial Se^{IV} concentration and incubation time. The absence of Se volatile compounds in biotic and abiotic controls (Figure 12C-D) suggested that they are produced by the bacterial cells. In addition, it is noteworthy that dimethyl disulfide (DMDS) was detected in both samples and controls since this compound could be involved in the formation of Se volatile species (Chasteen, 1993). Chasteen (1993) previously reported that a disproportionation reaction between DMDSe and DMDS to produce DMSeS is quite probable. The biotic and abiotic production of DMDS has been previously reported in the literature (Carrión et al., 2017; Higgins et al., 2006).

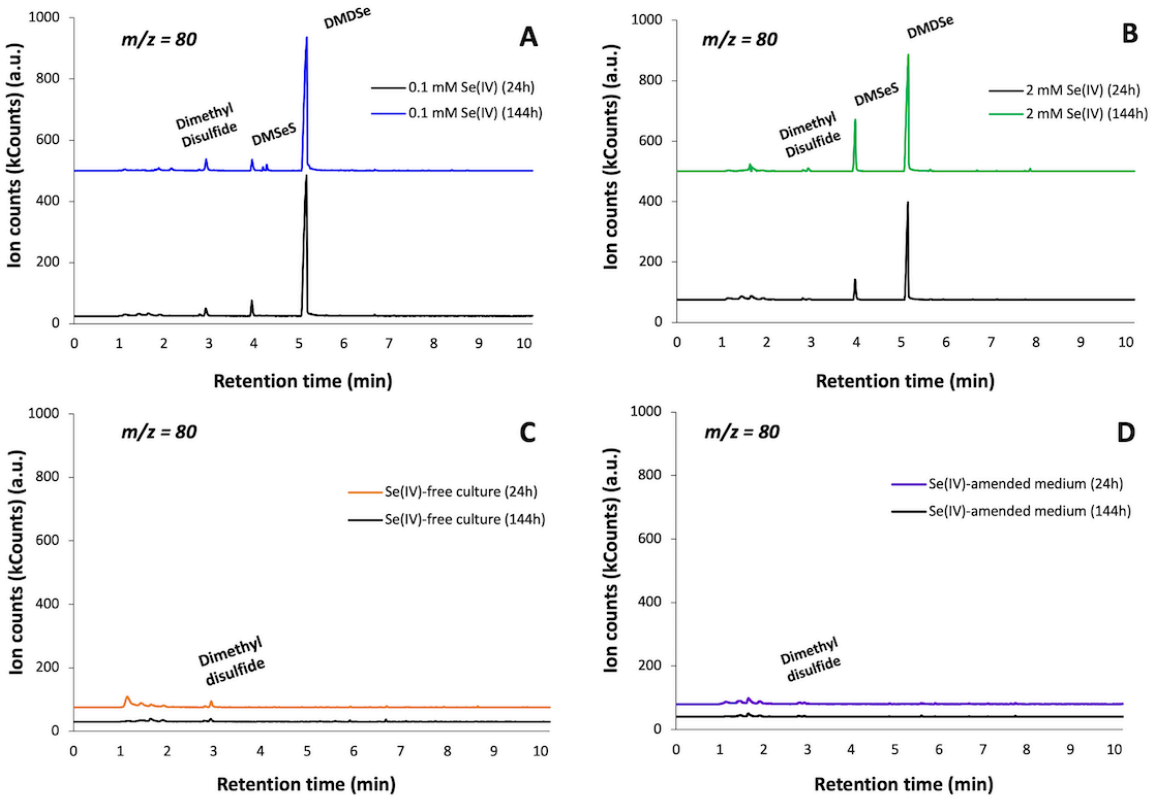

Figure 12. GC-MS chromatograms of the headspace gas of *S. bentonitica* cultures supplemented with Se^{IV} (0.1 and 2 mM) (A-B) and without Se^{IV} (C) after 24 and 144 h of incubation. Se^{IV}-amended medium (2 mM) chromatograms after 24 and 144 h of incubation were used as control (D). All GC-MS chromatograms were obtained by selecting the 80 m/z ion specific for selenium.

A number of microorganisms including phylogenetically-related species to *S. bentonitica* have been reported for their ability to produce volatile Se compounds largely in form of DMSe and DMDSe. Dungan et al. (2003) and Kagami et al. (2013) demonstrated the formation of DMSe, DMDSe and DMSeS by the bacterial species *Stenotrophomonas maltophilia* and *Pseudomonas stutzeri* NT-I, respectively. Bacteria were found to mainly generate DMSe as the most common form while DMDSe were produced in a lesser extent (Ranjard et al., 2003). In our case, *S. bentonitica* produces DMDSe and not DMSe. Less common methylated Se compounds such as

DMSeS, dimethyl selenyl disulphide (DMSeDS), dimethyl triselenide (DMTSe), and dimethyl selenone [$(CH_3)_2SeO_2$] have also been reported to be generated by several microbes (Burra et al., 2010; Reamer and Zoller, 1980). However, the specific mechanism involved in their production still remains unclear.

5. Discussion

The ability of the bacterial species *S. bentonitica* to reduce Se^{IV} to Se^0 forming Se nanostructures with different morphology (*e.g.* nanospheres, hexagons, polygons, and nanowires) has been described in a recently published work (Ruiz-Fresneda et al., 2018; Capítulo II). The time-dependent transformation of a-Se nanospheres to crystalline t-Se nanostructures was proposed as indicated by microscopy and spectroscopy results. Extracellular flagella-like proteins and organic matter produced by the cells seem to be involved in the transformation process serving as template for a-Se nanospheres aggregation.

In the present work a combination of spectroscopic (XPS, ATR-FTIR) and microscopic (STEM-HAADF) techniques were employed to confirm the involvement of biogenic proteins in the transformation of Se nanostructures. Biologically produced SeNPs were purified for a better analysis with these techniques. The STEM-HAADF results of the purified SeNPs showed the presence of crystalline nanostructures attached to extensive a-Se nanospheres aggregations, extremely supporting the proposed transformation process from amorphous to crystalline Se. The change in the shape of the nanospheres also agrees with the transformation hypothesis since the final crystalline products present different morphologies (*e.g.* hexagonal, polygonal, and nanowires). The conventional negative staining of these samples showed organics layers capping the purified SeNPs suggesting the existence of proteins surrounding them. Finally, the presence of amine rich organic material coating the SeNPs was confirmed by means of ATR-FTIR and XPS. The identification of amine rich proteins from these organic layers in the present study suggests the role of proteins on the nanospheres aggregation and transformation. These results are in agreement with the studies of Bao et al. (2016) and Debieux et al. (2011) who reported the critical role of proteins in the nucleation and self-assembly of SeNPs produced by *Thauera selenatis* and *Bacillus oryziterrae*, respectively. To the best of our knowledge, the aggregation of Se nanospheres would allow their precipitation and settlement and would be beneficial on the surroundings of the repository system of radioactive wastes. The qualitative identification of proteins associated to the SeNPs could contribute to the better understanding of the mechanisms implicated on their synthesis. However, the use of quantitative proteomic analysis would further improve our understanding about the involvement of specific proteins in the bioreduction process. Indeed, this would be helpful to enhance the production of SeNPs on

an industrial scale for many applications and bioremediation purposes. Several studies have recently included proteomic analysis to investigate the synthesis of SeNPs. Xu et al. (2018) reported that the organic layer of the SeNPs produced by the bacterial strain *Comamonas testosteroni* S44 are composed mainly by proteins as indicated quantitative analysis. Minor amounts of carbohydrates and lipids were detected, suggesting the major role of proteins in the formation of SeNPs. They reported that binding proteins to nanoparticles were nonspecific and could be a result of physicochemical processes, in contrast to previous studies indicating the role of specific proteins such as SefA (Debieux et al., 2011). However, they demonstrated that the charged amino acid rich proteins have a higher binding ability on the surface of the SeNPs. These results could be useful for the production of SeNPs by biologically produced proteins for industrial and medical applications. Future proteomic studies on the biogenic SeNPs produced by *S. bentonitica* are in progress in order to further investigate the possible role of proteins on the synthesis of SeNPs and hence on the mobilization of Se present within the repository system.

The Se reduction efficiency of *S. bentonitica* could be tested with a HPLC system coupled to ICP-MS. The results showed the complete Se^{IV} reduction under different initial concentrations assayed. The time course of Se^{IV} reduction by *S. bentonitica* is similar to other bacterial strains belonging to the same genus such as *S. maltophilia* SeITE02 (Lampis et al., 2017). Under 2 mM Se^{IV} stress SeITE02 strain is able to reduce up to 86% after 192 h of incubation. In contrast, *S. bentonitica* even present higher reduction efficiency with a 100% of reduced Se^{IV} at 120 h of incubation at the same Se^{IV} concentration. The high Se reduction efficiency of the bentonite isolate *S. bentonitica* would be beneficial within the radioactive disposal system, where Se^{IV} will be present (Dardenne et al., 2015). In addition, the obtained data would be really useful in the geochemical models used to study the influence of biogeochemical processes on Se mobility within the DGR system.

The local structure of the reduced Se was characterized by XAS. On the one hand, XANES region identified Se^0 as the oxidation state of the Se reduction products as previously suggested the colour change observed in the cultures. On the other hand, the EXAFS region showed the presence of two coordination shells at a bond distance of about 2.34-2.35 ± 0.02 Å for the first Se-Se_1 shell and about 3.63- 3.70± 0.02 Å for the second Se-Se_2 shell. It is well documented that the bond distance of the first Se-Se shell (Se-Se_1) is intimately related to the structure of Se nanostructures. The shortest bond length of this shell (2.32-2.34± 0.02 Å) is associated to red a-Se (Minaev et al., 2005). The largest Se-Se_1 bond distance (2.37 ± 0.02 Å) is related to t-Se (Popov, 1976). In the case of monoclinic Se (m-Se), the Se-Se_1 bond distance is calculated to be ranging from 2.32 to 2.34 ± 0.02 Å (Zhao et al., 1999). Therefore, the obtained Se-Se_1 bond

distance for the studied samples (2.34-2.35± 0.02Å) could correspond to the average distance of Se-Se_1 shell from different Se structures (amorphous, monoclinic and trigonal). The identification of a-Se and t-Se nanoparticles previously detected by STEM-HAADF and VP-FESEM (Ruiz-Fresneda et al., 2018; Capítulo II) supported this hypothesis. The bond distances obtained for the second Se-Se_2 shell correspond to crystalline Se according to Eswayah et al. (2017) who showed the EXAFS measurements of SeNPs produced by *M. capsulatus* and *M. Trichosporium* presented a Se-Se_2 at 3.69 Å. According to Scheinost and Charlet (2008), the Se-Se shell at 3.67-3.69 Å of Se reduced by Mackinawite minerals is in line with the structure of m-Se. Definitely, EXAFS suggested the presence of amorphous, monoclinic and trigonal Se according to the bond distances obtained in the nanostructures produced by *S. bentonitica*. The higher Debye-Waller factor (σ^2) of Se-Se_1 shell in the 24 h sample indicated the higher structural disorder of this sample in comparison with 72 and 144 h samples. This fact matches very well with microscopy results obtained in Ruiz-Fresneda et al. (2018) (Capítulo II), where amorphous SeNPs were predominantly observed at 24 h and higher structurally ordered (crystalline) Se were formed after this time.

To further investigate the reduction mechanism involved, the production of Se volatile species was studied. The biomethylation to volatile Se products leads to the removal of Se^{VI} and Se^{IV} and transference of Se from aquatic and terrestrial sites to the atmosphere in form of methyl selenides (Eswayah et al., 2016; Ranjard et al., 2003). It is well known the insolubility and limited bioavailability of methyl selenides in contrast to the highly reactive Se oxyanions (Doran et al. 1966). For this reason, methylation is considered one of the most important transformation processes in relation to bioremediation of Se. Losi and Frankenberger (1998) demonstrated that oxidation and resolubilization of Se^0 to Se^{IV} and Se^{VI} microbially induced in soil occurs at relatively low rates. Hence, the reduction of Se oxyanions to Se^0 could be only a provisional solution (Frankenberger and Arshad, 2001; Losi and Frankenberger, 1998). This fact makes biomethylation of Se to be one of the most promising technologies for the bioremediation of contaminated environments because it would allow the complete removal of Se from soil and water (Eswayah et al., 2016; Frankenberger and Arshad, 2001). The production of methylated Se compounds (DMDSe and DMSeS) by *S. bentonitica* confirmed the transformation to Se^{-II} oxidation state of the Se reduction products since methylation involve reduction to Se^{-II} when initial form is Se^{VI}, Se^{IV} and Se^0 (Eswayah et al., 2016). Both reduction and methylation of Se oxyanions (Se^{VI} and Se^{IV}) are considered a detoxification process for microorganisms since volatile compounds DMSe and DMDSe are 500 to 700 times less toxic than Se oxyanions and other derivatives (Ranjard et al., 2003). This fact suggests the potential positive influence that *S. bentonitica* would have in the planned repositories of radioactive wastes by converting toxic Se oxyanions to methylated Se species with lower toxicity. The

presence of dimethyl disulphide (DMDS) in the samples suggested its role in the formation of Se volatile species by a disproportionation reaction between DMDSe and DMDS to produce DMSeS as previously suggested Chasteen and Bentley (2003). However, more studies are required to determine the specific mechanism involved.

6. Conclusions

The present study demonstrated the reduction of the toxic selenium oxyanion Se^{IV} to less toxic species (Se^0 and volatile Se^{-II}) by the bacterium *S. bentonitica,* isolated from Spanish bentonites. The results clearly indicated the high efficiency and tolerance of *S. bentonitica* in reducing Se^{IV} and producing SeNPs and volatile methylated Se. The STEM-HAADF results support the transformation process from amorphous to crystalline Se proposed in a previous work. The local structure characterization of the Se^0 reduction products by means of XAS suggested the presence of amorphous, monoclinic, and trigonal Se and evidenced the transformation to Se crystals. Additionally, the detection of volatile methylated Se species such as DMDSe and DMSeS confirmed the ability of *S. bentonitica* to reduce Se^{IV} to the chemical species Se^{-II}. The bioproduction of methylated Se is getting attention as a promising tool for bioremediation purposes due to its lower toxicity comparing with Se oxyanions. Taken into account all above mentioned, the Se reduction products in form of Se^0 and Se^{-II} may play an important favorable role into the security of the DGR concept due to their lower toxixity.

The identification of organic layers mainly composed by amine rich material coating the biogenic SeNPs suggested the involvement of proteins in their synthesis and transformation. Consequently, proteins could influence their mobility and hence their fate in the environment. However, additional investigations are necessary to better understand the specific role of protein coating into the solubility and mobility of the Se reduction products through the surrounding environment of the deep disposal of radioactive wastes. Definitely, this work describes a new perspective on the potential impact of microorganisms on the Se mobility through the planned DGRs of radioactive wastes.

7. Conflicts of interest

The authors declare no competing financial interest.

8. Acknowledgements

This work was supported by Euratom research and training programme 2014 - 2018 under grant agreement no. 661880. The authors acknowledge the assistance of Maria del Mar Abad Ortega and Concepción Hernández Castillo, and Jaime Lazuen Alcón (Centro de Instrumentación Científica, University of Granada, Spain) for their help with microscopy and flow cytometry measurements. The authors also thank the assistance of Deborah Hammond (Sheffield Surface Analysis Centre, University of Sheffield, UK) and Jaime Gomez-Bolivar with the XPS analysis and XAS measurements, respectively.

9. Supplementary material

Table S1. Main infrared absorption bands and their tentative assignment found in the FTIR spectra of *S. bentonitica* (Kamnev, 2008; Naumann, 2000).

Wavenumber (cm^{-1})	Functional group assignment
3289	N-H stretching in Amides (Amide A) of proteins.
2960	C-H antisymmetric stretching vibrations in $-CH_3$ characteristics of fatty acid chains of membranes and amino acid side-chain.
2927	C-H antisymmetric stretching vibrations in $-CH_2$ characteristics of fatty acid chains of membranes and amino acid side-chain.
2874	C-H symmetric stretching vibrations in $-CH_3$
2855	C-H symmetric stretching vibrations in $-CH_2$ in fatty acids
1657	Stretching C=O in amides (amide I band) of proteins
1537	N-H bending and C-N stretching in amides (amide II band) of proteins. Asymmetric stretching for deprotonated COO^- groups
1401	C=O symmetric stretching vibrations of COO^- functional groups of amino acid side chains or free fatty acids.
1235	Vibrations of C-O in carboxylic groups. Double bond stretching of >P=O of general phosphoryl groups and phosphodiester of nucleic acids.
1062	P=O symmetric stretching in nucleic acids. Stretching vibrations of C-OH, C-O-C and C-C of polysaccharides.

Table S2. Surface composition determined by quantifying XPS survey scans.

Sample	Na	O	In	N	C	Se	S	P
Purified SeNPs (2 days n1)	<0.1	8.1	<0.1	8.1	66.3	10.9	<0.1	<0.1
Purified SeNPs (2 days n2)	<0.1	8.1	1.0	7.0	65.3	11.7	<0.1	<0.1
Purified SeNPs (6 days n1)	<0.1	7.3	<0.1	6.1	68.6	11.3	<0.1	<0.1
Purified SeNPs (6 days n2)	<0.1	10.5	3.5	6.9	63.4	10.0	<0.1	<0.1
Cell associated SeNPs (2 days n1)	0.3	16.6	<0.1	7.9	73.4	1.0	<0.1	<0.1
Cell associated SeNPs (2 days n2)	0.2	16.8	0.2	7.8	73.2	1.0	<0.1	<0.1
Cell biomass (6 days n1)	0.2	17.5	0.1	9.7	71.4	<0.1	0.2	1.1
Cell biomass (6 days n2)	0.2	17.4	0.2	9.6	71.2	<0.1	0.4	1.0
Cell associated SeNPs (6 days n2)	0.2	15.9	<0.1	9.0	72.4	1.5	<0.1	<0.1
Cell associated SeNPs (6 days n1)	0.2	16.0	<0.1	9.5	71.6	1.6	<0.1	<0.1

Figure S1. XPS high resolution spectra of carbon (C 1s), oxygen (O 1s), and nitrogen (N 1s) from the purified SeNPs, the cell associated SeNPs and the cell biomass of *S. bentonitica* after 144 h of incubation.

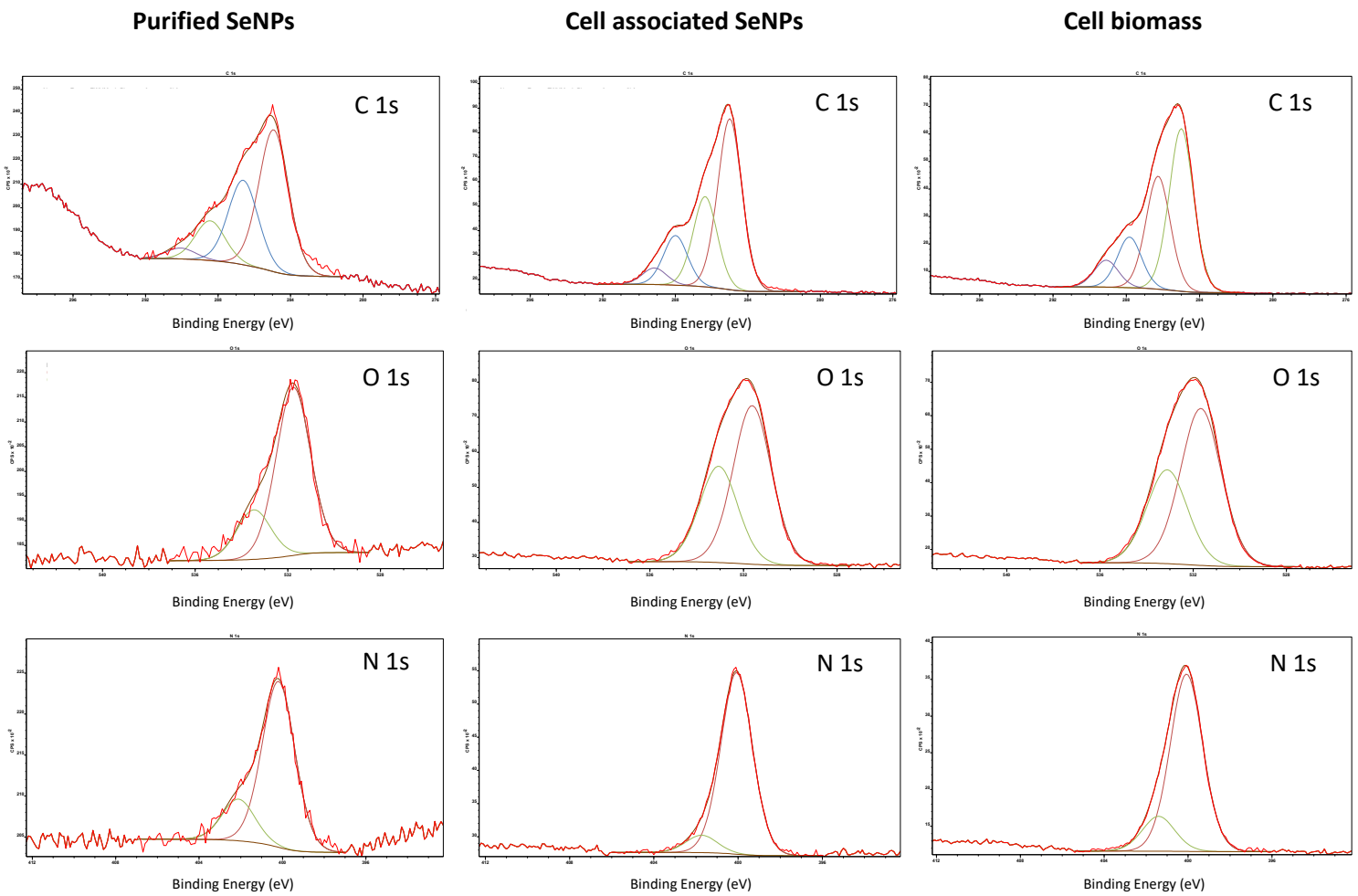

CAPÍTULO IV:

Bioreduction of selenite under anaerobic and alkaline conditions analogous to those expected at the deep geological repository system

Miguel A. Ruiz-Fresneda[1], Jaime Gomez-Bolivar[1], Maria M. Abad-Ortega[2], Isabel Guerra-Tschuschke[2], Mohamed L. Merroun[1]

[1]Department of Microbiology, University of Granada, Granada, Spain

[2]Centro de Instrumentación Científica (CIC), University of Granada, Granada, Spain

To be submitted to the journal Frontiers in Microbiology

1. Abstract

The environmental conditions of the planned geological disposal of radioactive waste including hyper-alkaline pH, radiation, or anoxia, are expected to be extremely harsh for microbial activity. However, it is thought that microbial communities will develop in these repositories having implications for geodisposal integrity and controlling the migration of radionuclides through the surrounding environment. Microbial use of a variety of electron acceptors that will be present in the geodisposal system may lead to the enzymatic reduction and hence immobilization of radionuclides. Nuclear waste will contain radioactive isotopes of selenium (Se) such as ^{79}Se, which has been identified as one of the main radionuclides in the geodisposal system. Here we use the bacterial species *Stenotrophomonas bentonitica*, isolated from clays that will be used as artificial barrier in repositories, to study the reduction of selenite (Se^{IV}) simulating geodisposal conditions. This bacterium is able to reduce toxic Se^{IV} anaerobically from neutral to alkaline pH (up to pH 10) producing elemental selenium (Se^0) nanospheres and nanowires. A transformation process from amorphous Se (a-Se) nanospheres to trigonal Se (t-Se) nanowires through the formation of monoclinic Se (m-Se) aggregates as intermediate step was proposed. The non-cell proliferation and low viability and activity rates of *S. bentonitica* cells under these stressful conditions are probably involved in the lower production of t-Se comparing to those obtained aerobically in previous studies. This fact suggested a slower transformation process under alkaline and anaerobic conditions. The less solubility of Se^0 and t-Se makes *S. bentonitica* a potential candidate for positively influence the security of the geodisposal system, most probably with lower efficiency rates than those obtained aerobically. This research will be useful for the security evaluation of repositories by predicting the possible microbial processes that may occur.

Keywords: *Stenotrophomonas bentonitica*, selenite, reduction, alkaline, anaerobic, disposal

2. Introduction

Nowadays, there is a growing concern about the extensive use of nuclear technology due to the increasing of radioactive waste inventory. The total amount of nuclear waste, extremely hazardous to the environment and living organisms, is expected to increase in the near future with the potential building of the next generation of nuclear reactors. For this reason, the deep geological repository (DGR) of intermediate and high-level waste (ILW and HLW) has been adopted by many countries to safely store and isolate them (IAEA, 2003). These radioactive residues will be disposed in steel, iron or concrete containers and backfilled with bitumen, cement matrix, or bentonite clays at a depth of 500-1000 m in different host rocks depending on the country. Clay formations will play a crucial role in many DGR design as host rock and engineered-barrier in France, Belgium, and Switzerland (Delage et al., 2010). Specifically, bentonite clays will be employed for mechanical, hydraulic and thermal protection of the containers because of their physical and geochemical properties (Alonso et al., 2004). Aerobic conditions are expected to dominate the DGR system after closure since oxygen will enter during the construction and operational periods. In the post-closure period, anaerobic conditions are expected to be established with a wide range of electron acceptors, organic matter and other compounds available. In addition, hyperalkaline (~ pH 12) conditions will dominate due to the extensive use of cementitious materials (Berner, 1992).

The environment within the DGR system is estimated to be extremely harsh for life. The presence of radionuclides, high-radiation levels, and limited space for microbial colonization, in addition to the above mentioned anaerobic and hyperalkaline conditions would restrict microbial viability and activity. However, it is well known the capacity of many microorganisms to colonize environments considered extreme as hyper-alkaline spring waters and hydrothermal vents (Maugeri et al., 2009; Pedersen et al., 2004). Indeed, it is assumed that different geochemical processes such as degradation of cellulose from packaging materials, disposable clothing, and surface wipes present in ILW can lead to the generation of nutrients and growth substrates that microorganisms can use to support growth. The resaturation of water after thousand years will probably result in the release of different chemical compounds from bitumen and concrete materials used in some DGR systems, including organic matter, electron donor and acceptors (NO_3^-), gases (H_2), etc. The utilization of electron donors and acceptors by anaerobic microorganisms could lead to enzymatic reduction and hence immobilization of radionuclides like U^{VI}, Tc^{VII}, Np^{V} or Se^{IV} within the geodisposal system (Borghese et al., 2014; Lloyd, 2003). It has been reported that selenium (Se) is present in the tetravalent oxidation state (+IV) in high-level radioactive waste (Dardenne et al., 2015). Water-soluble and toxic Se compounds commonly exist in the oxidation states +VI and +IV as selenite and selenate,

respectively, while insoluble and harmless Se compounds occurs in the oxidation state 0 as elemental Se (Antonioli et al., 2007). Microbial reduction of Se^{IV} has been reported under both aerobic and anaerobic conditions in a wide range of microorganisms. For example, some bacterial strains such as *Stenotrophomonas maltophilia* SeITE02, *Comamonas testosteroni* S44, and *Bacillus cereus* can reduce Se^{IV} to Se^{0} aerobically (Kora, 2018; Lampis et al., 2017; Tan et al., 2018). Se^{IV} can also be biotransformed anaerobically to Se^{0} by certain bacteria such as *Azoarcus* sp. CIB, *Stenotrophomonas maltophilia*, and *Shewanella oneidensis* MR-1 (Dungan et al., 2003; Fernández-Llamosas et al., 2016; Li et al., 2014b). Therefore, it is important to study the impact of microbial processes in the transport and mobility of Se through the geodisposal system under conditions relevant to a DGR (aerobic, anaerobic, alkaline conditions, etc.).

The aim of the present work is to study the reduction of Se^{IV} by the bentonite-isolated bacterium *Stenotrophomonas bentonitica* under anaerobic and alkaline conditions, comparable to those that will probably occur in future nuclear waste repositories. In a previous study, we described this interaction under aerobic conditions also of relevance to nuclear repositories (Ruiz-Fresneda et al., 2018; Capítulo II). Specifically, we demonstrated the aerobic bioreduction of Se^{IV} to different amorphous and crystalline Se^{0} nanostructures. Amorphous Se (a-Se) nanostructures seem to be transformed to Se crystals due to the role of organic matter. The results suggested *S. bentonitica* would decrease the solubility and hence the mobility of Se through the surrounding environment of DGRs. However, only few works have reported the impact of microbial processes on radionuclide mobility under alkaline conditions analogous to the DGR system (Smith et al., 2017; Williamson et al., 2014). To the best of our knowledge this is the first study describing the bioreduction of Se^{IV} to Se^{0} anaerobically at different pH conditions (from pH 7 to 10) by a bacterial strain isolated from Spanish bentonites (Almería, Spain), selected for DGRs due to their advantageous properties (Villar et al., 2006). Flow cytometry studies clearly showed that anoxia and Se^{IV} stress negatively affect bacterial viability and activity. Although small viability and activity levels were detected, no cell proliferation was found under these conditions. In-depth analysis by electron microscopy showed the production of individual and aggregated Se nanospheres and nanowires as reduction products after the Se-bacteria interaction under anaerobic and alkaline conditions (pH 10). The selected-area electron diffraction (SAED) pattern of individual Se nanospheres indicated their amorphous nature. However, Raman spectroscopy equipped to a variable pressure field emission scanning electron microscopy (VP-FESEM) indicated the crystalline structure of the Se aggregates (monoclinic Se) and nanowires (trigonal Se), suggesting a transformation process from amorphous to crystalline Se. Not only the oxidation state, but also the shape and the structure of the Se reduction products influence their solubility and mobility. This study further demonstrates the influence that *S. bentonitica* could have on the future DGR systems by reducing the toxicity and

mobility of Se^{IV} under anoxic and high-pH environment analogous to those that will develop in the disposal of radioactive waste.

3. Material and methods

3.1. Bacterial strain and growth conditions

The bacterial strain *S. bentonitica* employed in the present study was isolated from Spanish bentonite clays collected from Cabo Gata Nature Park (Almeria, Spain) (López-Fernández et al., 2014). The bacterial cells were grown aerobically in solid and liquid Luria-Bertani (LB) broth medium (tryptone 10 g/l, yeast extract 5 g/l and NaCl 10 g/l, pH 7.0 ± 0.2) at 28 ºC.

3.2. Anaerobic growth under selenite stress

S. bentonitica were growth in degassed R2A medium added with different electron donors (sodium acetate, citrate, pyruvate, etc.) and acceptor (sodium nitrate, iron (III) hydroxide, ferric citrate, etc.) in order to determine its ability to growth anaerobically. Cells were harvested at mid-exponential phase by centrifugation (10000 x g; 10 min) from LB cultures and washed with 30 mM PIPES buffer to remove the medium ingredients. Afterwards the cells were re-suspended in R2A supplemented with the corresponding electron donor and acceptor. Se^{IV} at different concentrations (0.1 to 1 mM) was added to the mixture from a 1M sodium selenite (Na_2SeO_3) (Sigma-Aldrich) stock solution. Finally, the suspensions were degassed using N_2 and incubated at 28ºC. Se^{IV}-untreated cells and R2A medium containing Se^{IV} were used as controls. All the measurements were performed in triplicate. The growth was determined by quantifying the total protein content in bacterial cell extracts using a modification of the method of Dhanjal and Cameotra (2010). A 1 ml aliquot of bacterial culture was taken at different time intervals to measure the growth based on the protein content of the cells by using the Bradford reagent (Bio-Rad®). Bovine serum albumin (BSA) was used as a standard.

3.3. Reduction of Se^{IV} under anaerobic and alkaline conditions

The Se^{IV} reduction ability of *S. bentonitica* was also assayed anaerobically under alkaline conditions (from pH 8 to 11) relevant for the DGR system. The samples were prepared as described in the section above (section 3.2.) by using sodium acetate and sodium nitrate as electron donor and acceptor, respectively. The pH of the solutions was adjusted by addition of acid ($HClO_4$) or base (NaOH) using a pH-meter CRISON© micro pH 2002 and sterilized by filtration through 0.22 μm nitrocellulose filters prior to degassing.

3.4. Flow cytometry

The cell viability and the metabolic activity of *S. bentonitica* in the presence of Se^{IV} under anoxic conditions were determined by using flow cytometry technique. For this purpose, the cultures were prepared as described in section 3.2 in the presence of acetate and nitrate with an initial concentration of Se^{IV} 2 mM. All experiments were conducted in triplicates. After 12, 60, and 144 h of incubation, the cells were collected by centrifugation at 11000 x g and 4 °C for 10 min. The resultant pellet was washed four times in phosphate buffered saline (PBS) pH 7. Then, the cells were dissolved in PBS adjusting the cellular density to approximately 10^6 cells/ml. For cell viability test, fluorescein diacetate (FDA) and propidium iodide (PI) were added into each sample to a final concentration of 20 µl/ml and 2 µl/ml respectively. For metabolic activity test, 3,30-dihexyloxacarbocyanine iodide (DiOC6) was employed to a final concentration of 20 µl/ml. Finally, the samples were analysed by Forward Scatter using a FACSCanto II™ cytometer (Becton Dickinson). Se^{IV}-free cultures and dead cells obtained by heating the biomass at 90 ºC served as controls.

3.5. Electron microscopy

VP-FESEM equipped with an X-ray detector Raman spectroscopy system enabled an in situ 3-D structural and elemental characterization of the reduced Se produced by the cells. Se^{IV}-amended cultures (2 mM) added with sodium acetate and sodium nitrate as electron donor and acceptor, respectively, were prepared for VP-FESEM after 144 h growing anaerobically at different pHs (7-10) as described in Ruiz-Fresneda et al. (2018) (Capítulo II). The samples were analysed under Variable Pressure Field Emission Scanning Electron Microscope Zeiss SUPRA 40VP.

The Se reduction products were also analysed by using scanning transmission electron microscopy (STEM) equipped with energy dispersive X-ray (EDX). EDX analysis was performed at 300 kV using a spot size of 4 Å and a live counting time of 50 s. The structural characterization of Se nanostructures were analysed by using SAED. The samples were prepared as described in Merroun et al. (2005) and examined under high-angle annular dark field scanning transmission electron microscope (HAADF-STEM) FEI TITAN G2 80-300. STEM specimen holders were cleaned by plasma prior to STEM analysis to minimize contamination.

4. Results and discussion

4.1. Se^{IV} reduction under anaerobic and neutral pH conditions

4.1.1. Se^{IV} reduction and growth profile

The growth and Se^{IV} reduction of *S. bentonitica* under anoxic conditions was evaluated in the presence of a wide range of added electron donors (sodium acetate, citrate pyruvate, etc.) and acceptors (sodium nitrate, iron (III) hydroxide, ferric citrate, etc.) at neutral pH conditions. Literature data show a great amount of compound that can be used by many microorganisms as electron donor and acceptor in reducing Se^{VI} and Se^{IV}. High reduction rate of Se^{IV} was achieved by *Veillonella atypica* when hydrogen (H_2) was used as electron donor under anaerobic conditions, but no reduction was appreciated when the cells were supplemented with acetate or formate as electron source (Pearce et al., 2008). On the other hand, Kessi and Hanselmann (2004) hyphotesized that reduced glutathione (GSH) function as the main electron donor reacting with Se^{IV} in *Rhodospirillum rubrum* and *Escherichia coli*. The possible role of GSH and other reactive thiols compounds in Se^{IV} reduction was also suggested within the genus *Stenotrophomonas* by *S. maltophilia* SeITE02 (Antonioli et al., 2007). Other electron sources such as acetate, lactate, formate, and pyruvate have been described to be used as electron donor in Se^{IV} reduction in *Geobacter sulfurreducens*, *Shewanella* sp. HN-41, and *Shewanella oneidensis* MR-1 (Klonowska et al., 2005; Li et al., 2014b; Pearce et al., 2009; Tam et al., 2010). Se^{IV} act as the terminal electron acceptor for many microorganisms (Nancharaiah and Lens, 2015). However the use of iron (Fe^{III}), nitrate (NO_3^-), nitrite (NO_2^-), sulphite (SO_3^{-2}) as electron acceptors by respiratory reductases can support the reduction of Se^{IV} in some microorganisms (Basaglia et al., 2007; DeMoll-decker and Macy, 1993). In the present study, the highest Se^{IV} reduction efficiency, quantified as red precipitate production, by the cells of *S. bentonitica* was observed when sodium acetate and nitrate was added.

Both acetates and nitrates are compounds that will be present in the geodisposal system of radioactive waste. Among other sources, acetate can derive from the oxidation of glucose, and degradation of phthalic acid esters (PVC plasticisers) characteristic of ILW, while nitrates are mainly contained within bitumen waste and as a product of nitrogen biogeochemical cycle (Abrahamsen et al., 2015; Bertron et al., 2014; Walczak et al., 2001). Thus, the presence of acetate and nitrates within the repositories could support the reduction of Se^{IV} by the cells of *S. bentonitica* when anaerobic conditions dominate. Consequently, they were selected for the rest of experiments as electron donor and acceptor sources. In addition, Se^{IV} reduction was also

observed when incubating anaerobically the *S. bentonitica* in PIPES buffer without addition of electron donor and acceptors, suggesting Se^{IV} could act as the terminal electron acceptor.

In the absence of Se^{IV}, only when the cultures were amended with sodium acetate and sodium nitrate, a limited increase in the total cell protein was observed during the first 12 h of incubation (Figure 1). However, no growth was detected in the presence of Se^{IV} at all concentrations tested (0.5 and 1 mM) (Figure 1), in contrast to previous studies revealing the capacity of this bacterium to growth aerobically under Se^{IV} stress (Ruiz-Fresneda et al. 2018; Capítulo II; Capítulo III). Consequently, these results suggested the toxic effect of Se^{IV} on *S. bentonitica* cells under anaerobic conditions. Nevertheless, the red precipitates produced in all the cultures amended with Se^{IV} clearly pointed out the ability of this bacterium to reduce Se^{IV} to Se^{0} anaerobically. Non-production of Se red precipitates in Se^{IV}-untreated cultures and Se^{IV}-treated media (abiotic controls) confirmed the Se^{IV} reduction as a biological process.

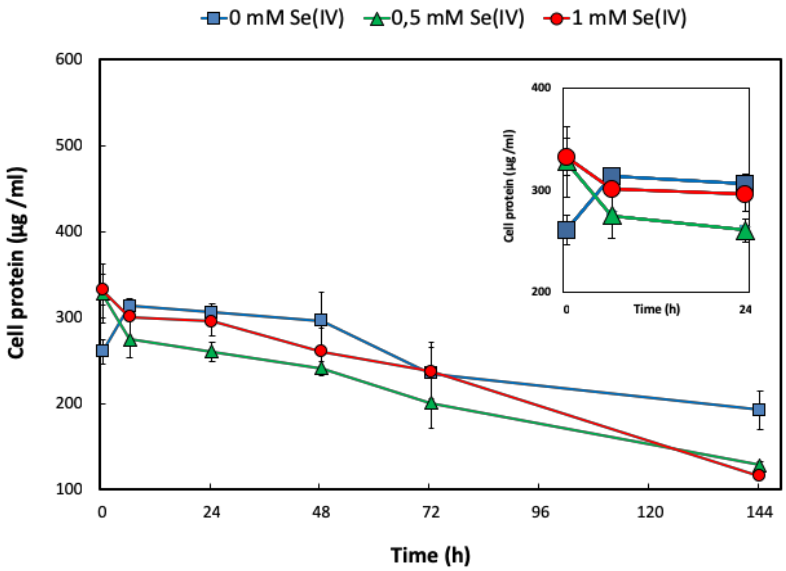

Figure 1. Anaerobic growth curves of *S. bentonitica* in R2A medium added with sodium acetate and sodium nitrate in the presence of different Se^{IV} concentrations (0 to 1 mM).The inset graph shows a magnification of the growth curve in the first 24 h. Data are presented as averages ± standard errors.

4.1.2. Cell viability and metabolic activity

The effect of Se^{IV} on cell viability of *S. bentonitica* was studied by the live-dead staining approach conducted with propidium iodide (PI) and fluorescein diacetate (FDA). PI enters to cells with damaged membranes staining nucleic acids of dead cells (Givan 2011), while FDA stains viable cells (Stubberfield and Shaw, 1990). With regard to the metabolic activity test, the fluorescent dye $DiOC_6$ was used in order to bind polarized membranes of active cells (David et al., 2011). The percentages of viable and active cells of *S. bentonitica* untreated and treated with

2 mM Se^{IV} incubating anaerobically at neutral pH from 12 h to 144 h are displayed in Figure 2. Cell viability was negatively affected by Se^{IV}. Specifically, 32.7, 41.5, and 1.7 % of cell populations were found to be viable after 12, 60, and 144 h of incubation, respectively, in presence of 2 mM Se^{IV}. In contrast, higher amount of viable cell population (100, 100, and 17.3 %) was observed in untreated samples at the same incubation times. Previous studies under aerobic conditions indicated the higher viability values of the cells after 144 h incubation in the presence of 2 mM Se^{IV} (Capítulo III). These results pointed out the great influence of anoxia and Se^{IV} on viability of *S. bentonitica* cells. On the other hand, the metabolic activity test generally showed a lower oxidative response under 2 mM Se^{IV} stress comparing with Se^{IV}-untreated cells at all times assayed except at 144 h. Specifically, 33.4, 45, and 50 % were found to be active after 12, 60, and 144 h at 2 mM Se^{IV} stress, while 85.6, 93.3, and 12.4 % of the cells were active in untreated samples. The increases on cell activity after 144 h in the presence of Se^{IV} comparing with Se^{IV}-untreated cells could be explained by the cellular metabolic response to Se^{IV} stress. Our previous studies under aerobic conditions showed a similar behaviour (Capítulo III).

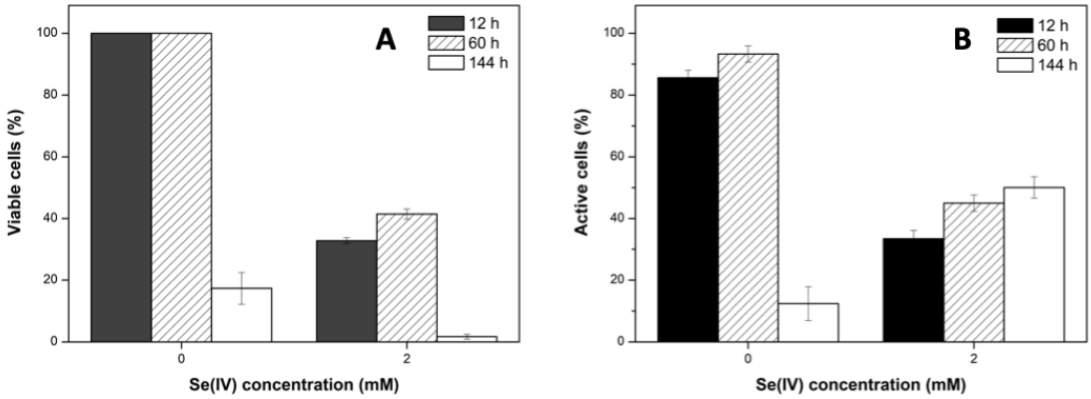

Figure 2. Percentage of viable (A) and active cells (B) of *S. bentonitica* under different Se^{IV} concentrations (0 and 2 mM) and contact times (12, 60, and 144 h) under anaerobic and neutral pH conditions.

4.2. Se^{IV} reduction under anaerobic and alkaline conditions

The Se reduction ability was also studied under anaerobic and alkaline pH conditions analogous to those expected in a DGR environment. The colour of the Se^{IV}-treated cultures (2 mM) of *S. bentonitica* turned reddish at pH 8, 9, and 10 (Figure 3). However, no red precipitates were observed at pH 11, probably due to non-proliferation of the cells under these conditions. The latter hypothesis is supported by previous investigations indicating *S. bentonitica* grows at pH 5-10 under aerobic conditions (Sánchez-Castro et al., 2017a). As described for the anaerobic experiments in section 4.1, no colour change in the Se^{IV}-untreated cultures and Se^{IV}-treated media confirmed the bioreduction of Se^{IV}. Many bacterial strains have been demonstrated to

reduce Se^{IV} anaerobically (Li et al. 2014a; Fernández-Llamosas et al. 2016). However, as far as we are concerned, this is the first study describing the microbial reduction of Se^{IV} at alkaline pH (up to pH 10) and anaerobic conditions. These results revealed the ability of the bentonite isolate *S. bentonitica* to reduce Se toxic forms to non-toxic Se under analogous conditions expected in the DGR system. Therefore, we propose this species of the genus *Stenotrophomonas* to contribute to the immobilization of Se within the DGR concept.

Figure 3. Cultures of *S. bentonitica* adjusted to pH 8, 9, 10, and 11 showing the reduction of 2 mM Se^{IV} from pH 8 to 10 as indicated by their reddish colour. Se^{IV}-untreated cultures and Se^{IV}-treated medium were employed as controls.

The effect of Se and the cells on the pH variation of the samples adjusted at pH 10 was studied by measuring the pH at different times during the incubation. Abiotic controls (Se^{IV}-treated media) showed no variation of the pH with increasing time and were around 10 during the entire assay (Figure 4). However, in the presence of bacteria, both untreated and treated cultures of *S. bentonitica* showed a decrease from pH 10 to pH 7 and 8, respectively, with increasing incubation time (Figure 4). Thus, the cells are responsible for this decrease in pH. This fact could be a consequence of the bacterial metabolic activity responding to these stressful conditions as suggested the flow cytometry results.

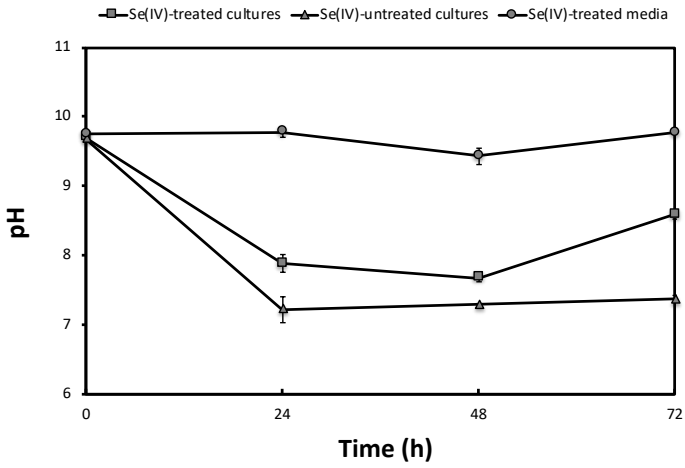

Figure 4. Time course of pH variation in Se^{IV}-treated (2 mM) and untreated cultures of *S. bentonitica* adjusted to pH 10 under anaerobic conditions. Se^{IV}-treated media ere employed as abiotic controls. Se^{IV} and cells was added at zero time. Each curve shows means based on the results of triplicates.

Rizoulis et al. (2012) studied the reduction of different electron acceptor of relevance to ILW in natural alkaline sediments set up at pH 10, 11, and 12. Similarly to our experiments, they noted a slight drop in pH during the incubation, probably due to the formation of CO_2 from the metabolism of lactate, acetate and other carbon source present in the sediments. In our case, *S. bentonitica* is able to oxidize acetate to CO_2, which in turn leads to the decrease of pH of the medium to 7-8 where Se^{IV} reduction occurs.

4.3. Electron microscopic characterization of Se^{IV} bioreduction products

Ultrathin sections showed electron-dense nanospheres produced by the cells of *S. bentonitica* on the surface and within the intracellular and extracellular space after 144 h incubating on Se^{IV} at neutral pH (Figure 5A-B). The size of both intracellular and extracellular nanospheres ranged between 100 and 200 nm (Figure 5A-B). EDX microanalysis confirmed their Se composition (Figure 5C). In addition, the SAED pattern derived from a single nanosphere revealed its amorphous nature (Figure 5D).

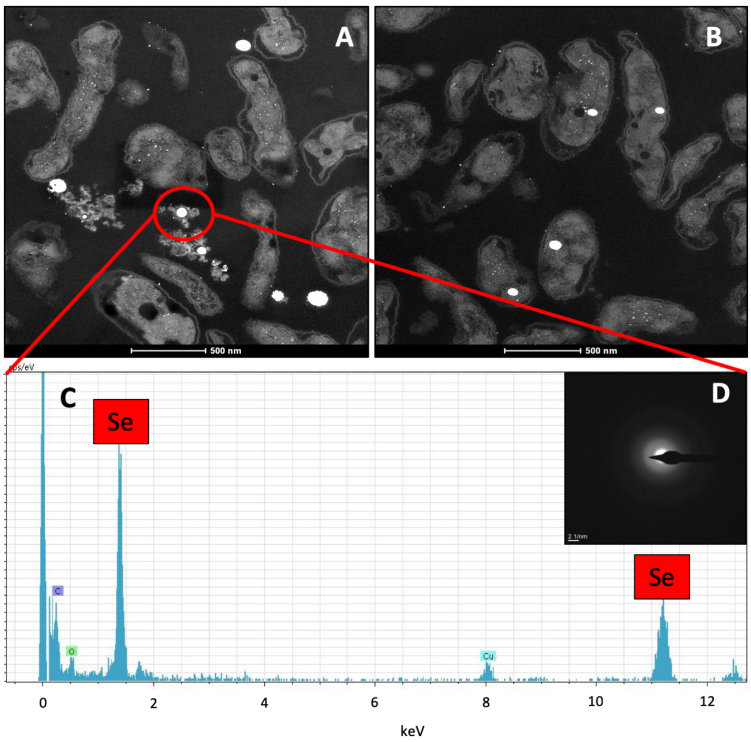

Figure 5. HAADF-STEM analysis of an ultrathin-sectioned *S. bentonitica* sample incubated anaerobically at neutral pH in the presence of 2 mM Se^{IV} (A-B). EDX analysis revealed the Se composition of the electron-dense nanospheres (C) located both intracellular and extracellularly (A-B). SAED pattern derived from an individual Se granule (D). Scale bars: 500 nm (A-B).

In the same way, we could observe the presence of individual Se nanospheres located extracellularly, intracellularly and also attached on the cell surface after 144 h of incubation anaerobically at pH 10 by using a VP-FESEM system (Figure 6A-D). In addition to Se, EDX microanalysis revealed the presence of S (Figure 6B), suggesting the relevant contribution of thiol-containing biomolecules such as GSH in the reduction pathway of Se^{IV}. The Se nanospheres formed aggregates (Figure 6C-D) as it was observed in aerobic cultures of *S. bentonitica* treated with Se^{IV} (Ruiz-Fresneda et al., 2018; Capítulo II). The formation of Se aggregates by *S. bentonitica* could lead to the transformation of a-Se nanospheres to trigonal Se (t-Se) nanostructures with high stability as reported by Ruiz Fresneda et al., (2018) when this bacterium was grown aerobically. The transformation from a-Se to t-Se consists of a time-dependent process. The a-Se nanospheres are initially released to the extracellular matrix from the cytoplasm (24 h) and start to form aggregates most probably on the axis of flagella-like proteins after 48-72 h. The aggregation of Se nanoparticles (SeNPs) using proteins as a template seem to play a crucial role during the transformation and crystallization mechanism (Ruiz-Fresneda et al., 2018; Wang et al., 2010). Finally, after 144 h the aggregates crystallize producing t-Se nanostructures with different shapes (nanowires, hexagons, and polygons) and size.

The Raman scattering spectrum derived from the observed Se nanospheres accumulations exhibited an intense peak at 254 cm^{-1} (Figure 6E). Kora and Rastogi (2016) suggested that resonance peak at 254 cm^{-1} could be accounted to a-Se as a result of irregularly Se atoms arrayed as disordered chains. These results differ with those previously obtained for the SeNPs synthesized by *S. bentonitica* under aerobic conditions, where a peak at 235 cm^{-1} corresponding to t-Se was observed. However, other authors indicated that the peak centred at 254 cm^{-1} was characteristic of crystalline monoclinic Se (m-Se) (Husen and Siddiqi, 2014; Zhang et al., 2011). Over the last century to many contradictory studies on a-Se structure have been reported (Jóvári et al. 2003). The three allotropes of m-Se have deep red colour and Se_8 rings as structural unit within their unit cell (Fernández-Martínez and Charlet, 2009). Amorphous Se (red or black) is thought to contain 2 polymeric chains (Se_n) and Se_8 monomeric rings (Cooper and Westbury 1974; Popov 1976). Therefore, it is very complicated to distinguish between a-Se and m-Se structure. Consequently, the Se aggregates produced by *S. bentonitica* cells could be amorphous or monoclinic, in contrast to individually distributed Se nanospheres described above as amorphous by means of SAED. However, it is well known that a-Se could be transformed to m-Se nanostructures and this in turn could be transformed to t-Se as one of the most thermodynamically stable phases (Chen et al., 2010; Wang et al., 2010). This suggests the formation of m-Se aggregates by *S. bentonitica* as an intermediate thermodynamic step during the transformation to t-Se. A great abundance of organic matter and organic filaments probably

corresponding to flagella-like proteins were detected surrounding the SeNPs and bacterial cells (Figure 7A-B). The VP-FESEM images clearly showed the SeNPs were embedded in this organic matrix mainly composed by proteins (Capítulo III), suggesting its role in the aggregation and transformation.

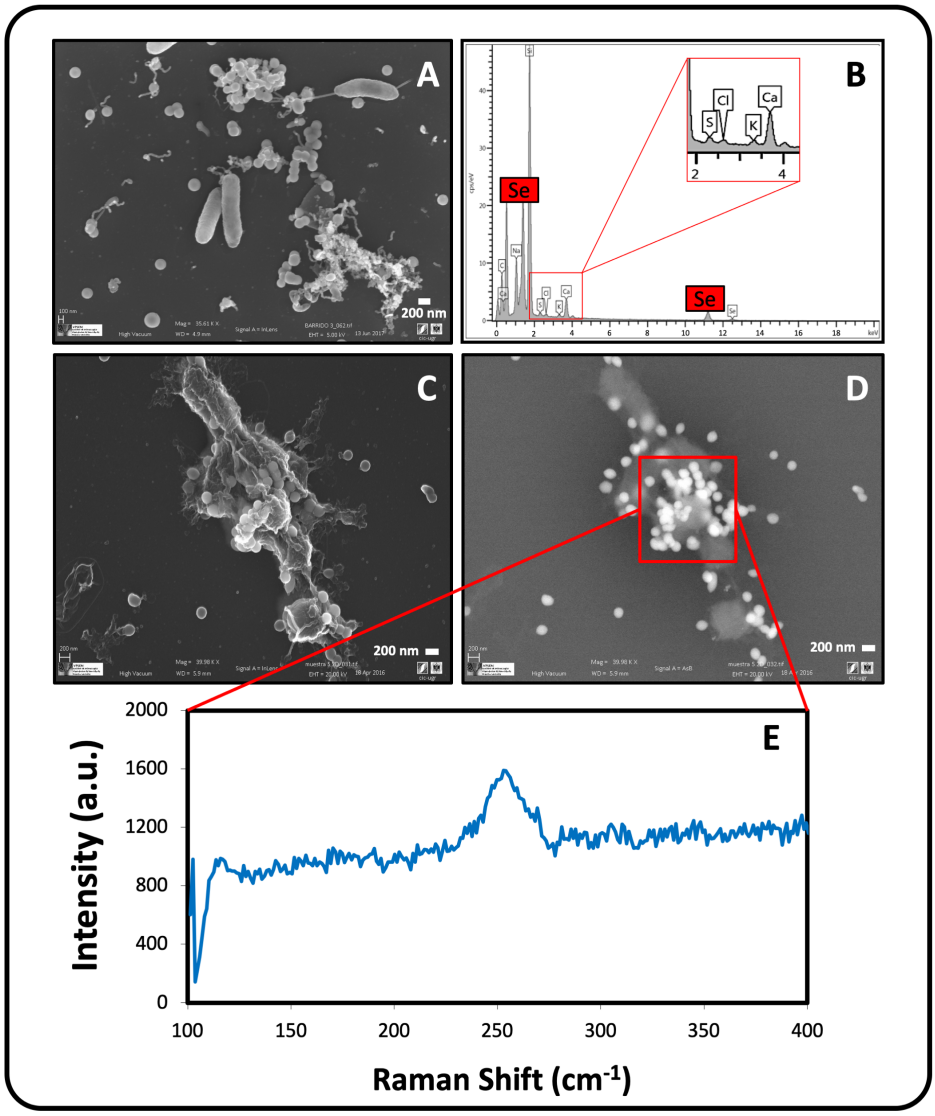

Figure 6. VP-FESEM micrographs of Se nanospheres located extracellularly, intracellularly and attached on lysed cells of *S. bentonitica* (A,C, and D) produced anaerobically at pH 10. EDX analysis showing the Se and S composition of the nanospheres (B). Raman analysis derived from Se nanospheres accumulations (E). Scale bars: 200 nm (A, C, D).

Finally, few extracellular Se nanowires could be detected in the proximity of Se aggregates (Figure 7B-D). The Raman scattering spectrum derived from the nanowires displayed two main peaks at 236 cm^{-1} and 254 cm^{-1} (Figure 7F). The resonance peak at 236 cm^{-1} could be associated to t-Se, while 254 cm^{-1} could be accounted, as mentioned before, to the intermediate

thermodynamic phase a-Se or m-Se. This fact confirmed that transformation process takes place, most probably following a similar mechanism reported by Ruiz-Fresneda et al., (2018) including several steps. The intracellular Se nanospheres seem to be released through the bacterial cell lysis as indicated the seriously damaged cells observed (Figure 8). After that, they formed aggregates within the extracellular matrix probably using cellular organic matter and flagella-like proteins as a template (Figure 8). Finally, the Se nanowires seem to originate from the accumulation and agregation of the nanospheres attached to these organic matter and protein filaments (Figure 8). During the proposed mechanism the crystallization from individual a-Se nanospheres to m-Se aggregates and t-Se nanowires seem to occur.

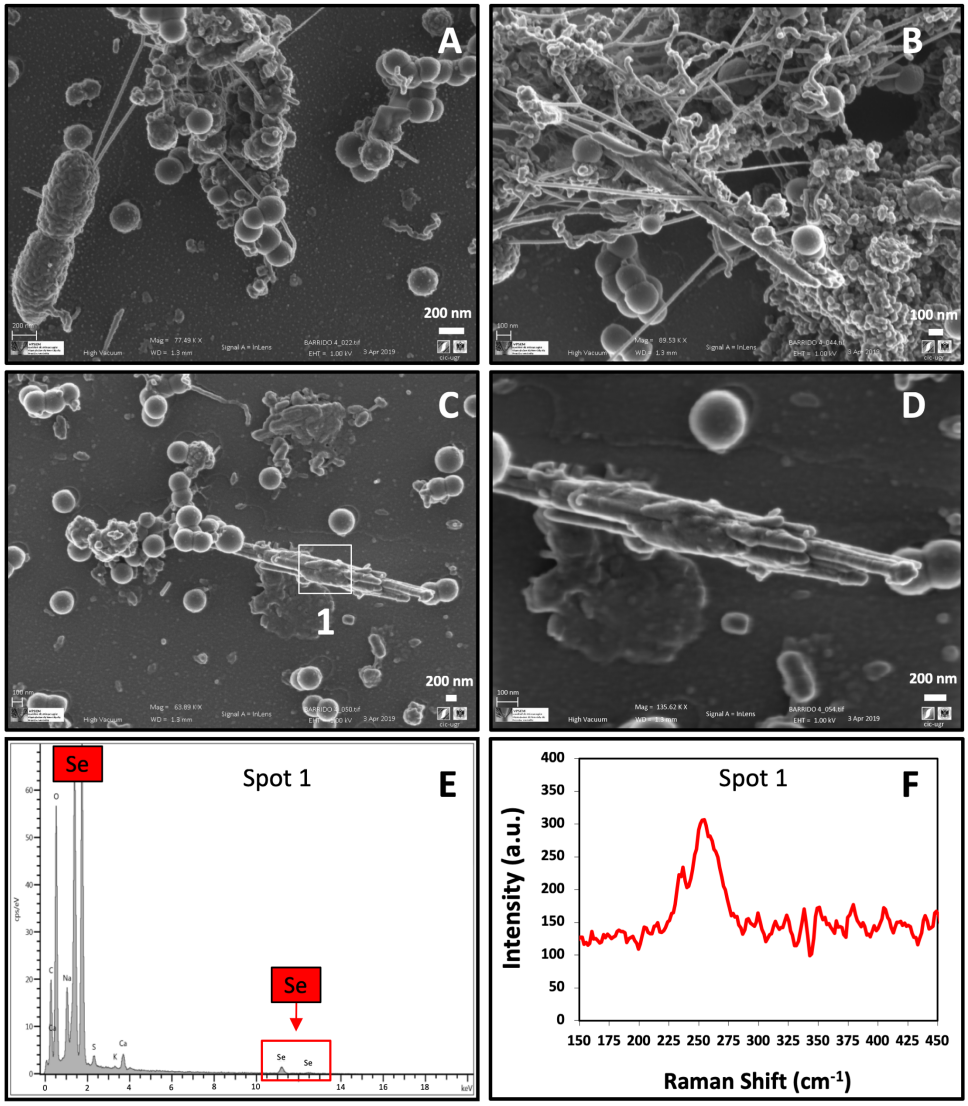

Figure 7. VP-FESEM pictures showing the presence of SeNPs associated to organic materials and filaments (A-B) and Se nanowires within the extracellular space (C-D) under anaerobic conditions at pH 10. EDX analysis derived from an individual nanowire indicating its Se composition (E). Raman scattering spectrum derived from the same nanowire (F). Scale bars: 200 nm (A, C, D) and 100 nm (B).

The low amount of nanowires observed in comparison with our previous studies conducted under oxic conditions (Ruiz-Fresneda et al., 2018; Capítulo II) pointed out that maybe under anaerobic and alkaline conditions the cells need longer incubation times to produce more Se crystals. A microscopic analysis of samples aerobically incubated agrees with the latter hypothesis as indicated the higher presence of Se crystal with increasing time from 15 to 30 days (Figure 9). The transformation it is likely to occur more slowly due to the harder conditions to which the cells were exposed. These conditions influenced the cell viability and proliferation as revealed flow cytometry, probably affecting the reduction and transformation process to Se crystals.

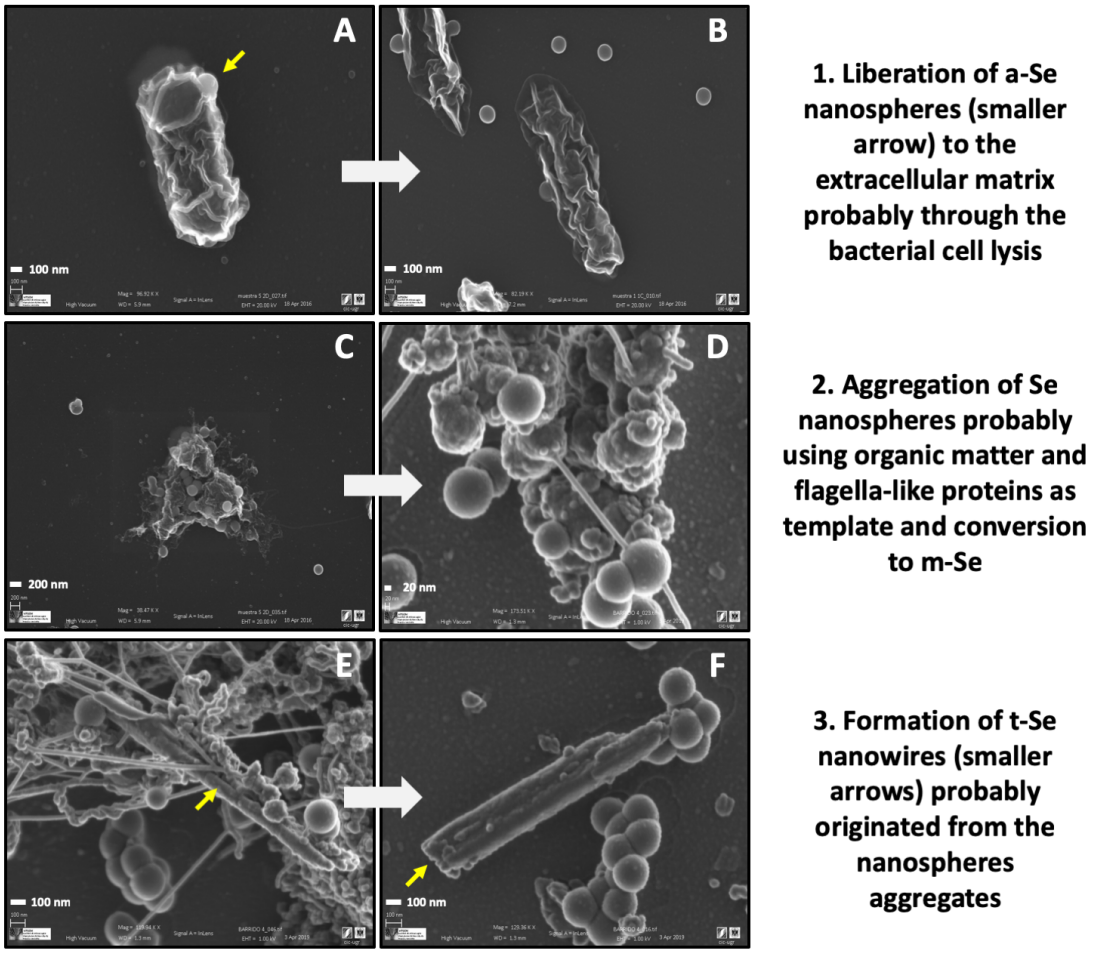

Figure 8. VP-FESEM images representing the proposed transformation from a-Se nanospheres to t-Se nanowires through the formation of m-Se aggregates an as intermediate step by using proteins as template. The images correspond to samples prepared by growing *S. bentonitica* anaerobically at pH 10. Scale bars: 100 nm (A,B,E,F), 200 nm (C), and 20 nm (D).

Definitely, the reduction from Se^{IV} to Se^{0} under DGR simulating conditions (anaerobic and alkaline) could have a positive impact onto the security of these systems due to the lower toxicity and mobility of Se at the zero valent oxidation state. However, the different Se

structures and shapes produced also must be taken into account for predicting the specific influence of *S. bentonitica* cells. It is generally assumed that SeNPs are insoluble and non-toxic (Husen and Siddiqi, 2014). In fact, microbially produced Se nanospheres have been demonstrated to be less toxic than oxidized Se species (Se^{VI} and Se^{IV}) (Benko et al., 2012). According to this, the production of Se nanospheres by *S. bentonitica* would be beneficial within the geodisposal system. In contrast, there are considerable uncertainties about the toxicity of SeNPs comparing to soluble oxidized forms as indicated some studies (Kumar et al., 2018; Li et al., 2008). Li et al. (2008) described the major toxicity of SeNPs in comparison with Se^{IV} in the fish *Oryzias latipes*. Kumar et al. (2018) reported the toxicity of SeNPs depend on the concentration, indicating that higher ones have toxic effect to the fish species *Pangasius hypophthalmus*. Consequently, further investigations are needed to conclude the toxicity level of SeNPs produced by *S. bentonitica*. On the other hand, the formation of crystalline Se in form of nanowires could have a positive impact on the repositories as indicated their lower mobility and higher settleability comparing to Se nanospheres and oxyanions (Jain et al., 2017; Lenz et al., 2009). The lesser extent of Se crystalline nanowires observed indicated a lower short-term efficiency of *S. bentonitica* in the immobilization of Se^{IV} present in the repositories when anaerobic and alkaline conditions dominate in comparison with aerobic studies (Ruiz-Fresneda et al., 2018; Capítulo II; Capítulo III).

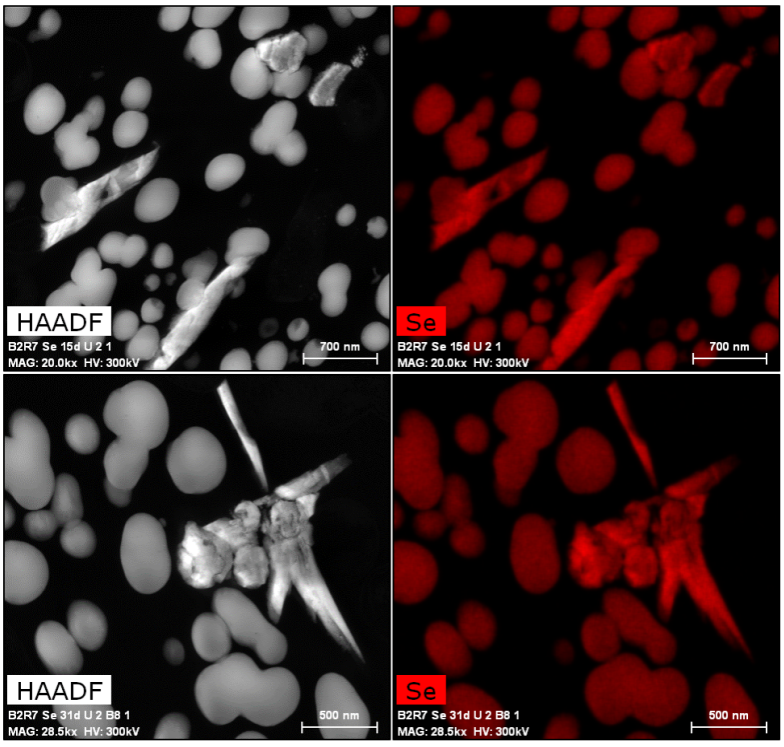

Figure 9. HAADF-STEM micrographs of Se nanostructures aerobically produced by *S. bentonitica* in the presence of 2 mM Se^{IV} for 15 days. Corresponding elemental maps showing the Se composition of the nanostructures. Scale bars: 700 nm (A-B) and 500 nm (C-D).

5. Conclusions

The present study described the ability of the bentonite-isolated *Stenotrophomonas bentonitica* to reduce Se^{IV} to Se^{0} under anaerobic and alkaline conditions simulating those expected in a DGR. Despite the low cell viability, activity and no growth of *S. bentonitica* in the presence of Se^{IV}, individual and aggregated Se nanospheres and lower amounts of Se nanowires were produced as a consequence of the bioreduction process. A combination of microscopic and spectroscopic techniques suggested the transformation from a-Se nanospheres to crystalline Se nanowires (t-Se) in a similar way as reported aerobically by Ruiz-Fresneda et al. (2018). A slower transformation process seem to occur due to the non-proliferation and low viability and activity rates of *S. bentonitica* cells, probably caused by these harder environmental conditions.

The redox transformation from toxic Se^{IV} to non-toxic Se^{0} and the formation of crystalline Se nanowires suggests *S. bentonitica* as a potential bacterial species for its positive effect on the safety of the DGR system in case of radionuclide escape. However, the slower transformation process suggested a lower short-term efficiency of *S. bentonitica* in the formation of crystalline Se and hence in the immobilization of Se when anaerobic and alkaline conditions dominate. Concerning the Se nanospheres produced by this bacterium, more studies are needed to determine their mobility within the DGR system. This study will help to further understanding the impact of microbial processes on the toxicity of Se in future disposal of radioactive waste.

6. Acknowledgements.

This work was supported by Euratom research and training programme 2014-2018 [grant agreement no. 661880]. The authors acknowledge the assistance of Concepción Hernández Castillo (Centro de Instrumentación Científica, University of Granada, Spain) for their help with sample preparation for microscopy. The authors also thank the assistance of Jaime Lazuen Alcón (Centro de Instrumentación Científica, University of Granada, Spain) with the flow cytometry measurements.

7. Conflicts of interest.

The authors declare no competing financial interest.

CAPÍTULO V:

Molecular binding of Eu^{III}/Cm^{III} by S*tenotrophomonas bentonitica* and its impact on the safety of future geodisposal of radioactive waste

Miguel A. Ruiz-Fresneda [1], Margarita López-Fernández [2] Marcos F. Martínez-Moreno [1], Henry Moll [2], Andrea Cherkouk [2], Yon Ju-Nam [3], Jesús J. Ojeda [3], Mohamed L. Merroun [1]

[1]Department of Microbiology, University of Granada, Granada, Spain

[2]Institute of Resource Ecology, Helmholtz-Zentrum Dresden-Rossendorf e.V., Dresden, Germany

[3]Systems and Process Engineering Centre, College of Engineering, Swansea University, Swansea, UK

To be submitted to the journal Environmental Science and Technology

1. Abstract

Microbial communities occurring in bentonite, considered as reference materials for safety barriers in the future deep geological repositories (DGRs), can influence the migration behaviour of radionuclides characteristic of radioactive waste such as curium (Cm^{III}). In the present work, the molecular scale interactions of Cm^{III} and its inactive analogue europium (Eu^{III}) with the indigenous bentonite bacterium *Stenotrophomonas bentonitica* were studied by using a novel multidisciplinary approach. Potentiometric studies of the cells surfaces showed remarkable high concentration of phosphate groups comparing to other bacteria, revealing the great potential of *S. bentonitica* in metal-binding mainly through phosphates. The concentrations of these groups is significantly lower for *S. bentonitica* cells exposed to Eu^{III} indicating that the Eu^{III} may be strongly bonded to phosphate sites. Infrared spectroscopy (ATR-FTIR) demostrated the role of carboxyl and phosphate groups in the Eu^{III} interaction. Specifically, carboxyl groups could form bidentate bridging complexes with Eu^{III}. X-ray photoelectron spectroscopy (XPS) confirmed the involvement of phosphates and suggested carboxyl groups from organic acids such as acetate in the Eu^{III} complexation. Additionally, time-resolved laser induced fluorescence spectroscopy (TRLFS) identified phosphoryl and carboxyl groups from bacterial envelopes and released complexing agents to be involved in the Eu^{III} coordination sites as indicated their luminescence lifetimes. Similarly, the lifetimes and the corresponding emission maxima at at 599.6 and 601.1 nm revealed two Cm^{III}-*S. bentonitica* species, also assigned to phosphoryl and carboxyl complexes. Microscopic and kinetics Eu binding studies indicated biosorption as the main interaction process. However, the few extracellular and intracellular complexes observed suggested that other mechanisms (e.g. biomineralization) could be involved. These results provided new findings in predicting the impact of microbial processes in the mobility of trivalent actinides and hence in the security of radioactive wastes disposal.

Keywords: europium, curium, bacteria, mobility, geodisposal

2. Introduction

The safe disposal of radioactive waste is crucial to ensure the security for future generations of human beings as well as for the biosphere. The implementation of deep geological repositories (DGRs) is planned in the near future for the safe storage of high level and long-lived radioactive wastes (NEA, 2010). DGR is a multi-barrier system where radioactive wastes, mainly generated by nuclear industry, will be encapsulated in metal containers surrounded by compacted bentonites, considered as artificial barriers, and emplaced in stable geological formations at a depth of about 500-1000 m (Stroes-Gascoyne et al., 2007). While metal containers and compacted bentonites are considered artificial barriers, host rock are seen as natural barrier for the DGR. A high microbial diversity in bentonite clay formations from Almería, (Spain), studied as an analogue of engineered barriers for repositories, has been previously reported (López-Fernández et al., 2015; 2014). Several studies have evidenced the impact that microbial processes may play in the corrosion of metal containers, which in turn could lead to the release of radionuclides to the surrounding environment (Meleshyn, 2011). They also seem to play a crucial role controlling the speciation and mobility of radionuclides present in radioactive wastes such as uranium (U) and curium (Cm) (Newsome et al., 2014). Therefore, understanding the migration behaviour and the environmental fate of radionuclides influenced by microorganisms will be essential for the risk assessment of repositories. Cm is a high toxic radionuclide as indicated by the high α activity of some isotopes such as ^{247}Cm and ^{248}Cm present in nuclear spent fuel (Gorietti et al., 2017; Kooyman et al., 2018). As a representative of trivalent actinides (An^{III}), Cm exhibits excellent luminescence properties that make it suitable to direct speciation studies at environmentally relevant metal concentration. Similarly, europium (Eu) was studied as representative inactive analogue of An^{III}, also providing excellent luminescence properties (Ansoborlo et al., 2007). This inactivity makes Eu^{III} an ideal element for Cm^{III} and americium (Am^{III}) studies, since Eu^{III} interaction experiments can be extrapolated to those of Cm^{III} (López-Fernández et al., 2018b).

Among other mechanisms, microbes can interact with actinides and lanthanides through their biosorption at the cell surfaces (Shukla et al., 2017). A large number of bacterial functional groups (carboxyl, phosphoryl, etc.) on microbial surfaces have been described to be effective for actinide complexation (Moll et al., 2014; Reitz et al., 2015). Cm^{III} and Eu^{III} form strong complexes with phosphoryl and carboxyl sites of the bacterial cell wall of *Sporomusa* sp. MT-2.99 and *Pseudomonas fluorescens* (Moll et al., 2014; 2013). Recently, yeasts and archaea have also been investigated for their ability to complex An^{III} (e.g. Cm) and trivalent lanthanides (Ln^{III}) (e.g. Eu). López-Fernández et al., (2018b) reported, for the first time, the role of carboxyl and phosphoryl groups from the envelopes of the yeast *Rhodotorula mucilaginosa* BII-R8 as

binding sites for Eu^{III} and Cm^{III}. The halophilic archaeon *Halobacterium noricense* DSM15987^{T} also interact with Cm^{III} and Eu^{III} forming phosphate complexes (Bader et al., 2019).

Since cell surfaces play a major role in the complexation of Cm^{III} and Eu^{III}, different spectroscopic and microscopic techniques should be applied to investigate the identities of functional groups and the corresponding mechanism involved in the biosorption of these elements. Attenuated total reflection-Fourier transform infrared (ATR-FTIR) spectroscopy, X-ray photoelectron spectroscopy (XPS), and time-resolved laser-induced fluorescence spectroscopy (TRLFS) are useful to determine the chemical speciation of these elements at environmental relevant conditions. Additionally, potentiometric titration studies would lead to the determination of types and abundance of metal binding sites at the cell surface (Fein et al., 2005; Ojeda et al., 2008). The higher the concentration of cell surface functional groups, the greater the availability of metal binding sites which enhance the efficiency of the biosorption process. While multidisciplinary approach combining different microscopic, spectroscopic, and potentiometric titration based methods were applied to investigate the interactions of U, as hexavalent actinide, with microbes (Krawczyk-Bärsch et al., 2018; Reitz et al., 2015), the microbial interaction with Cm and Eu were limited basically to TRLFS studies due to their fluorescence properties (Moll et al., 2014; 2013). To the best of our knowledge, this is the first study reporting the molecular interactions of the bacterial isolate *Stenotrophomonas bentonitica* with Eu^{III} and Cm^{III} by using a multidisciplinary approach including different spectroscopic, microscopic and potentiometrics studies. This will provide one of the most comprehensive studies on Eu^{III}/Cm^{III} interactions with bacterial cells to date.

S. bentonitica was isolated from Spanish bentonite clays (Almería, Spain) (López-Fernández et al., 2014), which have previously been well-characterized as a suitable analogue of engineered barrier for DGRs due to their physico-chemical properties (Villar et al., 2006). *S. bentonitica* cells have been previously described to influence the chemical speciation and thus the mobility of other elements characteristic of radioactive waste such as selenite (Se^{IV}) (Ruiz-Fresneda et al., 2018; Capítulo II; Capítulo III). Se^{IV} was reduced by *S. bentonitica* cells in form of Se^{0} nanoparticles with different shapes (spherical, hexagonal, polygonal and nanowires) and crystallographic properties (amorphous Se (a-Se) and trigonal Se (t-Se)). A time-dependent transformation process from a-Se nanospheres to more stable t-Se crystals was proposed, in which organic matter including cell proteins seem to be involved. These results suggested the mobility decrease of Se due to the higher settleability of Se crystals and the lower solubility of zero-valent Se (Breynaert et al., 2010; Lenz et al., 2009) through the surrounding environment of DGRs. Similarly, the present work attempts to study the effect that *S. bentonitica* may play on Eu^{III} and Cm^{III} environmental fate under aerobic and anaerobic conditions analogous to those

expected in geodisposal system of radioactive waste. This study will provide new insights on the influence of bentonite bacterial isolates in the immobilization of An^{III} within the concept of radioactive waste disposal, which in turn would help to evaluate the safety of the planned repositories.

3. Materials and Methods

3.1. Bacterial strain and growth conditions

The bacterial strain used in the present work was isolated from bentonite clay formations recovered from Almeria (Spain) (López-Fernández et al., 2014) and was recently described as a novel species named *Stenotrophomonas bentonitica* BII-$R7^T$ (Sánchez-Castro et al., 2017a; Capítulo I). The cells were grown aerobically in Luria-Bertani (LB) broth medium (tryptone 10g/l, yeast extract 5 g/l and NaCl 10 g/l, pH 7.0 ± 0.2) at 28 ºC on agitation (180 rpm).

3.2. Preparation of Eu^{III} and Cm^{III} stock solutions

An stock solution of Eu^{III} was prepared by dissolving europium chloride ($EuCl_3 \cdot 6H_2O$) (Sigma-Aldrich) in 0.1 M HCl to a final concentration of 10 mM. For the experiments, an Eu^{III} working solution was prepared diluting the stock in 0.1 M $NaClO_4$ to a final concentration of 30 μM. Analytical grade 0.1 M $NaClO_4$ (Merck, Darmstadt, Germany) was used as a background electrolyte. On the other hand, a stock solution of the long-lived Cm isotope ^{248}Cm (half-life: 3.4×10^5 years) was used as described in López-Fernández et al. (2018b). This solution had the following composition: 97.3% ^{248}Cm, 2.6% ^{246}Cm, 0.04% ^{245}Cm, 0.02% ^{247}Cm, and 0.009% ^{244}Cm in 1 M $HClO_4$. To prevent the carbonate complexation of Cm^{III} carbonate-free water and NaOH solution were used. The pH of the solutions was adjusted by addition of small volumes of acid ($HClO_4$) or base (NaOH) using an InLab Solids combination pH puncture electrode (Mettler-Toledo, Giessen, Germany) and sterilized by filtration through 0.22 μm nitrocellulose filters. In the case of anaerobic experiments, the solution was degassed with N_2 prior their use in a glove box under a N_2 atmosphere at 25 °C.

3.3. Cell viability and metabolic activity analysis

The cell viability and the metabolic activity of *S. bentonitica* exposed aerobically to 30 μM Eu^{III} were determined by using flow cytometry. The cells were collected by centrifugation (11000 x g; 4°C; and 10 min) after 24 and 48 h. The resultant pellet was washed three times in phosphate buffered saline (PBS) pH 7. Then, the cells were dissolved in PBS adjusting the cellular density

to approximately 10^6 cells/ml. For cell viability test, fluorescein diacetate (FDA) and propidium iodide (PI) were added into each sample to a final concentration of 20 µl/ml and 2 µl/ml, respectively. For metabolic activity test, 3,30-dihexyloxacarbocyanine iodide (DiOC6) was employed to a final concentration of 20 µl/ml. Finally, the samples were analysed by Forward Scatter using a FACSCanto II™ cytometer (Becton Dickinson). Eu^{III}-untreated cells and dead cells obtained by heating the biomass at 90 ºC served as controls. All experiments were done in triplicates.

3.4. Potentiometric titration of cell surfaces of *S. bentonitica* treated with Eu^{III}

Potentiometric titrations were carried out to characterize the chemistry of *S. bentonitica* surfaces in presence of Eu^{III} under aerobic conditions. All titrations were performed using a Metrohm Titrando 906 automatic titrator (Metrohm, UK) at 25 ºC. The temperature was kept constant and continuously monitored during the titration. The titrator was set to add successive acid or base only after a drift equal or less than 5 mV min^{-1} was achieved.

An amount of *S. bentonitica* equivalent to 0.4 g/L of dry biomass, previously washed four times with $NaClO_4$, was suspended in a vessel with 25 ml CO_2-free 0.1 M $NaClO_4$ solution containing 30 µM Eu^{III}. Bacterial samples suspended in 0.1 M $NaClO_4$ were employed as control. The suspension was titrated with 0.1 M HCl to pH 3.5 and then with 0.1 M NaOH to pH 10.0. To test the reversibility of the protonation-deprotonation behaviour, the suspension was back-titrated with 0.1 M HCl from pH 10.0 to 3.5. All the experiments were carried out in triplicate. The HCl and NaOH were previously standardized against primary standards. To calculate the acidity constant (p*K*a) values for the bacterial cells and the corresponding total concentration of the binding sites, data from four replicates of each titration curve was fitted using the program Protofit 2.1 rev1 (Turner and Fein, 2006). Variations in the experimental results are reported as the average ± standard derivation.

3.5. Eu^{III} biosorption experiments

S. bentonitica cells were collected at the exponential phase of growth by centrifugation (10000 x g; 10 min). The resultant pellet was washed three times with 0.1 M $NaClO_4$ and resuspended therein to obtain a final biomass concentration of 0.2 g/L. Then, the samples were contacted with 30 µM Eu^{III} solution and incubated at 120 rpm on a rotator shaker at room temperature. The Eu^{III}-bacteria suspensions were harvested by centrifugation (10000 x g; 10 min) after different incubation times (0, 0.5, 1, 2, 24 and 96 h for aerobic and 0, 1, 2, 18, 24 and 48 h for anaerobic experiments). Subsequently, 1 mL of the resultant supernatant was mixed with HNO_3

and measured by inductively coupled plasma mass spectrometry (ICP-MS) to estimate the Eu^{III} concentration. The amount of Eu^{III} adsorbed to the cells was calculated by subtracting the amount obtained in the supernatant from the initial Eu^{III} concentration. For the Eu^{III}-bacteria interaction under anaerobic conditions the samples were contacted with Eu^{III} under nitrogen atmosphere within a glove box. Eu^{III} solution (30 μM) without addition of cells was employed as control. All samples were performed in triplicate.

3.6. Attenuated total reflection-Fourier transform infrared (ATR-FTIR) spectroscopy

S. bentonitica cells were contacted aerobically with Eu^{III} solution to a final concentration of 30 μM at pH 6. After 48 hours, the samples were collected by centrifugation (2700 x g; 10 min) and washed with $NaClO_4$. Finally the samples were frozen in liquid nitrogen and subsequently lyophilized according to standard protocols (Ojeda et al., 2008; Omoike and Chorover, 2004) in order to perform ATR-FTIR measurements. Bacterial cells samples without addition of Eu^{III} were employed as controls.

ATR-FTIR measurements were performed on a Perkin Elmer Spectrum Two spectrometer, equipped with an ATR accessory, consisting of a diamond crystal at a fixed angle of 45º. 32 scans with spectral resolution 4 cm^{-1} and wavenumber range from 4000 to 400 cm^{-1} were collected for each sample. All measurements were performed in triplicate.

3.7. X-ray photoelectron spectroscopy (XPS)

For XPS analysis, Eu^{III}-treated cells of *S. bentonitica* were prepared as described in the section 3.6. The obtained powder was mounted on standard sample studs using double-sided adhesive tape. Non-treated cells were prepared as controls. XPS measurements were made on a KRATOS SUPRA Photoelectron Spectrometer at 10 KV and 20 mA using a monochromatic Al Kα X-ray source (1486.6 eV). The take-off angle was fixed at 90º. On each sample the data were collected from three randomly selected locations, and the area corresponding to each acquisition was 400 μm in diameter. Each analysis consisted of a wide survey scan (pass energy 160 eV, 1.0 eV step size) and high-resolution scan (pass energy 20 eV, 0.1 eV step size) for component speciation. All experiments were conducted in triplicate. The binding energies of the peaks were determined using the C_{1s} peak at 284.5 eV. The software CasaXPS 2.3.17 (Fairley, 2006) was used to fit the XPS spectra peaks. No constraint was applied to the initial binding energy values, and the Full Width at Half Maximum (FWHM) was maintained constant for the carbon contributions in a particular spectrum.

3.8. Time-resolved laser-induced fluorescence spectroscopy (TRLFS) analyses

3.8.1. TRLFS Eu^{III}/Cm^{III} bacteria sample preparation

TRLFS measurements were performed in order to determine Eu^{III}/Cm^{III} species involved in interactions with the bacterial cells. Cells of *S. bentonitica* were brought into contact with 30 µM Eu^{III} both aerobically and anaerobically and with 0.3 µM Cm^{III} aerobically, and collected as indicated in section 3.5. The inactivity and hence easy handling of Eu^{III} allowed the TRLFS studies under both respiring conditions. However, the high hazard and cost of Cm^{III} enabled to perform the studies only under aerobic conditions. The obtained pellets were washed and subsequently re-suspended in 5 ml of 0.1 M $NaClO_4$ for analysis by TRLFS. For Eu^{III}, the pH was kept constant at 6, while varying the incubation time (1, 24 and 48 h). For Cm^{III}, a pH dependent spectroscopic titration (pH 2.33 to 8.04) was carried out.

3.8.2. TRLFS experimental setup.

The time-resolved luminescence spectra were recorded using a unique pulsed flash lamp pumped Nd:YAG-OPO laser system (Powerlite Precision II 9020 laser equipped with a Green PANTHER EX OPO from Continuum, Santa Clara, CA, USA). The laser pulse energy, which was between 1.5 and 2.5 mJ depending on the excitation wavelength used, was monitored using a photodiode. The luminescence spectra were detected using an optical multi-channel analyzer-system, consisting of an Oriel MS 257 monochromator and spectrograph with a 300 or 1200 line mm^{-1} grating and an Andor iStar ICCD camera (Lot-Oriel Group, Darmstadt, Germany). The Eu^{III}/Cm^{III} single luminescence emission spectra were recorded in the 570–650 nm (1200 line mm^{-1} grating with 0.2 nm resolution) range. The time-dependent luminescence spectra were detected in the 500–700 nm (300 line mm^{-1} grating: high intensity with a lower resolution >0.6 nm) range. A constant time window of 1 ms length was applied. For Eu^{III} an excitation wavelength of 394 nm was used. Due to the high absorption of the F-band usually observed in Cm^{3+} excitation spectra, an excitation wavelength of 396 nm was used. For time-dependent emission decay measurements, the delay time between laser pulse and camera gating was scanned with time intervals between 10 and 25 µs. A more detailed description of the experimental setup data and evaluation of the luminescence spectra is described in Moll et al. (2014). The spectra were base-line and energy corrected and normalized using the ORIGIN 8.6G (OriginLab Corporation, USA) code. The lifetime of luminescent species was obtained also with this software.

The relative peak intensity ratio, which gives information about the ligand field of Eu^{III} and the coordination environment, was determined by forming the ratio for the integral intensities of the $^7F_2$ to $^7F_1$ band, as presented in Equation 1:

$$R_{E/M} = (^5D_0 \rightarrow {}^7F_2) / (^5D_0 \rightarrow {}^7F_1) \quad [1]$$

The intensities of I ($^5D_0 \rightarrow {}^7F_2$) and I ($^5D_0 \rightarrow {}^7F_1$) were calculated from the corresponding normalized peak areas. The number of coordinated water molecules was determined based on the equations of Kimura and colleagues (Kimura et al., 1996; Kimura and Choppin, 1994; Kimura and Kato, 1998), which is presented in Equation 2:

$$nH_2O = 1.07\ k_{exp} - 0.62 \text{ for } Eu^{III} \quad [2]$$

nH_2O = coordination number of water molecules

k_{exp} = reciprocal luminescence emission lifetime (ms)

The spectra deconvolutions of the pH-dependent Cm^{III} luminescence measurements were performed using the factor analysis software HypSpec (Gans et al., 1996).

3.9. STEM-HAADF analysis

The cellular location of Eu^{III} was analyzed by using scanning transmission electron microscopy (STEM) equipped with energy dispersive X-ray (EDX) for elemental composition analysis. EDX analysis was performed at 300 kV using a spot size of 4 Å and a live counting time of 50 s. The samples consisting of Eu^{III}-treated cells (30 µM) under aerobic and anaerobic conditions were prepared as described in Merroun et al. (2005) after 48 h of incubation. Finally, the samples were examined under high-angle annular dark field scanning transmission electron microscope (HAADF-STEM) FEI TITAN G2 80-300. STEM specimen holders were cleaned by plasma prior to STEM analysis to minimize contamination.

4. Results and discussion

4.1. Potentiometric titration studies

Bacterial cell walls are rich in functional groups (e.g. hydroxyl, phosphoryl, amino, and carboxylic moieties) that can protonate or deprotonate when interacting with their immediate surroundings (e.g. metals) and as a result the cell walls develop a net pH-dependent charge (Daughney and Fein, 1998; Fein et al., 2005; Haas et al., 2001; Ngwenya et al., 2003; Ojeda et

al., 2008; Plette et al., 1995). The concentration and characteristics of proton active carboxylic, hydroxyl, phosphate, phosphodiester, and amine groups on the cell surfaces play an important role in this respect, as they are responsible for the surface metal binding ability (Dittrich and Sibler, 2005). Therefore, the characterization of the cell surface chemical properties is needed to determine the types and abundance of these metal binding sites which in turn help to obtain accurate modeling of the mechanisms by which microbes interact with metals. In the present study, we applied acid-base titration methods to determine cell surface functional-group reactivity of the cells of the strain *S. bentonitica*.

The potentiometric titrations curves of *S. bentonitica* BII-R7 before and after Eu^{III} exposure are presented in Figures 1A and 1B. The concentration of deprotonated sites is standardized per mass of dry biomass (mol g^{-1}), and calculated according to Fein et al. (1997) as follows in Equation 3:

$$[H^+]_{consumed/released} = (C_a - C_b - [H^+] + [OH^-]) / m_b \quad [3]$$

Where m_b is the biomass concentration in the suspension (g/L), C_a and C_b are the concentrations of acid and base added at each step of a titration, and $[H^+]$ and $[OH^-]$ represent molar species concentrations of H^+ or OH^-. To calculate the acidity constants and the total concentration of each binding site, data from the titrations curves were fitted using ProtoFit 2.1 rev1 (Turner and Fein, 2006) using a Non-Electrostatic Model (NEM).

The titrated bacterial suspensions exhibit a protonation-deprotonation behaviour over the whole pH range studied (Figure 1A and 1B). No evidence of saturation was found with respect to proton adsorption, indicating that, even at pH 3.5, full protonation of the functional groups on the cell wall was not achieved. The shape of the titrations curves obtained suggested the presence of functional groups with close acid-base pK_a values, showing that although some small variability could be perceived in each set of the same bacterial sample, essentially reproducible results were obtained (the variation between the titration curves was below 6% of $[H^+]_{exchanged}$ between pH 3.5 and 10.0). Although a small hysteresis could be observed between acid and base titrations at the same ionic strength, results from reverse titrations did not vary strongly and suggested a reversible proton adsorption/desorption reaction.

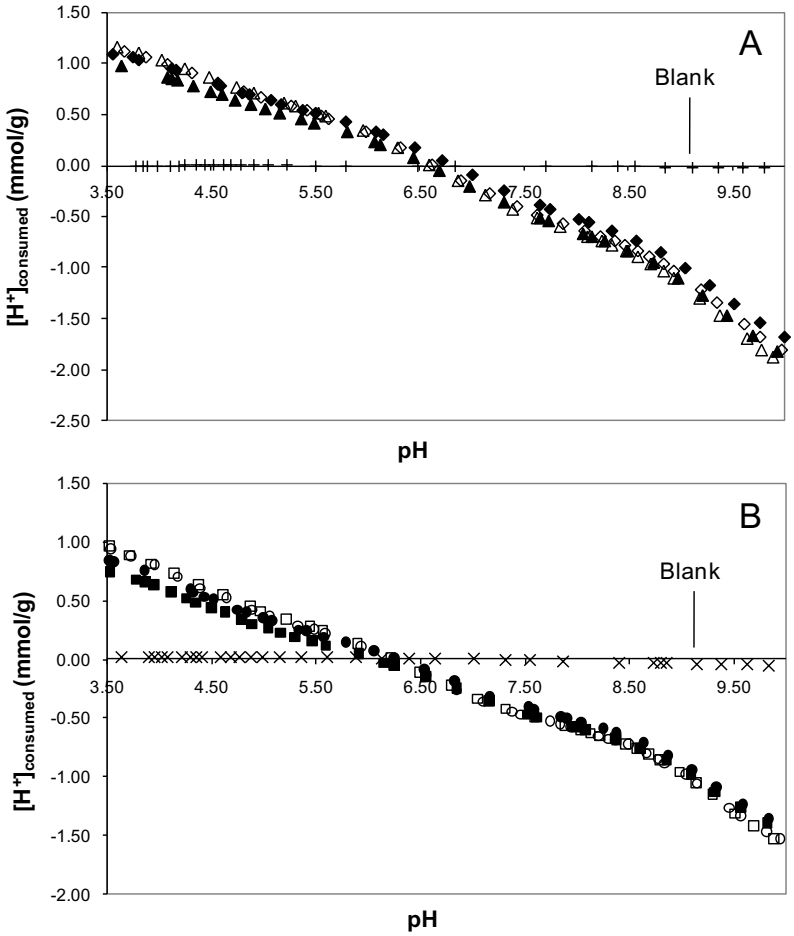

Figure 1. Representation of the potentiometric titrations of *S. bentonitica* in suspension in $NaClO_4$ (A) and in contact with Eu^{III} solution (B) after 48 hours of biosorption, compared with the background electrolyte. Closed symbols correspond to the forward titration data and open symbols correspond to back titration.

Table 1 summarizes the pK_a values for *S. bentonitica* before and after Eu^{III} exposure. The calculated values are 4.97 ± 0.08 and 4.78 ± 0.06 for pK_1, respectively, 6.88 ± 0.02 and 6.75 ± 0.13 for pK_2, respectively, and 9.43 ± 0.02 and 9.48 ± 0.11 for pK_3, respectively. The obtained pK_a values are representative of carboxylic groups for pK_1, phosphate groups for pK_2 and amine and hydroxyl groups for pK_3 (Dittrich and Sibler, 2005; Fein et al., 2005, 1997; Ngwenya et al., 2003; Ojeda et al., 2008; Yee et al., 2004; Yee and Fein, 2001). The existence of pH of zero proton charge (pH_{zpc}) indicated that *S. bentonitica* developed a positive net charge at low pH values, indicating the presence of at least one positively ionising, plausibly amino group. Models which only include negatively ionising groups such as carboxyl, phosphoryl and hydroxyl groups could not develop a net positive charge at low pH (Claessens et al., 2006). The pH_{zpc} around 5.7 also indicated that the cells are negatively charged at neutral pH = 7 and electrostatic attraction with positive-charged mineral surfaces or metals may be favourable.

The surface site densities obtained using ProtoFit are also presented in Table 1. The pK_a values for both bacterial samples are comparable, indicating similar concentration of the active functional groups on the cell wall. However, the concentrations corresponding to phosphate groups (C_2) is significantly lower for *S. bentonitica* cells exposed to Eu^{III}. This could suggest that the Eu^{III} may be strongly bonded to phosphate sites, making them now inaccessible to the protonation/deprotonation reaction. The considerable high concentration of phosphate groups at the surface of *S. bentonitica* (10.78 ± 0.31 x 10^{-4} mol/g) comparing with other bacterial species such as *Sphingomonas* sp. S15-S1 (3.16 ± 0.56 x 10^{-4} mol/g) and *B. sphaericus* JG-7B (2.19 ± 0.25 x 10^{-4} mol/g) (Merroun et al., 2011) (Table 1) pointed out the potential high metal-binding ability of *S. bentonitica*.

Table 1. Comparison of deprotonation constants and surface site concentrations for *S. bentonitica* and other strains from different studies.

Species	pK_1	pK_2	pK_3	C_1 (x 10^{-4}mol/g)	C_2 (x 10^{-4}mol/g)	C_3 (x 10^{-4}mol/g)	Model[a]	Reference
S. bentonitica + Electrolyte solution	4.97 ± 0.08	6.88 ± 0.02	9.43 ± 0.02	5.05 ± 0.31	10.78 ± 0.31	16.93 ± 1.45	NEM	This study
S. bentonitica + Eu(III) solution	4.78 ± 0.06	6.75 ± 0.13	9.48 ± 0.11	5.31 ± 0.22	7.56 ± 0.56	13.99 ± 1.12	NEM	This study
Aquabacterium commune, Gram-negative	3.5 ± 0.8	5.7 ± 0.9	9.1 ± 1.6	4.6 ± 1.5	1.9 ± 0.6	7.3 ± 3.1	NEM	Ojeda et al., 2008
B. sphaericus JG-7B, Gram-positive	4.37 ± 0.27	6.37 ± 0.31	9.95 ± 0.16	4.70 ± 0.55	2.19 ± 0.25	4.56 ± 0.77	NEM	Merroun et al., 2011
Sphingomonas sp. S15-S1, Gram-negative	4.27 ± 0.45	7.03 ± 0.86	9.92 ± 0.32	4.91 ± 1.04	3.16 ± 0.56	9.24 ± 2.97	NEM	Merroun et al., 2011
Enterobacteriaceae, Gram-negative	4.3 ± 0.2	6.9 ± 0.5	8.9 ± 0.5	5.0 ± 0.7	2.2 ± 0.6	5.5 ± 2.2	CCM	Ngwenya et al., 2003
Synechococcus Green, Gram-negative	4.85 ± 0.31	6.56 ± 0.2	8.76 ± 0.06	2.6 ± 0.4	1.9 ± 0.5	2.5 ± 0.4	CCM	Dittrich and Sibler; 2005
Synechococcus Red, Gram-negative	4.98 ± 0.16	6.69 ± 0.39	8.66 ± 0.21	7.4 ± 1.6	4.4 ± 0.8	4.8 ± 0.8	CCM	Dittrich and Sibler; 2005
Calothrix sp., Gram-negative	4.7 ± 0.4	6.6 ± 0.2	9.1 ± 0.3	3.28 ± 0.27	4.14 ± 0.31	7.16 ± 0.97	NEM	Yee et al., 2004
S. putrefaciens, Gram-negative	5.16 ± 0.04	7.22 ± 0.15	10.04 ± 0.67	0.32 ± 0.02	0.09 ± 0.01	0.38 ± 0.01	CCM	Haas et al., 2001
B. subtilis, Gram-positive	4.8 ± 0.14	6.9 ± 0.5	9.4 ± 0.6	12 ± 1	4.4 ± 0.2	6.2 ± 0.2	CCM	Fein et al., 1997

[a] CCM = Constant Capacitance Model; NEM = Non-electrostatic mode

The results of potentiometric titration experiments on the studied samples indicated that the cell surface groups capable for metal binding sites could involve carboxyl groups (pK around 3-5), phosphate groups (pK around 6-7), and hydroxyl and amine groups (pK > 8). These findings are in agreement with previous studies on bacterial surfaces (Fang et al., 2014; Liu et al., 2015; Ojeda et al., 2008). Liu et al., (2015) demonstrated the role of carboxyl, phosphoryl, and amino functional groups of *Synechococcus* sp. PCC 7002 cells as metal surface ligands by means of potentiometric titrations. In the case of Eu^{III} and Cm^{III}, their sorption with the surface cells of *B. subtilis* and *P. fluorescens* can be due to their coordination with carboxyl groups (Moll et al., 2013; Ozaki et al., 2004; Yao et al., 2016). In addition, Haas et al., (2001) showed that, in the presence of U^{VI}, sorption is accounted by using two separate adsorption reactions forming the

surface complexes >COO-UO_2^+ and >PO_4H-$UO_2(OH)_2$. Modeling results suggested that both Eu^{III} and U^{VI} form similar surface complexes, in agreement with data from extended X-ray absorption fine structure (EXAFS) spectroscopy (Estes, 2014). Consequently, phosphate and carboxyl groups could be expected to be involved in the binding of Eu^{III} as well. However, the potentiometric results only showed phosphate groups as the main potential binding sites in the pH range studied. It is probable that the extent of the carboxyl group involvement in the Eu^{III} binding is either too small to be detected by titration methods, or the sorption/desorption of Eu^{III} by the carboxylic groups is reversible at low pH.

4.2. Kinetics of Eu^{III} adsorption on the bacteria

Kinetics studies of Eu^{III} for *S. bentonitica* were performed in order to estimate the Eu^{III} removal capacity of this bacterial species with increasing time under aerobic and anaerobic conditions. To the best of our knowledge, this is the first study comparing the adsorption of Eu^{III} by bacterial cells under both respiration conditions. The maximum amount of Eu^{III} removal was around 12.9 ± 0.11 mg of Eu/g of dry biomass after 96 h of aerobic incubation (Figure S1). This amount corresponds to a 54 ± 0.44 % of Eu^{III} removed from the total amount of Eu in the solution. Higher values were obtained by Bader et al. (2019) in their bioassociation kinetics studies with the halophilic archaeon *Halobacterium noricense* DSM15987^T at the same Eu^{III} initial concentration (30 μM). They found that around 73% of Eu^{III} was removed after 1 week of incubation. Under anaerobic conditions the maximum amount of Eu^{III} removal was around 6.06 ± 0.25 mg of Eu/g of dry biomass after 18 h incubation (Figure S1). This amount corresponds to a 31.2 ± 1.3 % of Eu^{III} removal. The Eu^{III} removal increases with increasing contact time of incubation until equilibrium is attained under both conditions. However these results clearly showed that *S. bentonitica* cells have a higher removal capacity under aerobic conditions. This could be a consequence of the fact that anoxic conditions are more stressful for the bacterial cells, probably affecting the interaction process.

The results suggested the interaction is mediated not only by biosorption since this mechanism is generally defined as a quick process ocurring up to a few hours (Gadd, 2009). Specifically, the kinetic studies showed that time-dependent Eu interaction with the cells is a biphasic process. First, a rapid phase where 12.5 ± 0.73 and 13.9 ± 1 % of Eu^{III} removal was achieved (aerobically and anaerobically, respectively) within the first 2 h. This fast phase is usually associated to metabolic independent biosorption mechanism. Secondly, a slow phase occurs where Eu^{III} accumulation process reach equilibrium after 24 h. This phase could be controled by metabolically dependent interaction mechanisms such as intracellular accumulation,

bioprecipitation, etc. Similarly to our results, Gerber et al. (2016) also reported a two phasic process in the interaction of *Acidovorax facilis* with U^{VI}.

4.3. Characterization of Eu^{III}-*S.bentonitica* interactions using ATR-FTIR

Figure 2 shows the ATR-FTIR spectra obtained from *S. bentonitica* after being in contact with 30 µM Eu^{III} solution and with the electrolyte ($NaClO_4$) after 48 h incubation. The observed infrared bands corresponded to the presence of proteins, lipids, polysaccharides, polyphosphate groups, etc. The functional groups assigned to the infrared bands and the corresponding frequencies for the bacterial cells are summarised in Table S1.

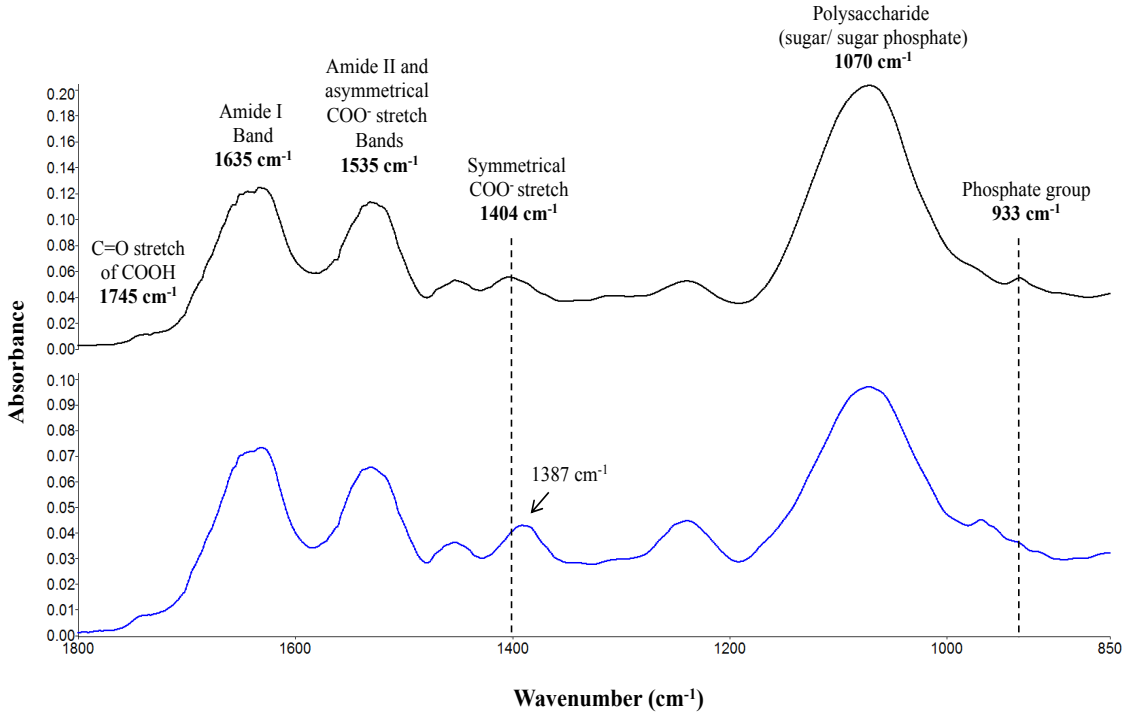

Figure 2. Comparison between the ATR-FTIR spectra for *S. bentonitica* cell suspensions in $NaClO_4$ (electrolyte) solution (top) and 30 µM Eu^{III} solution (bottom) after 48 hours.

The region between 3000 and 2800 cm^{-1} exhibited the typical C-H stretching vibrations (ν_{C-H}) corresponding to the CH_3 and $>CH_2$ functional groups present in the fatty acids and lipids, and the O-H stretching band (ν_{O-H}) corresponding to the presence of hydroxyl groups in the bacterial cells. Complementary information could be found at the region between 1800 and 750 cm^{-1}, where vibrations of C-H, $>CH_2$ and $-CH_3$ groups, amides, carbonyl groups and polysaccharides were observed. The peaks observed at 1308 and 1455 cm^{-1} could be attributed to the bending of $-CH_3$ and $>CH_2$ of proteins (δ_{CH2}, δ_{CH3}), and the signals at 1635 and 1535 cm^{-1} corresponded to the amide I and II bands, respectively. The amide I band is due to the stretching C=O ($\nu_{C=O}$) of

amides associated with proteins and the amide II band is actually a combination of bending N-H (δ_{N-H}) of amides and contributions from stretching C-N (ν_{C-N}) groups. The peak at 1455 cm^{-1} also conceals the amine III group. The peak around 1404 cm^{-1} is due to the symmetric stretching C-O of carboxylate groups ($\nu_{sym\ COO^-}$), and the peak corresponding to the asymmetric stretching vibration ($\nu_{asym\ COO^-}$) is concealed by the amide II band at 1535 cm^{-1}. The signal around 1745 cm^{-1} is actually a combination of two peaks: a signal corresponding to the vibrational C=O stretching ($\nu_{C=O}$) of carboxylic acids at 1747 cm^{-1} and another peak corresponding to the stretching C=O of ester functional groups from membrane lipids and fatty acids at 1730 cm^{-1} (Dittrich and Sibler, 2005; Jiang et al., 2004; Ojeda et al., 2008; Yee et al., 2004). The double bond stretching of >P=O of general phosphoryl groups and phosphodiester of nucleic acids could be observed at 1240 cm^{-1}. The stretching of P=O groups of polyphosphate products, nucleic acid phosphodiester and phosphorylated proteins can be found around 1070 cm^{-1}, and the peak at 933 cm^{-1} showed the asymmetric O-P-O stretching modes (Dittrich and Sibler, 2005; Jiang et al., 2004; Yee et al., 2004).

The ATR-FTIR spectra showed a shift in the band attributed to symmetric stretching of carboxylate groups (around 1404 cm^{-1}) to lower frequencies, when compared to the spectra of the cells in background electrolyte (Figure 2). Extensive studies made on metal complexes of carboxylic acids have established an empirical correlation between the position of the symmetric stretching ($\nu_{sym\ COO^-}$) and asymmetric stretching ($\nu_{asym\ COO^-}$) of carboxylate groups and the difference in frequency between them ($\Delta\nu$). The values of $\Delta\nu$ descend in the follow order: $\Delta\nu_{unidentate} > \Delta\nu_{brinding} \sim \Delta\nu_{free\ ionic} > \Delta\nu_{chelate(bidentate)}$ (Chu et al., 2004; Deacon and Phillips, 1980; Nakamoto, 2008; Tackett, 1989). As it can be observed in Figure 2 and Table S1, the asymmetric stretching ($\nu_{asym\ COO^-}$) of carboxylate groups is hidden by the amide II band, and therefore, it is difficult to determine if there was a shift in this band to higher or lower frequencies. However, Chu et al. (2004) and Deacon and Phillips (1980), after careful examinations of IR spectra of many acetates with known X-ray crystal structures, arrived at the conclusion that: i) for unidentates complexes, $\Delta\nu > 200\ cm^{-1}$ and the position of $\nu_{sym\ COO^-}$ is generally shifted to lower frequencies; ii) for bidentate chelating complexes, $\Delta\nu < 100\ cm^{-1}$ and the position of $\nu_{sym\ COO^-}$ is shifted to higher frequencies, whereas $\nu_{asym\ COO^-}$ is shifted to lower frequencies; and iii) for bidentate bridging complexes, $\Delta\nu \sim 160\ cm^{-1}$ and the position of $\nu_{sym\ COO^-}$ and $\nu_{asym\ COO^-}$ can shif in either direction (Chu et al., 2004). The symmetric stretching ($\nu_{sym\ COO^-}$) band for *S. bentonitica* in contact with Eu^{III} shifted to lower frequencies by ~15 cm^{-1} and the asymmetric stretching ($\nu_{asym\ COO^-}$) of carboxylate groups did not show a significant shift expressed as the appearance of an important shoulder near the amide II band (1535 cm^{-1}). Therefore, we could assume that $\Delta\nu$ must be around 150 cm^{-1}, suggesting that the carboxyl functional groups arising from the macromolecules of the cell wall of the bacterial cells could

form bidentate bridging complexes with the Eu^{III} metals. This is the first study demonstrating the ability of bacterial cells to interact with Eu in a bidentate bridging mode. EXAFS analysis is on-going and will provide more information about the local coordination of Eu associated with the cells.

The results also indicate that polysaccharides could also be involved in cell attachment. The lower intensity of the band found at 933 cm^{-1} of Eu^{III}-treated cells comparing with Eu^{III}-untreated cells suggested phosphate groups as candidates for Eu^{III} complexation.

4.4. Characterization of Eu^{III}-*S.bentonitica* interactions using XPS.

This method was applied to determine the local coordination of Eu^{III} at the cell surface of *S. bentonitica* approximately up to 5 nm (Kumar et al., 2015). The elemental composition of *S. bentonitica* surface, resulting from integrating the C_{1s}, O_{1s}, N_{1s} and P_{2p} from the wide scan spectrum can be seen in Figure 3. Sodium and chlorine were also detected as samples were washed with 0.1 M $NaClO_4$. Eu was also detected in the bacterial sample that was contacted for 48 hours with a 30 µM Eu^{III} solution. Nitrogen appeared at a binding energy of 399.99 eV, attributable to amine or amide groups of proteins (Dufrêne et al., 1997; Dufrêne and Rouxhet, 1996; Omoike and Chorover, 2004; Pradier et al., 2005; Van Der Mei et al., 2000). Phosphorus was found at a binding energy of 133.99 eV, and can be attributed to phosphate groups (Dufrêne et al., 1997; Dufrêne and Rouxhet, 1996; Van Der Mei et al., 2000). The presence of amine groups from proteins and phosphate groups based on the binding energies of N_{1s} and P_{2p} are in agreement with the results from potentiometric titrations (pK_a = 6.8 and pK_a = 9.4) and the FTIR spectra (adsorption bands at 1635 cm^{-1}, 1535 cm^{-1}, and 933 cm^{-1}).

XPS peaks corresponding to Eu_{3d} were analysed at high resolution to assess the nature of the Eu^{III} complex. The Eu_{3d} peak observed at 1135 eV was attributed to Eu-acetate according to Mercier et al. (2006). This observation suggests that the carboxyl groups from acetate play a key role in the complexation of Eu^{III} on the *S. bentonitica* cell wall, as previously indicated ATR-FTIR results. Previous studies showed the role of carboxyl groups from glutamic and aspartic acid present in proteins of the S-layer of *B. sphaericus* in the complexation of uranium and palladium (Fahmy et al., 2006; Merroun et al., 2005). Therefore, carboxyl groups of the glutamic acid of the peptidoglycan (PG) layer of *S. bentonitica* could be involved in the interaction of Eu^{III}.

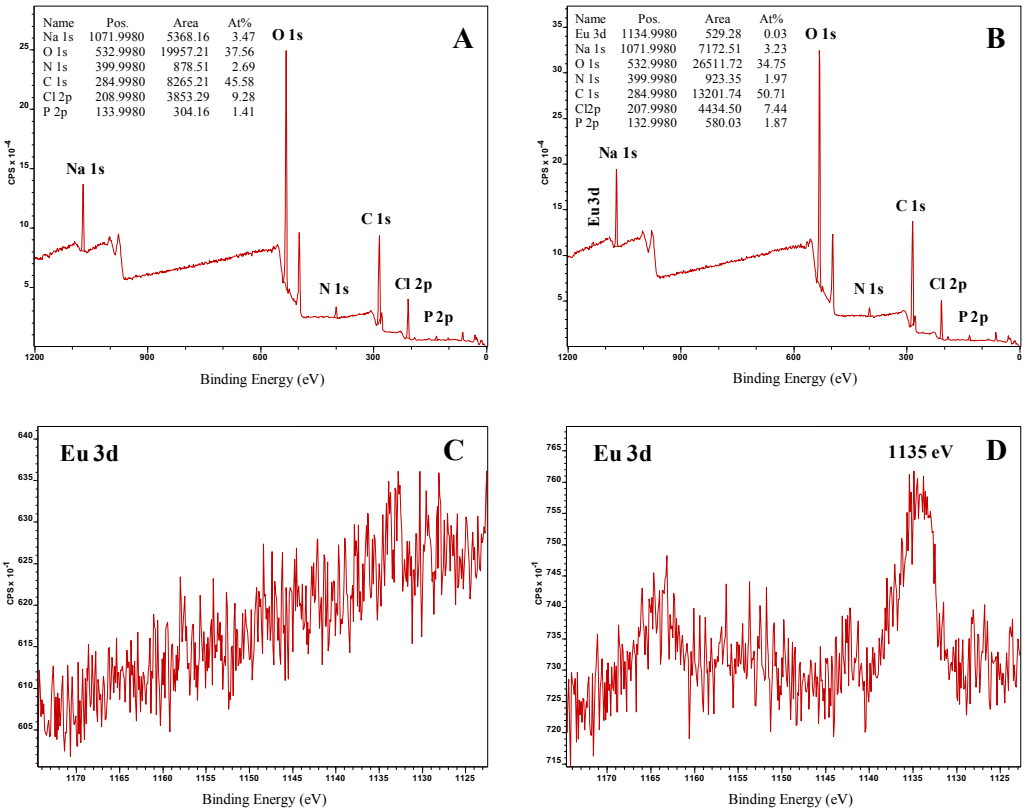

Figure 3. XPS spectra of *S. bentonitica* in the absence (A-B) and the presence of 30 µM Eu^{III} (C-D). The region belonging to Eu 3d (B and D) was scanned at high resolution.

4.5. TRLFS characterization of Eu^{III}/Cm^{III} interaction with *S. bentonitica*

Potentiometric titrations, ATR-FTIR, and XPS studies showed the involvement of phosphate and carboxyl groups in the coordination of Eu^{III} by the cells of *S. bentonitica*. In addition, TRLFS spectroscopy was also applied to confirm these Eu/bacteria structural data and also to investigate the complexation behavior of Cm^{III}, radioactive analogue of Eu^{III}, at much lower concentrations relevant to environmental conditions (0.3 µM).

4.5.1. Europium

The luminescence spectra depicted in Figure 4 showed the interaction of Eu^{III} with *S. bentonitica* through typical changes concerning cell addition after 1, 24 and 48 h incubating anaerobically at pH 6 in both supernatants and re-suspended cells. This suggested the complexation of Eu^{III} with bacterial surface functional groups and extracellular released complexing agents. In the supernatant and the re-suspended cells the $^7F_0$ transition appears at 579 nm with a slightly higher intensity than in the blank sample. This points to a different symmetry around the Eu^{III} center compared to the blank spectrum. The $^7F_0$ peak has a low intensity (up to 1 % of the total luminescence intensity) indicating the formation of Eu^{III}

complexes in the supernatants and the cells with a relatively high symmetry. The luminescence spectrum of Eu^{III} aqua ion (blank) is characterized by emission bands at 585-600 nm (magnetic dipole transition $^5D_0 \rightarrow {}^7F_1$) and 610-630 nm (hypersensitive transition $^5D_0 \rightarrow {}^7F_2$). An increased intensity of the hypersensitive $^7F_2$ transition at 617 nm moving from blank via supernatant to the re-suspended cells was discovered.

In the supernatants there was a systematic increase in the $^7F_2$ transition as a function of the incubation time (Figure 4A). This could indicate an increase in the release of complexing agents from the cells with increasing incubation time. The total organic carbon (TOC) content of the supernatant samples increased with the incubation time until 24 h of incubation (Figure S2), confirming that release of complexing substances from the cells. These results are in agreement with kinetic studies (section 4.2), in which the amount of Eu adsorbed increased with the incubation time. In the re-suspended cells there was a fast increase in the intensity of the $^7F_2$ transition after an incubation time of 1 h. Then, no systematic change in the spectra as a function of the incubation time could be observed (Figure 4B).

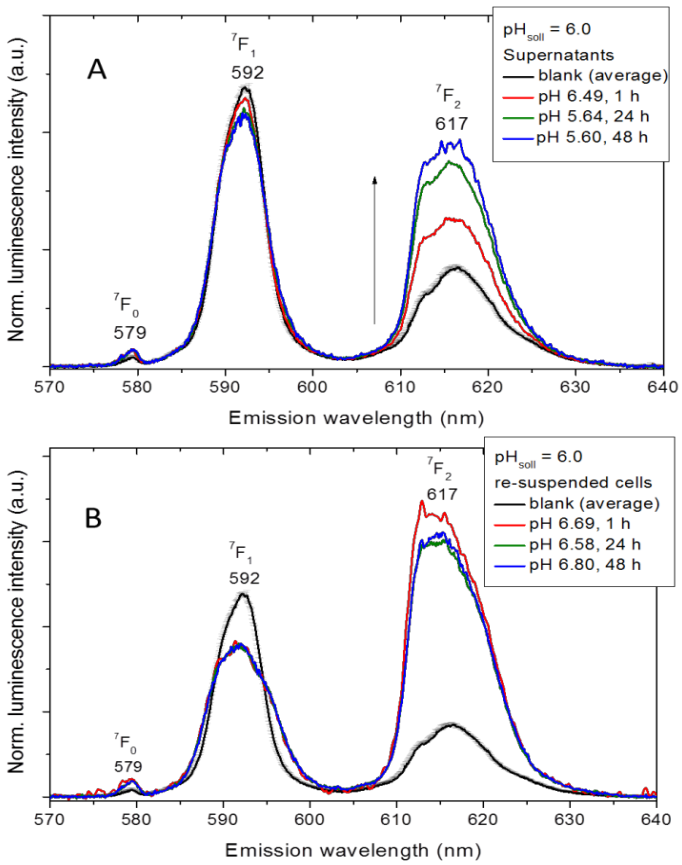

Figure 4. Luminescence emission spectra of 30 µM Eu^{III} measured for the supernatants after separating the *S. bentonitica* cells (0.2 g/l) (A) and the re-suspended cells (B) under anaerobic conditions at pH 6 and different incubation times (1, 24 and 48 hours) in 1 M $NaClO_4$.

In supernatant and re-suspended cells Eu^{III} appears in two different coordination environments. The short-lived component in supernatants was measured to be 117, 129 and 133 µs after 1, 24, and 48 h, respectively (Table 2). These lifetimes indicated a similar coordination environment after 24 and 48 h. The luminescence lifetime of 114 ± 5 µs found in the blank characterizes the Eu^{3+} ion. The short lifetime of 117 µs found in the supernatant indicated the presence of the Eu^{III} ion after 1 h of incubation. The longer lifetime, 387 to 500 µs, could indicate an interaction of Eu^{III} with released substances from the cells independently from the incubation time. However, the short lifetime, 130 µs, detected after 24 and 48 h could be a hint to another functionality most likely released from the cells (Table 2). In the case of re-suspended cells, a bi-exponential luminescence decay was measured indicating two coordination environments of Eu^{III}. The short-lived component showed luminescence lifetimes between 144 and 225 µs, whereas the long-lived component varied between 477 and 609 µs. In a first approximation, similar Eu^{III} species are formed for the short-lived component of the supernatant and re-suspended cells. In the same way, the long-lived component of both supernatant and re-suspended cells suggested a similar coordination environment but different from the one found for the short-lived component.

Table 2. Spectroscopic properties obtained from the Eu^{III}-*S. bentonitica* system at pH 6 using different incubation times and other relevant model systems.

Sample	$R_{E/M}$	Lifetime (µs)	Proposed species	Reference
Eu^{III} control	0.50 ± 0.05	114 ± 5	Eu^{3+}	This work
Supernatants **Eu^{III}-*S. bentonitica***				This work
1 h incubation	0.9	117; 387	Eu^{3+}; phosphoryl sites	
24 h incubation	1.2	129; 490	Carboxyl; phosphoryl	
48 h incubation	1.3	133; 500	Carboxyl; phosphoryl	
Cells **Eu^{III}-*S. bentonitica***				This work
1 h incubation	2.3	144; 477	Carboxyl; phosphoryl sites	
24 h incubation	2.1	174; 561	Carboxyl; phosphoryl	
48 h incubation	2.1	225; 609	Carboxyl; phosphoryl	
Eu^{III}-*Sporomusa* sp. MT-2.99	3.3	170	R-COO-Eu^{2+}	Moll et al. 2014
	1.8	515	R-O-PO_3H-Eu^{2+}	
Eu^{III}-*Bacillus subtilis*		230	Carboxyl sites	Markai et al. 2003
		730	Phosphoryl sites	
Eu^{III}-*Pseudomonas aeruginosa*		98-254	Carboxyl sites	Texier et al. 2000
		534-677	Phosphoryl sites	

By comparing our lifetime results with literature data, phosphoryl and carboxyl groups present on bacterial cell envelopes and bacterial released substances seem to play an important role in the Eu^{III} coordination sites characterized by, for instance, their individual luminescence lifetimes, probably in form of R-O-PO_3-Eu^{2+} (R-O-PO_3H-Eu^{2+} under acidic pH conditions) and R-COO-Eu^{2+}as revealed previous studies (Moll et al., 2014; Texier et al., 2000) (Table 2). It is important to note that the results here presented were very similar to those obtained aerobically and have comparable significance.

4.5.2. Curium

The chemical speciation of Cm^{III} with *S. bentonitica* cells was studied at trace (0.3 µM) Cm^{III} concentrations by using TRLFS. These measurements were conducted assuming that the influence of the luminescence properties of the microbial Cm^{III}-species dominates over the influence of soluble Cm^{III}-species with, for instance, released complexing agents. The pH-dependent spectroscopic Cm^{III} speciation in the cell suspensions is shown in Figure 5.

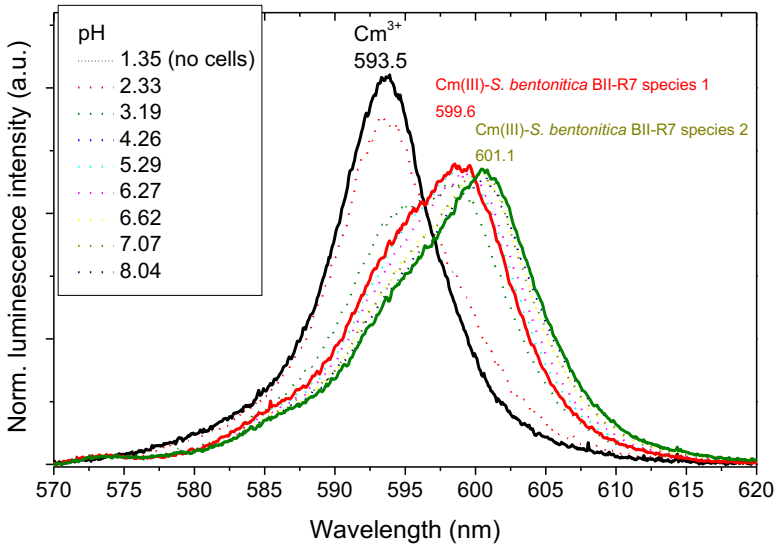

Figure 5. Luminescence emission spectra of 0.3 µM Cm^{III} in 0.1M $NaClO_4$ measured as a function of pH at a fixed biomass concentration of 0.2 $g_{dry\ weight}$/l.

From the dependencies found in the TRLFS spectra it can be concluded that there are two coordination environments of Cm^{III} due to interactions with functional groups of the cell surface and possibly with released complexing agents. Thus, the Hypspec analysis of the pH dependent emission spectra measurements revealed two Cm^{III} bacterial species (Figure 5). Cm^{III}-*S. bentonitica* species 1 was characterized by an emission maximum at 599.6 nm while Cm^{III}-*S. bentonitica* species 2 shows a more red shifted emission maximum at 601.1 nm. The extracted single component spectra of both species are shown in Figure 5. TRLFS of the supernatants and

the Cm^{III} loaded biomass after washing with 0.1M $NaClO_4$ showed that 73% of the detected Cm^{III} luminescence intensity remained in solution at pH 8.04. While, only 23% was associated to the biomass. This points to a complexation of Cm^{III} by substances released from the cells. In all cell containing samples, a bi-exponential luminescence decay was detected (Table 3). At pH 3.2 the short lifetime of 71 µs points to uncomplexed Cm^{3+}. Between pH 4 and 8 both lifetimes amounted to 120 ± 8 and 290 ± 23 µs. By comparing our results with literature a close agreement was found to the study of López-Fernández et al. (2018b). The long lifetime and the corresponding emission maximum matches with Cm^{III} interactions with microbial phosphoryl sites, whereas the short lifetime can be attributed to carboxyl interactions of Cm^{III}.

Table 3. Luminescence emission data of the Cm^{III}-*S. bentonitica* system including those of relevant model systems for comparison.

Species	Emission peak maximum (nm)	Lifetime (µs)	Reference
Cm^{III} (aq)	593.5	68 ± 5	This work
Cm^{III}-*S.bentonitica* BII-R7 species 1	599.6	290 ± 23	This work
Cm^{III}-*S.bentonitica* BII-R7 species 2	601.1	120 ± 8	This work
Cm^{III}-*R. mucilaginosa* BII-R8 species 1	599.6	240 ± 50	López-Fernández et al., 2018b
Cm^{III}-*R. mucilaginosa* BII-R8 species 2	601.5	123 ± 11	
Cm^{III}-*Sporomusa* sp. MT-2.99 complexes			Moll et al., 2014
R-O-PO_3H-Cm^{2+}	599.8	252 ± 46	
R-COO-Cm^{2+}	601.6	108 ± 15	
Cm^{III}-*Pseudomonas fluorescens* complexes			Moll et al., 2013
R-O-PO_3H-Cm^{2+}	599.6	390 ± 78	
R-COO-Cm^{2+}	601.9	121 ± 10	
Cm^{III}-*Paenibacillus* sp. complex			Lütke, 2013
R-O-PO_3H-Cm^{2+}	598.8	477 ± 73	

Summarizing, the TRLFS results indicated that phosphoryl and carboxyl groups of *S. bentonitica* present on bacterial cell envelopes and bacterial released substances seem to play an important role in the Eu^{III}/Cm^{III} coordination sites. Most probably, R-O-PO_3-Eu^{2+} and R-COO-Eu^{2+} complexes dominate the speciation as suggested previous studies (Moll et al., 2014; Texier et al., 2000). Specifically, the Eu^{III}-*S. bentonitica* complexes seem to have similar properties as

the surface species R-O-PO_3H-Eu^{2+}observed on cell envelopes of *Sporomusa* sp. MT-2.99 (Moll et al., 2014) as revealed the long lifetimes. Coordination site characterized by short lifetimes seem to interact with Eu^{III} with similar properties as the surface species R-COO-Eu^{2+} observed on cell envelopes of *Sporomusa* sp. MT-2.99 and *P. fluorescence* (Moll et al., 2014). Two different coordination environments of Cm^{III} with functional groups of the cell membrane and most probably with released complexing agents were detected. The lifetimes and the corresponding emission maximum can be attributed to carboxyl and phosphoryl interactions of Cm^{III}. Similarly, López-Fernández et al. (2018b) showed the involvement of organic carboxyl and phosphate groups of *Rhodotorula mucilaginosa* in the Eu^{III}/Cm^{III} complexation, demonstrating for the first time the coordination of Eu^{III} and Cm^{III} to yeast cells.

4.6. Cellular localization of Eu^{III} by STEM-HAADF

STEM-HAADF micrographs of thin sections of *S. bentonitica* cells exposed to Eu^{III} revealed the presence of electron-dense accumulations mainly at the cell surface (Figure 6A-D) under both aerobic and anaerobic conditions. In addition, very few extracellular (Figure 6A-D) and intracellular (Figure 6D) accumulations were also observed. EDX analysis (Figure 6E-F) and element-distribution mapping (Figure 7) derived from these accumulations indicated they were mainly composed of Eu and P. The detection of P in the EDX analysis of the Eu^{III} precipitates supports the involvement of functional groups containing phosphorus in their interaction with Eu^{III} as indicated previous results mentioned above. These results evidenced that biosorption of Eu^{III} as the main interaction mechanism with the cells of *S. bentonitica*. However, the presence of few extracellular and intracellular Eu^{III} precipitates indicated the interaction is not only mediated by biosorption and other processes such as bioaccumulation and bioprecipitation could be involved. This matches very well with the kinetics studies suggesting the implication of other interaction mechanisms.

The formation of outer membrane vesicles (OMVs) by *S. bentonitica cells* exposed to Eu^{III} was observed in the STEM-HAADF micrographs (Figure 6C-D). The production of OMVs by Gram-negative bacteria plays a prominent role in cell protection against hostile environments (Jan, 2017; Toyofuku et al., 2019). The production of OMVs represents a mechanism to alleviate stress through the packaging and release of stress-products (Klimentová and Stulík, 2015). Therefore, the vesicle formation mechanism of *S. bentonitica* cells could be involved in their Eu^{III} tolerance. In addition, the detection of extracellular precipitates could be a consequence of the release of intracellular accumulates through the formation of vesicles. However, further investigations are needed to confirm this hypothesis. To the best of our knowledge, this study provide for the first time the formation of vesicles by Gram-negative

bacteria in response to Eu^{III} stress. Our previous studies of *S. bentonitica* exposed to toxic selenite suggested a different mechanism for the release of intracellular accumulated selenium to the extracellular space since vesicles were not observed (Ruiz-Fresneda et al., 2018). This point out the versatility of this bacterium to response against different stress agents. The vesicle formation hyphotesis togheter with the low amount of Eu found intracelularly, discarded intracellular accumulation as a relevant mechanisms with a significant impact on the geodisposal security.

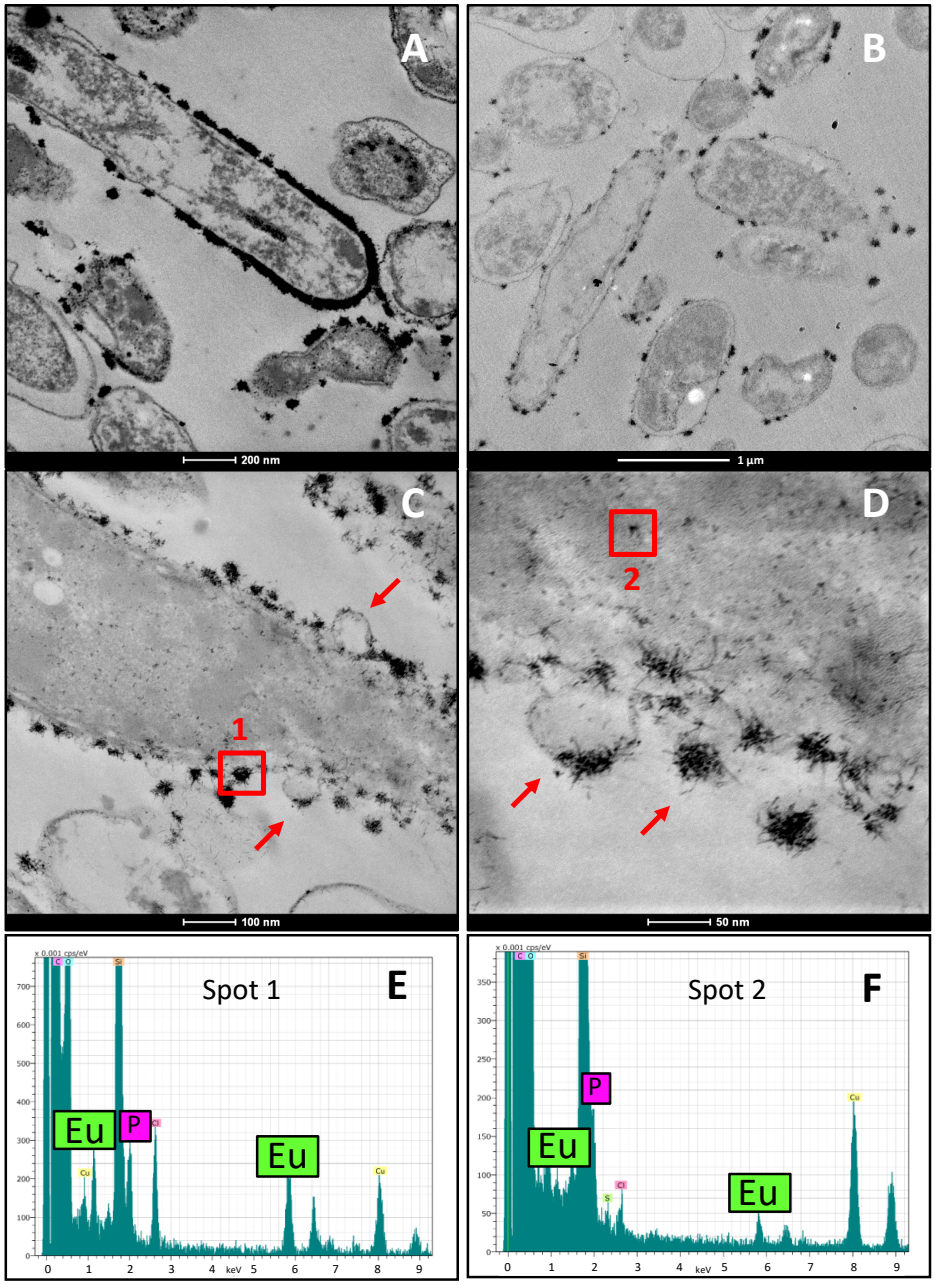

Figure 6. STEM-HAADF micrographs showing electron-dense accumulations at the cell surface, extracellular, and intracellularly under aerobic and anaerobic conditions (A-D). EDX analysis (E-F) confirmed the Eu^{III} and P composition of the accumulations. The formation of vesicles by *S. bentonitica* cells can also be observed (arrows) (C-D). Scale bars: 200 nm (A), 1µm (B), 100 nm (C), 50 nm (D).

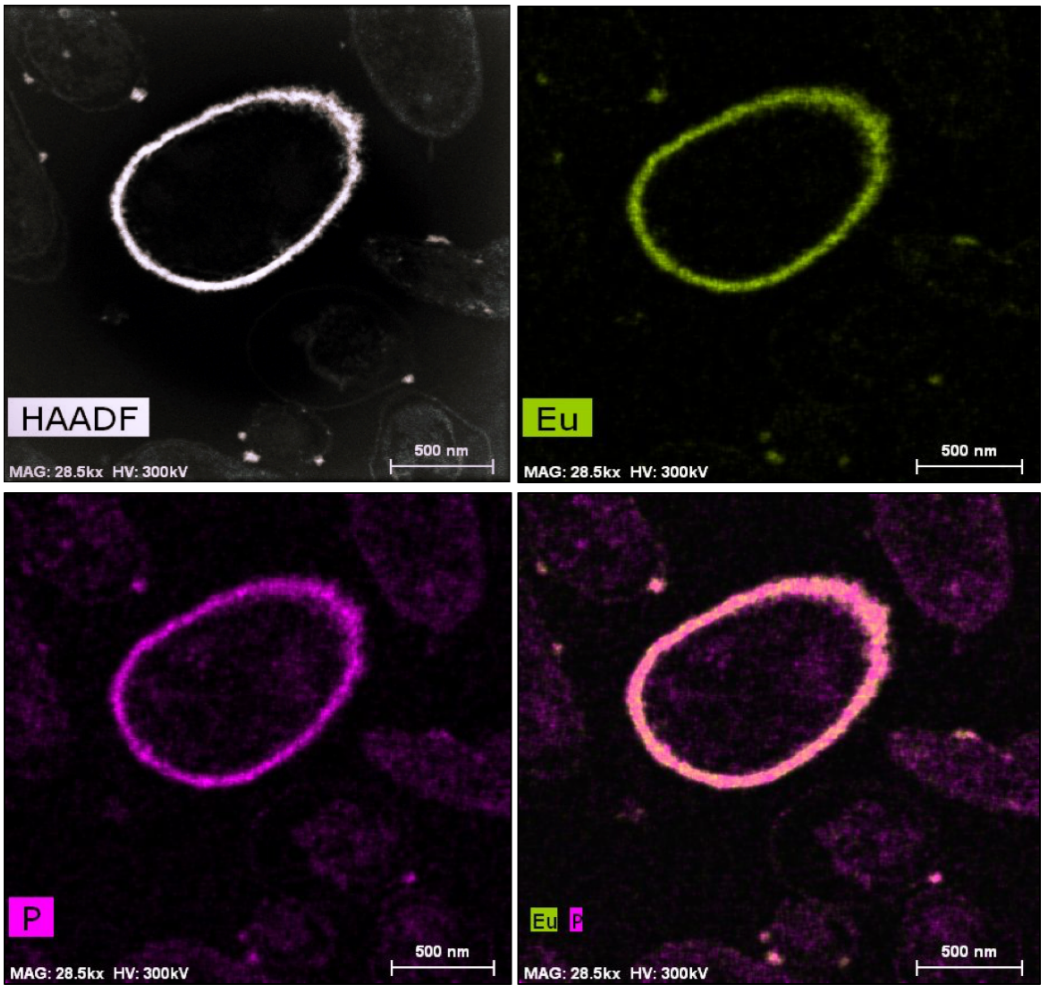

Figure 7. STEM-HAADF micrographs of thin sections clearly showing the adsorption of Eu^{III} on a *S. bentonitica* cell after 48 h growing aerobically on Eu^{III} 30 µM. Scale bars: 500 nm.

Microbial processes such as biosorption may enable the metal removal from contaminated aqueous solutions through the immobilization of bacterial biomass to inert supports (Gadd, 2004). The use of these devices in bioreactors is nowadays receiving attention for bioremediation purposes. The immobilization of microorganisms in minerals from bentonites and other materials through the formation of biofilms could lead in turn to the immobilization of bioadsorbed or bioaccumulated radionuclides. Genes coding for the formation of biofilms such as those involved in the formation of surface structures (*flhA, flhB, fliR, fliQ, fliP, fliN, fliM*) (Niba et al., 2007) or those encoding outer-membrane lipoproteins (*slp*) (Prigent-Combaret et al., 1999) have been reported to be present in the genome of *S. bentonitica* (Sánchez-Castro et al., 2017b; GenBank accession number MKCZ00000000). In addition, the production of flagella-like proteins by this bacterium, previously reported to influence the selenium nanoparticle transformation through their aggregation (Ruiz-Fresneda et al., 2018; Capítulo II; Capítulo III), could be involved in the formation of biofilms. Clark et al. (2007) demonstrated the role of flagella-like filaments produced by *Desulfovibrio vulgaris* in the establishment and

maintenance of biofilms between cells and silica oxide surfaces. Therefore, *S. bentonitica* could positively influence the safety of repositories by inducing the immobilization of radionuclides through the formation of biofilms. However, in the geodisposal context, biosorption could also lead to the mobilization of radionuclides since bacterial cells could disperse through groundwater. After biosorption, a long-term bioprecipitation process could be involved as suggested by kinetic studies and the extracellular Eu precipitates observed by STEM-HAADF. Bioprecipitation basically leads to the inmobilization of radionuclides since it is based on the conversion from soluble to insoluble forms though their precipitation with released cell ligands (carbonates, phosphates, etc.) (Rui et al., 2013; Shukla et al., 2017). Cell viability and metabolic activity of *S. bentonitica* cells under aerobic conditions are not very affected by Eu^{III} as indicated flow cytometry technique. In the presence of Eu^{III}, approximately 99 and 98 % of the cells were viable and active, repectively, similarly to those growing in the absence of Eu^{III} (data not showed). This would allow the cells to release inorganic phosphate probably involved in the Eu^{III} bioprecipitation process due to their previously reported phosphatase activity (Sánchez-Castro et al., 2017a; Sánchez-Castro et al., 2017b). However, the study of the local structure by means of X-ray absorption spectroscopy (XAS) is needed to confirm this hypothesis.

5. Conclusions

The present work demonstrated the interaction of Eu^{III}/Cm^{III} with functional groups from the cell surface and extracellular released complexing agents of *S. bentonitica* under aerobic and anaerobic conditions expected in future DGRs of radioactive waste. Carboxyl and phosphoryl groups seem to be involved in the Eu^{III}/Cm^{III} interaction as revealed a combination of several spectroscopic techniques and potentiometric titration. ATR-FTIR suggested carboxyl groups to form bidentate bridging complexes with Eu^{III}. Additionally, XPS analysis showed these groups from organic acids like acetate to be probably involved in the Eu^{III} complexation. The formed Eu^{III} complexes were mainly located at the cell surface as indicated microscopic analysis, indicating biosorption as the main interaction process. However, the presence of a few intracellular and extracellular Eu^{III} precipitates suggested that other mechanisms could be implicated such as bioaccumulation or bioprecipitation. The biphasic behaviour observed by kinetics studies agrees with the possible role of more than one mechanism. Definitely, the results here presented proposed *S. bentonitica* to play an important role in the immobilization of trivalent actinides through their biosorption and the potential ability of the cells to form biofilms within the DGR system. In addition, a possible bioprecipitation process carried out by the cells of *S. bentonitica* would lead to the immobilization of the present actinides. However, the low amount of intracellular Eu^{III} precipitates, discarded intracellular accumulation as a relevant mechanism with a significant impact in the repositories. In any case, it is difficult to determine

the influence of *S. bentonitica* since several interaction mechanisms with Eu^{III}/Cm^{III} seem to be involved and more evidences are necessary to demonstrate its specific role on the security of geodisposal system of nuclear waste. Although the exact mechanisms are unclear, the fact that S. *bentonitica* will impact the long-term safety case of these repositories is undoubtedly evident.

6. Conflicts of interest

The authors declare no competing financial interest.

7. Acknowledgements

This work was supported by Euratom research and training programme 2014-2018 under grant agreement no. 661880. Part of this work was co-financed by the European Radioecology Alliance mobility grant awarded to MAR-F. The authors acknowledge the assistance of Maria del Mar Abad Ortega and Concepción Hernández Castillo (Centro de Instrumentación Científica, University of Granada, Spain) for their help with microscopy measurements, and Dr James McGettrick (Swansea University, College of Engineering) for the help with the XPS measurements.

8. Supplementary material

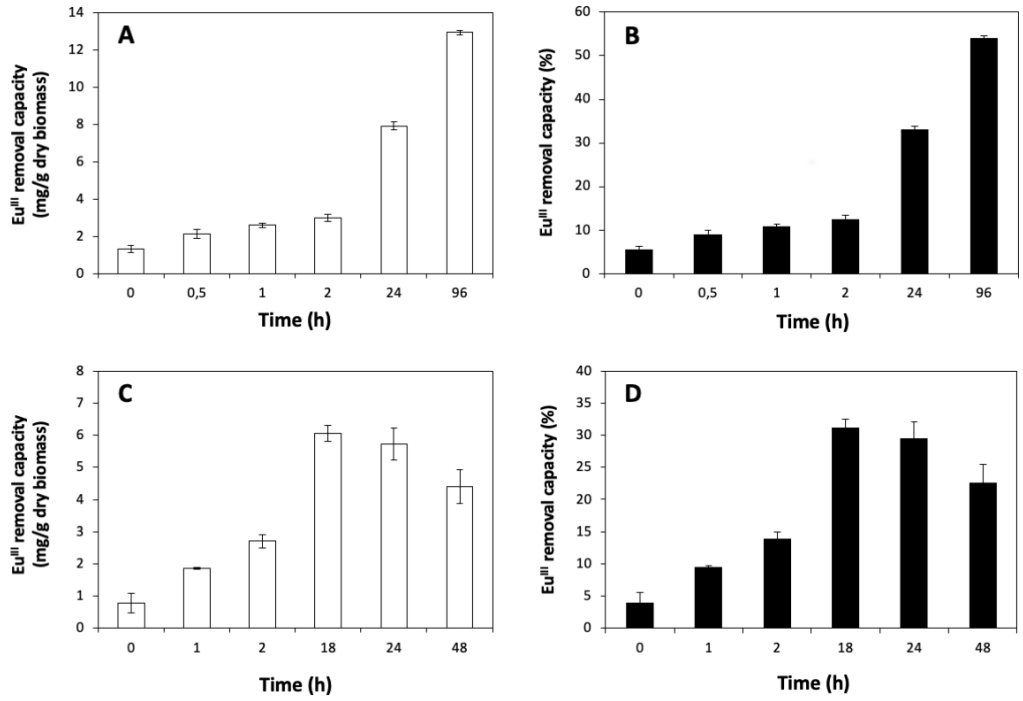

Figure S1. Time dependence in the Eu^{III} removal capacity of *S. bentonitica* cells under aerobic (A and B) and anaerobic (C and D) conditions. The Eu^{III} removal is expressed as mg of Eu per g of dry biomass and percentage.

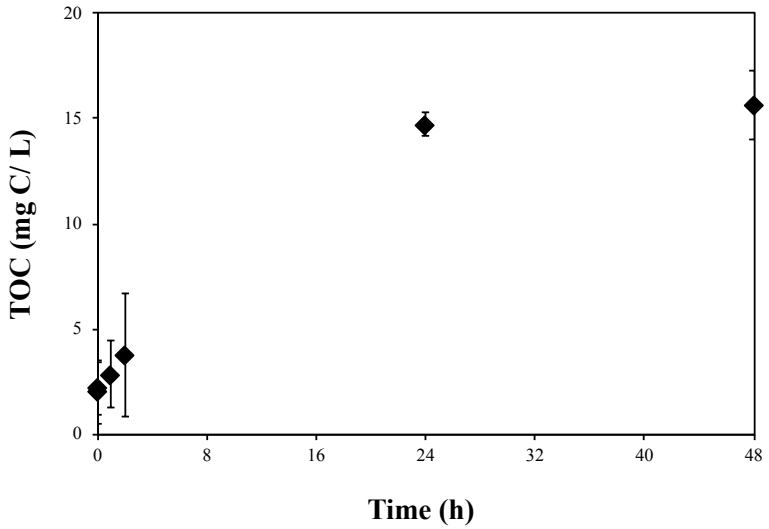

Figure S2. Total organic carbon as a function of time of supernatants obtained after Eu^{III}-*S. bentonitica* interaction under anaerobic conditions.

Table S1. Main infrared absorption bands of the bacterial cell functional groups (Conley, 1972; Dittrich and Sibler, 2005; Jiang et al., 2004; Ojeda et al., 2008; Schmitt and Flemming, 1998; Yee et al., 2004).

Wavenumber (cm^{-1})	Functional group assignment
1745	Stretching C=O of ester functional groups from membrane lipids and fatty acids; stretching C=O of carboxylic acids.
1635	Stretching C=O in amides (amide I band)
1531	N-H bending and C-N stretching in amides (amide II band). Asymmetric stretching for deprotonated COO^- groups.
1404	Symmetric stretching for deprotonated COO^- group.
1455	Bending CH_2/CH_3 (scissoring)
1308	Bending CH_2/CH_3
1300-1250	Vibrations of C-O from esters or carboxylic acids
1240	Vibrations of -COOH and C-O-H; Double bond stretching of >P=O of general phosphoryl groups and phosphodiester of nucleic acids.
1225	Stretching of P=O in phosphates.
1200-950	Asymmetric and symmetric stretching of PO_2^- and $P(OH)_2$ in phosphates; vibrations of C-OH, C-O-C and C-C of polysaccharides.
1070	Stretching P=O of phosphodiester, phosphorilated proteins or polyphosphate products.
933	Symmetric stretching vibration of phosphoryl groups.

DISCUSIÓN GENERAL

Hoy día es bien conocida la elevada diversidad microbiana existente en los diferentes componentes del sistema de almacenamiento geológico profundo (AGP) de residuos radiactivos, tales como la formación geológica hospedante y los materiales de sellado (ej. bentonitas) (Bachran et al., 2018; Itävaara et al., 2011; López-Fernández et al., 2015). Esta biodiversidad puede proceder tanto de las comunidades microbianas autóctonas presentes como de las introducidas durante la construcción, operación y mantenimiento de los AGPs. Los procesos microbianos llevados a cabo por estas comunidades pueden ejercer un notable impacto sobre la seguridad de los AGPs mediante: i) biocorrosión de contenedores metálicos, ii) producción de gases, iii) transformación de minerales de bentonita y iv) movilización o inmovilización de los radionúclidos presentes en los residuos radiactivos. La producción microbiana de gases (H_2, CO_2, CH_4) por parte de microorganismos metanógenos y sulfato-reductores, entre otros, podría afectar gravemente la integridad de las barreras mediante el aumento de la presión, así como dar lugar a la corrosión de los contenedores que protegen los residuos mediante la formación de H_2S (Bagnoud et al., 2016a; 2016b). Por otro lado, es bien sabido el efecto que pueden ejercer determinados microorganismos sobre la solubilidad, y por tanto sobre la movilidad, de los radionúclidos a través de procesos como bioacumulación intracelular, biotransformación, biosorción, biomineralización o quelación (Shukla et al., 2017). Estos procesos podrían ser beneficiosos o perjudiciales para la seguridad de los AGPs, según tenga lugar la movilización o la inmovilización del radionúclido en cuestión. Sin embargo, hasta la fecha, no son muchos los estudios realizados acerca del posible impacto de microorganismos aislados de materiales de referencia para los AGPs sobre la movilización de radionúclidos característicos de residuos radiactivos.

En esta tesis doctoral se estudió por primera vez la influencia que ejerce la cepa bacteriana *Stenotrophomonas bentonitica* BII-R7 sobre la movilidad de elementos característicos de residuos radiactivos como el selenio (Se) y el curio (Cm), y de representantes de actínidos trivalentes (An^{III}) como el europio (Eu), simulando las condiciones presentes en los AGPs. Para ello se empleó una metodología multidisciplinar que consistió principalmente en el uso de técnicas espectroscópicas, microscópicas, microbiológicas, radioquímicas y de química húmeda.

La caracterización a nivel molecular, fisiológico y bioquímico de la cepa de estudio permitió su clasificación como nueva especie bacteriana dentro del género *Stenotrophomonas*. El nombre *Stenotrophomonas bentonitica* BII-R7 fue finalmente escogido en referencia al tipo de arcilla de dónde fue aislada. La identificación en el genoma de la cepa de estudio de genes que codifican

para enzimas implicadas en la interacción con elementos característicos de residuos radiactivos, tales como el Se (ej. glutatión reductasa, tiorredoxina reductasa, etc.), y algunos actínidos como el uranio (U) (ej. fosfatasas), indicó su enorme potencial de interacción con los mismos (Sánchez-Castro et al., 2017b). De hecho, estudios previos realizados mostraron la capacidad de *S. bentonitica* para tolerar concentraciones de U de hasta 6 mM (López-Fernández et al., 2014). Se han descrito otras especies dentro del género *Stenotrophomonas* por su capacidad para interaccionar con metales pesados y otros elementos tóxicos, afectando a su especiación química y por tanto a su solubilidad y movilidad por el medio ambiente. Por ejemplo, la cepa *S. maltophilia* Sm777 tolera una amplia gama de elementos conocidos por su peligrosidad para el medio ambiente como son el selenio, el cadmio, el telurio, el cobre, la plata, el uranio y el plomo, entre otros (Pages et al., 2008). Otra cepa dentro de esta especie, *S. maltophilia* SeITE02, presenta una elevada resistencia al selenito (Se^{IV}) a través de su reducción a selenio elemental (Se^{0}) de menor movilidad (Lampis et al., 2017). Por todo lo citado anteriormente, se estudió la influencia ejercida por *S. bentonitica* sobre la movilidad de Se, Cm y Eu utilizando condiciones semejantes a las que tendrán lugar en los futuros AGPs.

Los primeros estudios demostraron la capacidad de *S. bentonitica* de reducir Se^{IV} a Se^{0} bajo condiciones aerobias y a temperatura ambiente, tal y como reflejó la producción de precipitados de color rojizo en los cultivos. Esta bioreducción es posible gracias a los elevados niveles de tolerancia al Se^{IV} que presentó la cepa de estudio, siendo 400 mM la concentración mínima inhibitoria (CMI). Estos resultados indicaron una resistencia al Se^{IV} muy elevada en comparación con otras especies bacterianas dentro del género *Stenotrophomonas*, como *S. maltophilia* SeITE02 y *S. maltophilia* Sm777, capaces de tolerar Se^{IV} hasta una concentración de 50 mM (Di Gregorio et al., 2005; Pages et al., 2008). El crecimiento bacteriano de *S. bentonitica* en presencia de Se^{IV} presentó una prolongación en la fase de adaptación de unas 48 horas, cuando alrededor del 50% del Se^{IV} estaba presente en solución. Este hecho sugirió que durante este periodo probablemente se lleva a cabo una expresión diferencial de genes que codifican para enzimas implicadas en la tolerancia al Se^{IV}. Después de la fase de adaptación, el crecimiento se vio negativamente afectado en comparación con cultivos bacterianos en ausencia de Se^{IV}. El crecimiento óptimo de los cultivos tratados con Se^{IV} (0.1-2 mM) se alcanzó una vez el 100% de Se^{IV} ha sido reducido, tal y como reflejaron los resultados obtenidos mediante cromatografía líquida (HPLC-*high-performance liquid chromatography*) acoplada a espectrometría de masas (ICP-MS- *inductively coupled plasm-mass spectometry*). Se trata, por tanto, de un proceso tremendamente eficaz con unos porcentajes de eliminación superiores a los de otras bacterias como *S. maltophilia* SeITE02, la cual reduce el 86% de Se^{IV} presente tras 192 horas de incubación con una concentración inicial de 2 mM de Se^{IV} (Lampis et al., 2017). De la misma forma que el crecimiento bacteriano, la viabilidad y la actividad metabólica se vieron

afectadas negativamente tal y como indicaron los resultados de citometría de flujo. A pesar de ello, las células de *S. bentonitica* se mantuvieron viables y activas en presencia de Se^{IV}.

El Se^{0} producido como consecuencia de la reducción se acumuló en forma de nanopartículas. Mediante el uso de microscopia electrónica y de varias técnicas espectroscópicas, se observó que estas nanopartículas presentaron diferentes morfologías (esferas, hexágonos, polígonos y nanofibras/nanohilos-del inglés *nanowires*) y propiedades cristalinas (amorfas y trigonales). La producción de nanoesferas de Se como consecuencia de la actividad reductora bacteriana a temperatura ambiente se ha estudiado previamente en numerosas cepas bacterianas como *Rhodopseudomonas palustris* N, *S. maltophilia*, *Methylococcus capsulatus*, o *Methylosinus trichosporium* OB3b (Dungan et al., 2003; Eswayah et al., 2017; Lampis et al., 2017; Li et al., 2014b). Sin embargo, la formación biológica de estructuras cristalinas en forma de *nanowires*, hexágonos o polígonos no se ha descrito en amplitud. Por lo que sabemos, tan sólo los estudios de Wang et al. (2010) demostraron la producción de nanoesferas y *nanowires* de Se a temperatura ambiente por la bacteria *Bacillus subtilis*. Más comúnmente si se ha observado la formación de cristales de Se (*nanowires*, hexágonos) través de procesos químicos que incluyen elevadas temperaturas (Chen et al., 2010; Ho et al., 2010). Es bien sabido que, desde un punto de vista termodinámico, las altas temperaturas pueden dar lugar a la formación de cristales de Se a partir de Se de naturaleza amorfa (Minaev et al., 2005). Por ello, este estudio proporciona un método sencillo, barato y respetuoso con el medio ambiente para la formación de nanopartículas de selenio (SeNPs) tanto cristalinas como amorfas, conocidas por su uso en numerosas aplicaciones tanto médicas como industriales (Wadhwani et al., 2016).

Durante las primeras 24 horas de incubación tiene lugar la producción, mayoritariamente a nivel intracelular, de nanopartículas esféricas de naturaleza amorfa (a-Se) por parte de las células de *S. bentonitica*. Tras 48-72 horas estas nanoesferas son liberadas por las células a nivel extracelular, probablemente a través de procesos de lisis celular, donde se empiezan a acumular formando grandes agregados. El análisis con espectroscopia de Raman de estos agregados sugirieron que un proceso de cristalización tiene lugar en los mismos, al detectarse la presencia de estructuras cristalinas. Finalmente, tras 144 horas de incubación, diferentes tipos de SeNPs cristalinas se empezaron a observar. El análisis estructural de estos cristales se realizó mediante una combinación de técnicas como difracción de rayos X (XRD-*X-ray diffraction*), espectroscopia de Raman, transformada rápida de Fourier (FFT-*Fast Fourier Transform*) y difracción de electrones (SAED-*selected-area electron diffraction*), los cuales indicaron su estructura trigonal (t-Se). Estas nanoestructuras cristalinas se observaron formando hexágonos, estructuras poligonales y *nanowires*. Es bien sabido que la forma de las nanoestructuras afecta a su estabilidad coloidal y a su carga superficial, lo que a su vez influye a su movilidad. Jain et al.

(2017) demostraron la menor estabilidad coloidal y movilidad de *nanowires* de Se en comparación con nanoesferas de Se, ambos producidos biológicamente por lodos granulares anaeróbicos. Además, se ha descrito con anterioridad que la cristalización de SeNPs aumenta su sedimentación, y por tanto, su inmovilización a través del ambiente (Lenz et al., 2009). Por todo lo citado anteriormente, la formación de *nanowires* cristalinos de t-Se por las células de *S. bentonitica* podría ser beneficiosa en cuanto a la seguridad de los AGPs de residuos radiactivos debido a su bajo grado de movilidad.

Estos resultados sugirieron que un proceso de transformación desde nanoesferas de Se amorfas a estructuras de Se cristalinas (trigonales) con respecto del tiempo tiene lugar. Wang et al. (2010) indicaron previamente un mecanismo de transformación de nanoesferas de Se monoclínico (m-Se) a *nanowires* de t-Se dependiente del tiempo por la bacteria *B. subtillis*. Según ellos, las proteínas celulares sintetizadas por esta bacteria juegan un papel crucial durante este proceso. Además de intervenir en la captura y reducción de los iones de Se^{IV}, las proteínas excretadas por *B. subtilis* parecen servir como punto de anclaje, permitiendo la acumulación y agregación de las nanopartículas producidas. Esta agregación podría ser una fase esencial para la formación de *nanowires* de t-Se según el modelo presentado por Wang et al. (2010). Mediante microscopia electrónica se observó que las SeNPs producidas por *S. bentonitica* se encuentran envueltas en una matriz de materia orgánica e incluso parecen acumularse en torno a unos filamentos que podrían tratarse de proteínas tipo flagelo. Estos hechos sugieren el posible rol de la materia orgánica, incluyendo proteínas y filamentos tipo flagelo, en la agregación de nanopartículas y por tanto en el proceso de transformación. El análisis mediante espectroscopia infrarroja (ATR-FTIR-*attenuated total reflectance-Fourier transform infrared spectroscopy*) y de fotoelectrones emitidos por rayos X (XPS-*X-ray photoelectron spectroscopy*) de las SeNPs purificadas permitió la detección de altas concentraciones de grupos amino y de aminoácidos, confirmando la presencia de proteínas en la matriz orgánica que las rodea. De forma similar a los estudios de Wang et al. (2010), otros trabajos indicaron la importante función de las proteínas en la nucleación y ensamblado de las SeNPs producidas por las especies bacterianas *Thauera selenatis* y *Bacillus oryziterrae* (Bao et al., 2016; Debieux et al., 2011). En este sentido, la agregación de nanoesferas de Se sintetizadas por *S. bentonitica*, junto con su transformación y cristalización, podrían permitir su inmovilización en los alrededores de los sistemas de almacenamiento de residuos radiactivos. Estudios proteómicos sobre esta interacción selenio-bacteria aportarían gran información sobre los mecanismos implicados en la síntesis y transformación de estas nanopartículas y, finalmente, sobre el efecto que *S. bentonitica* podría tener sobre la movilización de Se en el concepto de los AGPs.

La especiación y la estructura local de las nanopartículas producidas tras la reducción de Se^{IV} se caracterizaron mediante espectroscopia de absorción de rayos X (XAS-*X-ray absorption spectroscopy*). En base a las energías de ionización del electrón K de Se obtenidas en la región XANES (*X-ray absorption near-edge structure*) se identificó el estado de oxidación 0 (Se^0) de los productos de Se reducidos, tal y como sugirió previamente la coloración rojiza de los cultivos bacterianos. Por otra parte, los parámetros estructurales obtenidos en la región EXAFS (*extended X-ray absorption fine-structure*) indicaron la presencia de dos esferas de coordinación con una distancia radial de enlace de 2.34-2.35 ± 0.02 Å, para la primera esfera (Se-Se_1), y de 3.63- 3.70± 0.02 Å, para la segunda (Se-Se_2). Es bien sabido que las distancias de enlace de la esfera Se-Se_1 están íntimamente relacionadas con aspectos estructurales de nanopartículas. Las distancias de enlace de la esfera Se-Se_1 que oscilan entre 2.32-2.34± 0.02 Å corresponden con una estructura de Se amorfa o monoclínica (Minaev et al., 2005; Zhao et al., 1999), mientras que aquellas distancias sobre 2.37 ± 0.02 Å están relacionadas con Se trigonal (Popov, 1976). Por tanto, las distancias de enlace oscilantes entre 2.34-2.35 ± 0.02 obtenidas en nuestras muestras para la esfera Se-Se_1 podría corresponder a una distancia media procedente de las tres estructuras mencionadas (amorfo, monoclínico y trigonal). Esta hipótesis se encuentra apoyada por la presencia de a-Se y t-Se detectados previamente mediante los análisis con microscopia (HAADF/STEM-*high angle annular dark field scanning transmission electron microscopy* y VP-FESEM-*variable pressure field emission scanning electron microscopy*) (Ruiz-Fresneda et al., 2018; Capítulo II; Capítulo III). Las distancias de enlace obtenidas para la esfera Se-Se_2 oscilantes entre 3.63- 3.70± 0.02 Å podrían corresponder a Se cristalino de acuerdo con los estudios de Eswayah et al. (2017), cuyos resultados indicaron la presencia de cristales de Se producidos por las bacterias *M. capsulatus* y *M. Trichosporium* con una distancia de enlace en la esfera Se-Se_2 de 3.69 Å. Por otro lado, Scheinost y Charlet (2008) indicaron que la distancia de enlace 3.67-3.69 Å encontrada en Se reducido por minerales de Mackinawita corresponde a una estructura monoclínica. En definitiva, los resultados obtenidos con EXAFS parecen indicar la presencia de Se amorfo, monoclínico y/o trigonal en las nanoestructuras producidas por *S. bentonitica*. Este hecho, junto con los altos valores obtenidos del factor Debye-Waller (σ^2) en las nanoestructuras producidas a tiempos menores (24 h), en comparación con las producidas tras 72 y 144 h, concuerdan muy bien con el proceso de transformación y cristalización propuesto.

La producción de seleniuros volátiles metilados tales como DMDSe (*dimethyl diselenide*) y DMSeS (*dimethyl selenenyl sulphide*) por *S. bentonitica* proporcionó una nueva vía para la eliminación de Se^{IV} debido a la menor solubilidad y biodisponibilidad de los mismos (Ranjard et al., 2003). Estos resultados confirmaron la transformación del Se reducido por *S. bentonitica* a Se en el estado de oxidación –II. La biometilación es un proceso que implica reacciones de

reducción cuando la forma inicial es Se^{VI}, Se^{IV} o Se^{0} (Eswayah et al., 2016). Tanto la reducción como la biometilación son procesos considerados de detoxificación para los microorganismos, ya que los compuestos de Se metilados son entre 500 y 700 veces menos tóxicos que los oxoaniones de Se (Ranjard et al., 2003). Por este motivo, *S. bentonitica* podría tener una influencia potencialmente positiva sobre la seguridad de los AGPs mediante la conversión del Se tóxico en especies metiladas con una menor solubilidad y toxicidad.

La reducción de Se^{IV} mediada por *S. bentonitica* también se estudió en condiciones anaeróbicas, alcalinas y en presencia de determinados nutrientes y fuentes de electrones con el fin de simular las condiciones que estarán presentes en los sistemas de AGP. La producción de precipitados rojos en los cultivos de *S. bentonitica* revelaron la capacidad de esta bacteria en reducir Se^{IV} a Se^{0} anaeróbicamente. De entre las diferentes fuentes utilizadas como donador y aceptor de electrones, fue en presencia de acetato y nitrato cuando se observaron las mayores tasas de reducción. Bajo estas condiciones también se observó que la reducción de Se^{IV} tiene lugar desde pH neutro hasta pH 10. Estos resultados sugirieron que la reducción de Se^{IV} podría ocurrir en los sistemas de AGP una vez domine un ambiente anaerobio y alcalino tras el cierre de los mismos. Además, la presencia de productos de degradación, nutrientes y fuentes de electrones en estos sistemas (Abrahamsen et al., 2015) podría aumentar la eficiencia de reducción. Sin embargo, estas condiciones fueron realmente desfavorables para las células ya que no se observó crecimiento bacteriano. Los resultados de citometría de flujo indicaron una menor viabilidad y actividad celular en comparación con los datos obtenidos en aerobiosis (Capítulo III), especialmente tras 144 horas de incubación cuando la transformación de las nanoesferas de Se tiene lugar. De forma similar a los experimentos realizados bajo condiciones aerobias, los productos de la reducción de Se se acumularon alrededor de filamentos y materia de origen orgánico en forma de nanoesferas (distribuidas individualmente y formando agregados), *nanowires* y otros tipos de nanoestructuras, tras 144 horas de incubación. La presencia de *nanowires* cristalinos (t-Se), así como de fases termodinámicas de Se intermedias (a-Se y m-Se) de las nanoesferas, confirmaron que tiene lugar un proceso de transformación similar al previamente descrito en Ruiz-Fresneda et al. (2018) (Capítulo II). La menor cantidad de nanoestructuras cristalinas observadas en anaerobiosis y alcalinosis, sugirió que *S. bentonitica* requiere mayores tiempos de incubación para la formación de cristales de Se bajo estas condiciones. Análisis previos realizados mediante HAADF/STEM sobre muestras incubadas en aerobiosis durante 15 y 30 días apoyaron esta hipótesis, al mostrar una mayor cantidad de cristales de Se con el tiempo. Por ello, un proceso de transformación con mayor lentitud parece tener lugar, probablemente debido al menor crecimiento, viabilidad y actividad celular existentes bajo estas condiciones de mayor estrés.

En definitiva, la reducción a Se^0 podría tener una influencia positiva en cuanto a la seguridad de los futuros almacenamientos de residuos, debido a la menor movilidad del Se en este estado de oxidación. Sin embargo, también hay que tener en cuenta la toxicidad según la forma y cristalinidad de los productos de reducción. Benko et al. (2012) demostraron que las nanoesferas de Se son menos tóxicas que los oxoaniones Se^{VI} y Se^{IV}. Otros estudios indicaron que la toxicidad depende de la especie que se utilice como referencia. Por ejemplo, los experimentos llevados a cabo en el pez *Oryzias latipes* parecen indicar la mayor toxicidad de SeNPs en comparación con Se^{IV} (Li et al., 2008). Por ello, estudios en mayor profundidad sobre la movilidad y toxicidad de nanoesferas de Se deben realizarse para determinar el papel de esta bacteria en estos sistemas. Por el contrario, tal y como se ha discutido anteriormente, se ha descrito la menor movilidad de las nanoestructuras de Se cristalinas y en forma de *nanowires* producidas biológicamente (Jain et al., 2017; Lenz et al., 2009). Por esta razón, *S. bentonitica* podría tener una influencia positiva sobre la seguridad de los AGPs.

Además de elementos como el Se, una gran diversidad de An^{III}, como por ejemplo el Cm^{III}, están presentes en los residuos radiactivos. La bacteria de estudio de esta Tesis Doctoral demostró su habilidad para interaccionar con el Cm^{III}, conocido representante de An^{III}, y el Eu^{III}, conocido representante inactivo de An^{III}, mediante una combinación de numerosas técnicas espectroscópicas y microscópicas que proporcionaron uno de los estudios más completos realizados hasta la fecha. Debido a su inactividad y menor peligrosidad, desde un punto de vista radiactivo, el Eu^{III} se utilizó principalmente para la realización de los experimentos, tanto en condiciones aerobias como anaerobias relevantes en el ámbito de los AGPs. Estudios potenciométricos revelaron la presencia de grupos funcionales en la superficie celular de *S. bentonitica* que podrían servir como sitios de unión para el Eu^{III}: grupos carboxilo (pKa 3-5), grupos fosfato (pKa 6-7), grupos hidroxilo y grupos amino (pKa>8). Trabajos anteriores ya indicaron la capacidad de sorción de Eu, Cm, y U por grupos carboxilo y fosfato de superficies celulares bacterianas como *B. subtilis, P. fluorescens, S. putrefaciens* (Haas et al., 2001; Moll et al., 2013; Yao et al., 2016). La concentración de grupos carboxilo, amino e hidroxilo obtenidas mediante el uso de ProtoFit 2.1 fueron similares en presencia y en ausencia de Eu^{III}. Es probable que el proceso de sorción de Eu^{III} por estos grupos sea reversible a pHs bajos o que la cantidad de grupos involucrados en la unión sea demasiado pequeña para ser detectada mediante este método. Sin embargo, la concentración de grupos fosfato fue considerablemente menor en presencia de Eu^{III}. Esto sugirió una fuerte unión del Eu^{III} a los fosfatos de la superficie celular de *S. bentonitica*, haciéndolos inaccesibles a la reacción protonación/desprotonación y por tanto a su medida. La concentración de grupos fosfato en la superficie celular de *S. bentonitica* ($10.78 \pm 0.31 \times 10^{-4}$ mol/g) fue considerablemente mayor que en otras bacterias como *Sphingomonas* sp. S15-S1 ($3.16 \pm 0.56 \times 10^{-4}$ mol/g) y *B. sphaericus* JG-7B ($2.19 \pm 0.25 \times 10^{-4}$ mol/g) (Merroun et

al., 2011). Este hecho destacó la potencial alta capacidad de unión a metales y otros elementos tóxicos de *S. bentonitica*.

La técnica de ATR-FTIR aportó más información sobre la naturaleza de los grupos funcionales bacterianos implicados en la interacción con Eu^{III}. Los espectros de *S. bentonitica* en contacto con Eu^{III} mostraron un desplazamiento en la banda de tensión simétrica correspondiente a grupos carboxilato (1400 cm^{-1} aproximadamente) hacia frecuencias más bajas en comparación con los espectros control de *S. bentonitica* en ausencia de Eu^{III}. Numerosos estudios han establecido una relación empírica entre la posición de las bandas de tensión simétricas y asimétricas de los grupos carboxilato ($\nu_{sym\ COO^-}$, $\nu_{asym\ COO^-}$) y la diferencia de frecuencia entre ellas ($\Delta\nu$) (Chu et al., 2004; Deacon y Phillips, 1980; Nakamoto, 2008; Tackett, 1989). Según estos trabajos, los valores de diferencia de frecuencia ($\Delta\nu$) varían de forma descendente según el tipo de complejo formado de la siguiente manera: $\Delta\nu_{unidentado} > \Delta\nu_{puente} \sim \Delta\nu_{ión\ libre} > \Delta\nu_{quelante\ (bidentado)}$. Tras examinar cuidadosamente los espectros infrarrojos de muchos acetatos con estructuras cristalinas de rayos X conocidas, Chu et al. (2004) y Deacon y Phillips (1980) llegaron a la conclusión de que:

- Para los complejos unidentados, la diferencia de frecuencia es superior a 200 cm^{-1} ($\Delta\nu$ >200 cm^{-1}) y la posición de las bandas de tensión de COO^- simétrico ($\nu_{sym\ COO^-}$) generalmente se desplaza hacia frecuencias menores.

- Para los complejos quelantes bidentados, la diferencia de frecuencia es inferior a 100 cm^{-1} ($\Delta\nu$ <100 cm^{-1}) y la posición de las bandas de tensión de COO^- simétrico ($\nu_{sym\ COO^-}$) y del asimétrico ($\nu_{asym\ COO^-}$) se desplazan hacia frecuencias mayores y menores, respectivamente.

- Para los complejos puente, la diferencia de frecuencia es aproximadamente 160 cm^{-1} ($\Delta\nu$ ~ 160 cm^{-1}) y la posición de las bandas de tensión de COO^- simétrico ($\nu_{sym\ COO^-}$) y del asimétrico ($\nu_{asym\ COO^-}$) pueden desplazarse en cualquier dirección (Chu et al., 2004).

En presencia de Eu^{III}, la tensión asimétrica de los grupos carboxilato ($\nu_{asym\ COO^-}$) no se puede observar por superposición con la banda de las amidas secundarias (Amida II), por lo que es difícil determinar si hay un desplazamiento de esta banda hacia otras frecuencias. Lo que si parece seguro es que no muestra un desplazamiento significativo, ya que sobrepasaría el pico de las amidas II. Por otro lado, en presencia de Eu^{III}, la tensión simétrica de los grupos carboxilato ($\nu_{sym\ COO^-}$) se desplaza unos 15 cm^{-1} hacia frecuencias menores. Todo ello parece indicar que la diferencia de frecuencia entre la tensión simétrica y la asimétrica debe estar sobre los 150 cm^{-1},

sugiriendo que los grupos carboxilo de las macromoléculas presentes en la superficie celular de las células de *S. bentonitica* forman complejos puente con Eu^{III}. Además, la menor intensidad de la banda a 933 cm^{-1} correspondiente a bandas de tensión de O-P-O asimétrico (Dittrich y Sibler, 2005; Jiang et al., 2004; Yee et al., 2004) en los espectros de células expuestas a Eu^{III}, indicó la posible interacción de los grupos fosfato con este elemento. Al igual que las técnicas anteriores, el análisis de la composición elemental a nivel superficial de estas muestras mediante XPS también indicó la presencia de grupos fosfato. Además, el pico correspondiente a Eu_{3d} (1135 eV) fue atribuido a la unión de Eu^{III} con grupos carboxilo procedentes de moléculas orgánicas, tales como acetato (Mercier et al., 2006). Este hecho sugirió el importante papel de los grupos carboxilo de aminos ácidos (ej. ácido glutámico) presentes en las paredes celulares de *S. bentonitica* en la acomplejación de Eu^{III}, tal y como indicaron los resultados obtenidos por Merroun et al. (2005) en la interacción de paladio con la capa S de *B. sphaericus*. En definitiva, los estudios potenciométricos, junto con las técnicas de espectroscopia (ATR-FTIR y XPS) demostraron que los grupos fosfatos y carboxilo presentes en las superficies celulares de *S. bentonitica* parecen intervenir en la complejación de Eu^{III}.

Con el fin de confirmar estos resultados y aportar una caracterización más completa, se utilizó la espectroscopia de fluorescencia (TRLFS-*time-resolved laser-induced fluorescence spectroscopy*). Mediante esta técnica se comparó la complejación de Eu^{III} y de Cm^{III}, como análogo activo de Eu^{III}, por la bacteria *S. bentonitica* en condiciones aerobias y anaerobias relevantes para los sistemas de AGP. Los parámetros obtenidos mediante esta técnica (energía de las bandas de emisión y tiempos de vida de fluorescencia de los complejos formados) indicaron la complejación de Eu^{III}/Cm^{III} con grupos fosforilo y carboxilo de la superficie celular y de sustancias liberadas por la bacteria. De acuerdo con estos resultados, procesos microbianos como la biosorción y la bioprecipitación podrían estar implicados en la interacción. Comparando nuestros resultados con estudios previos, probablemente los complejos formados se encuentren en forma de R-O-PO_3-Eu^{2+} y R-COO-Eu^{2+} (Moll et al., 2014; Texier et al., 2000). Los complejos de Eu^{III} formados por *S. bentonitica* parecen presentar propiedades similares a los complejos R-O-PO_3H-Eu^{2+} observados en las envueltas celulares de la bacteria *Sporomusa* sp. MT-2.99 (Moll et al., 2014) tal y como revelaron los tiempos de vida largos obtenidos. Por otro lado, los sitios de unión caracterizados por los tiempos de vida cortos parecen interaccionar con Eu^{III} de forma semejante a los complejos R-COO-Eu^{2+} observados en la superficie celular de *Sporomusa* sp. MT-2.99 y *P. fluorescence* (Moll et al., 2014). Resultados similares se obtuvieron por López-Fernández et al. (2018b) con la levadura *Rhodotorula mucilaginosa*, capaz de interaccionar con Eu^{III} y Cm^{III} a través de grupos carboxilo y fosfato.

Finalmente, los análisis de microscopia electrónica (HAADF/STEM) revelaron la presencia de acúmulos de Eu^{III} principalmente alrededor de la superficie bacteriana de *S. bentonitica*. En menor medida, los complejos de Eu^{III} formados se localizaron extra e intracelularmente. La detección de fósforo (P) en los precipitados de Eu^{III} coincide con los resultados que indicaron la implicación de los grupos fosfato en la complejación de Eu^{III} y Cm^{III}. Por consiguiente, la interacción de *S. bentonitica* con Eu^{III} ocurre principalmente mediante un proceso de biosorción a través de las superficie bacteriana. Sin embargo, la presencia de acúmulos extra e intracelulares sugirió que otros procesos como la bioacumulacíon o la bioprecipitación podrían estar involucrados. Este hecho concuerda con los estudios cinéticos de adsorción de Eu^{III} por esta bacteria, que también indicaron la posible participación de varios mecanismos de interacción. Las micrografías de HAADF/STEM también mostraron la formación de vesículas de membrana externa en células expuestas a Eu^{III}. Este proceso podría estar implicado en el mecanismo de interacción con este elemento. Algunas bacterias Gram-negativas producen estas vesículas en respuesta a agentes de estrés como mecanismo de protección mediante su acumulación y liberación al espacio extracelular (Jan, 2017; Klimentová y Stulík, 2015; Toyofuku et al., 2019). Por tanto, la presencia de acúmulos de Eu^{III} extracelulares podría ser consecuencia de su liberación desde el interior celular a través de la formación de vesículas. Por lo que sabemos, esta es la primera vez que se describe este mecanismo de formación de vesículas por bacterias Gram-negativas en respuesta a estrés inducido por Eu^{III}. Este proceso es completamente diferente del presentado anteriormente en respuesta al Se^{IV}, donde las nanoesferas de Se reducido localizadas intracelularmente podrían liberarse tras la lisis celular. Este hecho destaca la versatilidad de *S. bentonitica* a la hora de responder frente a diferentes agentes estresantes.

Procesos microbianos como la biosorción pueden dar lugar a la eliminación de metales y compuestos contaminantes de soluciones acuosas a través de la inmovilización de la biomasa microbiana en soportes inertes (Gadd, 2004). De hecho, el uso de estos dispositivos en biorreactores está actualmente adquiriendo una gran atención para fines en biorremediación. La inmovilización de microorganismos a través de la formación de biopelículas en ciertos minerales de las bentonitas u otros materiales presentes podría dar lugar, a su vez, a la inmovilización de radionúclidos bioadsorbidos dentro del marco de los AGPs. Genes implicados en la formación de biopelículas como *flhA, flhB, fliR, fliQ, fliP, fliN, fliM* (involucrados en la formación de estructuras de superficie para la adhesión celular durante la formación de biopelículas) (Niba et al., 2007), y *slp* (codificante para lipoproteínas estructurales de membrana externa relevantes en las fases iniciales de la formación de biopelículas) (Prigent-Combaret et al., 1999) han sido descritos en el genoma de *S. bentonitica* (Sánchez-Castro et al., 2017b; GenBank accession number MKCZ00000000). Como consecuencia de ello, esta cepa

podría influir positivamente en la seguridad de estos almacenamientos. Sin embargo, la biosorción también podría dar lugar a la movilización de radionúclidos, ya que los microorganismos podrían dispersarse a través de aguas subterráneas. Después de la biosorción, un proceso generalmente rápido (Gadd, 2009), procesos de bioprecipitación a largo plazo podrían tener lugar, tal y como sugirieron los resultados obtenidos mediante los estudios cinéticos y los precipitados de Eu extracelulares observados con HAADF/STEM. La bioprecipitación induciría la inmovilización de radionúclidos ya que da lugar a la formación de precipitados insolubles a partir de elementos solubles que precipitan con ligandos liberados por la célula (fosfatos, etc.) (Rui et al., 2013; Shukla et al., 2017). La viabilidad y actividad metabólica de *S. bentonitica* bajo condiciones aeróbicas apenas se vio afectada por la presencia de Eu^{III}, donde prácticamente el 99% de las células se mantuvieron viables y activas. Esto permitiría a las células liberar fosfatos inorgánicos que podrían precipitar con Eu^{III} debido a su actividad fosfatasa previamente descrita (Sánchez-Castro et al., 2017a; Sánchez-Castro et al., 2017b). Sin embargo, el estudio de la estructura local de estos complejos a través de XAS sería necesario para confirmar la bioprecipitación. Por todo lo indicado anteriormente, *S. bentonitica* podría afectar positivamente la seguridad de los futuros almacenamientos mediante la inmovilización de An^{III} a través de su biosorción y de su potencial habilidad para formar biopelículas dentro del sistema de AGP. Por otro lado, la bioprecipitación de actínidos presentes en los alrededores de los AGPs podría conducir a su inmovilización, afectando positivamente a la seguridad de los mismos. Finalmente, la poca cantidad de precipitados de Eu intracelulares, descarta la bioacumulación como un proceso con un impacto significativo en la seguridad de los AGPs. En cualquier caso, es difícil determinar la influencia de *S. bentonitica*, ya que diferentes mecanismos de interacción con Cm^{III} y Eu^{III} podrían llevarse a cabo. En este sentido, serían necesarias más evidencias para demostrar el papel específico que esta bacteria tendrá en la seguridad de los almacenamientos de residuos radiactivos.

CONCLUSIONES

Los resultados obtenidos durante el desarrollo de esta Tesis Doctoral nos permiten establecer las siguientes conclusiones:

1. Los análisis moleculares y fenotípicos confirmaron de manera inequívoca que la cepa de estudio de esta Tesis Doctoral (*Stenotrophomonas* sp. BII-R7) representa una nueva especie bacteriana dentro del género *Stenotrophomonas*, para la cual el nombre *Stenotrophomonas bentonitica* fue propuesto.

2. *S. bentonitica* es capaz de reducir Se^{IV} a Se^{0} bajo condiciones aerobias, anaerobias y alcalinas de relevancia en los futuros sistemas de almacenamiento de residuos radiactivos dando lugar a la formación de nanopartículas de Se con diferente morfología (esferas, hexágonos, polígonos y nanofibras/nanohilos) y estructura (amorfa y cristalina).

3. Un proceso de transformación dependiente del tiempo desde nanoesferas de Se amorfo (a-Se) a nanoestructuras de Se trigonal (t-Se) cristalino, mediante la formación de Se monoclínico (m-Se) cristalino como fase intermedia, parece tener lugar. Esta transformación sucede más lentamente bajo un ambiente anóxico y alcalino en comparación con un ambiente aeróbico, probablemente debido a la menor proliferación celular, viabilidad y actividad metabólica de *S. bentónica* ante estas condiciones de mayor estrés.

4. El material proteico que envuelve las nanopartículas de Se, junto con los filamentos proteicos tipo flagelo característicos de este género bacteriano, parecen tener un papel primordial en el proceso de transformación al permitir la agregación de las nanoesferas.

5. La producción de compuestos volátiles metilados de Se (DMDSe y DMSeS) por las células de *S. bentonitica* reveló la volatilización como otro de los mecanismos implicados en la interacción con Se.

6. Los resultados obtenidos sobre las interacciones con Se sugieren una potencial influencia positiva de las células de *S. bentonitica* sobre la seguridad de los almacenamiento de residuos radiactivos, debido a la conocida menor movilidad y toxicidad de los productos de reducción de Se obtenidos.

7. La combinación de una amplia variedad de técnicas espectroscópicas (TRLFS, XPS, FTIR, etc.) demostró la interacción de *S. bentonitica* con Eu^{III} y Cm^{III} mediante un proceso de biosorción. Los grupos carboxilo y fosforilo presentes en las superficies celulares y en agentes acomplejantes liberados al medio extracelular parecen intervenir en la interacción, probablemente en forma de complejos $R\text{-}COO\text{-}Eu^{2+}$ y $R\text{-}O\text{-}PO_3\text{-}Eu^{2+}$.

8. La presencia de precipitados de Eu^{III} observados mediante microscopia (STEM-HAADF) tanto a nivel de superficie como extracelular e intracelularmente sugirió que otros mecanismos de interacción, además de la biosorción, como la bioacumulación y la bioprecipitación podrían estar involucrados.

9. Los resultados obtenidos sobre las interacciones con Eu^{III} y Cm^{III} sugieren el potencial efecto positivo de *S. bentonitica* sobre la seguridad de los futuros almacenamientos de residuos radiactivos mediante la inmovilización de actínidos trivalentes, principalmente a través de su biosorción y posible bioprecipitación.

CONCLUSIONS

The results obtained in the present Doctoral Thesis allow us to establish the following conclusions:

1. The molecular and phenotypic analysis confirmed unequivocally that the strain of study of this Doctoral Thesis (*Stenotrophomonas* sp. BII-R7) represents a new bacterial species within the genus *Stenotrophomonas*, for which the name *Stenotrophomonas bentonitica* was proposed.

2. *S. bentonitica* is able to reduce Se^{IV} to Se^{0} under aerobic, anaerobic, and alkaline conditions of relevance in the future repository system of radioactive wastes, producing Se nanoparticles with different morphology (nanospheres, hexagons, polygons, and nanowires)) and structure (amorphous and crystalline).

3. A time-dependent transformation process of amorphous Se (a-Se) nanospheres to crystalline trigonal Se (t-Se) nanostructures through the formation of monoclinic Se (m-Se) as intermediate phase seem to occur. This transformation is slower under anoxic and alkaline environments comparing with aerobic conditions, probably due to the lower cellular proliferation, viability, and activity of *S. bentonitica* under these more stressful conditions.

4. The protein material capping the Se nanoparticles and flagella-like proteins characteristic of this bacterial genus, seem to play an important role in the transformation process enabling the aggregation of the nanospheres.

5. The production of volatile methylated compounds of Se (DMDSe y DMSeS) by the cells of *S. bentonitica* pointed out volatilization as another of the mechanisms involved in the interaction with Se.

6. The results obtained on the interactions with Se suggest a potential positive impact of *S. bentonitica* cells on the safety of the repository system of radioactive waste, due to the well-known lower mobility and toxicity of the Se reduction products.

7. The combination of a wide variety of spectroscopic techniques (TRLFS, XPS, FTIR, etc.) demonstrated the interaction of *S. bentonitica* with Eu^{III} y Cm^{III} through a biosorption process. Carboxyl and phosphoryl groups from cell envelopes and complexing agents released to the

extracellular matrix seem to play an important role in the interaction most probably in the form of R-COO-Eu^{2+} and R-O-PO_3-Eu^{2+} complexes.

8. The presence of Eu^{III} precipitates observed extracellularly, intracellularly, and attached to the cell surface by microscopy (STEM-HAADF) suggested that other interaction mechanisms, in addition to biosorption, such as bioaccumulation and bioprecipitation, could be involved.

9. The results obtained on the interactions with Eu^{III} y Cm^{III} suggested the potential positive effect of *S. bentonitica* on the safety of future repositories of radioactive waste by the immobilization of trivalent actinides, mainly through their biosorption and possible bioprecipitation.

REFERENCIAS

Abrahamsen, L., Arnold, T., Brinkmann, H., Leys, N., Merroun, M., Mijnendonckx, K., Moll, H., Polvika, P., Sevcu, J., Small, J., Vikman, M., Wouters, K., 2015. A review of anthropogenic organic wastes and their degradation behaviour. Microbiology In Nuclear waste Disposal (MIND Proj). Available from: https://igdtp.eu/wp-content/uploads/2017/10/MIND-2015-12-D1.1-ReviewOfAnthropogenicOrganicWastes.pdf

Ahonen, L., Pedersen, K., Small, J., Mijnendonckx, K., Weetjens, E., Wouters, K., 2016. Year One Evaluation Report. Microbiology In Nuclear waste Disposal (MIND Proj). Available from:http://www.mind15.eu/wp-content/uploads/2015/11/MIND-Deliverable-3.1-Y1-Evaluation.pdf

Albino, V., Ardito, L., Dangelico, R.M., Messeni Petruzzelli, A., 2014. Understanding the development trends of low-carbon energy technologies: A patent analysis. Appl. Energy. 135, 836-854. https://doi.org/10.1016/j.apenergy.2014.08.012

Alonso, J., Becker, D.A., Storck, R., Besnus, F., Pellegrini, D., Serres, C., Johnson, L., Hart, J., Marivoet, J., Vieno, T., Nordman, H., Petkovsek, B., 2004. Bentonite barriers in integrated performance assessment (Benipa). European Commission, Nuclear Science and Technology, Report EUR 21023 EN. Available from: http://elibrary.cenn.org/Report/Bentonite%20Barries%20in%20Integrated%20Performance%20Assessment%20Benipa/Part_2.pdf

Altenburgera, P., Kämpfer, P., Makristathis, A., Lubitz, W., Busse, H.J., 1996. Classification of bacteria isolated from a medieval wall painting. J. Biotechnol. 47 (1), 39-52. https://doi.org/10.1016/0168-1656(96)01376-4

Altmann, S., 2008. 'Geo'chemical research: A key building block for nuclear waste disposal safety cases. J. Contam. Hydrol. 102 (3-4), 174–179. https://doi.org/10.1016/j.jconhyd.2008.09.012

Ankudinov, A., Ravel, B., 1998. Real-space multiple-scattering calculation and interpretation of x-ray-absorption near-edge structure. Phys. Rev. B - Condens. Matter Mater. Phys. 58 (12-15), 7565–7576. https://doi.org/10.1103/PhysRevB.58.7565

Ansoborlo, E., Bion, L., Doizi, D., Moulin, C., Lourenco, V., Madic, C., Cote, G., Van der Lee, J., Moulin, V., 2007. Current and future radionuclide speciation studies in biological media. Radiat. Prot. Dosimetry 127 (1-4), 97–102. https://doi.org/10.1093/rpd/ncm258

Antonioli, P., Lampis, S., Chesini, I., Vallini, G., Rinalducci, S., Zolla, L., Righetti, P.G., 2007. *Stenotrophomonas maltophilia* SeITE02, a new bacterial strain suitable for bioremediation of selenite-contaminated environmental matrices. Appl. Environ. Microbiol. 73 (21), 6854–63. https://doi.org/10.1128/AEM.00957-07

Anzai, Y., Kim, H., Park, J.Y., Wakabayashi, H., Oyaizu, H., 2000. Phylogenetic affiliation of the *Pseudomonas* based on 16S rRNA sequence. Int. J. Syst. Evol. Microbiol. 50 (Pt 4), 1563-1589. https://doi.org/10.1099/00207713-50-4-1563

Assih, E.A., Ouattara, A.S., Thierry, S., Cayol, J.L., Labat, M., Macarie, H., 2002. *Stenotrophomonas acidaminiphila* sp. nov., a strictly aerobic bacterium isolated from an upflow anaerobic sludge blanket (UASB) reactor. Int. J. Syst. Evol. 52 (Pt 2), 559-568. Microbiol. https://doi.org/10.1099/00207713-52-2-559

Atwood D.A., (ed.), 2010. Radionuclides in the Environment (EIC Books). Weinheim: WILEY, 2913. Available from: https://www.wiley.com/en-us/Radionuclides+in+the+Environment-p-9781118632697

Auling, G., Busse, H.-J., Pilz, F., Webb, L., Kneifel, H., Claus, D., 1991. Rapid Differentiation, by Polyamine Analysis, of *Xanthomonas* Strains from Phytopathogenic *Pseudomonas* and Other Members of the Class Proteobacteria Interacting with Plants. Int. J. Syst. Bacteriol. 41, 223–228. https://doi.org/10.1099/00207713-41-2-223

Ayangbenro, A.S., Babalola, O.O., 2017. A new strategy for heavy metal polluted environments: A review of microbial biosorbents. 14 (1), 94. Int. J. Environ. Res. Public Health. https://doi.org/10.3390/ijerph14010094

Bachran, M., Kluge, S., López-Fernández, M., Cherkouk, A., 2018. Microbial Diversity in an Arid , Naturally Saline Environment. Microb. Ecol. 1-12. https://doi.org/10.1007/s00248-018-1301-2

Bader, M., Moll, H., Steudtner, R., Lösch, H., Drobot, B., Stumpf, T., Cherkouk, A., 2019. Association of Eu(III) and

Cm(III) onto an extremely halophilic archaeon. Environ. Sci. Pollut. Res. 26 (9), 9352–9364 https://doi.org/10.1007/s11356-019-04165-7

Bagnoud, A., de Bruijn, I., Andersson, A.F., Diomidis, N., Leupin, O.X., Schwyn, B., Bernier-Latmani, R., 2016a. A minimalistic microbial food web in an excavated deep subsurface clay rock. 92(1). FEMS Microbiol. Ecol. https://doi.org/10.1093/femsec/fiv138

Bagnoud, A., Chourey, K., Hettich, R.L., De Bruijn, I., Andersson, A.F., Leupin, O.X., Schwyn, B., Bernier-Latmani, R., 2016b. Reconstructing a hydrogen-driven microbial metabolic network in Opalinus Clay rock, in: Nature Communications. 7, 12770. https://doi.org/10.1038/ncomms12770

Ballantyne, A.P., Alden, C.B., Miller, J.B., Tans, P.P., White, J.W.C., 2012. Increase in observed net carbon dioxide uptake by land and oceans during the past 50 years. Nature. 488, 70-72. https://doi.org/10.1038/nature11299

Bao, P., Xiao, K.Q., Wang, H.J., Xu, H., Xu, P.P., Jia, Y., Häggblom, M.M., Zhu, Y.G., 2016. Characterization and potential applications of a selenium nanoparticle producing and nitrate reducing bacterium *Bacillus oryziterrae* sp. nov. Sci. Rep. 6, 34054. https://doi.org/10.1038/srep34054

Barkleit, A., Moll, H., Bernhard, G., 2009. Complexation of uranium(VI) with peptidoglycan. Dalt. Trans. 0 (27), 5379-5385. https://doi.org/10.1039/b818702a

Basaglia, M., Toffanin, A., Baldan, E., Bottegal, M., Shapleigh, J.P., Casella, S., 2007. Selenite-reducing capacity of the copper-containing nitrite reductase of *Rhizobium sullae*. FEMS Microbiol. Lett. 269 (1), 124–130. https://doi.org/10.1111/j.1574-6968.2006.00617.x

Bassil, N.M., Bryan, N., Lloyd, J.R., 2015. Microbial degradation of isosaccharinic acid at high pH. ISME J. 9 (2), 310-320. https://doi.org/10.1038/ismej.2014.125

Beekes, M., Lasch, P., Naumann, D., 2007. Analytical applications of Fourier transform-infrared (FT-IR) spectroscopy in microbiology and prion research. Vet. Microbiol. 123 (4), 305-319 https://doi.org/10.1016/j.vetmic.2007.04.010

Bengtsson, A., Pedersen, K., 2016. Microbial sulphate-reducing activity over load pressure and density in water saturated Boom Clay. Appl. Clay Sci. 132-133, 542-541. https://doi.org/10.1016/j.clay.2016.08.002

Benko, I., Nagy, G., Tanczos, B., Ungvari, E., Sztrik, A., Eszenyi, P., Prokisch, J., Banfalvi, G., 2012. Subacute toxicity of nano-selenium compared to other selenium species in mice. Environ. Toxicol. Chem. 31 (12), 2812–2820. https://doi.org/10.1002/etc.1995

Berg, G., Ballin, G., 1994. Bacterial Antagonists to *Verticillium dahliae* Kleb. J. Phytopathol. 141 (1), 99-110. https://doi.org/10.1111/j.1439-0434.1994.tb01449.x

Berner, U.R., 1992. Evolution of pore water chemistry during degradation of cement in a radioactive waste repository environment. Waste Manag. 12 (2-3), 201–219. https://doi.org/10.1016/0956-053X(92)90049-O

Bertron, A., Jacquemet, N., Erable, B., Sablayrolles, C., Escadeillas, G., Albrecht, A., 2014. Reactivity of nitrate and organic acids at the concrete-bitumen interface of a nuclear waste repository cell. Nucl. Eng. Des. 268, 51-57. https://doi.org/10.1016/j.nucengdes.2013.11.085

Binks, P.R., Nicklin, S., Bruce, N.C., 1995. Degradation of hexahydro-1,3,5-trinitro-1,3,5-triazine (RDX) by *Stenotrophomonas maltophilia* PB1. Appl. Environ. Microbiol. 61 (4), 1318-1322.

Bish, D.L., Post, J.E., (Eds.), 1990. Modern powder diffraction. Reviews in Mineralogy. Vol 20. Washington, The Mineralogical Society of America, 369p. Available from: https://books.google.es/books?hl=es&lr=&id=4696DwAAQBAJ&oi=fnd&pg=PR2&dq=Modern+powder+diffraction,+in:+Reviews+in+Mineralogy&ots=447EEChy7d&sig=1Wl92sqTvuyNZzjviQjIjhuLxU#v=onepage&q=Modern%20powder%20diffraction%2C%20in%3A%20Reviews%20in%20Mineralogy&f=false

Borghese, R., Baccolini, C., Francia, F., Sabatino, P., Turner, R.J., Zannoni, D., 2014. Reduction of chalcogen oxyanions and generation of nanoprecipitates by the photosynthetic bacterium *Rhodobacter capsulatus*. J. Hazard. Mater. 269, 24–30. https://doi.org/10.1016/j.jhazmat.2013.12.028

Breynaert, E., Scheinost, A.C., Dom, D., Rossberg, A., Vancluysen, J., Gobechiya, E., Kirschhock, C.E.A., Maes, A., 2010. Reduction of Se(IV) in boom clay: XAS solid phase speciation. Environ. Sci. Technol. 44 (17), 6649–

6655. https://doi.org/10.1021/es100569e

Briggs, D., Seah, M. P., 1983. Practical Surface Analysis by Auger and X-ray photoelectron spectroscopy. New York, John Wiley & Sons, 533p. https://doi.org/10.1002/sia.740060611

Brim, H., McFarlan, S.C., Fredrickson, J.K., Minton, K.W., Zhai, M., Wackett, L.P., Daly, M.J., 2000. Engineering *Deinococcus radiodurans* for metal remediation in radioactive mixed waste environments. Nat. Biotechnol. 18, 85-90. https://doi.org/10.1038/71986

Brosius, J., Dull, T.J., Sleeter, D.D., Noller, H.F., 1981. Gene organization and primary structure of a ribosomal RNA operon from *Escherichia coli*. J. Mol. Biol. 148 (2), 107-127. https://doi.org/10.1016/0022-2836(81)90508-8

Buchs, B., Evangelou, M.W.H., Winkel, L.H.E., Lenz, M., 2013. Colloidal properties of nanoparticular biogenic selenium govern environmental fate and bioremediation effectiveness. Environ. Sci. Technol. 47 (5), 2401–2407. https://doi.org/10.1021/es304940s

Burns, P.C., Ewing, R.C., Navrotsky, A., 2012.Nuclear Fuel in a Reactor Accident [Review]. Science. 335 (6073), 1184-8. https://doi.org/10.1126/science.1211285

Burra, R., Pradenas, G.A., Montes, R.A., Vásquez, C.C., Chasteen, T.G., 2010. Production of dimethyl triselenide and dimethyl diselenenyl sulfide in the headspace of metalloid-resistant *Bacillus* species grown in the presence of selenium oxyanions. Anal. Biochem. 396 (2), 217–222. https://doi.org/10.1016/j.ab.2009.09.026

Busse, H.-J., Bunka, S., Hensel, A., Lubitz, W., 1997. Discrimination of Members of the Family *Pasteurellaceae* Based on Polyamine Patterns. Int. J. Syst. Bacteriol. 47, 698–708. https://doi.org/10.1099/00207713-47-3-698

Busse, J., Auling, G., 1988. Polyamine Pattern as a Chemotaxonomic Marker within the Proteobacteria. Syst. Appl. Microbiol. 11 (1), 1-8. https://doi.org/10.1016/S0723-2020(88)80040-7

Butler, C.S., Debieux, C.M., Dridge, E.J., Splatt, P., Wright, M., 2012. Biomineralization of selenium by the selenate-respiring bacterium *Thauera selenatis* . Biochem. Soc. Trans. 40 (6), 1239-1243. https://doi.org/10.1042/bst20120087

Calvin, S., 2013. XAFS for Everyone. London, Taylor & Francis: CRC Press, 457p. https://doi.org/10.1201/b14843

Carrión, O., Pratscher, J., Curson, A.R.J., Williams, B.T., Rostant, W.G., Colin Murrell, J., Todd, J.D., 2017. Methanethiol-dependent dimethylsulfide production in soil environments. ISME J. 11 (10), 2379-2390 https://doi.org/10.1038/ismej.2017.105

Chabert, C., Warin, D., Leudet, A., Milot, J.F., Saturnin, A., Lagrange, M.H., Hoorelbeke, J. M., 2012. Impact of minor actinide transmutation options on interim storage and geological disposal: The French Case. In: Proceedings of the Twelfth Information Exchange Meeting on Actinide and Fission Product Partitioning and Transmutation; 2012 Sep 24-27; Prague. Issy-les-Moulineaux (France): Nuclear Energy Agency of the OECD (NEA); 2013. pp. 131-140. Available from http://inis.iaea.org/search/search.aspx?orig_q=RN:44100547

Challenger, F., 1945. Biological Methylation. Chem. Rev. 36 (3), 315–361. https://doi.org/10.1021/cr60115a003

Chandwadkar, P., Misra, H.S., Acharya, C., 2018. Uranium biomineralization induced by a metal tolerant: *Serratia* strain under acid, alkaline and irradiated conditions. Metallomics. 10 (8), 1078-1088 https://doi.org/10.1039/c8mt00061a

Chasteen, T.G., 1993. Confusion between dimethyl selenenyl sulfide and dimethyl selenone released by bacteria. Appl. Organomet. Chem. 7 (5), 335–342. https://doi.org/10.1002/aoc.590070507

Chasteen, T.G., Bentley, R., 2003. Biomethylation of Selenium and Tellurium : Microorganisms and Plants. Chem. Rev. 103 (1), 1-26. https://doi.org/10.1021/cr010210+

Chen, H., Shin, D.W., Nam, J.G., Kwon, K.W., Yoo, J.B., 2010. Selenium nanowires and nanotubes synthesized via a facile template-free solution method. Mater. Res. Bull. 45 (6), 699–704. https://doi.org/10.1016/j.materresbull.2010.02.016

Chhibber, S., Zgair, A.K., 2009. Involvement of *Stenotrophomonas maltophilia* Flagellin in Bacterial Adhesion to Airway Biotic Surfaces : An in Vitro Study. Am.J. Biomed. Sci. 2009. 1 (3), 188–195. https:// doi: 10.5099/aj090300188

Choudhary, S., Sar, P., 2009. Characterization of a metal resistant *Pseudomonas* sp. isolated from uranium mine for its potential in heavy metal (Ni^{2+}, Co^{2+}, Cu^{2+}, and Cd^{2+}) sequestration. Bioresour. Technol. 100 (9), 2482-2492. doi.org/10.1016/j.biortech.2008.12.015

Chu, H.A., Hillier, W., Debus, R.J., 2004. Evidence that the C-Terminus of the D1 Polypeptide of Photosystem II Is Ligated to the Manganese Ion that Undergoes Oxidation during the S1 to S2 Transition: An Isotope-Edited FTIR Study. Biochemistry. 43 (11), 3152-3166. https://doi.org/10.1021/bi035915f

Claessens, J., van Lith, Y., Laverman, A.M., Van Cappellen, P., 2006. Acid-base activity of live bacteria: Implications for quantifying cell wall charge. Geochim. Cosmochim. Acta. 70 (2), 267-276. https://doi.org/10.1016/j.gca.2005.09.006

Clark, M.E., Edelmann, R.E., Duley, M.L., Wall, J.D., Fields, M.W., 2007. Biofilm formation in *Desulfovibrio vulgaris* Hildenborough is dependent upon protein filaments. Environ. Microbiol. 9 (11), 2844-2854. https://doi.org/10.1111/j.1462-2920.2007.01398.x

Collins, R.N., Saito, T., Aoyagi, N., Payne, T.E., Kimura, T., Waite, T.D., 2011. Applications of Time-Resolved Laser Fluorescence Spectroscopy to the Environmental Biogeochemistry of Actinides. J. Environ. Qual. 40 (3), 731-741. https://doi.org/10.2134/jeq2010.0166

Cologgi, D.L., Speers, A.M., Bullard, B.A., Kelly, S.D., Reguera, G., 2014. Enhanced uranium immobilization and reduction by *Geobacter sulfurreducens* biofilms. Appl. Environ. Microbiol. 80 (21), 6638–6646. https://doi.org/10.1128/AEM.02289-14

Colthup, N.B., Daly, L.H., Wiberley, S.E., 1990. Introduction to Infrared and Raman Spectroscopy. London, Academic Press., 547p. https://doi.org/10.1016/C2009-0-21628-X

Conley, R.T., 1972. Infrared Spectroscopy. Boston, Allyn and Bacon, 293p.

Cooper, W.C., westbury, A., 1974. "The structure of Selenium", in Selenium, edited by R. A. Zingaro and W. C. Cooper (Van Nostrand Reinhold Company, New York, 1974), Chap. 3, pp. 87–147

Dardenne, K., González-Robles, E., Rothe, J., Müller, N., Christill, G., Lemmer, D., Praetorius, R., Kienzler, B., Metz, V., Roth, G., Geckeis, H., 2015. XAS and XRF investigation of an actual HAWC glass fragment obtained from the Karlsruhe vitrification plant (VEK). J. Nucl. Mater. 460, 209–215. https://doi.org/10.1016/j.jnucmat.2015.02.021

Daughney, C.J., Fein, J.B., 1998. The effect of ionic strength on the adsorption of H^+, Cd^{2+}, $Pb^{2+}$and Cu^{2+} by *Bacillus subtilis* and *Bacillus licheniformis*: A surface complexation model. J. Colloid Interface Sci. 198, 53-77. https://doi.org/10.1006/jcis.1997.5266

David, F., Berger, A., Hänsch, R., Rohde, M., Franco-Lara, E., 2011. Single cell analysis applied to antibody fragment production with *Bacillus megaterium*: Development of advanced physiology and bioprocess state estimation tools. Microb. Cell Fact. 10, 23. https://doi.org/10.1186/1475-2859-10-23

Deacon, G.B., Phillips, R.J., 1980. Relationships between the carbon-oxygen stretching frequencies of carboxylato complexes and the type of carboxylate coordination. Coord. Chem. Rev. 33 (3), 227-250. https://doi.org/10.1016/S0010-8545(00)80455-5

Debieux, C.M., Dridge, E.J., Mueller, C.M., Splatt, P., Paszkiewicz, K., Knight, I., Florance, H., Love, J., Titball, R.W., Lewis, R.J., Richardson, D.J., Butler, C.S., 2011. A bacterial process for selenium nanosphere assembly. Proc. Natl. Acad. Sci. 108 (33), 13480-13485. https://doi.org/10.1073/pnas.1105959108

Delage, P., Cui, Y.J., Tang, A.M., 2010. Clays in radioactive waste disposal. J. Rock Mech. Geotech. Eng. 2 (2), 111–123. https://doi.org/10.3724/SP.J.1235.2010.00111

DeMoll-decker, H., Macy, J.M., 1993. The periplasmic nitrite reductase of *Thauera selenatis* may catalyze the reduction of selenite to elemental selenium. Arch. Microbiol. 160 (3), 241–247. https://doi.org/10.1007/BF00249131

Dhanjal, S., Cameotra, S.S., 2010. Aerobic biogenesis of selenium nanospheres by *Bacillus cereus* isolated from coalmine soil. Microb. Cell Fact. 9, 52. https://doi.org/10.1186/1475-2859-9-52

Di Gregorio, S., Lampis, S., Vallini, G., 2005. Selenite precipitation by a rhizospheric strain of *Stenotrophomonas* sp.

isolated from the root system of *Astragalus bisulcatus*: a biotechnological perspective. Environ. Int. 31 (2), 233–41. https://doi.org/10.1016/j.envint.2004.09.021

Diep, P., Mahadevan, R., Yakunin, A.F., 2018. Heavy metal removal by bioaccumulation using genetically engineered microorganisms. Front. Bioeng. Biotechnol. 6, 157. https://doi.org/10.3389/fbioe.2018.00157

Diesen, V., Forsberg, K., Jonsson, M., 2017. Effects of cellulose degradation products on the mobility of Eu(III) in repositories for low and intermediate level radioactive waste. J. Hazard. Mater. 340, 384-389. https://doi.org/10.1016/j.jhazmat.2017.07.008

Dittrich, M., Sibler, S., 2005. Cell surface groups of two picocyanobacteria strains studied by zeta potential investigations, potentiometric titration, and infrared spectroscopy. J. Colloid Interface Sci. 286 (2), 487-495. https://doi.org/10.1016/j.jcis.2005.01.029

Dobias, J., Suvorova, E.I., Bernier-Latmani, R., 2011. Role of proteins in controlling selenium nanoparticle size. Nanotechnology. 22 (19), 195605. https://doi.org/10.1088/0957-4484/22/19/195605

Dobrowolski, R., Szcześ, A., Czemierska, M., Jarosz-Wikołazka, A., 2017. Studies of cadmium(II), lead(II), nickel(II), cobalt(II) and chromium(VI) sorption on extracellular polymeric substances produced by *Rhodococcus opacus* and *Rhodococcus rhodochrous*. Bioresour. Technol. 225, 113-120. https://doi.org/10.1016/j.biortech.2016.11.040

Don MacElroy, J.M., 2016. Closing the carbon cycle through rational use of carbon-based fuels. Ambio 45 (Suppl 1), 5–14. https://doi.org/10.1007/s13280-015-0728-7

Dowdle, P.R., Oremland, R.S., 1998. Microbial oxidation of elemental selenium in soil slurries and bacterial cultures. Environ. Sci. Technol. 32 (23), 3749–3755. https://doi.org/10.1021/es970940s

Dufrêne, Y.F., Rouxhet, P.G., 1996. X-ray photoelectron spectroscopy analysis of the surface composition of *Azospirillum brasilense* in relation to growth conditions. Colloids Surfaces B Biointerfaces. 7 (5-6), 271-279. https://doi.org/10.1016/0927-7765(96)01295-7

Dufrêne, Y.F., Van der Wal, A., Norde, W., Rouxhet, P.G., 1997. X-ray photoelectron spectroscopy analysis of whole cells and isolated cell walls of gram-positive bacteria: Comparison with biochemical analysis. J. Bacteriol. 179 (4), 1023–1028. https://doi.org/10.1128/jb.179.4.1023-1028.1997

Dungan, R.S., Yates, S.R., Frankenberger, W.T., 2003. Transformations of selenate and selenite by *Stenotrophomonas maltophilia* isolated from a seleniferous agricultural drainage pond sediment. Environ. Microbiol. 5 (4), 287–295. https://doi.org/10.1046/j.1462-2920.2003.00410.x

Duro, L., Domènech, C., Grivé, M., Roman-Ross, G., Bruno, J., Källström, K., 2014. Assessment of the evolution of the redox conditions in a low and intermediate level nuclear waste repository (SFR1, Sweden). Appl. Geochemistry. 49, 192-205. https://doi.org/10.1016/j.apgeochem.2014.04.015

Estes, S., 2014. Toward understanding the thermodynamics and mechanisms of actinide sorption reactions. Dissertation, Clemson University. Available from: https://tigerprints.clemson.edu/all_dissertations/1426

Eswayah, A.S., Smith, T.J., Gardiner, P.H.E., 2016. Microbial transformations of selenium species of relevance to bioremediation. Appl. Environ. Microbiol. 82 (16), 4848-4859. https://doi.org/10.1128/AEM.00877-16

Eswayah, A.S., Smith, T.J., Scheinost, A.C., Hondow, N., Gardiner, P.H.E., 2017. Microbial transformations of selenite by methane-oxidizing bacteria. Appl. Microbiol. Biotechnol. 101 (17), 6713–6724. https://doi.org/10.1007/s00253-017-8380-8

Fahmy, K., Merroun, M., Pollmann, K., Raff, J., Savchuk, O., Hennig, C., Selenska-Pobell, S., 2006. Secondary structure and Pd(II) coordination in S-layer proteins from *Bacillus sphaericus* studied by infrared and X-ray absorption spectroscopy. Biophys. J. 91 (3), 996-1007. https://doi.org/10.1529/biophysj.105.079137

Fairley, N., 2006. CasaXPS 2.3.17 ed.; Casa Software Ltd. Available from: www.casaxps.com

Fang, L., Yang, S., Huang, Q., Xue, A., Cai, P., 2014. Biosorption mechanisms of Cu(II) by extracellular polymeric substances from *Bacillus subtilis*. Chem. Geol. 386, 143-151. https://doi.org/10.1016/j.chemgeo.2014.08.017

Fein, J.B., Boily, J.F., Yee, N., Gorman-Lewis, D., Turner, B.F., 2005. Potentiometric titrations of *Bacillus subtilis*

cells to low pH and a comparison of modeling approaches. Geochim. Cosmochim. Acta. 69 (5), 1123–1132. https://doi.org/10.1016/j.gca.2004.07.033

Fein, J.B., Daughney, C.J., Yee, N., Davis, T.A., 1997. A chemical equilibrium model for metal adsorption onto bacterial surfaces. Geochim. Cosmochim. Acta. 61 (16), 3319-3328. https://doi.org/10.1016/S0016-7037(97)00166-X

Felsenstein, J., 2005. PHYLIP - Phylogeny inference package - v3.6. Dep. Genome Sci. Univ. Washington, Seattle. https://doi.org/10.1111/j.1096-0031.1989.tb00562.x

Fernández-Llamosas, H., Castro, L., Blázquez, M.L., Díaz, E., Carmona, M., 2016. Biosynthesis of selenium nanoparticles by *Azoarcus* sp. CIB. Microb. Cell Fact. 15, 109. https://doi.org/10.1186/s12934-016-0510-y

Fernández-Martínez, A., Charlet, L., 2009. Selenium environmental cycling and bioavailability: a structural chemist point of view. Rev. Environ. Sci. Bio/Technology. 8 (1), 81–110. https://doi.org/10.1007/s11157-009-9145-3

Féron, D., Crusset, D., 2014. Microbial induced corrosion in French concept of nuclear waste underground disposal. Corros. Eng. Sci. Technol. 49 (6), 540-547. https://doi.org/10.1179/1743278214y.0000000193

Finkmann, W., Altendorf, K., Stackebrandt, E., Lipski, A., 2000. Characterization of N_2O-producing *Xanthomonas*-like isolates from biofilters as *Stenotrophomonas nitritireducens* sp. nov., *Luteimonas mephitis* gen. nov., sp. nov. and *Pseudoxanthomonas broegbernensis* gen. nov., sp. nov. Int. J. Syst. Evol. Microbiol. 50 (Pt 1), 273-282. https://doi.org/10.1099/00207713-50-1-273

Fomina, M., Gadd, G.M., 2014. Biosorption: current perspectives on concept, definition and application. Bioresour. Technol. 160, 3-14. https://doi.org/10.1016/j.biortech.2013.12.102

Francis, A.J., Nancharaiah, Y. V., 2015. In situ and ex situ bioremediation of radionuclide-contaminated soils at nuclear and norm sites, in: Environmental Remediation and Restoration of Contaminated Nuclear and Norm Sites. pp. 185-236. https://doi.org/10.1016/B978-1-78242-231-0.00009-0

Frankenberger, W.T, Arshad, M., 2001. Bioremediation of selenium-contaminated sediments and water. BioFactors 14 (1-4), 241–254. https://doi.org/10.1002/biof.5520140130

Friedman, N.D., Korman, T.M., Fairley, C.K., Franklin, J.C., Spelman, D.W., 2002. Bacteraemia due to *Stenotrophomonas maltophilia*: An analysis of 45 episodes. J. Infect. 45 (1), 47–53. https://doi.org/10.1053/jinf.2002.0978

Fultz, B., Howe, J.M., 2008. Transmission electron microscopy and diffractometry of materials. New York, Springer, 747p. https://doi.org/10.1007/978-3-540-73886-2

Gadd, G.M., 2009. Biosorption: critical review of scientific rationale, environmental importance and significance for pollution treatment. J. Chem. Technol. Biotechnol. 84 (1), 13-28. https://doi.org/10.1002/jctb.1999

Gadd, G.M., 2004. Microbial influence on metal mobility and application for bioremediation, in: Geoderma. 122 (2-4), 109-119. https://doi.org/10.1016/j.geoderma.2004.01.002

Gans, P., Sabatini, A., Vacca, A., 1996. Investigation of equilibria in solution. Determination of equilibrium constants with the HYPERQUAD suite of programs. Talanta. 43 (10), 1739-1753. https://doi.org/10.1016/0039-9140(96)01958-3

Gates, B., Mayers, B., Cattle, B., Xia, Y., 2002. Synthesis and characterization of uniform nanowires of trigonal selenium. Adv. Funct. Mater. 12 (3), 219–227. https://doi.org/10.1002/1616-3028(200203)12:3<219::AID-ADFM219>3.0.CO;2-U

Ge, S., Ge, S.C., 2016. Simultaneous Cr(VI) reduction and Zn(II) biosorption by *Stenotrophomonas* sp. and constitutive expression of related genes. Biotechnol. Lett. 38 (5), 877-884. https://doi.org/10.1007/s10529-016-2057-8

Gerber, U., Zirnstein, I., Krawczyk-Bärsch, E., Lünsdorf, H., Arnold, T., Merroun, M.L., 2016. Combined use of flow cytometry and microscopy to study the interactions between the gram-negative betaproteobacterium *Acidovorax facilis* and uranium (VI). J. Hazard. Mater. 317, 127-134. https://doi.org/10.1016/j.jhazmat.2016.05.062

Gerstner, E., 2009. The hybrid returns. Nature 460, 25–28. https://doi.org/10.1038/460025a

Ghosh, A., Saha, P.D., 2013. Optimization of copper bioremediation by *Stenotrophomonas maltophilia* PD2. J. Environ. Chem. Eng. 1 (3), 159-163. https://doi.org/10.1016/j.jece.2013.04.012

Givan, A.L., 2011. Flow Cytometry: An Introduction, in: Hawley, T.S., Hawley, R.G. (Eds.). Flow Cytometry Protocols. pp. 1–29. https://doi.org/10.1007/978-1-61737-950-5

González Orive, A., Pissinis, D.E., Diaz, C., Miñán, A., Benítez, G.A., Rubert, A., Daza Millone, A., Rumbo, M., Hernández Creus, A., Salvarezza, R.C., Schilardi, P.L., 2014. Self-assembly of flagellin on Au(111) surfaces. J. Colloid Interface Sci. 433, 86–93. https://doi.org/10.1016/j.jcis.2014.07.016

Gorietti, D., Giardina, I., Arginelli, D., Battisti, P., 2017. Determination of plutonium, americium and curium isotopes in radioactive metal wastes deriving from nuclear decommissioning. J. Radioanal. Nucl. Chem. 314 (3), 1785–1792. https://doi.org/10.1007/s10967-017-5553-y

Goris, J., Konstantinidis, K.T., Klappenbach, J.A., Coenye, T., Vandamme, P., Tiedje, J.M., 2007. DNA-DNA hybridization values and their relationship to whole-genome sequence similarities. Int. J. Syst. Evol. Microbiol. 57 (Pt 1), 81-91. https://doi.org/10.1099/ijs.0.64483-0

Grouzdev, D.S., Safonov, A. V, Babich, T.L., Tourova, T.P., Krutkina, M.S., Nazina, T.N., 2018. Draft Genome Sequence of a Dissimilatory U(VI)-Reducing Bacterium, *Shewanella xiamenensis* Strain DCB2-1, Isolated from Nitrate- and Radionuclide-Contaminated Groundwater in Russia. Genome Announc. 6, e00555-18. https://doi.org/10.1128/genomeA.00555-18

Günther, A., Geipel, G., Bernhard, G., 2007. Complex formation of uranium(VI) with the amino acids l-glycine and l-cysteine: A fluorescence emission and UV-Vis absorption study. Polyhedron. 26 (1), 59-65. https://doi.org/10.1016/j.poly.2006.07.030

Haas, J.R., Dichristina, T.J., Wade, R., 2001. Thermodynamics of U(VI) sorption onto *Shewanella putrefaciens*. Chem. Geol. 180 (1), 33–54. https://doi.org/10.1016/S0009-2541(01)00304-7

Hamed, M.M., Holiel, M., El-Aryan, Y.F., 2017. Removal of selenium and iodine radionuclides from waste solutions using synthetic inorganic ion exchanger. J. Mol. Liq. 242, 722–731. https://doi.org/10.1016/j.molliq.2017.07.035

Handa, Y., Tazato, N., Nagatsuka, Y., Koide, T., Kigawa, R., Sano, C., Sugiyama, J., 2016. *Stenotrophomonas tumulicola* sp. nov., a major contaminant of the stone chamber interior in the Takamatsuzuka Tumulus. Int. J. Syst. Evol. Microbiol. 66 (3), 1119-1124. https://doi.org/10.1099/ijsem.0.000843

Hedrich, S., Schlömann, M., Barrie Johnson, D., 2011. The iron-oxidizing proteobacteria. Microbiology. 157, 1551-1564. https://doi.org/10.1099/mic.0.045344-0

Herbel, M.J., Blum, J.S., Oremland, R.S., Borglin, S.E., 2003. Reduction of elemental selenium to selenide: Experiments with anoxic sediments and bacteria that respire se-oxyanions. Geomicrobiol. J. 20 (6), 587–602. https://doi.org/10.1080/713851163

Heylen, K., Vanparys, B., Peirsegaele, F., Lebbe, L., De Vos, P., 2007. *Stenotrophomonas terrae* sp. nov. and *Stenotrophomonas humi* sp. nov., two nitrate-reducing bacteria isolated from soil. Int. J. Syst. Evol. Microbiol. 57 (Pt 9), 2056-2061. https://doi.org/10.1099/ijs.0.65044-0

Higgins, M.J., Chen, Y.-C., Yarosz, D.P., Murthy, S.N., Maas, N.A., Glindemann, D., Novak, J.T., 2006. Cycling of volatile organic sulfur compounds in anaerobically digested biosolids and its implications for odors. Water Environ. Res. 78 (3), 243-252. https://doi.org/10.2175/106143005X90065

Ho, C.T., Kim, J.W., Kim, W.B., Song, K., Kanaly, R.A., Sadowsky, M.J., Hur, H.-G., 2010. *Shewanella*-mediated synthesis of selenium nanowires and nanoribbons. J. Mater. Chem. 20, 5899-5905. https://doi.org/10.1039/b923252d

Horvath, A., Rachlew, E., 2016. Nuclear power in the 21st century: Challenges and possibilities. Ambio. 45 (Suppl 1), 38-49. https://doi.org/10.1007/s13280-015-0732-y

Hulanicki, A., Maj-Żurawska, M., Glab, S., 2013. TITRIMETRY | Potentiometry. Encyclopedia of Analytical Science, 2005, pp 114-121. https://doi.org/10.1016/B978-0-12-409547-2.00546-1

Hunter, W.J., 2014. A *Rhizobium selenitireducens* protein showing selenite reductase activity. Curr. Microbiol. 68 (3), 311–316. https://doi.org/10.1007/s00284-013-0474-7

Hunter, W.J., Kuykendall, L.D., 2007. Reduction of selenite to elemental red selenium by *Rhizobium* sp. strain B1. Curr. Microbiol. 55 (4), 344–349. https://doi.org/10.1007/s00284-007-0202-2

Hupert-Kocurek, K., Saczyńska, A., Piotrowska-Seget, Z., 2013. Cadmium increases catechol 2,3-dioxygenase activity in *Variovorax* sp. 12S, a metal-tolerant and phenol-degrading strain. Antonie van Leeuwenhoek, Int. J. Gen. Mol. Microbiol. 104 (5), 845-853. https://doi.org/10.1007/s10482-013-9997-y

Husen, A., Siddiqi, K.S., 2014. Plants and microbes assisted selenium nanoparticles: characterization and application. J. Nanobiotechnology 12, 28. https://doi.org/10.1186/PREACCEPT-4680053311297707

IAEA, 2018. Status and trends in spent fuel and radioactive waste management. Vienna, International Atomic Energy Agency. Nuclear Energy Series No. NW-T-1.14, 74. Available from: https://www-pub.iaea.org/MTCD/Publications/PDF/P1799_web.pdf

IAEA, 2016. Nuclear Power and the Paris Agreement. Vienna, International Atomic Energy Agency. Available from: https://www.iaea.org/sites/default/files/16/11/np-parisagreement.pdf.

IAEA, 2015. Climate change and nuclear power 2015. Vienna, International Atomic Energy Agency. https://www-pub.iaea.org/MTCD/Publications/PDF/CCANP2015Web-78834554.pdf

IAEA, 2009a. Data Classification of radioactive waste : safety guide [Internet]. Vienna, International Atomic Energy Agency. IAEA safety standards series, no. GSG-1) STI/PUB/1419. Available from: https://www-pub.iaea.org/MTCD/Publications/PDF/Pub1419_web.pdf

IAEA, 2009b. Status and trends of nuclear technologies: Report of the International Project on Innovative Nuclear Reactors and Fuel Cycles (INPRO). Vienna, International Atomic Energy Agency. Available from: https://www-pub.iaea.org/MTCD/Publications/PDF/TE_1622_Web.pdf

IAEA, 2003. Scientific and technical basis for geological disposal of radioactive wastes. Vienna, International Atomic Energy Agency. Technical reports series, n. 413. STI/DOC/010/413. Available from: https://www-pub.iaea.org/MTCD/Publications/PDF/TRS413_web.pdf

Ikemoto, S., Suzuki, K., Kaneko, T., Komagata, K., 1980. Characterization of strains of *Pseudomonas maltophilia* which do not require methionine. Int. J. Syst. Bacteriol. 5, 43. https://doi.org/10.1099/00207713-30-2-437

Ikonen, J., Voutilainen, M., Söderlund, M., Jokelainen, L., Siitari-Kauppi, M., Martin, A., 2016. Sorption and diffusion of selenium oxyanions in granitic rock. J. Contam. Hydrol. 192, 203–211. https://doi.org/10.1016/j.jconhyd.2016.08.003

Itävaara, M., Nyyssönen, M., Kapanen, A., Nousiainen, A., Ahonen, L., Kukkonen, I., 2011. Characterization of bacterial diversity to a depth of 1500m in the Outokumpu deep borehole, Fennoscandian Shield. FEMS Microbiol. Ecol. 77 (2), 295-309. https://doi.org/10.1111/j.1574-6941.2011.01111.x

Jain, R., Jordan, N., Tsushima, S., Hübner, R., Weiss, S., Lens, P.N.L., 2017. Shape change of biogenic elemental selenium nanomaterials from nanospheres to nanorods decreases their colloidal stability. Environ. Sci. Nano. 4, 1054–1063. https://doi.org/10.1039/C7EN00145B

Jan, A.T., 2017. Outer Membrane Vesicles (OMVs) of gram-negative bacteria: A perspective update. Front. Microbiol. 8, 1053. https://doi.org/10.3389/fmicb.2017.01053

Jiang, W., Saxena, A., Song, B., Ward, B.B., Beveridge, T.J., Myneni, S.C.B., 2004. Elucidation of functional groups on gram-positive and gram-negative bacterial surfaces using infrared spectroscopy. Langmuir. 20 (26), 11433-11442. https://doi.org/10.1021/la049043+

Jörg, G., Bühnemann, R., Hollas, S., Kivel, N., Kossert, K., Van Winckel, S., Gostomski, C.L. v., 2010. Preparation of radiochemically pure ^{79}Se and highly precise determination of its half-life. Appl. Radiat. Isot. 68 (12), 2339–2351. https://doi.org/10.1016/j.apradiso.2010.05.006

Jorgensen, E., (Ed.), 2010. Ecotoxicology. Amsterdam, Elsevier Sci., 402p.

Jóvári, P., Delaplane, R.G., Pusztai, L., 2003. Structural models of amorphous selenium. Phys. Rev. B - Condens. Matter Mater. Phys. 67 (17), 172201. https://doi.org/10.1103/PhysRevB.67.172201

Jucker, B.A., Harms, H., Zehnder, A.J.B., 1996. Adhesion of the positively charged bacterium *Stenotrophomonas* (*Xanthomonas*) *maltophilia* 70401 to glass and teflon. J. Bacteriol. 178 (18), 5472–5479. https://doi.org/10.1128/jb.178.18.5472-5479.1996

Jukes, T.H., Cantor, C.R., 1969. Evolution of protein molecules, in: Mammalian protein metabolism. New York, Academic Press, pp. 21-132. https://doi.org/10.1016/B978-1-4832-3211-9.50009-7

Kagami, T., Narita, T., Kuroda, M., Notaguchi, E., Yamashita, M., Sei, K., Soda, S., Ike, M., 2013. Effective selenium volatilization under aerobic conditions and recovery from the aqueous phase by *Pseudomonas stutzeri* NT-I. Water Res. 47(3), 1361–1368. https://doi.org/10.1016/j.watres.2012.12.001

Kamnev, A.A., 2008. FTIR spectroscopic studies of bacterial cellular responses to environmental factors, plant-bacterial interactions and signalling. Spectroscopy. 22 (2-3), 83–95. https://doi.org/10.3233/SPE-2008-0329

Kamnev, A.A., Mamchenkova, P. V., Dyatlova, Y.A., Tugarova, A. V., 2017. FTIR spectroscopic studies of selenite reduction by cells of the rhizobacterium *Azospirillum brasilense* Sp7 and the formation of selenium nanoparticles. J. Mol. Struct. 1140, 106–112. https://doi.org/10.1016/j.molstruc.2016.12.003

Kämpfer, P., Kroppenstedt, R.M., 1996. Numerical analysis of fatty acid patterns of coryneform bacteria and related taxa. Can. J. Microbiol. 42 (10), 989-1005. https://doi.org/10.1139/m96-128

Kämpfer, P., Steiof, M., Dott, W., 1991. Microbiological characterization of a fuel-oil contaminated site including numerical identification of heterotrophic water and soil bacteria. Microb. Ecol. 21 (1), 227-251. https://doi.org/10.1007/BF02539156

Kaparullina, E., Doronina, N., Chistyakova, T., Trotsenko, Y., 2009. *Stenotrophomonas chelatiphaga* sp. nov., a new aerobic EDTA-degrading bacterium. Syst. Appl. Microbiol. 32 (3), 157-162. https://doi.org/10.1016/j.syapm.2008.12.003

Kaur, G., Iqbal, M., Bakshi, M.S., 2009. Biomineralization of fine selenium crystalline rods and amorphous spheres. J. Phys. Chem. C. 113 (31), 13670–13676. https://doi.org/10.1021/jp903685g

Keller, A.A., Wang, H., Zhou, D., Lenihan, H.S., Cherr, G., Cardinale, B.J., Miller, R., Zhaoxia, J.I., 2010. Stability and aggregation of metal oxide nanoparticles in natural aqueous matrices. Environ. Sci. Technol. 44 (6), 1962–1967. https://doi.org/10.1021/es902987d

Kessi, J., Hanselmann, K.W., 2004. Similarities between the abiotic reduction of selenite with glutathione and the dissimilatory reaction mediated by *Rhodospirillum rubrum* and *Escherichia coli*. J. Biol. Chem. 279 (49), 50662–50669. https://doi.org/10.1074/jbc.M405887200

Kietäväinen, R., Purkamo, L., 2015. The origin, source, and cycling of methane in deep crystalline rock biosphere. Front. Microbiol. 6, 725. https://doi.org/10.3389/fmicb.2015.00725

Kim, H. Bin, Srinivasan, S., Sathiyaraj, G., Quan, L.H., Kim, S.H., Bui, T.P.N., Liang, Z.Q., Kim, Y.J., Yang, D.C., 2010. *Stenotrophomonas ginsengisoli* sp. nov., isolated from a ginseng field. Int. J. Syst. Evol. Microbiol. 60 (Pt 7), 1522-1526. https://doi.org/10.1099/ijs.0.014662-0

Kimura, T., Choppin, G.R., 1994. Luminescence study on determination of the hydration number of Cm(III). J. Alloys Compd. 213-214, 313-317. https://doi.org/10.1016/0925-8388(94)90921-0

Kimura, T., Choppin, G.R., Kato, Y., Yoshida, Z., 1996. Determination of the Hydration Number of Cm(III) in Various Aqueous Solutions. Radiochim. Acta. 72 (2), 61-64. https://doi.org/10.1524/ract.1996.72.2.61

Kimura, T., Kato, Y., 1998. Luminescence study on hydration states of lanthanide(III)-polyaminopolycarboxylate complexes in aqueous solution. J. Alloys Compd. 275-277, 806-810. https://doi.org/10.1016/S0925-8388(98)00446-0

Klimentová, J., Stulík, J., 2015. Methods of isolation and purification of outer membrane vesicles from gram-negative bacteria. Microbiol. Res. 170, 1-9. https://doi.org/10.1016/j.micres.2014.09.006

Klonowska, A., Heulin, T., Vermeglio, A., 2005. Selenite and tellurite reduction by *Shewanella oneidensis*. Appl.

Environ. Microbiol. 71 (9), 5607-5609. https://doi.org/10.1128/AEM.71.9.5607-5609.2005

Kohli, R., 2012. Methods for monitoring and measuring cleanliness of surfaces, in: Developments in surface contamination and cleaning. William Andrew Publishing, pp. 107–178. https://doi.org/10.1016/B978-1-4377-7883-0.00003-1

Kolhe, N., Zinjarde, S., Acharya, C., 2018. Responses exhibited by various microbial groups relevant to uranium exposure. Biotechnol. Adv. 36 (7), 1828-1846. https://doi.org/10.1016/j.biotechadv.2018.07.002

Komagata, K., 1985. Bacteria (1)- the aerobic bacteria, in: Hasegawa, T. (Ed.), Classification and Identification of Microorganisms. Tokyo, Gakkai Shuppan, pp. 99–161.

Kónya, J., Nagy, N.M., 2018. Environmental Radioactivity. In: Kónya J., Nagy, N.M. (Eds.). Nuclear and Radiochemistry. 2nd ed. Netherlands: Elsevier. pp. 399-419. Available from: https://doi.org/10.1016/B978-0-12-813643-0.00013-5.

Kooyman, T., Buiron, L., Rimpault, G., 2018. A comparison of curium, neptunium and americium transmutation feasibility. Ann. Nucl. Energy 112, 748–758. https://doi.org/10.1016/j.anucene.2017.09.041

Kora, A.J., 2018. *Bacillus cereus*, selenite-reducing bacterium from contaminated lake of an industrial area: a renewable nanofactory for the synthesis of selenium nanoparticles. Bioresour. Bioprocess. 5, 30. https://doi.org/10.1186/s40643-018-0217-5

Kora, A.J., Rastogi, L., 2016. Bacteriogenic synthesis of selenium nanoparticles by *Escherichia coli* ATCC 35218 and its structural characterisation. IET Nanobiotechnol. 11 (2), 179-184. https://doi.org/10.1049/iet-nbt.2016.0011

Kovacs, N., 1956. Identification of *Pseudomonas pyocyanea* by the oxidase reaction. Nature. 178, 703. https://doi.org/10.1038/178703a0

Krawczyk-Bärsch, E., Gerber, U., Müller, K., Moll, H., Rossberg, A., Steudtner, R., Merroun, M.L., 2018. Multidisciplinary characterization of U(VI) sequestration by *Acidovorax facilis* for bioremediation purposes. J. Hazard. Mater. 347, 233–241. https://doi.org/10.1016/j.jhazmat.2017.12.030

Kumar, N., Krishnani, K.K., Singh, N.P., 2018. Comparative study of selenium and selenium nanoparticles with reference to acute toxicity, biochemical attributes, and histopathological response in fish. Environ. Sci. Pollut. Res. 25 (9), 8914-8927. https://doi.org/10.1007/s11356-017-1165-x

Kumar, S., Prakash, R., Singh, V., 2015. Synthesis, characterization, and applications of europium oxide: A review. Rev. Adv. Sci. Eng. 4 (4), 247–257. https://doi.org/10.1166/rase.2015.1102

Kumar, S., Stecher, G., Tamura, K., 2016. MEGA7: Molecular Evolutionary Genetics Analysis Version 7.0 for Bigger Datasets. Mol. Biol. Evol. 33 (7), 1870-1874. https://doi.org/10.1093/molbev/msw054

Lampis, S., Zonaro, E., Bertolini, C., Bernardi, P., Butler, C.S., Vallini, G., 2014. Delayed formation of zero-valent selenium nanoparticles by *Bacillus mycoides* SeITE01 as a consequence of selenite reduction under aerobic conditions. Microb. Cell Fact. 13 (1), 35. https://doi.org/10.1186/1475-2859-13-35

Lampis, S., Zonaro, E., Bertolini, C., Cecconi, D., Monti, F., Micaroni, M., Turner, R.J., Butler, C.S., Vallini, G., 2017. Selenite biotransformation and detoxification by *Stenotrophomonas maltophilia* SeITE02: Novel clues on the route to bacterial biogenesis of selenium nanoparticles. J. Hazard. Mater. 324 (Pt A), 3-14. https://doi.org/10.1016/j.jhazmat.2016.02.035

Le Caër, S., 2011. Water radiolysis: influence of oxide surfaces on H_2 production under ionizing radiation. Water. 3 (1), 235-253. https://doi.org/10.3390/w3010235

Lee, I., Kim, Y.O., Park, S.C., Chun, J., 2016. OrthoANI: An improved algorithm and software for calculating average nucleotide identity. Int. J. Syst. Evol. Microbiol. 66 (2), 1100-1103. https://doi.org/10.1099/ijsem.0.000760

Lee, M., Woo, S.G., Chae, M., Shin, M.C., Jung, H.M., Ten, L.N., 2011. *Stenotrophomonas daejeonensis* sp. nov., isolated from sewage. Int. J. Syst. Evol. Microbiol. 61, 598-604. https://doi.org/10.1099/ijs.0.017780-0

Lehto, J., Huo, X., 2011. Chemistry and analysis of radionuclides: laboratory techniques and methodology.

weinheim: WILEY-VCH Verlag & Co. KGaA. Available from: https://www.wiley.com/en-us/Chemistry+and+Analysis+of+Radionuclides%3A+Laboratory+Techniques+and+Methodology-p-9783527633029

Lelieveld, J., Kunkel, D., Lawrence, M.G., 2012. Global risk of radioactive fallout after major nuclear reactor accidents. Atmos. Chem. Phys. 12 (9), 4245–4258. https://doi.org/10.5194/acp-12-4245-2012

Lenz, M., van Aelst, A.C., Smit, M., Corvini, P.F.X., Lens, P.N.L., 2009. Biological production of selenium nanoparticles from waste waters. Adv. Mater. Res. 71-73, 721-724. https://doi.org/10.4028/www.scientific.net/AMR.71-73.721

Leupin, O.X., Bernier-Latmani, R., Bagnoud, A., Moors, H., Leys, N., Wouters, K., Stroes-Gascoyne, S., 2017. Fifteen years of microbiological investigation in Opalinus Clay at the Mont Terri rock laboratory (Switzerland). Swiss J. Geosci. 110 (1), 343-354. https://doi.org/10.1007/s00015-016-0255-y

Li, B., Liu, N., Li, Y., Jing, W., Fan, J., Li, D., Zhang, L., Zhang, X., Zhang, Z., Wang, L., 2014a. Reduction of selenite to red elemental selenium by *Rhodopseudomonas palustris* strain N. PLoS One. 9 (4), e95955. https://doi.org/10.1371/journal.pone.0095955

Li, D.B., Cheng, Y.Y., Wu, C., Li, W.W., Li, N., Yang, Z.C., Tong, Z.H., Yu, H.Q., 2014b. Selenite reduction by *Shewanella oneidensis* MR-1 is mediated by fumarate reductase in periplasm. Sci. Rep. 4, 1–7. https://doi.org/10.1038/srep03735

Li, H., Zhang, J., Wang, T., Luo, W., Zhou, Q., Jiang, G., 2008. Elemental selenium particles at nano-size (Nano-Se) are more toxic to Medaka (*Oryzias latipes*) as a consequence of hyper-accumulation of selenium: A comparison with sodium selenite. Aquat. Toxicol. 89 (4), 251–256. https://doi.org/10.1016/j.aquatox.2008.07.008

Li, X., Li, Y., Li, S., Zhou, W., Chu, H., Chen, W., Li, I.L., Tang, Z., 2005. Single crystalline trigonal selenium nanotubes and nanowires synthesized by sonochemical process. Cryst. Growth Des. 5 (3), 911–916. https://doi.org/10.1021/cg049681q

Libert, M., Bildstein, O., Esnault, L., Jullien, M., Sellier, R., 2011. Molecular hydrogen: an abundant energy source for bacterial activity in nuclear waste repositories. Phys. Chem. Earth. 36 (17-18), 1616-1623. https://doi.org/10.1016/j.pce.2011.10.010

Liu, Y., Alessi, D.S., Owttrim, G.W., Petrash, D.A., Mloszewska, A.M., Lalonde, S. V., Martinez, R.E., Zhou, Q., Konhauser, K.O., 2015. Cell surface reactivity of *Synechococcus* sp. PCC 7002: implications for metal sorption from seawater. Geochim. Cosmochim. Acta. 169, 30-44. https://doi.org/10.1016/j.gca.2015.07.033

Lloyd, J.R., 2003. Microbial reduction of metals and radionuclides. FEMS Microbiol. Rev. 27 (2-3), 411-425. https://doi.org/10.1016/S0168-6445(03)00044-5

López-Fernández, M., Cherkouk, A., Vilchez-Vargas, R., Merroun, M.L., 2015. Bacterial diversity in bentonites, engineered barrier for deep geological disposal of radioactive wastes. Microbial Ecology. 70 (4), 922-935. https://doi.org/10.1007/s00248-015-0630-7

López-Fernández, M., Fernández-Sanfrancisco, O., Moreno-García, A., Martín-Sánchez, I., Sánchez-Castro, I., Merroun, M.L., 2014. Microbial communities in bentonite formations and their interactions with uranium. Appl. Geochemistry 49, 77–86. https://doi.org/10.1016/j.apgeochem.2014.06.022

López-Fernández, M., Vilchez-Vargas, R., Jroundi, F., Boon, N., Pieper, D., Merroun, M.L., 2018a. Microbial community changes induced by uranyl nitrate in bentonite clay microcosms. Appl. Clay Sci. 160, 206-216. https://doi.org/10.1016/j.clay.2017.12.034

López-Fernández, M., Moll, H., Merroun, M.L., 2018b. Reversible pH-dependent curium(III) biosorption by the bentonite yeast isolate *Rhodotorula mucilaginosa* BII-R8. J. Hazard. Mater. 370, 156-163. https://doi.org/10.1016/j.jhazmat.2018.06.054

Losi, M.E., Frankenberger, W.T.J., 1998. Microbial oxidation and solubilization of precipitated elemental selenium in soil. J. Environ. Qual. 27 (4), 836-843. https://doi.org/10.2134/jeq1998.00472425002700040018x

Ludwig, W., Strunk, O., Westram, R., Richter, L., Meier, H., Yadhukumar, A., Buchner, A., Lai, T., Steppi, S., Jacob, G., Förster, W., Brettske, I., Gerber, S., Ginhart, A.W., Gross, O., Grumann, S., Hermann, S., Jost, R., König, A., Liss, T., Lüßbmann, R., May, M., Nonhoff, B., Reichel, B., Strehlow, R., Stamatakis, A.,

Stuckmann, N., Vilbig, A., Lenke, M., Ludwig, T., Bode, A., Schleifer, K.H., 2004. ARB: A software environment for sequence data. Nucleic Acids Res. 32 (4), 1363-1371. https://doi.org/10.1093/nar/gkh293

Lütke, L., 2013. Interaction of selected actinides (U, Cm) with bacteria relevant to nuclear waste disposal. Dissertation, TU Dresden. Available from: https://www.hzdr.de/FWR/DOCS/Publications/Dissertation_Laura_Luetke.pdf

Ma, B., Charlet, L., Fernandez-Martinez, A., Kang, M., Madé, B., 2018. Review of the retention mechanisms of redox-sensitive radionuclides in multi-barrier systems. Appl. Geochemistry. 100, 414-431. https://doi.org/10.1016/J.APGEOCHEM.2018.12.001

Maleke, M., Valverde, A., Vermeulen, J.-G., Cason, E., Gomez-Arias, A., Moloantoa, K., Coetsee-Hugo, L., Swart, H., van Heerden, E., Castillo, J., 2019. Biomineralization and Bioaccumulation of europium by a thermophilic metal resistant bacterium. Front. Microbiol. 10, 81. https://doi.org/10.3389/fmicb.2019.00081

Markai, S., Andrès, Y., Montavon, G., Grambow, B., 2003. Study of the interaction between europium (III) and *Bacillus subtilis*: fixation sites, biosorption modeling and reversibility 262 (2) 351–361. https://doi.org/10.1016/S0021-9797(03)00096-1

Mattox, D.M., 2010. Substrate ("Real") surfaces and surface modification, in: handbook of Physical Vapor Deposition (PVD) processing. Oxford, Elsevier, pp. 25-72. https://doi.org/10.1016/B978-0-8155-2037-5.00002-2

Maugeri, T.L., Lentini, V., Gugliandolo, C., Italiano, F., Cousin, S., Stackebrandt, E., 2009. Bacterial and archaeal populations at two shallow hydrothermal vents off Panarea Island (Eolian Islands, Italy). Extremophiles. 13 (1), 199–212. https://doi.org/10.1007/s00792-008-0210-6

McBroom, A.J., Kuehn, M.J., 2007. Release of outer membrane vesicles by Gram-negative bacteria is a novel envelope stress response. Mol. Microbiol. 63 (2), 545–558. https://doi.org/10.1111/j.1365-2958.2006.05522.x

Meier-Kolthoff, J.P., Auch, A.F., Klenk, H.P., Göker, M., 2013. Genome sequence-based species delimitation with confidence intervals and improved distance functions. BMC Bioinformatics. 14, 60. https://doi.org/10.1186/1471-2105-14-60

Meleshyn, A., 2011. Microbial Processes Relevant for Long-Term Performance of Radioactive Waste Repositories in Clays. Gesellschaft für Anlagen-und Reaktorsicherheit (GRS) mbH. GRS – 291. Available from: https://www.grs.de/sites/default/files/pdf/GRS-291.pdf.

Mercier, F., Alliot, C., Bion, L., Thromat, N., Toulhoat, P., 2006. XPS study of Eu(III) coordination compounds: Core levels binding energies in solid mixed-oxo-compounds EumXxOy. J. Electron Spectros. Relat. Phenomena. 150 (1), 21-26. https://doi.org/10.1016/j.elspec.2005.08.003

Merroun, M.L., Nedelkova, M., Ojeda, J.J., Reitz, T., Fernández, M.L., Arias, J.M., Romero-González, M., Selenska-Pobell, S., 2011. Bio-precipitation of uranium by two bacterial isolates recovered from extreme environments as estimated by potentiometric titration, TEM and X-ray absorption spectroscopic analyses. J. Hazard. Mater. 197, 1–10. https://doi.org/10.1016/j.jhazmat.2011.09.049

Merroun, M.L., Raff, J., Rossberg, A., Hennig, C., Reich, T., Selenska-Pobell, S., 2005. Complexation of uranium by cells and S-layer sheets of *Bacillus sphaericus* JG-A12. Appl. Environ. Microbiol. 71 (9), 5532-5543. https://doi.org/10.1128/AEM.71.9.5532-5543.2005

Merroun, M.L., Selenska-Pobell, S., 2008. Bacterial interactions with uranium: an environmental perspective. J. Contam. Hydrol. 102 (3-4), 285-295. https://doi.org/10.1016/j.jconhyd.2008.09.019

Miller, J., 1972. Experiments in molecular genetics. Cold Spring Harbor, NY: Cold Spring Harbor Laboratory.

Minaev, V. S., Timoshenkov, S.P., Kalugin, V. V., 2005. Structural and phase transformations in condensed selenium. J. Optoelectron. Adv. Mater. 7 (4) , 1717–1741.

Mishra, A., Malik, A., 2013. Recent advances in microbial metal bioaccumulation. Crit. Rev. Environ. Sci. Technol. 43 (11), 1162-1222. https://doi.org/10.1080/10934529.2011.627044

Moll, H., Glorius, M., Barkleit, A., Rossberg, A., Bernhard, G., 2009. The mobilization of actinides by microbial ligands taking into consideration the final storage of nuclear waste: Interactions of Selected Actinides U(VI),

Cm(III), and Np(V) with Pyoverdins Secreted by Pseudomonas fluorescens and Related Model Compounds. Forschungszentrum Dresden-Rossendorf, Dresden. Final Report BMBF Project No.: 02E9985. Available from: http://hzdr.qucosa.de/api/qucosa%3A21603/attachment/ATT-0/

Moll, H., Lütke, L., Bachvarova, V., Cherkouk, A., Selenska-Pobell, S., Bernhard, G., 2014b. Interactions of the Mont Terri Opalinus Clay Isolate *Sporomusa* sp. MT-2.99 with Curium(III) and Europium(III). Geomicrobiol. J. 31 (8), 682–696. https://doi.org/10.1080/01490451.2014.889975

Moll, H., Lütke, L., Barkleit, A., Bernhard, G., 2013. Curium(III) speciation studies with cells of a groundwater strain of *Pseudomonas fluorescens*. Geomicrobiol. J. 30 (4), 337-346. https://doi.org/10.1080/01490451.2012.688927

Moore, E.R.B., Krüger, A.S., Hauben, L., Seal, S.E., De Baere, R., De Wachter, R., Timmis, K.N., Swings, J., 1997. 16s rRNA gene sequence analyses and inter- and intrageneric relationships of *Xanthomonas* species and *Stenotrophomonas maltophilia*. FEMS Microbiol. Lett. 151 (2), 145-53. https://doi.org/10.1016/S0378-1097(97)00152-3

Nakamoto, K., 2008. Infrared and raman spectra of inorganic and coordination compounds: part B: applications in coordination, organometallic, and bioinorganic chemistry, Sixth Edit. ed, Infrared and Raman Spectra of Inorganic and Coordination Compounds: Part B: Applications in Coordination, Organometallic, and Bioinorganic Chemistry. https://doi.org/10.1002/9780470405888

Nakayama, T., Homma, Y., Hashidoko, Y., Mizutani, J., Tahara, S., 1999. Possible role of xanthobaccins produced by *Stenotrophomonas* sp. strain SB-K88 in suppression of sugar beet damping-off disease. Appl. Environ. Microbiol. 65 (10), 4334–4339.

Nancharaiah, Y. V., Lens, P.N.L., 2015. Ecology and biotechnology of selenium-respiring bacteria. Microbiol. Mol. Biol. Rev. 79 (1), 61-80. https://doi.org/10.1128/mmbr.00037-14

Naumann, D., 2000. Infrared Spectroscopy in Microbiology in: Meyers R. A., (Ed.). Encyclopedia of Analytical Chemistry. Chichester, John Wiley & Sons Ltd, pp. 102–131.

NEA, 2015. Nuclear Technology Roadmap: Nuclear Energy. Paris, Nuclear Energy Agency. Available from: https://www.oecd-nea.org/pub/techroadmap/techroadmap-2015.pdf

NEA, 2010. Radioactive Waste in Perspective. Paris, Nuclear Energy Agency. Available from: https://www.oecd-nea.org/ndd/pubs/2010/6350-waste-perspective.pdf

Nei, M., Kumar, S., 2000. Molecular Evolution and Phylogenetics, New York. Oxford University Press.

Newsome, L., Morris, K., Lloyd, J.R., 2015. Uranium biominerals precipitated by an environmental isolate of *Serratia* under anaerobic conditions. PLoS One. 10 (7), e0132392. https://doi.org/10.1371/journal.pone.0132392

Newsome, L., Morris, K., Lloyd, J.R., 2014. The biogeochemistry and bioremediation of uranium and other priority radionuclides. Chem. Geol. 363, 164-184. https://doi.org/10.1016/j.chemgeo.2013.10.034

Ngwenya, B.T., Sutherland, I.W., Kennedy, L., 2003. Comparison of the acid-base behaviour and metal adsorption characteristics of a gram-negative bacterium with other strains. Appl. Geochemistry. 18 (4), 527-538. https://doi.org/10.1016/S0883-2927(02)00118-X

Ni, T.W., Staicu, L.C., Nemeth, R.S., Schwartz, C.L., Crawford, D., Seligman, J.D., Hunter, W.J., Pilon-Smits, E.A.H., Ackerson, C.J., 2015. Progress toward clonable inorganic nanoparticles. Nanoscale. 7 (41), 17320–17327. https://doi.org/10.1039/C5NR04097C

Niba, E.T.E., Naka, Y., Nagase, M., Mori, H., Kitakawa, M., 2007. A genome-wide approach to identify the genes involved in biofilm formation in *E. coli*. DNA Res. 14 (6), 237–246. https://doi.org/10.1093/dnares/dsm024

Ojeda, J.J., Romero-González, M.E., Bachmann, R.T., Edyvean, R.G.J., Banwart, S.A., 2008. Characterization of the cell surface and cell wall chemistry of drinking water bacteria by combining XPS, FTIR spectroscopy, modeling, and potentiometric titrations. Langmuir. 24 (8), 4032–4040. https://doi.org/10.1021/la702284b

Omoike, A., Chorover, J., 2004. Spectroscopic study of extracellular polymeric substances from *Bacillus subtilis*: Aqueous chemistry and adsorption effects. Biomacromolecules. 5 (4), 1219-1230.

https://doi.org/10.1021/bm034461z

Ormerod, R.M., 2001. Surface chemistry: electron yield spectroscopy. Encycl. Mater. Sci. Technol. pp. 9006–9008. https://doi.org/10.1016/B0-08-043152-6/01623-5

Ozaki, T., Gillow, J.B., Kimura, T., Ohnuki, T., Yoshida, Z., Francis, A.J., 2004. Sorption behavior of europium(III) and curium(III) on the cell surfaces of microorganisms, in: Radiochimica Acta. 92 (9-11), 741–748. https://doi.org/10.1524/ract.92.9.741.55006

Pages, D., Rose, J., Conrod, S., Cuine, S., Carrier, P., Heulin, T., Achouak, W., 2008. Heavy metal tolerance in *Stenotrophomonas maltophilia*. PLoS One. 3 (2), e1539. https://doi.org/10.1371/journal.pone.0001539

Palleroni N.J., Bradbury J.F., 1993. *Stenotrophomonas*, a new bacterial genus for *Xanthomonas maltophilia* (Hugh 1980) Swings et al.1983. Int. J. Syst. Bacteriol. 43, 606-609. https://doi.org/10.1099/00207713-43-3-606

Paterson-Beedle, M., Macaskie, L.E., Lee, C.H., Hriljac, J.A., Jee, K.Y., Kim, W.H., 2006. Utilisation of a hydrogen uranyl phosphate-based ion exchanger supported on a biofilm for the removal of cobalt, strontium and caesium from aqueous solutions. Hydrometallurgy. 83 (1-4), 141-145. https://doi.org/10.1016/j.hydromet.2006.03.020

Patil, P.P., Midha, S., Kumar, S., Patil, P.B., 2016. Genome sequence of type strains of genus *Stenotrophomonas*. Front. Microbiol. 7, 309. https://doi.org/10.3389/fmicb.2016.00309

Pearce, C.I., Coker, V.S., Charnock, J.M., Pattrick, R.A.D., Mosselmans, J.F.W., Law, N., Beveridge, T.J., Lloyd, J.R., 2008. Microbial manufacture of chalcogenide-based nanoparticles via the reduction of selenite using *Veillonella atypica*: An in situ EXAFS study. Nanotechnology. 19 (15), 155603. https://doi.org/10.1088/0957-4484/19/15/155603

Pearce, C.I., Pattrick, R.A.D., Law, N., Charnock, J.M., Coker, V.S., Fellowes, J.W., Oremland, R.S., Lloyd, J.R., 2009. Investigating different mechanisms for biogenic selenite transformations: *Geobacter sulfurreducens*, *Shewanella oneidensis* and *Veillonella atypica*. Environ. Technol. 30 (12), 1313-1326. https://doi.org/10.1080/09593330902984751

Pedersen, K., 2013. Metabolic activity of subterranean microbial communities in deep granitic groundwater supplemented with methane and H_2. ISME J. 7, 839–849. https://doi.org/10.1038/ismej.2012.144

Pedersen, K., Nilsson, E., Arlinger, J., Hallbeck, L., O'Neill, A., 2004. Distribution, diversity and activity of microorganisms in the hyper-alkaline spring waters of Maqarin in Jordan. Extremophiles. 8 (2), 151–164. https://doi.org/10.1007/s00792-004-0374-7

Picot, J., Guerin, C.L., Le Van Kim, C., Boulanger, C.M., 2012. Flow cytometry: retrospective, fundamentals and recent instrumentation. Cytotechnology. 64 (2), 109-30. https://doi.org/10.1007/s10616-011-9415-0

Plette, A.C.C., van Riemsdijk, W.H., Benedetti, M.F., van der Wal, A., 1995. pH dependent charging behavior of isolated cell walls of a gram-positive soil bacterium. J. Colloid Interface Sci. 173 (2), 354-363. https://doi.org/10.1006/jcis.1995.1335

Popov, A., 1976. Correlation between the molecular structure and properties of amorphous selenium. J. Phys. C Solid State Phys. 9 (24), 675. https://doi.org/10.1088/0022-3719/9/24/001

Porcelli, D., 2018. Radioactivity. In: White W.M. (Ed.) Encyclopedia of Geochemistry: A Comprehensive Reference Source on the Chemistry of the Earth. Cham: Springer International Publishing. pp. 1295-1298. Available from: https://doi.org/10.1007/978-3-319-39312-4_269

Pradier, C.M., Rubio, C., Poleunis, C., Bertrand, P., Marcus, P., Compère, C., 2005. Surface characterization of three marine bacterial strains by fourier transform IR, X-ray photoelectron spectroscopy, and time-of-flight secondary-ion mass spectrometry, correlation with adhesion on stainless steel surfaces. J. Phys. Chem. B. 109 (19), 9540-9549. https://doi.org/10.1021/jp044705p

Prakash, D., Gabani, P., Chandel, A.K., Ronen, Z., Singh, O. V., 2013. Bioremediation: a genuine technology to remediate radionuclides from the environment. Microb. Biotechnol. 6 (4), 349-360. https://doi.org/10.1111/1751-7915.12059

Prakash, N.T., Sharma, N., Prakash, R., Raina, K.K., Fellowes, J., Pearce, C.I., Lloyd, J.R., Pattrick, R.A.D., 2009. Aerobic microbial manufacture of nanoscale selenium: exploiting nature's bio-nanomineralization potential.

Biotechnol. Lett. 31, 1857–1862. https://doi.org/10.1007/s10529-009-0096-0

Prăvălie, R., Bandoc, G., 2018. Nuclear energy: between global electricity demand, worldwide decarbonisation imperativeness, and planetary environmental implications. J. Environ. Manage. 209, 81–92. https://doi.org/10.1016/j.jenvman.2017.12.043

Prigent-Combaret, C., Vidal, O., Dorel, C., Lejeune, P., 1999. Abiotic surface sensing and biofilm-dependent regulation of gene expression in *Escherichia coli*. J. Bacteriol. 181 (19), 5993-6002.

Pruesse, E., Peplies, J., Glöckner, F.O., 2012. SINA: Accurate high-throughput multiple sequence alignment of ribosomal RNA genes. Bioinformatics. 28 (14), 1823-1829. https://doi.org/10.1093/bioinformatics/bts252

Ramos, P.L., Van Trappen, S., Thompson, F.L., Rocha, R.C.S., Barbosa, H.R., de Vos, P., Moreira-Filho, C.A., 2011. Screening for endophytic nitrogen-fixing bacteria in Brazilian sugar cane varieties used in organic farming and description of *Stenotrophomonas Pavanii* sp. nov. Int. J. Syst. Evol. Microbiol. 61 (Pt 4), 926-931 https://doi.org/10.1099/ijs.0.019372-0

Ranjard, L., Nazaret, S., Cournoyer, B., 2003. Freshwater bacteria can methylate selenium through the thiopurine methyltransferase pathway. Appl. Environ. Microbiol. 69 (7), 3784–3790. https://doi.org/10.1128/AEM.69.7.3784-3790.2003

Rauschenbach, I., Posternak, V., Cantarella, P., McConnell, J., Starovoytov, V., Häggblom, M.M., 2013. *Seleniivibrio woodruffii* gen. nov., sp. nov., a selenate- and arsenate-respiring bacterium in the *Deferribacteraceae*. Int. J. Syst. Evol. 63 (Pt 10), 3659-3665. Microbiol. https://doi.org/10.1099/ijs.0.043547-0

Ravel, B., Newville, M., 2005. ATHENA, ARTEMIS, HEPHAESTUS: Data analysis for X-ray absorption spectroscopy using IFEFFIT. J. Synchrotron Radiat. 12, 537–541. https://doi.org/10.1107/S0909049505012719

Reamer, D.C., Zoller, W.H., 1980. Selenium biomethylation products from soil and sewage sludge. Science. 208 (4443), 500–502. https://doi.org/10.1126/science.208.4443.500

Reasoner, D.J., Geldreich, E.E., 1985. A new medium for the enumeration and subculture of bacteria from potable water. Appl. Environ. Microbiol. 49 (1), 1-7.

Reitz, T., Merroun, M.L., Rossberg, A., Steudtner, R., Selenska-Pobell, S., 2011. Bioaccumulation of U(VI) by *Sulfolobus acidocaldarius* under moderate acidic conditions. Radiochim. Acta. 99 (9), 543-554. https://doi.org/10.1524/ract.2011.1848

Reitz, T., Rossberg, A., Barkleit, A., Steudtner, R., Selenska-Pobell, S., Merroun, M.L., 2015. Spectroscopic study on uranyl carboxylate complexes formed at the surface layer of *Sulfolobus acidocaldarius*. Dalt. Trans. 44 (6), 2684-2692. https://doi.org/10.1039/c4dt02555e

Richter, M., Rossello-Mora, R., 2009. Shifting the genomic gold standard for the prokaryotic species definition. Proc. Natl. Acad. Sci. 106 (45), 19126-19131. https://doi.org/10.1073/pnas.0906412106

Rizoulis, A., Steele, H.M., Morris, K., Lloyd, J.R., 2012. The potential impact of anaerobic microbial metabolism during the geological disposal of Intermediate-level waste. Mineral. Mag. 76 (8), 3261–3270. https://doi.org/10.1180/minmag.2012.076.8.39

Rockström, J., Steffen, W., Noone, K., Persson, Å., Chapin, F.S., Lambin, E.F., Lenton, T.M., Scheffer, M., Folke, C., Schellnhuber, H.J., Nykvist, B., de Wit, C.A., Hughes, T., van der Leeuw, S., Rodhe, H., Sörlin, S., Snyder, P.K., Costanza, R., Svedin, U., Falkenmark, M., Karlberg, L., Corell, R.W., Fabry, V.J., Hansen, J., Walker, B., Liverman, D., Richardson, K., Crutzen, P., Foley, J.A., 2009. A safe operating space for humanity. Nature. 461, 472-475. https://doi.org/10.1038/461472a

Rossbach, S., Wilson, T.L., Kukuk, M.L., Carty, H.A., 2000. Elevated zinc induces siderophore biosynthesis genes and a *zntA*-like gene in *Pseudomonas fluorescens*. FEMS Microbiol. Lett. 191 (1), 61–70. https://doi.org/10.1016/S0378-1097(00)00371-2

Roux, M., Sarret, G., Pignot-Paintrand, I., Fontecave, M., Coves, J., 2001. Mobilization of selenite by *Ralstonia metallidurans* CH34. Appl. Environ. Microbiol. 67 (2), 769–773. https://doi.org/10.1128/AEM.67.2.769-773.2001

Rui, X., Kwon, M.J., O'Loughlin, E.J., Dunham-Cheatham, S., Fein, J.B., Bunker, B., Kemner, K.M., Boyanov, M.I., 2013. Bioreduction of hydrogen uranyl phosphate: Mechanisms and U(IV) products. Environ. Sci. Technol. 47 (11), 5668–5678. https://doi.org/10.1021/es305258p

Ruiz-Fresneda, M.A., Delgado Martín, J., Gómez Bolívar, J., Fernández Cantos, M. V., Bosch-Estévez, G., Martínez Moreno, M.F., Merroun, M.L., 2018. Green synthesis and biotransformation of amorphous Se nanospheres to trigonal 1D Se nanostructures: Impact on Se mobility within the concept of radioactive waste disposal. Environ. Sci. Nano. 5, 2103–2116. https://doi.org/10.1039/c8en00221e

Rupp, H., Weser, U., 1975. X-ray photoelectron spectroscopy of some selenium containing amino acids. Bioinorg. Chem. 5 (1), 21–32. https://doi.org/10.1016/S0006-3061(00)80217-3

Ryan, R.P., Monchy, S., Cardinale, M., Taghavi, S., Crossman, L., Avison, M.B., Berg, G., van der Lelie, D., Dow, J.M., 2009. The versatility and adaptation of bacteria from the genus *Stenotrophomonas*. Nat. Rev. Microbiol. 7, 514–25. https://doi.org/10.1038/nrmicro2163

Sabaty, M., Avazeri, C., Pignol, D., Vermeglio, A., 2001. Characterization of the reduction of selenate and tellurite by nitrate reductases. Appl. Environ. Microbiol. 67 (11), 5122–5126. https://doi.org/10.1128/AEM.67.11.5122-5126.2001

Saito, T., Aoyagi, N., Kimura, T., 2015. Time-resolved laser-induced fluorescence spectroscopy combined with parallel factor analysis: a robust speciation technique for UO_2^{2+}. J. Radioanal. Nucl. Chem. 303 (2), 1129–1132. https://doi.org/10.1007/s10967-014-3465-7

Saito, T., Sao, H., Ishida, K., Aoyagi, N., Kimura, T., Nagasaki, S., Tanaka, S., 2010. Application of parallel factor analysis for time-resolved laser fluorescence spectroscopy: implication for metal speciation study. Environ. Sci. Technol. 44 (13), 5055–5060. https://doi.org/10.1021/es9036995

Sánchez-Castro, I., Ruiz-Fresneda, M.A., Bakkali, M., Kämpfer, P., Glaeser, S.P., Busse, H.J., López-Fernández, M., Martínez-Rodríguez, P., Merroun, M.L., 2017a. *Stenotrophomonas bentonitica* sp. nov., isolated from bentonite formations. Int. J. Syst. Evol. Microbiol. 67 (8), 2779–2786. https://doi.org/10.1099/ijsem.0.002016

Sánchez-Castro, I., Bakkali, M., Merroun, M.L., 2017b. Draft genome sequence of *Stenotrophomonas bentonitica* BII-R7, a selenite-reducing bacterium isolated from Spanish bentonites. Genome Announc. 5 (31), e00719-17. https://doi.org/10.1128/genomeA.00719-17

Sarathchandra, S.U., Watkinson, J.H., 1981. Oxidation of elemental selenium to selenite by *Bacillus megaterium*. 211 (4482), 600-601. Science. https://doi.org/10.1126/science.6779378

Scheinost, A.C., Charlet, L., 2008. Selenite reduction by mackinawite, magnetite and siderite: XAS characterization of nanosized redox products. Environ. Sci. Technol. 42 (6), 1984-1989. https://doi.org/10.1021/es071573f

Schlegel, M.L., Necib, S., Daumas, S., Blanc, C., Foy, E., Trcera, N., Romaine, A., 2016. Microstructural characterization of carbon steel corrosion in clay borehole water under anoxic and transient acidic conditions. Corros. Sci. 109, 126-144. https://doi.org/10.1016/j.corsci.2016.03.022

Schmitt, J., Flemming, H.C., 1998. FTIR-spectroscopy in microbial and material analysis. Int. Biodeterior. Biodegrad. 41 (1), 1-11. https://doi.org/10.1016/S0964-8305(98)80002-4

Schnohr, C.S., Ridgway, M.C., 2015. Introduction to X-Ray Absorption Spectroscopy, in: Schnohr, C.S., Ridgway, M.C. (Eds.). X-Ray Absorption Spectroscopy of Semiconductors. Heildelberg, Springer, Series in Optical Sciences, 355p. https://doi.org/10.1007/978-3-662-44362-0

Senior, N., Newman, R., Wang, S., Diomidis, N., 2017. Understanding and quantifying the anoxic corrosion of carbon steel in a Swiss L/ILW repository environment. Corros. Eng. Sci. Technol. 52 (Suppl 1), 78-83. https://doi.org/10.1080/1478422X.2017.1303102

Sharma, J., Beard, B.C., 1990. Fundamentals of X-ray Photoelectron Spectroscopy (XPS) and its applications to explosives and propellants, in: Bulusu, S.N. (Ed.), Chemistry and Physics of Energetic Materials. Netherlands, Dordrecht, Springer, pp. 569–585. https://doi.org/10.1007/978-94-009-2035-4_25

Shin, Y., Blackwood, J.M., Bae, I.T., Arey, B.W., Exarhos, G.J., 2007. Synthesis and stabilization of selenium nanoparticles on cellulose nanocrystal. Mater. Lett. 61 (21), 4297–4300. https://doi.org/10.1016/j.matlet.2007.01.091

Shukla, A., Parmar, P., Saraf, M., 2017. Radiation, radionuclides and bacteria: an in-perspective review. J. Environ. Radioact. 180, 27–35. https://doi.org/10.1016/j.jenvrad.2017.09.013

Sitaud, B., Solari, P.L., Schlutig, S., Llorens, I., Hermange, H., 2012. Characterization of radioactive materials using the MARS beamline at the synchrotron SOLEIL. J. Nucl. Mater. 425 (1-3), 238–243. https://doi.org/10.1016/j.jnucmat.2011.08.017

Skoog, D.A., Holler, F.J., Crouch, S.R., 2007. Principles of Instrumental Analysis. Belmont, Thomson Brooks Cole.

Smart, N.R., Rance, A.P., Reddy, B., Hallbeck, L., Pedersen, K., Johansson, A.J., 2014. *In situ* evaluation of model copper-cast iron canisters for spent nuclear fuel: a case of microbiologically influenced corrosion (MIC). Corros. Eng. Sci. Technol. 49 (6), 548-553. https://doi.org/10.1179/1743278214Y.0000000213

Smart, N.R., Reddy, B., Rance, A.P., Nixon, D.J., Frutschi, M., Bernier-Latmani, R., Diomidis, N., 2017. The anaerobic corrosion of carbon steel in compacted bentonite exposed to natural Opalinus Clay porewater containing native microbial populations. Corros. Eng. Sci. Technol. 52 (Suppl 1), 101-112. https://doi.org/10.1080/1478422X.2017.1315233

Smith, S.L., Boothman, C., Williams, H.A., Ellis, B.L., Wragg, J., West, J.M., Lloyd, J.R., 2017. Microbial impacts on ^{99m}Tc migration through sandstone under highly alkaline conditions relevant to radioactive waste disposal. Sci. Total Environ. 575, 485–495. https://doi.org/10.1016/j.scitotenv.2016.08.126

Solari, P.L., Schlutig, S., Hermange, H., Sitaud, B., 2009. MARS, a new beamline for radioactive matter studies at SOLEIL. J. Phys. Conf. Ser. 190 (1), 012042. https://doi.org/10.1088/1742-6596/190/1/012042

Song, D., Li, X., Cheng, Y., Xiao, X., Lu, Z., Wang, Y., Wang, F., 2017. Aerobic biogenesis of selenium nanoparticles by *Enterobacter cloacae* Z0206 as a consequence of fumarate reductase mediated selenite reduction. Sci. Rep. 7, 3239. https://doi.org/10.1038/s41598-017-03558-3

Sonkusre, P., Nanduri, R., Gupta, P., Cameotra, S.S., 2014. Improved extraction of intracellular biogenic selenium nanoparticles and their specificity for cancer chemoprevention. J. Nanomed. Nanotechnol. 5 (2), 194. https://doi.org/10.4172/2157-7439.1000194

Srivastava, N., Mukhopadhyay, M., 2013. Biosynthesis and structural characterization of selenium nanoparticles mediated by *Zooglea ramigera*. Powder Technol. 244, 26–29. https://doi.org/10.1016/j.powtec.2013.03.050

Stackebrandt, E., Frederiksen, W., Garrity, G.M., Grimont, P.A.D., Kämpfer, P., Maiden, M.C.J., Nesme, X., Rosselló-Mora, R., Swings, J., Trüper, H.G., Vauterin, L., Ward, A.C., Whitman, W.B., 2002. Report of the ad hoc committee for the re-evaluation of the species definition in bacteriology. Int. J. Syst. Evol. Microbiol. 52 (Pt 3), 1043-1047. https://doi.org/10.1099/00207713-52-3-1043

Staicu, L.C., Ackerson, C.J., Cornelis, P., Ye, L., Berendsen, R.L., Hunter, W.J., Noblitt, S.D., Henry, C.S., Cappa, J.J., Montenieri, R.L., Wong, A.O., Musilova, L., Sura-de Jong, M., van Hullebusch, E.D., Lens, P.N.L., Reynolds, R.J.B., Pilon-Smits, E.A.H., 2015. *Pseudomonas moraviensis* subsp. stanleyae, a bacterial endophyte of hyperaccumulator *Stanleya pinnata*, is capable of efficient selenite reduction to elemental selenium under aerobic conditions. J. Appl. Microbiol. 119 (2), 400–410. https://doi.org/10.1111/jam.12842

Stamatakis, A., 2006. RAxML-VI-HPC: Maximum likelihood-based phylogenetic analyses with thousands of taxa and mixed models. Bioinformatics. 22 (21), 2688-2690. https://doi.org/10.1093/bioinformatics/btl446

Stolz, A., Busse, H.J., Kämpfer, P., 2007. *Pseudomonas knackmussii* sp. nov. Int. J. Syst. Evol. Microbiol. 57 (Pt 3), 572-576. https://doi.org/10.1099/ijs.0.64761-0

Stroes-Gascoyne, S., Hamon, C.J., Dixon, D.A., Martino, J.B., 2007. Microbial analysis of samples from the tunnel sealing experiment at AECL's Underground Research Laboratory. Phys. Chem. Earth 32 (1-7), 219–231. https://doi.org/10.1016/j.pce.2006.01.002

Stubberfield, L.C.F., Shaw, P.J.A., 1990. A comparison of tetrazolium reduction and FDA hydrolysis with other measures of microbial activity. J. Microbiol. Methods. 12 (3-4), 151–162. https://doi.org/10.1016/0167-7012(90)90026-3

Stylo, M., Neubert, N., Roebbert, Y., Weyer, S., Bernier-Latmani, R., 2015. Mechanism of uranium reduction and immobilization in *Desulfovibrio vulgaris* Biofilms. Environ. Sci. Technol. 49 (17), 10553-10561. https://doi.org/10.1021/acs.est.5b01769

Svensson-Stadler, L.A., Mihaylova, S.A., Moore, E.R.B., 2012. *Stenotrophomonas* interspecies differentiation and identification by *gyrB* sequence analysis. FEMS Microbiol. Lett. 327 (1), 15-24. https://doi.org/10.1111/j.1574-6968.2011.02452.x

Tabak, H.H., Lens, P., Van Hullebusch, E.D., Dejonghe, W., 2005. Developments in bioremediation of soils and sediments polluted with metals and radionuclides - 1. Microbial processes and mechanisms affecting bioremediation of metal contamination and influencing metal toxicity and transport. Rev. Environ. Sci. Biotechnol. 4 (3), 115–156. https://doi.org/10.1007/s11157-005-2169-4

Tackett, J.E., 1989. FT-IR characterization of metal acetates in aqueous solution. Appl. Spectrosc. 43 (3), 483-489. https://doi.org/10.1366/0003702894202931

Tam, K., Ho, C.T., Lee, J.-H., Lai, M., Chang, C.H., Rheem, Y., Chen, W., Hur, H.-G., Myung, N. V., 2010. Growth mechanism of amorphous selenium nanoparticles synthesized by *Shewanella* sp. HN-41. Biosci. Biotechnol. Biochem. 74 (4), 696-700. https://doi.org/10.1271/bbb.90454

Tan, Y., Wang, Yuantao, Wang, Yu, Xu, D., Huang, Y., Wang, D., Wang, G., Rensing, C., Zheng, S., 2018. Novel mechanisms of selenate and selenite reduction in the obligate aerobic bacterium *Comamonas testosteroni* S44. J. Hazard. Mater. 359, 129-138. https://doi.org/10.1016/j.jhazmat.2018.07.014

Tan, Y., Yao, R., Wang, R., Wang, D., Wang, G., Zheng, S., 2016. Reduction of selenite to Se(0) nanoparticles by filamentous bacterium *Streptomyces* sp. ES2-5 isolated from a selenium mining soil. Microb. Cell Fact. 15 (1), 157. https://doi.org/10.1186/s12934-016-0554-z

Texier, A.C., Andrés, Y., Illemassene, M., Le Cloirec, P., 2000. Characterization of lanthanide ions binding sites in the cell wall of *Pseudomonas aeruginosa*. Environ. Sci. Technol. 34 (4), 610–615. https://doi.org/10.1021/es990668h

Tindall, B.J., 1990a. A Comparative Study of the Lipid Composition of *Halobacterium saccharovorum* from Various Sources. Syst. Appl. Microbiol. 13 (2), 128-130. https://doi.org/10.1016/S0723-2020(11)80158-X

Tindall, B.J., 1990b. Lipid composition of *Halobacterium lacusprofundi*. FEMS Microbiol. Lett. 66 (1-3), 199-202. https://doi.org/10.1016/0378-1097(90)90282-U

Tišáková, L., Pipíška, M., Godány, A., Horník, M., Vidová, B., Augustín, J., 2013. Bioaccumulation of ^{137}Cs and ^{60}Co by bacteria isolated from spent nuclear fuel pools. J. Radioanal. Nucl. Chem. 295 (1), 737–748. https://doi.org/10.1007/s10967-012-1932-6

Toyofuku, M., Nomura, N., Eberl, L., 2019. Types and origins of bacterial membrane vesicles. Nat. Rev. Microbiol. 17, 13-24. https://doi.org/10.1038/s41579-018-0112-2

Turner, B.F., Fein, J.B., 2006. Protofit: A program for determining surface protonation constants from titration data. Comput. Geosci. 32 (9), 1344–1356. https://doi.org/10.1016/j.cageo.2005.12.005

UNSCEAR, 2013. Sources, effects and risks of ionizing radiation: Report to the General Assembly with Scientific Annexes. UNSCEAR 2013 Report. New York, United Nations, 2014. Available from: http://www.unscear.org/unscear/en/publications/2013_1.html

Van Der Mei, H.C., De Vries, J., Busscher, H.J., 2000. X-ray photoelectron spectroscopy for the study of microbial cell surfaces. Surf. Sci. Rep. 39 (1), 1-24. https://doi.org/10.1016/S0167-5729(00)00003-0

Videla, H.A., Herrera, L.K., 2009. Understanding microbial inhibition of corrosion. A comprehensive overview. Int. Biodeterior. Biodegrad. 63 (7), 896-900. https://doi.org/10.1016/j.ibiod.2009.02.002

Villar, M.V., Pérez del Villar, L., Martín, P.L., Pelayo, M., Fernández, A.M., Garralon, A., Cuevas, J., Leguey, S., Caballero, E., Huertas, F., Jimenez de Cisneros, C., Linares, J., Reyes, E., Delgado, A., Fernandez-Soler, J.M., Astudillo, J., 2006. The study of Spanish clays for their use as sealing materials in nuclear waste repositories : 20 years of progress. J. Iber. Geol. 32, 15–36.

Vogel, M., Fischer, S., Maffert, A., Hübner, R., Scheinost, A.C., Franzen, C., Steudtner, R., 2018. Biotransformation and detoxification of selenite by microbial biogenesis of selenium-sulfur nanoparticles. J. Hazard. Mater. 344, 749–757. https://doi.org/10.1016/j.jhazmat.2017.10.034

Von Schenck, H., Källström, K., 2014. Reactive transport modelling of organic complexing agents in cement

stabilized low and intermediate level waste. Phys. Chem. Earth. 70-71, 114-126. https://doi.org/10.1016/j.pce.2013.11.005

Vuori, S., 1995. The environmental and ethical basis of the geological disposal of long-lived radioactive waste. ATS Ydintekniikka, 24(3), 16-17.

Wadhwani, S.A., Shedbalkar, U.U., Singh, R., Chopade, B.A., 2016. Biogenic selenium nanoparticles: current status and future prospects. Appl. Microbiol. Biotechnol. 100 (6), 2555-2566. https://doi.org/10.1007/s00253-016-7300-7

Walczak, I., Libert, M.-F., Camaro, S., Blanchard, J.-M., 2001. Quantitative and qualitative analysis of hydrosoluble organic matter in bitumen leachates. Agronomie. 21 (3), 247-257. https://doi.org/10.1051/agro:2001121

Wang, F., Li, D., Mao, C., 2008. Genetically modifiable flagella as templates for silica fibers: from hybrid nanotubes to 1D periodic nanohole arrays. Adv. Funct. Mater. 18 (24), 4007–4013. https://doi.org/10.1002/adfm.200800889

Wang, T., Yang, L., Zhang, B., Liu, J., 2010. Extracellular biosynthesis and transformation of selenium nanoparticles and application in H_2O_2 biosensor. Colloids Surfaces B Biointerfaces. 80 (1), 94–102. https://doi.org/10.1016/j.colsurfb.2010.05.041

Wang, Y., Shu, X., Zhou, Q., Fan, T., Wang, T., Chen, X., Li, M., Ma, Y., Ni, J., Hou, J., Zhao, W., Li, R., Huang, S., Wu, L., 2018. Selenite reduction and the biogenesis of selenium nanoparticles by *Alcaligenes faecalis* Se03 isolated from the gut of *Monochamus alternatus* (Coleoptera: Cerambycidae). Int. J. Mol. Sci. 19 (9), 2799. https://doi.org/10.3390/ijms19092799

Wayne, L., Moore, W.E.C., Stackebrandt, E., Kandler, O., Colwell, R.R., Krichevsky, M.I., Truper, H.G., Murray, R.G.E., Wayne, L.G., Grimont, P.A.D., Brenner, D.J., Starr, M.P., Moore, L.H., 1987. Report of the Ad Hoc Committee on Reconciliation of Approaches to Bacterial Systematics. Int. J. Syst. Evol. Microbiol. 37 (4), 463–464. https://doi.org/10.1099/00207713-37-4-463

Williamson, A.J., Morris, K., Law, G.T.W., Rizoulis, A., Charnock, J.M., Lloyd, J.R., 2014. Microbial reduction of U(VI) under alkaline conditions: Implications for radioactive waste geodisposal. Environ. Sci. Technol. 48 (22), 13549–13556. https://doi.org/10.1021/es5017125

Wolf, A., Fritze, A., Hagemann, M., Berg, G., 2002. *Stenotrophomonas rhizophila* sp. nov., a novel plant-associated bacterium with antifungal properties. Int. J. Syst. Evol. Microbiol. 52 (Pt 6), 1937-1944. https:// doi.org/10.1099/00207713-52-6-1937

Xu, Di., Yang, L., Wang, Y., Wang, G., Rensing, C., Zheng, S., 2018. Proteins enriched in charged amino acids control the formation and stabilization of selenium nanoparticles in *Comamonas testosteroni* S44. Sci. Rep. 8, 4766. https://doi.org/10.1038/s41598-018-23295-5

Yamada, A., Miyashita, M., Inoue, K., Matsunaga, T., 1997. Extracellular reduction of selenite by a novel marine photosynthetic bacterium. Appl. Microbiol. Biotechnol. 48 (3), 367–372. https://doi.org/10.1007/s002530051064

Yang, H.C., Im, W.T., Kang, M.S., Shin, D.Y., Lee, S.T., 2006. *Stenotrophomonas koreensis* sp. nov., isolated from compost in South Korea. Int. J. Syst. Evol. Microbiol. 56 (Pt 1), 81-84. https://doi.org/10.1099/ijs.0.63826-0

Yang, T., Chen, M.L., Wang, J.H., 2015. Genetic and chemical modification of cells for selective separation and analysis of heavy metals of biological or environmental significance. TrAC - Trends Anal. Chem. 66, 90-102. https://doi.org/10.1016/j.trac.2014.11.016

Yao, T., Wu, X., Chen, X., Xiao, Y., Zhang, Y., Zhao, Y., Li, F., 2016. Biosorption of Eu(III) and U(VI) on *Bacillus subtilis*: Macroscopic and modeling investigation. J. Mol. Liq. 219, 32-38. https://doi.org/10.1016/j.molliq.2016.01.101

Yarza, P., Richter, M., Peplies, J., Euzeby, J., Amann, R., Schleifer, K.H., Ludwig, W., Glöckner, F.O., Rosselló-Móra, R., 2008. The All-Species Living Tree project: A 16S rRNA-based phylogenetic tree of all sequenced type strains. Syst. Appl. Microbiol. 31 (4), 241-250. https://doi.org/10.1016/j.syapm.2008.07.001

Yee, N., Benning, L.G., Phoenix, V.R., Ferris, F.G., 2004. Characterization of metal-cyanobacteria sorption reactions: a combined macroscopic and infrared spectroscopic investigation. Environ. Sci. Technol. 38 (3), 775-782. https://doi.org/10.1021/es0346680

Yee, N., Fein, J., 2001. Cd adsorption onto bacterial surfaces: a universal adsorption edge? Geochim. Cosmochim. Acta. 65 (13), 2037-2042. https://doi.org/10.1016/S0016-7037(01)00587-7

Yi, H., Srinivasan, S., Kim, M.K., 2010. *Stenotrophomonas panacihumi* sp. nov., isolated from soil of a ginseng field. J. Microbiol. 48 (1), 30-35. https://doi.org/10.1007/s12275-010-0006-0

Yoon, S.H., Ha, S.M., Kwon, S., Lim, J., Kim, Y., Seo, H., Chun, J., 2017. Introducing EzBioCloud: A taxonomically united database of 16S rRNA gene sequences and whole-genome assemblies. Int. J. Syst. Evol. Microbiol. 67 (5), 1613-1617. https://doi.org/10.1099/ijsem.0.001755

Yu, Q., Szymanowski, J., Myneni, S.C.B., Fein, J.B., 2014. Characterization of sulfhydryl sites within bacterial cell envelopes using selective site-blocking and potentiometric titrations. Chem. Geol. 373, 50-58. https://doi.org/10.1016/j.chemgeo.2014.02.027

Hussain, S.Z., Maqbool, K., 2014. GC-MS: Principle, Technique and its application in Food Science. Int J Curr Sci. 13, 116-126.

Zawadzka, A.M., Crawford, R.L., Paszczynski, A.J., 2006. Pyridine-2,6-bis(thiocarboxylic acid) produced by Pseudomonas stutzeri KC reduces and precipitates selenium and tellurium oxyanions. Appl. Environ. Microbiol. 72 (5), 3119–3129. https://doi.org/10.1128/AEM.72.5.3119-3129.2006

Zhang, J., Song, H., Chen, Z., Liu, S., Wei, Y., Huang, J., Guo, C., Dang, Z., Lin, Z., 2018. Biomineralization mechanism of U(VI) induced by *Bacillus cereus* 12-2: The role of functional groups and enzymes. Chemosphere. 206, 682-692. https://doi.org/10.1016/j.chemosphere.2018.04.181

Zhang, W., Chen, Z., Liu, H., Zhang, L., Gao, P., Li, D., 2011. Biosynthesis and structural characteristics of selenium nanoparticles by *Pseudomonas alcaliphila*. Colloids Surfaces B Biointerfaces. 88 (1), 196–201. https://doi.org/10.1016/j.colsurfb.2011.06.031

Zhang, X., Gu, P., Liu, Y., 2019. Decontamination of radioactive wastewater: state of the art and challenges forward. Chemosphere. 215, 543–553. https://doi.org/10.1016/j.chemosphere.2018.10.029

Zhao, Y.H., Lu, K., Liu, T., 1999. EXAFS study of structural characteristics of nanocrystalline selenium with different grain sizes. Phys. Rev. B - Condens. Matter Mater. Phys. 59, 11117–11120. https://doi.org/10.1103/PhysRevB.59.11117

Zheng, S., Su, J., Wang, L., Yao, R., Wang, D., Deng, Y., Wang, R., Wang, G., Rensing, C., 2014. Selenite reduction by the obligate aerobic bacterium *Comamonas testosteroni* S44 isolated from a metal-contaminated soil. BMC Microbiol. 14, 204. https://doi.org/10.1186/s12866-014-0204-8

Żymankowska-Kumon, 2016. Ecological assessment of foundry binders from cold-box technology by gas chromatography method. World Sci. News 57, 554–561.